ADSORPTIVE REMOVAL OF METALLIC AND NON-METALLIC POLLUTANTS FROM WATER BY CHEMICALLY MODIFIED NATURAL ION EXCHANGER

A THESIS SUBMITTED TO THE

CENTRAL DEPARTMENT OF CHEMISTRY

INSTITUTE OF SCIENCE AND TECHNOLOGY

TRIBHUVAN UNIVERSITY

NEPAL

FOR THE AWARD OF

DOCTOR OF PHILOSOPHY

IN CHEMISTRY

BY

BHOJ RAJ POUDEL

DECEMBER 2022

ADSORPTIVE REMOVAL OF METALLIC AND NON-METALLIC POLLUTANTS FROM WATER BY CHEMICALLY MODIFIED NATURAL ION EXCHANGER

A THESIS SUBMITTED TO THE

CENTRAL DEPARTMENT OF CHEMISTRY

INSTITUTE OF SCIENCE AND TECHNOLOGY

TRIBHUVAN UNIVERSITY

NEPAL

FOR THE AWARD OF

DOCTOR OF PHILOSOPHY

IN CHEMISTRY

BY

BHOJ RAJ POUDEL

DECEMBER 2022

EXTERNAL EXAMINERS

The Title of Ph.D. Thesis : "Adsorptive Removal of Metallic and Non-Metallic Pollutants from Water by Chemically Modified Natural Ion Exchanger"

Name of Candidate : Mr. Bhoj Raj Poudel

External Examiners:

(1)   Prof. Dr. Ajaya Bhattarai
        Department of Chemistry
        Mahendra Morang Aadarsha Multiple Campus
        Tribhuvan University
        Biratnagar, NEPAL

(2)   Prof. Dr. Satendra Pal Singh
        Department of Physics
        Lucknow University
        Uttar Pradesh, INDIA

(3)   Prof. Dr. Hak Yong Kim
        Department of Nano Convergence Engineering
        Jeonbuk National University
        Jeonju, SOUTH KOREA

January 20, 2023

Dr. Surendra Kumar Gautam
Assistant Dean

DECLARATION

Thesis entitled **"Adsorptive Removal of Metallic and Non-Metallic Pollutants from Water by Chemically Modified Natural Ion Exchanger"** which is being submitted to the Central Department of Chemistry, Institute of Science and Technology (IOST), Tribhuvan University, Nepal for the award of the degree of Doctor of Philosophy (Ph.D.), is a research work carried out by me under the supervision of Prof. Dr. Megh Raj Pokhrel, of Central Department of Chemistry, Tribhuvan University and co-supervised by Asst. Prof. Dr. Hari Paudyal, of Central Department of Chemistry, Tribhuvan University.

This research is original and has not been submitted earlier in part or full in this or any other form to any university or institute, here or elsewhere, for the award of any degree.

....

Bhoj Raj Poudel

RECOMMENDATION

This is to recommend that **Mr. Bhoj Raj Poudel** has carried out research entitled **"Adsorptive Removal of Metallic and Non-Metallic Pollutants from Water by Chemically Modified Natural Ion Exchanger"** for the award of Doctor of Philosophy (Ph.D.) in **Chemistry** under our supervision. To our knowledge, this work has not been submitted for any other degree.

He has fulfilled all the requirements laid down by the Institute of Science and Technology (IOST), Tribhuvan University, Kirtipur for the submission of the thesis for the award of Ph.D. degree.

....
Prof. Dr. Megh Raj Pokhrel
(Supervisor)
Professor
Central Department of Chemistry
Tribhuvan University
Kirtipur, Kathmandu, Nepal

....
Dr. Hari Paudyal
(Co-supervisor)
Assistant Professor
Central Department of Chemistry
Tribhuvan University
Kirtipur, Kathmandu, Nepal

DECEMBER 2022

पत्र संख्या:
Ref. No.:

LETTER OF APPROVAL

Date: December 01, 2022

On the recommendation of **Prof. Dr. Megh Raj Pokhrel** and **Dr. Hari Paudyal,** this Ph.D. thesis submitted by **Mr. Bhoj Raj Poudel,** entitled **"Adsorptive Removal of Metallic and Non-Metallic Pollutants from Water by Chemically Modified Natural Ion Exchanger"** is forwarded by Central Department Research Committee (CDRC) to the Dean, IOST, T.U.

....

Prof. Dr. Jagadeesh Bhattarai

Professor,

Head

Central Department of Chemistry

Tribhuvan University

Kirtipur, Kathmandu

Nepal

ACKNOWLEDGEMENTS

....

Bhoj Raj Poudel

December 2022

ABSTRACT

Metallic and non-metallic pollutant in water sources poses a great threat to the environment and all living organisms, including humans. Adsorption is the most economical, simple, and effective method for treating water containing both heavy metals and non-metals. To develop an alternative to activated carbon and synthetic ion-exchange resins, it is necessary to investigate all feasible agro-based low-cost biosorbents and analyze their feasibility for removing metallic and non-metallic pollutants. The main goal of the current work is to examine the biosorption performances of three types of novel biosorbents/ion-exchangers prepared from pomegranate peel waste such as zirconium-loaded saponified pomegranate peel (SPP@Zr) for the sorption of As(V), As(III) and phosphate; TiO_2 impregnated pomegranate peel (PP@TiO_2) for the sorption of As(III) and saponified pomegranate peels (SPP) for the sorption of Pb(II)/Cd(II) from aqueous solution. After a simple chemical modification, the pomegranate peel (PP) waste has the potential biosorption properties for cationic (Pb(II) and Cd(II)) and anionic (arsenate, arsenite, and phosphate) contaminants. The methyl ester portion of pomegranate pectin was saponified by lime water treatment to adsorb metal cations, by increasing the carboxyl functional groups. The active sites for anions were developed after loading with Zr(IV) ions or impregnating TiO_2.

Zeta potential analysis, FE-SEM, EDX, XRD, FTIR, and XPS analyses were utilized to characterize the obtained biosorbents. The biosorption study was done using batch methods. The adsorbate solution pH, adsorbent dosage, and contact time to attain equilibrium were optimized in batch mode. To evaluate the biosorption isotherm, the effect of the initial concentration of adsorbate ion on biosorption was investigated. A thermodynamics study was conducted to evaluate spontaneity and heat change for the biosorption of As(V) on SPP@Zr. It also investigated how coexisting ions affected the biosorption of the adsorbate ion onto the biosorbent. Studies on desorption and reusability were carried out to assess the practical utility of the prepared biosorbent. Based on the characterization and experimental results, the underlying mechanism of biosorption was investigated.

The maximum adsorptive capacities (q_m) of SPP@Zr towards As(V), As(III), and phosphate were 83.33, 72.52, and 123.15 mg/g, respectively. As(V) and phosphate

were strongly adsorbed at pH 4.0, while As(III) was strongly adsorbed at pH 9.5. The q_m of PP@TiO$_2$ towards As (III) was 76.92 mg/g at neutral pH. The q_m of the SPP was evaluated as 229.88 mg/g and 174.52 mg/g for Pb(II) and Cd(II), respectively. All the biosorption processes were found to be best fitted to the Langmuir isotherm model and the pseudo-second-order kinetic model. Thermodynamic studies revealed the biosorption of As(V) onto SPP@Zr was endothermic and spontaneous. The biosorption As(V) and As(III) was not affected by the addition of co-existing anions such as chloride, sulfate, or bicarbonate. The presence of phosphate ions, however, may significantly slow down the biosorption of arsenic onto SPP@Zr and SPP@ TiO$_2$. Similarly, the presence of carbonate ions interfered with the biosorption of phosphate onto SPP@Zr. The co-existing cations such as K^+, Ni^{2+}, $Cu^{2+,}$ and Co^{2+} showed negligible effects on Pb(II)/Cd(II) removal by SPP. Using a 0.1 M NaOH solution, adsorbed arsenic and phosphate were eluted without any leakage of the loaded zirconium. An eluent concentration of 0.1 M HNO$_3$ can be used for the effective desorption of Pb(II) and Cd(II) ions from exhausted SPP for safe disposal. All three biosorbents demonstrated exceptional reusability and stability for up to five biosorption-desorption cycles. The arsenic and phosphate biosorption and desorption mechanisms were inferred to be ligand exchange reactions between coordinating hydroxyl ions of loaded Zr(IV) ions on SPP@Zr and aqueous solution arsenate/arsenite/phosphate anions. Likewise, Pb(II) and Cd(II) ions can be adsorbed onto SPP by replacing the Ca^{2+} ions of the SPP through a cation exchange mechanism. Finally, the SPP@Zr was used to remove arsenic from real groundwater samples, and it was shown to be very effective in the uptake of arsenic much lower than the mark of drinking water tolerance threshold (10 μg/L) established by WHO and USEPA.

The SPP@Zr, PP@TiO$_2$, and SPP based on pomegranate peel developed in our laboratory proved to be effective ion-exchangers for removing arsenic, phosphate, lead, and cadmium ions from contaminated water, as in the case of plastic materials like commercial synthetic ion exchangers.

LIST OF ACRONYMS AND ABBREVIATIONS

EDX	:	Energy Dispersive X-ray Spectroscopy
FTIR	:	Fourier Transform Infrared Spectroscopy
PZC	:	Point of Zero Charge
UV	:	Ultraviolet
ΔG^{o}	:	Change in Standard Gibbs Free Energy
ΔH^{o}	:	Change in Standard Enthalpy
ΔS^{o}	:	Change in Standard Entropy
AAS	:	Atomic Absorption Spectroscopy
AR	:	Analytical Reagent
q_m	:	Maximum Biosorption Capacity
b	:	Langmuir Constant
K_F	:	Freundlich Constant
C_e	:	Equilibrium Concentration
C_0	:	Initial Concentration
R_L	:	dimensionless Separation Factor
1/n	:	Heterogeneity Factor Related to the Biosorption Intensity
K_C	:	Thermodynamic Equilibrium Constant
K_D	:	Distribution Coefficient
PFO	:	Pseudo First Order
PSO	:	Pseudo Second Order
FE-SEM	:	Field Emission Scanning Electron Microscopy
ICP-MS	:	Inductively Coupled Plasma - Mass Spectroscopy
ICP-OES	:	Inductively Coupled Plasma- Optical Emission Spectroscopy
XPS	:	X-ray Photoelectron Spectroscopy
PXRD	:	Powder X-ray Diffraction
RPP	:	Raw Pomegranate Peel
SPP	:	Saponified Pomegranate Peel
SPP@Zr	:	Zr(IV) Loaded Saponified Pomegranate Peel
$PP@TiO_2$	:	TiO_2 Impregnated Pomegranate Peel
WHO	:	World Health Organization
US-EPA	:	United State Environmental Protection Agency

LIST OF SYMBOLS

λ :   Wavelength

θ :   Bragg Diffraction Angle

V   :   Volt

ºC   :   Degree Celsius

K   :   Kelvin

R   :   Universal Gas Constant

R^2 :   Correlation Coefficient

χ^2 :   Chi Square

LIST OF TABLES

LIST OF FIGURES

xviii

TABLE OF CONTENTS

CHAPTER 1

INTRODUCTION

1.1 Introduction

Water is one of the most necessary things for a living organism. Freshwater makes up just 3.5% of the total amount of water on Earth, and just 0.01% of that is appropriate for human use (Hinrichsen & Tacio, 2002). Water consumption and wastewater production increased because of rapid urbanization and population growth. Untreated wastewater is being haphazardly disposed of by households, institutions, and industries severely degrading the water quality in developing nations. In recent decades, water pollution has been into surface waterways or by the intrusion of untreated sewage and chemical pollutants into water bodies. Additionally, it might be seen as the injection of wastes into the surface runoff, which then flows through surface waterways and eventually reaches underground water sources. The most significant environmental issue in the world is water pollution, which is defined as "the presence of chemical, biological compounds, or factors that make a specific body of water less suitable for some beneficial uses" (Schweitzer & Noblet, 2018). The type and level of pollution in water affect its quality. To stop the deterioration of water quality, the WHO and the USEPA developed guidelines for polluting species in water (USEPA, 2017). Under these guidelines, there is no considerable or foreseeable danger to human health from drinking water pollution (Schweitzer & Noblet, 2018). The contaminations, however, might result in serious diseases and disorders if they exceed the permissible limit. As a result, it is important to treat the water systems using methods that are both energy and cost-efficient (Carolin *et al.*, 2017).

1.2 Water pollution

The contamination of water results from either naturally occurring sources, or anthropogenic sources (the several activities embarked on by a human). Although certain heavy metals or trace elements can dissolve in natural water during the hydrological cycle, anthropogenic sources are the main cause of water pollution (Saifuddin M & Kumaran, 2005). The main activities contributing to pollution are the indiscriminate dumping of municipal, industrial, and residential sewage into rivers, lakes, waterways, and streams. Every day, sewage and effluent are thought to be

dumped into the water, amounting to about 2 million tonnes worldwide. 90% of untreated sewage and 70% of untreated effluents are dumped into surface waters in developing countries (Azizullah *et al.*, 2011). The primary sources of water pollution include industries like ceramics, textiles, food, food processing, tanning leather, medicines, steel, fertilizer, petrochemical plants, and oil mills (Sial *et al.*, 2006). Their production operations result in the creation of large volumes of wastewater containing noxious heavy metals like Ni, As, Hg, Pb, Cd, Zn, Cu, Cr, Co, as well as cations and anions like Na^+, K^+, Ca^{2+}, Cl^-, and CO_3^{2-} as well as several other pollutants like phosphate, nitrites, and nitrates, as well as organic compounds (Sial *et al.*, 2006; Ullah *et al.*, 2009). Waste from home and community sources, as well as the pervasive usage of agrochemicals in agricultural activities, are the main causes of water pollution (Alengebawy *et al.*, 2021). **Figure 1** shows the different anthropogenic sources of heavy metals.
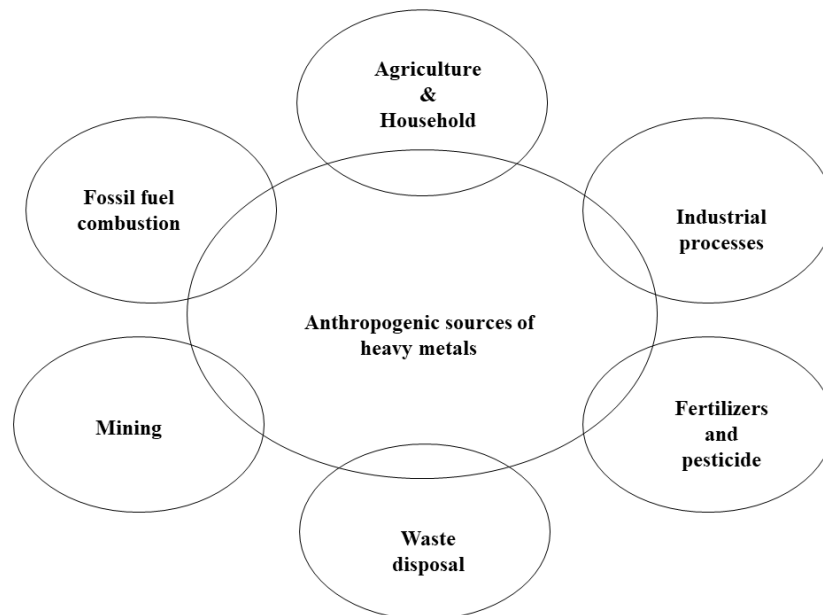
Figure 1: Anthropogenic sources of heavy metal pollution.

Several contaminants are classified into various categories that are thought to be vigorous water pollutants. They are toxic and seriously harm people and other species when they reach a maximum permissible limit. Pathogens (bacteria, viruses, and protozoa), inorganic pollutants (acid, salts, and toxic metals), organic pollutants (dyes, and polycyclic aromatic hydrocarbon), anions (nitrates, phosphates, fluorides, and sulphates), and water-soluble radioactive substances are the most common. The US-

EPA has classified some trace metals, including Cd, Pb, Hg, Cu, Cr, Zn, Ni, and As, as priority control pollutants because of their toxicity, bioaccumulation, and inability to degrade (Wang *et al.*, 2017). Even though some heavy metals like Cu, Zn, and Cr, are essential for human health, an excessive amount of them can be damaging to the body (Pandey & Madhuri, 2014).

1.3 Heavy metals and their impacts

The term heavy metal refers to "the group of toxic metals and metalloids having an atomic density higher than 5.0 g/cm^3" (Nies, 1999). The term is widely recognized and usually applied to the elements such as Cadmium (8.65 g/cm^3), Chromium (7.14 g/cm^3), Cobalt (8.90 g/cm^3), Copper (8.95 g/cm^3), Lead (11.34 g/cm^3), Mercury (13.53 g/cm^3), Nickel (8.91 g/cm^3) and Zinc (7.14 g/cm^3) which are associated with pollution and toxicity problems. A metalloid such as arsenic (As) (5.73 g/cm^3) can be poisonous even at very low concentrations. Increased urbanization and fast industrial expansion have resulted in the release of noxious heavy metal ions into water bodies and soil. Even in trace concentrations, they are exceedingly harmful to human health and the ecosystem (Li *et al.*, 2018; Poudel *et al.*, 2020; Rathore *et al.*, 2021). Contamination of noxious heavy metals including Pb(II), Hg(II), and Cd(II) in water has attracted considerably greater attention over the decades due to their non-biodegradability and toxicity at low concentrations, bioaccumulation potential, and neurotoxic and carcinogenic effects (Rathore *et al.*, 2017; Yadav *et al.*, 2021; Zhang *et al.*, 2021).

Heavy metals can enter our systems through air, food, water, or direct skin contact in residential, industrial, agricultural, and pharmaceutical contexts (Cao *et al.*, 2015; Kong *et al.*, 2011). Since heavy metals cannot be metabolized by the body, they accumulate in both soft and hard tissues (Ghodbane & Hamdaoui, 2008). High exposure levels are not necessary for hazardous consequences to manifest in people because heavy metal accumulation occurs over time and negative effects become more pronounced when levels of exposure exceed acceptable limits (Khuzestani & Souri, 2013). Some essential metals in elevated concentrations are noxious as they produce oxidative stress by producing free radicals (Ghosh & Singh, 2005; Barakat & Kumar, 2014). In humans, oxidative stress is the cause of many illnesses and ailments. Heavy metals are hazardous as they may substitute for necessary metals in

pigments and enzymes and thus disturb the function of the living organism. An organism's biochemical cycles are significantly altered when non-essential heavy metals are present. The toxicity is frequently more pronounced in animals at higher trophic levels because metal ions bioaccumulate in the environment and are biomagnified up the food chain (Ahluwalia & Goyal, 2007). Living beings can absorb metal ions because of their high solubility in aquatic conditions, and they can accumulate in the body in significant amounts. **Figure 2** shows the pathway of heavy metals transfer from their originating sources to the human body.
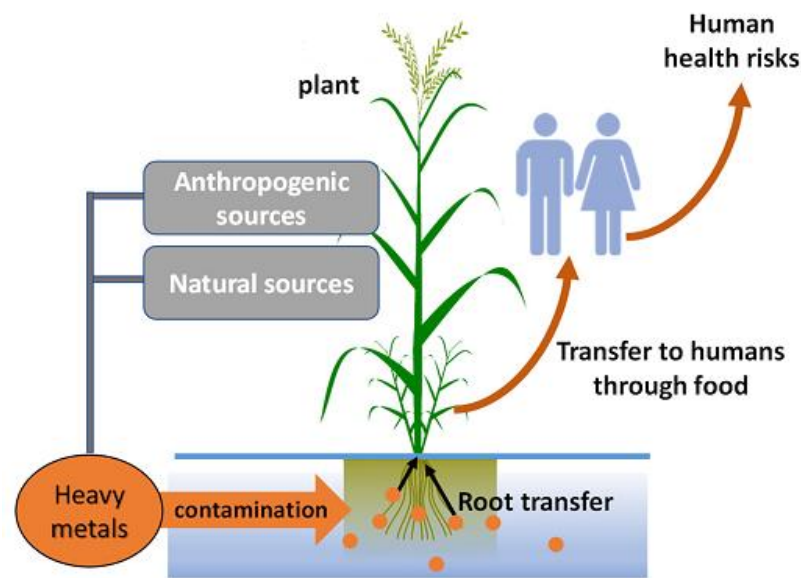
Figure 2: Pathway of heavy metals transfer from their originating sources to humans (Uddin *et al.*, 2021).

1.3.1 Arsenic

Arsenic (As) is a naturally occurring metalloid with At. No. = 33, At. Wt. = 74.921, density = 5.727 g/cm^3, M.P. = 817°C and B.P. = 614°C (Mohan & Pittman, 2007). The health impacts of arsenic-contaminated groundwater on people are diverse. It is a hazardous and non-essential component of biological systems that can harm the skin, neurological and circulatory systems, cause cancer, and even result in death (Zhang *et. al.*, 2007; Poudel *et. al.*, 2020). It is expected that drinking water contaminated with arsenic severely affects 94 to 220 million people worldwide. (Podgorski & Berg, 2020). A massive (94%) of the people at peril are in Southeast Asia (Podgorski & Berg, 2020; Uppal *et. al.*, 2019; Davydiuk *et. al.*, 2020). Arsenic pollution in groundwater and surface water can be caused by anthropogenic factors including

4

industrial effluents, mining, burning fossil fuels, agricultural chemicals, pigments, and paints, or geogenic factors such as soil and rock weathering and volcanic emissions (Rajendran &Thangavelu, 2021; Naujokas *et. al*., 2013). Arsenic contamination of food and water is the main way that humans are exposed to it (Davydiuk et. al., 2020). WHO and USEPA have set a maximum permissible limit (MCL) for arsenic in drinking water of 10 µg/L because of its exposure concern and severe noxiousness (WHO, 2017; USEPA, 2017). As a result, effective and affordable arsenic removal from polluted water is of emerging concern. Arsenic exposure, specifically through drinking water, has been linked to several complications, including dermatological effects, cardiovascular effects, pulmonary illnesses, reproductive effects, and neurological consequences in both adults and children (Abdul *et al.*, 2015). The key consequences of arsenic on major organ systems are illustrated in **Figure 3**.
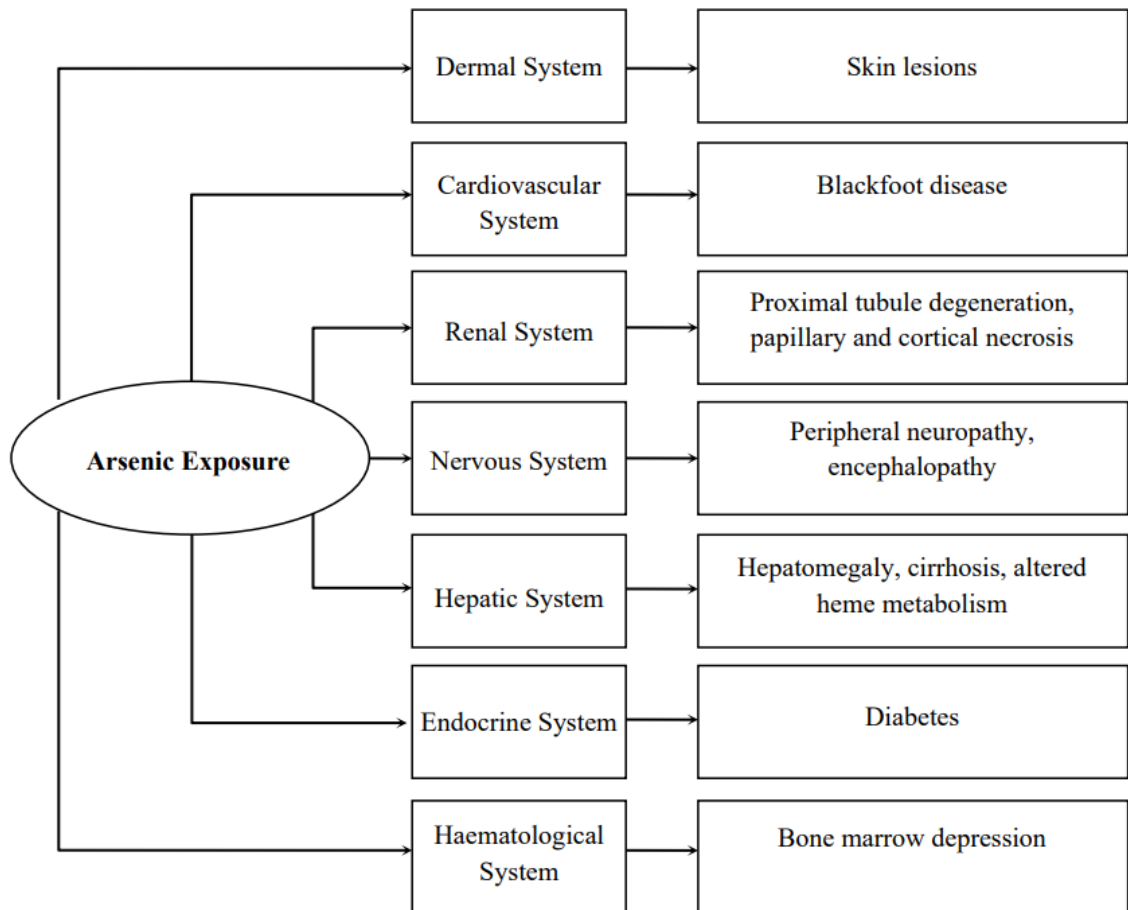
Figure 3: The key effects of arsenic on major organ systems (Abdul *et al.*, 2015).

In the aquatic environment, arsenic may be found in both organic and inorganic forms. The primary forms are inorganic arsenate and arsenite, which are the most

dangerous to human health and are classified as "Class A" human carcinogens (Nhiem *et. al.*, 2021). Arsenic species concentration depends on the redox potential and pH of the solution. The trivalent form (H_3AsO_3, $H_2AsO_3^-$) is prevalent in the reducing environment, while the pentavalent form ($H_2AsO_4^-$, $HAsO_4^{2-}$) is prevalent in the oxidizing environment (Nhiem *et. al.*, 2021; Ghimire *et. al.*, 2002).

1.3.2 Lead

Lead (Pb) is one of the most toxic heavy metals with At. No. = 82, At. Wt. = 207.20, Density = 11.34 g/cm^3, M. P. = 327.46°C and B. P. = 1749°C. Contamination and exposure to Pb(II) ions have been reported to be toxic even at ppb levels (Abdullah *et al.*, 2020). Various anthropogenic sources, such as the battery industry, lead pipes, and taps, coal combustion, mining, metal polishing, paints, medical equipment, use of gasoline additives such as tetra ethyl lead (TEL), and electronic devices, readily discharge toxic Pb(II) ions into the aquatic environment (Alqadami *et al.*, 2020; Ekrayem *et al.*, 2021). Lead pollution in water is mostly caused by lead-acid batteries. Such used lead acid batteries can contaminate the surrounding environment with lead if they are dumped improperly (Sherchand *et al.*, 2014). Lead enters the human body by ingestion, inhalation, or food and can cause kidney damage, anemia, cardiovascular illness, mental retardation, and problems with the reproductive system (Anantha & Kota, 2016; Zhang *et al.*, 2021). Lead accumulation in the body during pregnancy can be harmful to the unborn child (UNEP 2013). The MCL for lead in drinking water has been set at 10 and 15 µg/L, respectively, by the WHO and USEPA (Ekka *et al.*, 2015). As a result, efficient and cost-effective treatment of Pb(II) ions from wastewater is required to keep lead concentrations below tolerance levels. Lead pollution levels in the ground and surface water resources of the Indian subcontinent range from 5 to 317 ppb (Bhardwaj *et al.*, 2020; Yadav *et al.*, 2021). Thus, even a trace concentration of Pb(II) ions in water are extremely dangerous.

1.3.3 Cadmium

One of the most hazardous heavy metals is Cd with At. No. = 48, At. Wt. = 112.41, density = 8.69 g/cm^3, M.P. = 321°C and B.P. = 767°C. It is another heavy metal that causes human cancer, and it is listed as the seventh most hazardous substance provided by Agency for Toxic Substances and Disease Registry (ATSDR). High

water solubility makes Cd (II) and its compounds more bioavailable and mobile in soil. Because of the high bioconcentration factors, mollusks and microbes can transfer Cd with ease. It is thought of as a serious contaminant because the free ionic form of Cd (II) is easily absorbed by organisms in water, has a high solubility in water, and bioaccumulates quickly in soil (Qi *et al.*, 2018). By inhaling Cd-containing fumes, Cd is easily absorbed by 10% and enters the digestive tract. The WHO has established a Cd tolerance level for portable water of 3 µg/L (Barakat & Kumar, 2014; Hubicki & Kołodyńska, 2012). Persistent exposure to Cd can cause lung cancer as well as damage the kidneys and bones. The most serious form of Cd poisoning in humans is called "itai-itai," a condition characterized by excruciating bone pain. The metabolism of essential elements including Zn, Fe, Cu, Mn, Se, and Ca is altered because of Cd accumulation in the intestines, kidneys, and glands. The cadmium-containing fumes and dust may be the cause of lung problems and emphysema (Hubicki & Kołodyńska 2012). **Table 1** lists the probable health impacts, the WHO (2017) permissible levels for potable water, and the sources of several toxic heavy metals.

Table 1: Various sources and impacts of toxic metals, including their toxicity mechanisms, and WHO, 2017 permissible limits for drinking water (Abbas *et al.*, 2016; Barakat & Kumar, 2014; Ayele *et al.*, 2021; Jaishankar *et al.*, 2014).

Heavy metals	Sources	Effects	Mechanisms of toxicity	Permissible limits (µg/L)
Arsenic	Fungicides, pesticides, electronics, metallurgical industries, mining-byproduct, and combustion of fossil fuel	Internal cancer, skin rashes, bronchitis, vascular disease, acute poisoning, and death	Biotransformation of toxic inorganic arsenic gets methylated.	10
Lead	Automobile emission, electronics, mining, plumbing, paint, coal burning, pesticides, landfill leachate	damage to the fetal brain, gastrointestinal damage, conditions affecting the neurological system, circulatory system, and liver	An imbalance exists between the formation of antioxidants needed to detoxify reactive intermediates and the creation of free radicals; replacing monovalent cations like Na+ and other divalent cations like Ca(II), Mg(II).	10

Cadmium	Electroplating, electronics, pesticide, fertilizers, nuclear fission plant, metalliferous mining, landfill leachate, and battery manufacturing	Kidney damage, renal disorder, a human carcinogen, bronchitis, gastrointestinal damage	Binding with cysteine, glutamate, histidine, and aspartate ligands; binding to cysteine-rich proteins such as metallothioneins.	3
Chromium	Leather tanners, metal finishers, dyes and pigments, chrome plating, and wood preservation	Normocytic, hypochromic anemia, leukopenia, Headache, diarrhea, nausea, vomiting, carcinogenic, mutagenesis changes, lung tumors	Cr(VI) interaction with biological reductants like thiols and ascorbate	50
Mercury	Batteries, paper and paint industries, pesticides, electronics, waste disposal, landfill leachate	Chronic pain from rheumatoid arthritis, kidney, cardiovascular, central nervous system, protoplasm toxicity, eyes, and muscle illnesses	Binding to freely available thiols; Attachment to the selenohydryl and sulfhydryl groups	6
Nickel	Electrolysis, paint formulation, printed circuit board, metalliferous mining, metal finishing industry	Dermatitis, nausea, chronic asthma, coughing, a human carcinogen, gastrointestinal damage	Substituting the essential metal from metalloproteins. attaching to non metalloenzyme catalytic residues	70
Zinc	Metal finishing industry, metal plating, metalliferous mining, agricultural materials, fertilizers, brass manufacturing, plumbing	Skin, nervous system, gastrointestinal damage, Depression, lethargy	Reactive oxygen species production and activation of the mitogen-activated protein kinase pathway	50

1.4 Non-metallic pollutants

Human health and aquatic ecosystems are negatively impacted by an overabundance of various non-metals, such as phosphorous (as phosphate ions), fluorine (as fluoride ions), and nitrogen (as ammonium and nitrate ions).

1.4.1 Phosphorous

One of the sixteen elements necessary for plant growth is phosphorus (P) (Yadav *et al.*, 2019). It is also an essential component of the animal body's teeth, bones, phospholipids, DNA, RNA, and ATP (Karachalios, 2013; Schaum, 2018). P is also used in industrial applications such as fertilizers, detergents, paints, corrosion

inhibitors, drinks, and medications (Sasidharan *et al.*, 2022). Phosphorous has a big impact on daily living, but it is a non-renewable resource that cannot be made artificially (Karabegovic *et al.*, 2013). The global P reserve is currently overexploited for a variety of purposes, and it may run out in 40-150 years (Boer *et al.*, 2019; Ohtake & Tsuneda, 2019). Alternative sources of phosphorous are now urgently needed (Hanief & Laursen, 2019). From another angle, eutrophication is likely to occur when phosphorous concentrations in water bodies approach 0.02 mg/L (Mallampati & Valiyaveettil, 2013). The aquatic medium may become depleted of dissolved oxygen because of the significant oxygen consumption required for the breakdown of dead algae, jeopardizing the survival of aquatic species (Jyothi *et al.*, 2012). Loss of the water's quality, biodiversity, and economic and recreational worth could arise as a result. In addition to lowering the quality of drinking water, phosphate leaching into the groundwater through the subsoil poses a threat to both human and animal health. Osteoporosis and renal damage from consuming a high phosphate concentration must be reported (Mor *et al.*, 2016).

Phosphorous enters natural water bodies through sewage discharges, agricultural runoff, and rock weathering (Sasidharan *et al.*, 2021; Xu *et al.*, 2011). Despite being chemically unstable and prone to oxidation into the pentavalent state, trivalent phosphorus is one of the two main oxidation states of phosphorus. Oxo-anions, which are forms of phosphorus, can be found in aqueous solutions (Pokhrel *et al.*, 2019). Many national and international water standard authorities have restricted the effluent discharge criteria for total phosphorous to safeguard surface water from such undesirable phenomena. The US-EPA recommends that the stringent discharge limit be less than 0.05 mg/L and the MCL of phosphorus be 0.1 mg/L (Huang *et al.*, 2009). The WHO recommends a maximum phosphate concentration in drinking water of 5 mg/L (WHO, 2017). Consequently, to comply with strict rules, proper treatment methods are required (Kalmykova & Fedje, 2013).

1.5 Methods for removal of hazardous materials from water

The removal of metallic and non-metallic contaminants from wastewater currently uses a variety of treatment techniques, including chemical precipitation, chemical oxidation, electrochemical treatment, reverse osmosis, ion exchange, membrane technology, filtering (Sarma *et al.*, 2015), and coagulation (Won *et al.*, 2014). They

have been utilized and developed to remove hazardous pollutants from wastewater at high concentrations. Some of the disadvantages of each treatment technology include toxic sludge production that would require additional treatment and large amounts of chemical reagents; complicated operation and maintenance; low efficiency in the purification of water polluted with trace levels of heavy metals; high operating costs; high energy consumption; and the production of a secondary waste product (Sarma *et al.*, 2015; Poudel *et al.*, 2021). In large-scale applications, adsorption using activated carbon is prohibitively costly (Wang & Chen, 2009). As a result, most of those treatment methods are not considered to be sustainable treatment technologies. This has prompted the researcher to look for alternative cost-effective wastewater treatment solutions. Brief descriptions of some methods for removing toxic metallic and non-metallic ions from wastewater are presented here.

1.5.1 Reverse osmosis

A semipermeable membrane is used in the reverse osmosis method of water treatment to eliminate ions, molecules, and bigger particles from drinking water. Applied pressure is utilized to counteract osmotic pressure in reverse osmosis. Chemical potential variations in the solvent cause osmotic pressure. Many forms of dissolved and suspended species, including bacteria, may be removed from water using reverse osmosis, which is utilized in both industrial operations and the production of potable water. The solute is kept on the pressurized side of the membrane while the pure solvent is permitted to pass through. This membrane should not allow big molecules or ions to pass through the pores or holes to be 'selective, but it should enable smaller components of the solution, such as solvent molecules, to flow freely. This technique has been used to separate different metallic and non-metallic ions from the aqueous phase (Bodalo *et al.*, 2005; Sehn, 2008). For the separation of dissolved species from aqueous solutions, reverse osmosis is used. Dilute solutions, however, it has substantial operating and maintenance expenses (Lin *et al.*, 2005).

1.5.2 Chemical precipitation

Coagulating agents including alum, lime, Fe salts, and organic polymers are used to precipitate metal ions. It is common practice to chemically precipitate heavy metals using lime or sodium hydroxide as their hydroxides. The metal carbonate precipitated

with calcium or sodium carbonate is very limited. The sulfide precipitation method can also be used to get rid of heavy metals. The most used method for treating effluents containing metal ions today is chemical precipitation (Zubair *et al.*, 2008). In the case of non-metal, for instance, fluoride can be precipitated with calcium and aluminum salts, but the treated water has a high pH, making it challenging to remove extra contaminants (Martínez-Miranda *et al.*, 2011).

By adding salts of multi-valent metal ions to create precipitates of insoluble metal phosphates, which are then separated by sedimentation, phosphorous is removed using the chemical precipitation approach (Bashar *et al.*, 2018; Biswas *et al.*, 2008b; Gibbons, 2010; Silva Simplicio, 2020). Iron and aluminum chloride or sulphate, as well as calcium hydroxide, are the most used chemicals for this purpose. The reactions below demonstrate how these chemicals combine with phosphate (Nieminen, 2010).

$$Al^{3+} + PO_4^{3-} \longrightarrow AlPO_4\downarrow$$

$$Fe^{3+} + PO_4^{3-} \longrightarrow FePO_4\downarrow$$

$$5\,Ca^{2+} + 3\,PO_4^{3-} + OH^- \longrightarrow Ca_5(PO_4)_3\,(OH)\downarrow$$
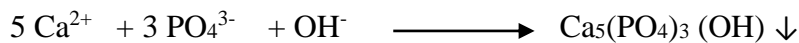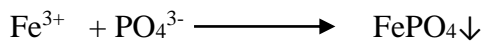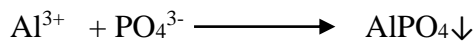
The downsides of the chemical precipitation approach include sludge formation, high chemical costs, effluent neutralization requirements, and insufficient efficiency for pollutants, both metallic and non-metallic, at low concentrations (Kumar & Pal, 2015). Handling sludge will raise treatment costs and need a lot of space (Sengupta & Pandit, 2011). Sludge produced chemically has a high impurity level and a low bioavailability, making it unusable (Nieminen, 2010).

1.5.3 Electro-dialysis

Semi-permeable ion-selective membranes are used in the electro-dialysis procedure to separate the ionic components (heavy metals or non-metals), which need electrical energy as a driving force (Mohammadi *et al.*, 2005). Cations and anions migrate toward their respective electrodes when an electrical potential is placed between the two electrodes (Lambert *et al.*, 2006). The membranes may transport ions with a positive or negative charge and reject ions with an opposite charge because they are selective. Consequently, ions may be removed or separated via dialysis (Akpor &

Muchie, 2010). Chemical precipitation of salts with limited solubility on the membrane surface is the main drawback of the electrodialysis procedure for wastewater treatment. The method hasn't been widely used in full-scale metal ion removal from wastewater.

1.5.4 Solvent extraction

The distribution of solute in an organic and aqueous phase is the goal of solvent (liquid-liquid) extraction. The aqueous solution having metallic or non-metallic ions is combined with the appropriate chelating reagent and relevant organic solvent to recover the metals or non-metals. Metal enters the organic phase. Problems with classical solvent extraction include solvent loss, phase separation, emulsion formation, flooding, and loading in column contactors (such as packed towers) and mixer settlers (Lin & Juang, 2002).

1.5.5 Ion exchange

Ion exchange is a reversible process that involves exchanging ions from contaminated water for equivalence ions on an immovable solid phase known as ion exchange resins (Martin *et al.*, 2009). Insoluble ion exchangers include loosely held ions in the form of insoluble salts, which might be naturally occurring zeolites or synthetically produced organic resins, primarily polymeric resins derived from hydrocarbons. It permits ion exchange materials to exchange either positively charged ions (cation exchangers) or negatively charged ions (anion exchangers) (Karachalios, 2013). In a solid resin, anions, and cations present in water exchange, release ions with comparable charges (Kanamarlapudi *et al.*, 2018).

This method can eliminate a trace concentration of pollutants ions present in wastewater. Proteins, cellulose, and living cells are examples of natural ion exchange materials, but polystyrene with sulfonate groups (cation exchangers) and amine groups (anion exchangers) is the most widely used synthetic resin. Because of its ease of operation and flexibility to variations in feed flow rates, temperatures, and compositions, the ion exchange technique is useful (Awual & Jyo, 2011; Li *et al.*, 2016). Important barriers to its widespread application include low selectivity in the presence of co-ions and high operating expenses because of the frequent use of reagents (Biswas *et al.*, 2008a; Karachalios, 2013).

1.5.6 Phytoremediation

One biological technique used to remediate contaminants in wastewater, including hazardous metallic and non-metallic ions, is phytoremediation. This approach has advantages for ecological, green space, and decreased aesthetics in addition to wastewater treatment. Using certain plant species, phytoremediation is a technique for eliminating environmental pollutants (metals, non-metals, pesticides, solvents, crude oils, and their derivatives) in soil, air, or water. Numerous plant species, such as *Vetiveria sp.*, *Typha sp.*, and *Cyperus sp.*, are frequently used in this field (Chen *et al.*, 2004; Danh *et al.*, 2009). The disadvantages include the considerable time it takes to remove metals and the difficulty in regenerating the plant for further treatment.

1.5.7 Adsorption

Adsorption is an economically viable alternative to conventional techniques for removing metallic and non-metallic contaminants from wastewater. Adsorption is a physicochemical process that commonly involves the mass transfer of the substances (adsorbate) from the gas or liquid phase to the surface and or the interface of the solid phase (adsorbent) (Li *et al.*, 2021; Demirbas, 2008). The adsorbent is the substance that the adsorption occurs on, while adsorbate is the substance that is adsorbed (Grassi *et al.*, 2012). Adsorption is a mass transfer method used to remediate wastewater, moving mass from the wastewater's liquid phase to the adsorbent solid surface. Adsorption occurs commonly in industrial applications and can be found in several natural, physical, biological, and chemical systems. Activated carbon, silica gel, and alumina are the most popular industrial adsorbents. Because of its outstanding sorption capacity correlating to its large specific surface area, activated carbon is one of the materials that are most extensively utilized in environmental applications (Okada *et al.*, 2004). **Figure 4** depicts the main processes involved in adsorption (Babalola, 2018). Both the adsorbate and the adsorbent have specific characteristics that are dependent on their specific components (De Gisi *et al.*, 2016). The adsorption process may be divided into two categories according to the strength of the attraction between the adsorbent and adsorbate:

 - ➢ Physical adsorption or physisorption
 - ➢ Chemical adsorption or chemisorption
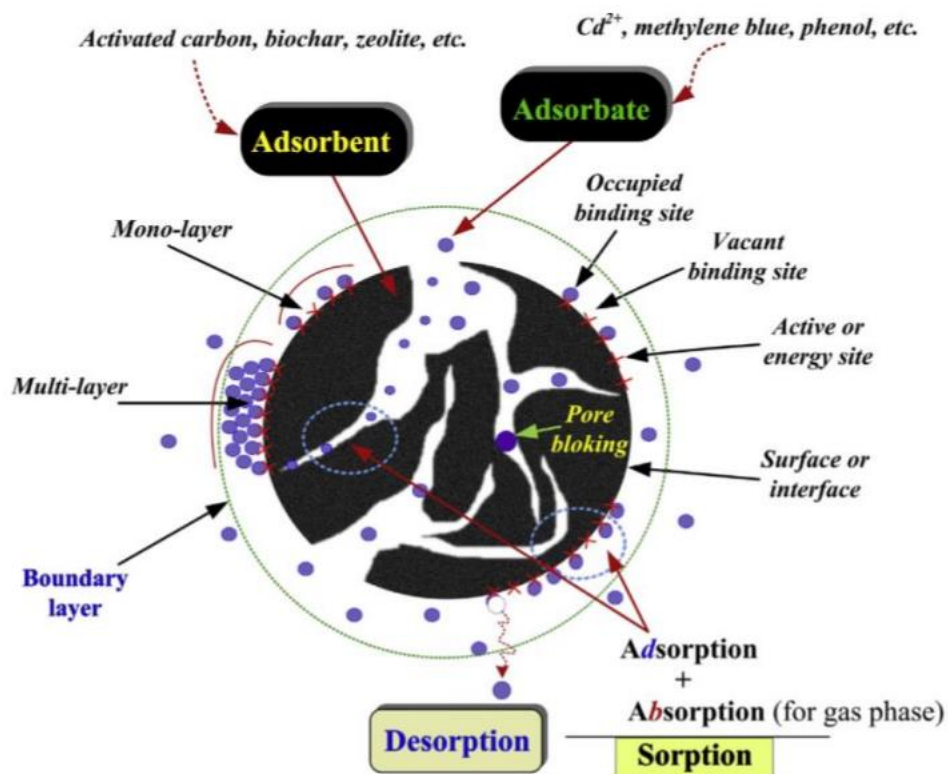
Figure 4: Processes and terminology used in adsorption (adapted from Babalola, 2018)

Physical adsorption, also known as vander Walls adsorption, is the result of the vander Waals force of interaction. The heat in this form of adsorption is on the range of 20 to 40 kJ/mol (Aryal *et al.* 2011). The physical adsorption process is reversible and quick to initiate. Monolayer adsorption and multilayer adsorption are the two forms of physical adsorption. Multilayer adsorption might occur in the adsorbent and be readily disrupted as the temperature rises. In chemisorption, the adsorbate and the adsorbent surface interact chemically and electrostatically. The heat of adsorption in this technique normally varies from 40 to 400 kJ/mol (Aryal *et al.* 2011). It is known as activated adsorption because it has relatively high activation energy. Chemical adsorption involves either electron transfer or sharing, or the formation of chemical bonds between molecules.

Physical adsorption is a reversible process that takes place below or near the critical temperature of the material being adsorbed. On the other hand, chemisorption is an irreversible process because of the potent electrostatic attraction between the adsorbent and the adsorbate. Physical adsorption works well, especially when the temperature is near the fluid's critical temperature. Unlike physical adsorption,

14

chemisorption only takes place on a specific solid surface for a given fluid and happens at temperatures substantially higher than the critical temperature. Adsorption in a monolayer is the outcome of chemisorption. Physical adsorption is an exothermic process because it is followed by a drop in the free energy and entropy of the adsorption system. If conditions were met, both types of adsorptions might happen at once or in succession (Grassi *et al.*, 2012). The term "sorption" is occasionally used to describe the process since it can be difficult to discern whether adsorption is brought on by chemical or physical causes.

The three steps of the adsorption process are typically (a) the transfer of the pollutant from the bulk solution to the sorbent surface, (b) diffusion from the external surface into the pores of the adsorbents, and (c) adsorption between the adsorbate and the active sites of the adsorbent (Elwakeel *et al.*, 2020). As seen in **Figure 5**, interactions between pollutants and adsorbent surfaces frequently may occur through surface complexation, precipitation, ion exchange, electrostatic attraction, and physical adsorption.
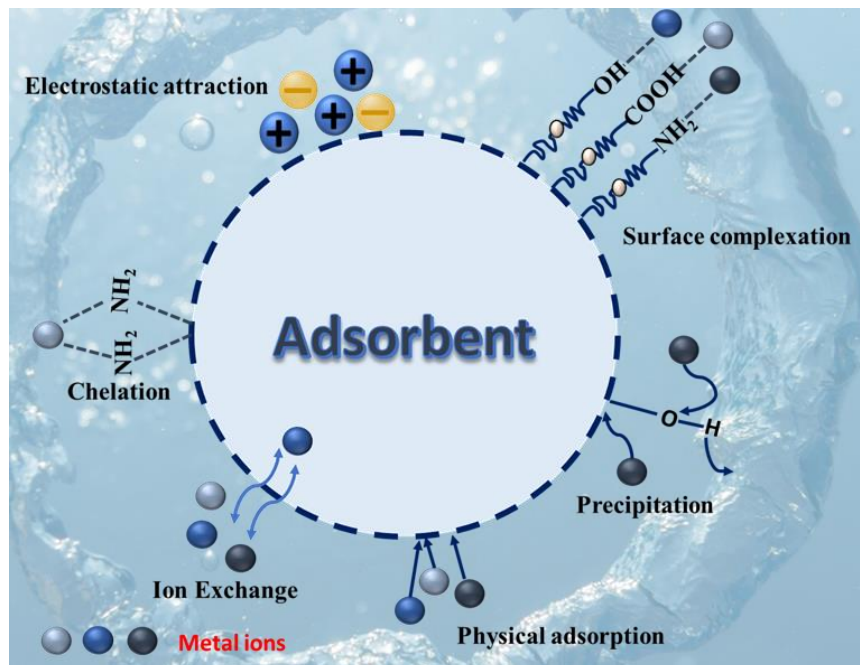
Figure 5: Various mechanisms occurring in the adsorption process

Most methods, however, have several drawbacks, including high costs, inadequate metal elimination, the production and dumping of hazardous metal sludge, and the inability to treat water with even trace amounts of arsenic (Sharma & Shon, 2009). The best method for removing trace levels of contaminants is adsorption (Mohan &

Pittman, 2007; Aryal *et. al.*, 2011). Activated carbon is frequently used as an adsorbent in adsorption, although it is quite costly, non-selective, and not usually widely accessible in significant quantities (Chuang *et. al.*, 2005).

Biosorption is a type of adsorption that uses biological substances like plant wastes or microbes (Sarma *et al.*, 2015). The confiscation of metallic and non-metallic species and particles from solution by biomaterials is known as biosorption. Sorbents of biological origin (biomasses) can impound pollutants, lowering the concentration of contaminants in aqueous solutions significantly (Wang & Chen, 2009). Some of the key benefits of biosorption over other traditional treatment methods are the low cost, high efficiency, wide selectivity in heavy metals uptake, wide availability of biosorbents, the low production of toxic sludge, the viability of recovering heavy metals by desorption, and the potential for renewing biosorbents. Utilizing waste materials to create affordable sorbents helps to reduce and reuse created garbage (Ali *et al.*, 2012; Ding *et al.*, 2012; Won *et al.*, 2014).

1.6 Adsorption studies

Batch and column operations are often used to assess adsorbent performance in adsorption systems. Batch methods are commonly used to assess the capability of a substance to adsorb as well as the sorption capacity of the adsorbent. Batch methods seldom yield data that can be effectively used in industrial and domestic systems since they are often limited to laboratory size. On the other hand, column operations provide data that may be helpful in both industrial and domestic systems (Maji *et al.*, 2007; Ranjan *et al.*, 2009).

1.6.1 Batch adsorption studies

In a small conical flask or centrifuging tube, a fixed mass of adsorbent and a fixed volume of an adsorbate solution with a known concentration and controlled pH are mixed using the batch technique.

A mechanical shaker/centrifuging machine is used to shake/centrifuge the flask/tube at room temperature for a set amount of time. The adsorbate solution is separated, and the equilibrium concentration after adsorption is measured. The adsorption process is influenced by several factors, including the pH of the adsorbate solution, the

biosorbent dosage, agitation duration, initial concentration of adsorbate, and temperature. By altering one parameter while leaving the other parameter constant, the influence of each parameter may be investigated. The equilibrium adsorption capacity (q_e) of adsorbent for adsorbate is evaluated by utilizing **Equation 1.1** (Ghimire et. al., 2002). The % adsorption (% A) of adsorbate was evaluated by applying **Equation 1.2**.

$$q_e = \frac{(C_o - C_e)\ V}{m} \qquad\qquad (1.1)$$

$$\%\ A = \frac{(C_o - C_e)}{C_o} \times 100 \qquad\qquad (1.2)$$

where q_e is the equilibrium sorption capacity (mg/g), C_0 and C_e are the primary and final adsorbate concentrations (mg/L), respectively, V is the amount of adsorbate solution (mL), and m is the mass of adsorbent in gram.

1.7 Variables influencing the adsorption of metallic or non-metallic ions

The degree of adsorption effectiveness may be influenced by several variables, including pH, contact duration, the kind of adsorbent and adsorbate ions, concentrations of the adsorbent and adsorbate ions, temperature, and the presence of co-existing ions.

1.7.1 The pH of the adsorbate solution

The pH of the solution is significant because it influences the aqueous chemistry of adsorbate ions, as well as the action of the external functional groups of biosorbent (Vijayaraghavan & Yun, 2008). The speciation and sorption availability of metallic and non-metallic ions are substantially influenced by pH. Because of the rise in negatively charged surface groups, the biosorption ability of metal cations enhances with rising pH, although this is not a linear relationship (Wang and Chen, 2009). A higher pH results in less H^+ ion presence and more active functional group sites that are free and exposed (negative charge), which enhances adsorption by luring metal cations. On the other hand, the biosorption capacity of metal and non-metal anions improves as pH decreases because the positively charged surface functional groups of biosorbents are increasing (Aryal *et al.*, 2010). The total surface charge on the biosorbent became positive at low pH (very acidic pH), and the presence of

hydronium ions prevents metal cations from accessing surface functional groups via repulsive forces. At elevated pH levels in the solution, the metallic ions may precipitate and form hydroxides, obstructing the biosorption process (Vijayaraghavan & Yun, 2008).To comprehend how pH impacts biosorption, it is crucial to understand the point of zero charges (pH_{PZC}). The pH_{PZC} denotes an adsorbent with a pH of zero net surface charge. The colloidal system displays zero zeta potential at pH_{pzc}, which means that the particles stay stationary in an electric field. When the pH of the biosorbent surface is above its pH_{pzc}, the adsorbent surface is negatively charged attracting metal cations and repelling metal/nonmetal anions. Conversely, the adsorbent surface is positively charged and attracts anions while rejecting cations below pH_{pzc} (Sherlala *et al.*, 2018).

There is an ideal pH value for each metal ion at which maximal adsorption of that ion occurs. For cationic metals, this pH occurs in the basic region; for anionic metals and non-metals, it occurs in an exceptional instance at low pH levels (Uysal & Ar, 2007). the optimal pH for various metal and non-metal ions removal by different adsorbents should be varied (Liu *et al.*, 2019), due to differences in metal electronegativity and standard reduction potential (Peng *et al.*, 2017).

1.7.2 Specific surface area of biosorbent

The biosorption of metallic or non-metallic pollutants is closely correlated with the specific surface area of biomass. By dividing biomass into smaller pieces or converting it to a finer powder form, the surface area can be increased. A higher number of surface binding sites will be exposed due to the increased surface area of biomass, boosting biosorption and shortening the contact time (Vijayaraghavan & Yun, 2008).

1.7.3 Bisorbent dose

The Biosorption of heavy metallic or non-metallic ions is influenced by the biosorbent dose utilized in the sorption medium, and the dose has a significant impact on the extent of biosorption (Aryal *et al.*, 2011). The biosorbent dose is usually expressed in the amount of biosorbent in grams added per liter of the adsorbate solution. The % removal of metal and non-metal ions during adsorption increases with the increase of biosorbent dose while that of the equilibrium biosorption capacity is decreased. This

is because of the rise in the number of binding sites. On the other hand, a reduction in biosorption capacity with increased biosorbent dosage might be owing to the biosorption medium's significant constraints on ionic species mobility, resulting in the unsaturation of certain attaching sites in the biosorption process (Tangaromsuk *et al.*, 2002).

1.7.4 Initial concentration of adsorbate ions

The initial metal/non-metal ion concentration plays a vital role in the biosorption process. If the amount of biomass is kept constant, the biosorption capacity of biosorbent for metal or non-metal ions will rise when the initial concentration is increased. In general, raising the initial concentration of metal/non-metal ions increases adsorption capacity by increasing the concentration gradient between the adsorbent and solution; however, this is only true before equilibrium is reached (Sherlala *et al.*, 2018). It is obvious that increasing adsorbate ion concentrations increase sorbed ions per unit mass of biosorbent since the initial adsorbate concentration provides the necessary energy to overcome the resistance to adsorbate ion mass transfer between the aqueous and solid phases (Dursun, 2006). The biosorption capacity may increase with concentration due to improved interactions between adsorbate (metal and non-metal ions) and the surface of the biomass.

1.7.5 Effect of temperature

The temperature of the biosorption medium is one of the factors that have a major impact on the biosorption of metal or non-metal ions. Whether a process is exothermic or endothermic will determine this. Temperature affects the kinetic process by varying the contact of the adsorbate ions with the solid surface as well as solubility. As a result of increased surface activity and the kinetic energy of the solute at higher temperatures, the biosorption of metallic or non-metallic ions often increases, leading to an effective collision of these ions with biomass species (Khambhaty *et al.*, 2009). At higher temperatures, however, certain binding sites may be physically damaged (Padmavathy, 2008). Since ambient conditions at room temperature are widely favored for practical applications, conducting biosorption in this setting is always recommended (Vijayaraghavan & Yun, 2008).

1.7.6 Effect of competitive ions

Natural water comprises several competitive ions that might compete with the adsorbate for a limited number of active sorption sites, affecting the sorption capacity of the biosorbent. Interfering co-ions are commonly found in industrial as well as natural water, and their occurrence in water is likely to result in interference and competition for adsorption sites. Biosorption of metallic or non-metallic ions can be optimized if the influence of co-ions or competing ions is fully understood (Aryal & Liakopoulou-Kyriakides, 2011). Typically, contaminated water comprises a variety of ionic components, such as metal and non-metal ions. The existence of competitive ions may increase or decrease the biosorption capacity of biosorbent because of the enhanced number of surface binding sites resulting from co-existing ion sorption or competing processes on surface binding sites of biosorbent (Mohan and Pittman, 2007). The concentration of co-existing ions influences the electrostatic interaction which influences particle aggregation.

1.8 Selection of metallic/non-metallic ions for the biosorption

Heavy metals comprise radionuclides, precious metals, and toxic metals. Environmental concerns make it important to remove toxic heavy metal ions and radionuclides from polluted water. The health of people and aquatic ecosystems is negatively impacted by excesses of various non-metals including phosphorous (as phosphate ions), fluorine (as fluoride ion), and nitrogen (as ammonium and nitrate ions). Therefore, it is necessary to consider the removal of such metallic and non-metallic ions from contaminated water.

1.9 Kinetics of biosorption

The biosorption kinetic studies are very useful in determining the biosorption rate, and the time needed to reach biosorption equilibrium. Kinetic studies are carried out to determine the rate-limiting step and biosorption mechanisms like mass transfer, diffusion, and chemical reaction. A variety of mathematical models have been used in the literature to investigate kinetic studies. In this study, the fitness of experimental kinetic data of target metal or non-metal removal by biosorbent was examined utilizing three common kinetic models namely, pseudo-first-order (PFO), pseudo-second-order (PSO), and Webber-morris intra-particle diffusion model. These kinetic

models may examine whether the biosorption process comprises physisorption or chemisorption.

1.9.1 Pseudo-first order (PFO) kinetics

Possibly the first empirical model to represent the rate of adsorption of the solid-liquid interface is the PFO equation, commonly referred to as the Lagergren equation (Eris & Azizian, 2017). The PFO rate equation (Lagergren, 1898) explains the rate of adsorption based on the adsorption capacity of the adsorbent. It assumes that the rate of occupying sorption sites is proportional to the number of unoccupied sites (Iqbal *et al.*, 2009). The non-linear form of the model is denoted as **Equation 1.3**:

$$q_t = q_e \left(1 - e^{-k1t}\right) \tag{1.3}$$

This non-linear equation is modified to give the linear forms as **Equation 1.4** (Tran et. al., 2017).

$$\log (q_e - q_t) = \log q_e - \frac{k_1}{2.303}\, t \tag{1.4}$$

where q_e and q_t in mg g^{-1} are the biosorption capacity at equilibrium and at time t, correspondingly, and k_1, (min^{-1}) is the rate constants of PFO kinetic. A straight line is obtained by plotting $\log (q_e - q_t)$ versus t with a negative slope equal to $K_1/2.303$ and intercept equal to $\log q_e$. The slope and intercept yield the values of k_1 and q_e, respectively.

1.9.2 Pseudo-second order (PSO) kinetics

The PSO kinetic model also relies on the sorption capability of the adsorbent. It is predicated on the notion that the adsorption rate is related to the square of the number of vacant sites (Ho & McKay, 1999). Two presumptions form the basis of this approach. The first presumption is that two reactions will happen concurrently throughout the adsorption process, and the second is that one reaction will happen quicker and achieve equilibrium more rapidly than the other while the adsorption process is still ongoing. The non-linear version of the equation is represented as:

$$q_t = \frac{q_e^2 k_2 t}{1 + q_e k_2 t} \tag{1.5}$$

This non-linear equation is restructured to get the linear forms as **Equation 1.6**.

$$\frac{t}{q_t} = \frac{1}{k_2 q_e^2} + \frac{1}{q_e} t \qquad\qquad (1.6)$$

where k_2 (g/mg. min) is the PSO kinetics rate constant. A straight line can be obtained by plotting t/q_t versus t. The value of k_2 and q_e can be evaluated from the slope and intercept respectively. It should be obvious that only when the adsorbate concentration fluctuates considerably can the PSO equation be used (Eris & Azizian, 2017). The adsorption is seen to be a chemical process in this paradigm, and it happens when the adsorbent and the adsorbate share or exchange electrons.

1.9.3 Webber-Morris intra-particle diffusion model

The Weber and Morris model was used to examine the kinetics data to clarify the diffusion mechanism and rate-limiting stage in the biosorption process.
 (Weber & Morris, 1963) (**Equation 1.7**).

$$q_t = k_{2,i\,W\&B}\, t^{0.5} + c \qquad\qquad (1.7)$$

where q_t is the quantity of adsorbate adsorbed (mg/g) at time t (min), $k_{2,iW\&B}$ (mg g^{-1} min$^{-0.5}$) is the Weber Morris rate constant, and c (mg g^{-1}) is the intercept of the intraparticle diffusion equation, which provides information on the thickness of the boundary layer (Moreira et. al., 2019). Film diffusion, intraparticle diffusion, and biosorption were generally thought to be the three consecutive steps that make up the biosorption process. First, it involved the external mass transfer of metal or non-metal ions through the boundary layer to the external surface of the biosorbent. Second, it involved intraparticle diffusion, in which the metal or non-metal ions diffused through the pores of the biosorbent from the exterior surface to the internal surface. Last, the biosorption of adsorbate ions onto the binding sites of the biosorbent was then performed until equilibrium was reached (Michalak *et al.*, 2013).

The slope of the linear plot of q_t versus $t^{0.5}$ may be used to get the $k_{2,i\,W\&B}$. The greater the 'c', the more the contribution of the surface sorption in the rate-limiting step. When the plot of q_t vs $t^{0.5}$ is linear and crosses the origin, then intraparticle diffusion is the only rate-controlling step. When the plots do not pass through the origin, this further demonstrates that intraparticle diffusion is not the only rate-limiting step, but those other kinetic models may also affect the rate of biosorption. The boundary layer effect is suggested by the plot's intercept. The stronger impact of surface biosorption

on the rate-controlling step is shown by the greater value of the intercept (Weber and Morris, 1963).

1.9.4 Boyd kinetic model

Boyd's equation (Boyd *et al.*, 1947) may be used to assess the kinetic results, which can be represented as.

$$F = 1 - \frac{6}{p^2} \cdot \exp(-B_t) \qquad (1.8)$$

Where B represents the Boyd constant and F represents the fractional achievement of equilibrium. F can be represented as follows at time t.

$$F = \frac{q_t}{q_e} \qquad (1.9)$$

Where q_e and q_t are, respectively, the adsorption capacity (mg/g) at equilibrium and time t. The following kinetic expression results from substituting the value of F in Equation (1.10).

$$Bt = -0.4977 - \ln\left(1 - \frac{q_t}{q_e}\right) \qquad (1.10)$$

To get the values of Bt at various starting solute concentrations, utilize equation (1.10). The relationship between the computed Bt values and time (t) indicates whether the rate of the biosorption process is externally-transport-controlled (film diffusion) or interparticle-transport-controlled.

1.10 Adsorption Isotherms

The relation between the equilibrium concentration of adsorbate in solution at constant temperature (C_e) and the quantity of adsorbate per unit mass of adsorbent q_e (mg/g) is known as the adsorption isotherm. It stands for the equilibrium relationship that describes how the adsorbent's surface interacts with the adsorbate ions. The quantity of adsorbate that is attached to the surface of the adsorbent is represented graphically by the adsorption isotherm. The phenomena controlling either the retention or mobility of material from aqueous media to a solid phase at constant temperature and pH are depicted in the graph (Foo & Hameed, 2010). Sorption equilibrium happens when an adsorbate in any phase encounters the adsorbent for a sufficient period. When the adsorption process approaches equilibrium, the isotherm parameters give qualitative details on the nature of the adsorbate-adsorbent interaction

as well as the correlation between the concentration of adsorbate and its degree of accumulation onto adsorbent surfaces. They also explain the biosorption mechanism and indicate surface properties and affinities of binding sites of biosorbents. To explain the adsorption process, several adsorption isotherms models have been constructed. In this study, the Langmuir and Freundlich isotherm models were used to simulate the biosorption of metallic or non-metallic ions onto biosorbent surfaces.

1.10.1 Langmuir adsorption isotherm

According to the Langmuir isotherm model, monolayer adsorption takes place on a homogeneous surface with identically affine and energetic binding sites without interaction between adsorbents (Langmuir, 1916). The maximal biosorption capacity (q_{max}), which corresponded to a total monolayer coverage on the surface of the biosorbent, is the most significant parameter that could be derived from this model. As a result, the model views the adsorption process as a chemisorption (Wang & Guo, 2020; Al-Ghouti & Da'ana, 2020). The Langmuir model is described by **Equation (1.11)**.

$$q_e = \frac{q_m b C_e}{1 + b C_e} \qquad (1.11)$$

It can be expressed linearly according to **Equation (1.12)** as:

$$\frac{C_e}{q_e} = \frac{1}{q_m\, b} + \frac{C_e}{q_m} \qquad (1.12)$$

where q_e and q_m (mg/g), respectively, represent the equilibrium and maximum adsorption capacity corresponding to full monolayer coverage, and b (L/mg) represents the Langmuir equilibrium constant related to adsorption energy (Langmuir, 1918). The slope and intercept of a plot of C_e/q_e vs C_e are used to determine the values of q_m and b.

Additionally, **Equation 1.13** was used to establish the dimensionless separation factor (R_L), which was used to clarify the key aspects of the Langmuir model (Hall *et al.*, 1966); (Wang & Guo, 2020)**:**

$$R_L = \frac{1}{1 + (b C_o)} \qquad (1.13)$$

The Langmuir model is implied by the R_L value, where $R_L = 1$ denotes a linear biosorption isotherm, $R_L > 1$ denotes unfavorable biosorption, $0 < R_L < 1$ denotes favorable biosorption, and $R_L = 0$ denotes irreversible biosorption (Al-Ghouti & Da'ana, 2020).

1.10.2 Freundlich adsorption isotherm

This model assumed that the biosorption took place on the heterogeneous surface of the biosorbent with the interaction between multilayer adsorption of adsorbate (Freundlich, 1907; Wang & Guo, 2020; Al-Ghouti & Da'ana, 2020). **Equation 1.14** describes the Freundlich model.

$$q_e = K_F (C_e)^{1/n} \qquad (1.14)$$

Equation 1.15 allows it to be represented in the linear form as:

$$\log q_e = \log K_F + \left(\frac{1}{n}\right) \log C_e \qquad (1.15)$$

where K_F $[(mg/g)(L/g)^{1/n}]$ denotes the Freundlich constant related to biosorption capacity and $1/n$ denotes the dimensionless heterogeneity factor related to the biosorption intensity. A graph of $\log q_e$ *vs* $\log C_e$ is plotted and the value of $1/n$ and K_F are calculated.

1.11 Adsorption thermodynamics

Estimating the entire heat and energies involved with biosorption processes is made easier by using the fundamental thermodynamic properties of the adsorption system. Standard Gibbs free energy change (ΔG^o) and standard entropy change (ΔS^o) are both considered in environmental engineering practice to ascertain the spontaneity of the process. The degree of spontaneity in the biosorption process is indicated by the standard Gibbs free energy change (ΔG^o). The adsorption process occurs spontaneously if the Gibbs free energy changes the adsorption from a non-equilibrium to an equilibrium state at constant pressure and the temperature has a negative value ($\Delta G^o < 0$). The isotherm constants and experimental data at various temperatures were used to compute the parameters ΔG^0, ΔH^0, and ΔS^0. Using **Equation 1.16**, the values of ΔG^0 (kJ/mol) for the adsorption process were determined.

$$\Delta G^o = -RT \ln K_C \qquad (1.16)$$

where T denotes temperature (K), K_C denotes thermodynamic equilibrium constant (dimensionless), and R denotes universal gas constant (dimensionless). Using the result of the experiment's measurement of the Langmuir constant (b), the value of K_C related to biosorption was assessed. **Equation 1.17** may be used to easily take the K_C into account as a dimensionless parameter when a biosorption experiment is conducted in water and b has units of L/mg (Tran et. al., 2017; Xu et. al., 2021; Poudel *et al.*, 2021).

$$K_C = b \times 55.5 \times 1000 \times M_w \qquad (1.17)$$

where M_w is the molar mass of arsenic. Up to -20 kJ/mol, ΔG^o value is compatible with physical adsorption (physisorption), but ΔG^o values beyond -40 kJ/mol indicate chemical adsorption (chemisorption).

Equation 1.18 shows that for a certain temperature, ΔG^0 is also related to the ΔH^0 and ΔS^0 by thermodynamics.

$$\Delta G^o = \Delta H^o - T\Delta S^o \qquad (1.18)$$

The following equation is produced when Eq. (1.16) is substituted into Eq. (1.18).

$$\ln K_C = -\frac{\Delta H^o}{RT} + \frac{\Delta S^o}{R} \qquad (1.19)$$

The van't Hoff equation **(Equation 1.19)** may be used to determine how temperature affects adsorption equilibrium. Calculating ΔH^o and ΔS^o from a van't Hoff plot of ln K_C *vs* 1/T yields a straight line. The magnitude of ΔH^o also reveals the nature of biosorption, which might be physical or chemical. The ΔH^o values between 2.1 and 20.9 kJ/mol correlate to physisorption, in contrast, values between 20.9 and 418.4 kJ/mol prefer the chemisorptions. Entropy change (ΔS^o) values that are positive or negative indicate a rise or reduction in randomness at the solid/solution interface when a metallic or non-metallic ion is sorbed onto biosorbents.

1.12 Column adsorption studies

For an industrial application or real wastewater treatment, adsorption in a fixed-bed column packed with adsorbent is preferable (Paudyal *et al.*, 2013; Roy *et al.*, 2013;

Singh & Pant, 2006). Thus, experimental results acquired from the laboratory scale fixed-bed column are supportive for scheming an adsorption column for industrial applications. Tests for fixed-bed column adsorption were performed in a glass column with a predetermined inner diameter and height (see **Figure 6**). Before packing the adsorbent into the column, it is first soaked with DI water. Following that, the wet adsorbent is packed into a column.
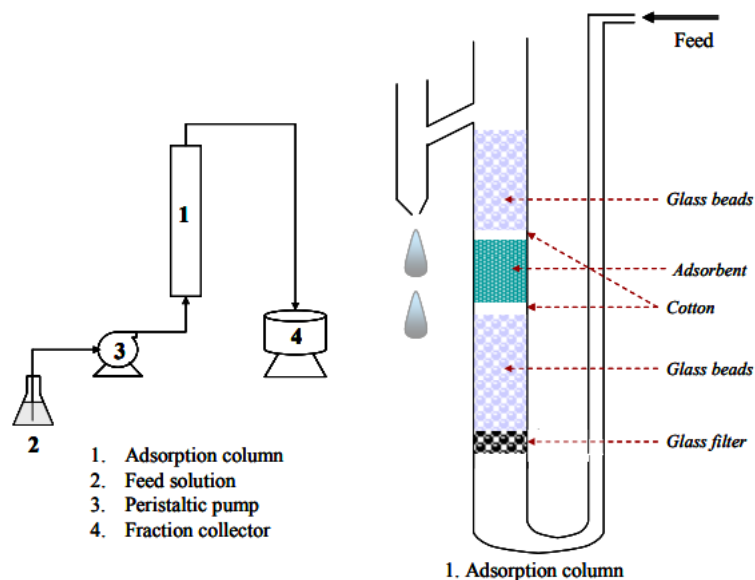
Figure 6: Schematic diagram for the column experiments (Figure adapted with permission from Biswas *et al.*, 2008a, Copyright, Elsevier)

The column is first filled with glass beads, then a layer of cotton, and finally wet absorbent. Once more, a cotton layer is packed into the remaining space of the column before glass beads. Glass beads or cotton wool can provide equal inlet flow, reduce adsorbent loss, and maintain the column's proper liquid distribution. During the continuous flow, the glass bead acts as a support and stops the adsorbent from floating. Before the sorption test, the column is conditioned by passing DI water for 5 h at the same pH as the test solution. The controller (peristaltic pump) is used to control the flow rate of the sample solution through the column. The effluent samples for the measurement were collected at each regular interval with the help of a fraction collector. Fresh adsorbents quickly adsorb the adsorbate during the early phases of column operations because there are a lot of accessible adsorption sites. Due to the adsorbent's decreasing efficiency as the effluent flows continuously, the adsorbate is slowly adsorbed. Eventually, the column reaches saturation, and no further adsorption

can take place (Patel, 2019). The column adsorption tests are performed to confirm how well the adsorbent performs at varying flow rates, initial adsorbate concentrations, and bed heights.

1.12.1 Analysis of breakthrough curve parameters

Examining the breakthrough curve is crucial for determining how well a column performs. Evaluating the parameters of the breakthrough curve can do this. The curve reveals the column's capacity to remove adsorbate ions from a fixed bed. It is given as a ratio of adsorbate concentration (mg/L) in the effluent and the intake, C_e/C_i, as a function of time (min) after flow began. **Equation 1.20** provides the total quantity of adsorbate ion sorbed onto the packed column, q_{total} (mg), and the dynamic biosorption capacity, q_e (mg/g) (Paudyal *et al.*, 2013; Sharma & Singh, 2013).

$$q_{total} = \frac{QA}{1000} = \frac{Q}{1000} \int_{t=0}^{t=total} C_{ads}\, dt \qquad (1.20)$$

$$q_e = \frac{q_{total}}{M} \qquad (1.21)$$

where t_{total}, Q, A, M, and C_{ads} stand for, respectively, the total flow period (min) for the column to reach exhaustion, volumetric flow rate (mL/min), area under the breakthrough curve, the quantity of biosorbent packed in the column (g), the difference in the initial and the effluent adsorbate concentration at time t caused by biosorption (mg/L).

Equation 1.22 may be used to determine the mass transfer zone (MTZ), which is calculated as the length of the biosorption zone (cm) in the column (Bulgariu & Bulgariu, 2013):

$$MTZ = Z\, \frac{(t_E - t_B)}{t_E} \qquad (1.22)$$

where Z denotes the height of the bed (cm); t_B denotes the breakthrough time (min), and t_E is the exhaustion duration (min).

1.12.2 The breakthrough curve modeling

For the proper design and optimization of the column for the adsorption process system, the breakthrough curve must be predicted. For this, several mathematical models have been put out. Three mathematical models, namely the Yoon-Nelson model, the Thomas model, the Adams-Bohart model, and the BDST model, were used in this work to examine the dynamic adsorption performance of the adsorbent.

1.12.2.1 Adams-Bohart model

This model presupposes that equilibrium is not instantaneous also that external mass transfer regulates the adsorption rate (Quintelas *et al.*, 2013). For analyzing the first portion of the breakthrough curve ($C_e/C_i = 0$ to 0.5) this model is suitable (Sharma & Singh, 2013). The following **Equation 1.23** is a representation of this model:

$$\ln\left(\frac{C_e}{C_i}\right) = K_{AB}\,C_i t - K_{AB}N_0\,\frac{Z}{U_0} \qquad (1.23)$$

where C_i and C_e (mg/L) represent the influent and effluent adsorbate concentration, K_{AB} (L/mg.min) denotes the kinetic constant, N_0 (mg/L) represents the biosorption capacity of the biosorbent per unit volume of the bed, Z (cm) represents the bed depth, U_0 (cm/min) represents the linear velocity, that is evaluated by dividing the flow rate (cm^3 /min) by the column section area (cm^2). This model can be assessed from the linear plot of $\ln(C_e/C_i)$ *vs* t and can be used to estimate the constants K_{AB} and N_0.

1.12.2.2 Thomas model

This model assumes that mass transfer at the interface rather than chemical interactions restrict adsorption, and experimental results exhibit Langmuir isotherms and second-order kinetics (Foo *et al.*, 2013). This is appropriate for illustrating the entire breakthrough curve (Bulgariu & Bulgariu, 2013). The following **Equation 1.24** may be used to express the Thomas model in linear form (Paudyal *et al.*, 2013):

$$\ln\left(\frac{C_i}{C_e} - 1\right) = k_{TH}\frac{q_0 M}{Q} - k_{TH}C_i t \qquad (1.24)$$

where k_{Th} denotes Thomas rate constant (mL/min.mg), qe represents the equilibrium biosorption capacity (mg/g), M represents the mass of biosorbent (g), and Q denotes

the feed rate (mL/min). The linear plot of ln (C_i/C_e − 1) vs t allowed for the evaluation of the values k_{Th} and q_e.

1.12.2.3 Yoon-Nelson model

This model presumes that the probability of biosorption for each adsorbate ion decreases at a rate that is proportionate to its probability of both biosorption and breakthrough of biosorbent from the biosorbent (Mthombeni *et al.*, 2018). In the later phases of the breakthrough curve, the Yoon-Nelson model, like the Thomas model, may reduce the shortcomings of the Adams-Bohart model. The Yoon-Nelson model's linear expression is presented by the following **Equation 1.25** (Sharma & Singh, 2013):

$$\ln\left(\frac{C_e}{C_i - C_e}\right) = k_{YN} - \tau k_{YN} \qquad (1.25)$$

where τ denotes the amount of time required for a 50% adsorbate breakthrough in minutes and k_{YN} denotes the Yoon-Nelson rate constant (min^{-1}).

1.10.2.4 Bed depth service time (BDST) model

The BDST model predicts that bed depth and service time will be linearly related for a certain breakthrough concentration. Instead of attempting to predict the whole breakthrough curve, this model predicts the moment at which a certain breakthrough concentration will happen for a particular bed depth and flow rate. Past studies state that this model does a good job of explaining the first 10 to 50% of the breakthrough curve (Jain *et al.*, 2013). **Equation 1.26** provides the linear expression of BDST model (Paudyal *et al.*, 2013):

$$t_B = \frac{N_0 Z}{C_i U_0} - \frac{1}{k_b C_i} \ln\left(\frac{C_i}{C_b} - 1\right) \qquad (1.26)$$

where N_0 is the column adsorption capacity (mg/L), t_B denotes the service period of column (in hours), C_b denotes the outflow concentration at breakthrough point (mg/L), and k_b denotes the rate constant [L/(mg.h)]. The BDST parameters, N_0, and k_b, are computed from the time versus bed depth graphs.

1.13 Pomegranate peel, its composition, and possible applications

A little tree that may grow to a height of 5-8 m, the pomegranate (*Punica granatum L.*) is mostly farmed on the Iranian Plateau, the Himalayas in northern India, North Pakistan, Azerbaijan, Afghanistan, the Mediterranean region, and Russia (shown in **Figure 7(a)**). The scientific classification of pomegranate is shown in **Table 2**.

Table 2: Scientific classification of pomegranate (Melgarejo *et al.*, 2020).

Kingdom:	Plantae
Division/Phylum:	Magnoliophyta
Class:	Magnoliopsida
Subclass:	Rosidae
Order:	Myrtales
Family:	Punicaceae
Genus:	Punica
Species:	*granatum*
Binomial name:	*Punica granatum*

Different parts of a tree, including leaves, blossoms, barks, fruits, and seeds, have been used to treat illnesses (Pathak *et al.*, 2016). Its delicious flavor, excellent nutritional content, and numerous medical benefits make it one of the most well-liked fruits in the world. The nations with the most pomegranate production are India, Iran, and China (Hernández *et al.*, 2012). Pomegranate fruits are normally eaten fresh or as processed products as juice, jams, wine, and sauce for salad. Pomegranate peel (PP), which can make up to 30% of the weight of the fruit, is typically thrown as a waste residue and is easily available for free or very little cost (Ben-Ali, 2021). The food processing and agricultural sectors create massive quantities of fruit peels, which are then either composted or discarded on public lands or bodies of water, creating an environmental risk. Fruit peels are cheap and widely available, so using them to make value-added products is a novel way to use them sustainably. Gallic acid and ellagic acid are two significant hydroxybenzoic acids found in pomegranate peel. Additionally, it includes flavone derivatives and hydroxycinnamic acids. These tannins, which may be used as an anti-inflammatory, antibacterial, and antioxidant therapy, make up much of the pomegranate peel (Lansky & Newman, 2007; Saad *et al.*, 2012; Xi *et al.*, 2017). These benefits of the pomegranate peel's components can

be exploited for therapeutic (Hasnaoui *et al.*, 2014), dyeing (Ajmal *et al.*, 2014), and adhesive uses (Saad *et al.*, 2015). Unstudied pomegranate peel has the potential to be a highly effective biosorbent for removing hazardous contaminants from water. It is possible to properly recycle pomegranate peel to make inexpensive biosorbents that efficiently remove pollutants without causing the creation of any secondary pollutants. It may be converted into biosorbents to remove harmful pollutants, adding economic value to these low-cost biowastes, and offering a sustainable, cost-effective, and environmentally acceptable alternative to the current treatment methods.

Figure 7: Photograph of (a) Pomegranate tree; (b) Pomegranate peels.

Pathak *et al.* (2016) analyzed the composition of Indian pomegranate peel. The chemical analysis exhibited that its main ingredients were C, O, and H. The Indian pomegranate peel composition was 35.96% of C, 58.38% of O, 4.92% of H, 0.65% of N, and 0.09% of S. The findings of the proximate and ultimate analyses of Indian pomegranates are shown in **Table 3** (Pathak *et al.*, 2016).

Table 3: Proximate and ultimate analysis of pomegranate peel

Proximate analysis				Ultimate analysis				
% moisture	% Ash	% volatile matter	% fixed carbon	% C	% O	% H	% N	% S
10.43	3.63	85.68	0.25	35.96	58.38	4.92	0.65	0.09

The pomegranate peel has enough functional groups (e.g. hydroxyl, carboxyl, and carbonyl) due to its predominance of cellulose, pectin, hemicellulose, lignin, and other low molecular weight substances. It is a good source of natural pectin and comprises around 10-15% of pectin (Gavlighi *et al.*, 2018; Yang *et al.*, 2018b). In this research, pomegranate peel was chosen to prepare an adsorbent for its pectin content. Pectin is a naturally occurring carboxylated polysaccharide where pectic acid is

partially esterified by a methyl group (**Figure 8**). It functions as an intracellular and intercellular cementing material. It can bind to several organic and inorganic substances with molecular interactions. Pectin can be easily saponified with lime ((Ca(OH)$_2$) to give calcium pectate (Pangeni *et al.*, 2014). In this work, saponified pomegranate peel (SPP) was used as a Ca-type natural pectin-based cation exchange resin alternative to conventional synthetic cation exchange resins for removing Pb(II) and Cd(II) ions from the aquatic medium. Similarly, for removing anionic pollutants (arsenate, arsenite, and phosphate), anion exchange resins are prepared by loading Zr(IV) ions on saponified pomegranate peels (Poudel *et al.*, 2021) or impregnating TiO$_2$ onto pomegranate peels (Poudel *et al.*, 2020). After Zr(IV) loading, new active sites for anionic species are expected to be formed. In this study, the adsorption of arsenate, arsenite, and phosphate by Zr(IV) loaded saponified pomegranate peel, As(III) adsorption by TiO$_2$ impregnated pomegranate peel, and Pb(II)/Cd(II) adsorption by saponified (lime treated) pomegranate peel were studied in details.
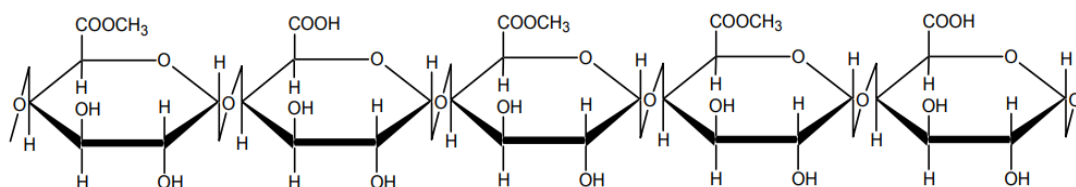
Figure 8: Cellulosic network of pectin

1.14 Rationale of the study

The global community is very concerned about water pollution, but poor nations like Nepal are particularly affected. The surface water and groundwater of Nepal are polluted by both metallic and non-metallic pollutants. Heavy metals (As, Pb, Cd, and Hg) and non-metals represent a major risk to both human health and the environment due to their acute toxicity. The government's major goal is to find cost-effective ways to address the problems, thus academics are being funded to investigate different remediation strategies that will work in Nepal's current economic conditions. Current treatment available technologies have substantial shortcomings, like high capital and operating expenses, the production of hazardous sludge, challenging operation and maintenance, and high energy consumption. Finding a treatment technology that is economically viable, easy to use, effective, and sustainable is, therefore, crucial to safeguard our surface water resources and, ultimately, our health from heavy metal

and non-metal contamination. The pollution of arsenic in Nepal is a significant issue. The problem is most severe in the Western Terai region (near Nawalparasi district), where the level of arsenic contamination in groundwater of shallow wells is approximately 70 times the WHO limit of 10 µg/L (Mueller & Hug, 2018; Shrestha *et al.*, 2014). Industrial effluents of Kathmandu valley are contaminated with several heavy metals. In the metropolitan regions, the Bagmati River's sediments are severely contaminated by untreated municipal wastewater and industrial effluents. The main cause of river pollution is also the high volume of vehicles. Lead, cadmium, arsenic, copper, and zinc are the major contaminants in the Bagmati River (Ghimire *et al.*, 2022; Kayastha, 2015). The degree of phosphate poisoning in the groundwater and surface water of urban areas of Nepal is a severe issue that is now causing eutrophication in lakes and rivers, a reduction in dissolved oxygen, and toxicity to aquatic life.

The proven advantages of the adsorption process over other conventional techniques are nowadays of the greatest importance. Since 1927, activated carbon has been used to adsorb toxic metallic and non-metallic ions from water (Netzer & Hughes, 1984), but its usage in wastewater treatment will be hampered by the high price of commercial activated carbon and its import into Nepal. Nowadays, synthetic ion-exchange resins are widely utilized as adsorbents since activated carbons are non-selective. They also have non-degradable characteristics, as well as the multistep chemical synthesis approach, which not only raises treatment costs but also causes problems in the post-treatment process.

Agricultural waste and/or biomaterials are among those adsorbents that are of the biggest relevance due to their accessibility, low cost, and reasonably high adsorption capacities. In addition, it is more conceivable that such adsorbents will be commercially viable. Using agricultural waste as biosorbents not only removes toxic pollutants at a reduced cost but also achieves the objective of trash reuse and recycling. It will offer an ideal technology for utilizing and converting locally accessible agricultural waste into valuable products that can be commercialized for the purification of water. Additionally, it is fitted well with the Green Chemistry principle of "use of renewable resources" (Srivastava & Goyal, 2010). Agricultural wastes have several characteristics that make them desirable sources for developing

adsorbents. They have an appropriate chemical composition (cellulose, hemicelluloses, pectin, proteins, and lipids) with carboxyl, hydroxyl, carbonyl, and amino acid functional groups. As a result, they can readily be involved in chemical reactions including metal loading, polymerization, and grafting reaction (Xu *et al.*, 2010). It establishes a basis for the synthesis of certain functional polymers from agricultural waste (Benyoucef & Amrani, 2011). A wide variety of agricultural waste and biomaterials have so far been investigated to develop effective and affordable adsorbents. Hitherto, rice husk, seaweed, sugarcane bagasse, charcoal, fungal biomass, yeast biomass, algae, fruit peel, and so forth have been investigated by researchers considering their possibility of being converted as adsorbents. Pomegranate peel is an agricultural by-product generated in juicing factories, which can be modified into a suitable adsorbent for the removal of cationic and anionic pollutants. It was selected as the biosorbent to analyze in this study since it is a typical waste in Nepal.

For the adsorptive sequestration of metallic and non-metallic contaminants from an aqueous medium, modification of biomaterials to acquire the same kinds of functional moiety onto the polymeric chain of biopolymers should be employed instead of synthetic ion-exchange resin. Several attempts to generate comparable functionalized natural ion-exchangers utilizing agricultural wastes are now underway. The galacturonic acid groups found in pectic substances in polysaccharides are effective in remediating cationic pollutants (Pb(II), Cd(II)), contributing to polysaccharide's ion exchange characteristics (Aksu & İşoğlu, 2005; Kartel *et al.*, 1999). In general, pectic and lignocellulosic substances are saponified with alkali, which improves their features such as water retention and swelling, increases their cation binding/exchange capacity, and allows them to be employed successfully for removing Pb(II) and Cd(II). The cation exchange capacity of pomegranate peels was increased due to the addition of additional carboxyl groups to the biopolymer skeleton (Arslanoğlu *et al.*, 2021; Pangeni *et al.*, 2014). In addition, for the removal of oxyanions of arsenic and phosphorous from water, pomegranate peel powder can be modified into anion exchange resins by loading Zr(IV) ions after saponification. The oxygen donor-containing species have a strong electrostatic and coordinative affinity for the Zr(IV) cation. Additionally, Zr(IV) modified biosorbents have the benefit of a low rate of leaching and are safe for human health (Biswas *et al.*, 2008b; Nguyen *et al.*, 2020;

Rahman *et al.*, 2021). This study is a pioneering effort in the field since it makes use of chemically modified pomegranate peels for the biosorption of arsenate, arsenite, phosphate, Pb(II), and Cd(II). Additionally, to the best of my knowledge, no studies have been conducted on the use of SPP as a cation exchanger for removing Pb (II) and Cd (II), PP@TiO2 as an efficient biosorbent for removing As(III), and SPP@Zr as an anion exchanger for removing oxyanions of arsenic and phosphorous.

The functionalization of biopolymers from pomegranate peels achieves similar types of functional moieties on the polymeric chain that can be used as an alternative material to synthetic ion-exchange resins for removing charged contaminants from water.

1.15 Objectives

1.15.1 General objectives

The general objective of the present study is the preparation and characterization of natural ion-exchangers from pomegranate peels as alternative materials to replace synthetic ion-exchangers and evaluation of their viability for the removal of some toxic metallic ions (As(V), As(III), Pb(II), and Cd(II)), and non-metallic ion (phosphate ions) from water

1.15.2 Specific objectives

The specific objectives of the current research are:

1. Preparation and characterization of saponified pomegranate peel loaded with zirconium (SPP@Zr) as an anion exchanger and investigation of its selectivity for the removal of oxyanions of arsenic (arsenate and arsenite) and phosphorous (phosphate) from water
2. Preparation and characterization of pomegranate peel impregnated with TiO_2 (PP@TiO_2) as a low-cost biosorbent, and evaluation evaluation of its biosorption performance for As (III) from water.
3. Preparation and characterization of saponified pomegranate peel (SPP) as a cation exchanger and investigation of its biosorption performance for Pb(II) and Cd(II) ions from water.

4. Elucidation of the influence of operational parameters (pH, contact time, concentration of adsorbate ions, temperature, and coexisting ions) for removing targeted cationic or anionic pollutants.

5. Investigation of mathematical models (kinetics, isotherms, and thermodynamics) and adsorption mechanisms of the studied biosorption processes.

6. Evaluation of the desorption of pollutants and recyclability of exhausted biosorbent.

7. Application of the prepared ion exchanger to natural water samples collected from a contaminated area.

CHAPTER 2

LITERATURE REVIEW

2.1 Agro-wastes as biosorbents

New biosorbents must be developed to remove metallic and non-metallic contaminants from wastewater. There are numerous commercial biosorbents for biosorption, including activated carbon and chelating ion exchange resins, however, their costs are frequently high, and they have disposal issues. As researchers continued their quest for less expensive biosorbents, they largely concentrated on the utilization of cheap biosorbents made from industrial by-products, agro-wastes, and other naturally occurring materials for removing metallic and non-metallic contaminants from water. The use of low-cost biosorbents in the biosorption process is being researched and is thought to be a novel method for treating wastewater. The use of agro-wastes in wastewater treatment acts as a replacement for conventional biosorbents and is an effective, environmentally friendly, affordable, and simple way for removing metals and non-metals from wastewater.

In order to produce a favorable chelating environment for removing arsenic, Ghimire *et al.* (2002) explored the utilization of orange juice residue that had been changed through phosphorylation and then loaded with Fe(III). The metal loaded biosorbent was used in batch-wise and column-based arsenic removal studies. As(III) biosorption was favored under alkaline conditions while As(V) at acidic conditions. For As(V) and As(III), correspondingly, the optimal pH value was found to be 3.1 and 10.0, and the maximal biosorption capacity was found to be 0.94 and 0.91 mol/kg.

Biswas *et al.* (2008a) used orange waste loaded with Zr(IV) for removing both As(V) and As(III) from an aquatic environment. The PSO rate equation for biosorption capacity and correlation coefficients was used to characterize the biosorption kinetics of arsenic at various doses. Between pH 9 and 10, As(III) was strongly adsorbed, while As(V) was effectively adsorbed in the pH span of 2.0 to 6.0. They discovered that the Zr(IV)-loaded SOW gel's highest biosorption capacities for As(V) and As(III) were 88 mg/g and 130 mg/g, correspondingly.

Biswas *et al.* (2008b) explored the removal of phosphorus from water using a saponified orange waste gel that was loaded with Zr(IV). The kinetic behavior and pH

dependence of P biosorption from water were studied. It was observed that the generated gel had a maximum adsorption capacity to remove P of 57 mg-P/g, which was four times greater than that of the commercially available zirconium ferrite biosorbent. The maximum removal efficiency was seen at low pH levels, exceeding 85% even at pH 9.0.

The iron-impregnated coir pith (CP-Fe-I) was used by Krishnan & Haridas (2008) to remove phosphate from sewage and aqueous streams. Batch studies were utilized to investigate the impacts of pH, beginning phosphate concentration, contact time, and biosorbent dose on the biosorption of phosphate. The highest phosphate biosorption from an aqueous solution was observed at pH 3.0. A comparison study of the phosphate biosorption utilizing CP-Fe-I and CP revealed that the former is 5 to 6 times more efficient than the latter. The kinetic analysis showed that PSO kinetics was used in the biosorption process. The Langmuir isotherm model was used for biosorption.

Homagai et al. (2010) investigated the heavy metal removal ability of charred xanthated sugarcane bagasse (CXSB) to remove various heavy metal ions. FTIR results and elemental assessment were used to characterize the biosorbent. The data of equilibrium sorption best suited the Langmuir isotherm model and PSO kinetic model. The removal of various metal ions from wastewater may be accomplished using CXSB as a selective biosorbent.

Govindaswamy et al. (2011) studied the special phytoremediation capability of arsenic by dried roots of water hyacinth for the synthesis of cos-effective biosorbent. For batch and continuous column tests, dried hyacinth roots (DHR) were produced by washing, drying, and powdering water hyacinth roots. Water that had 300 g/L of arsenic was spiked with various amounts of DHR. In the batch testing, it was determined that a concentration of 20 g/L DHR was sufficient to remove more than 90% of the arsenic. Continuous column tests were carried out utilizing a 2-liter column based on the outcomes of the batch test. With a biosorption capacity of around 260 g As/g DHR, a continuous column was utilized to treat 15 liters of water with 300 g/L of arsenic to below 20 g/L using 50 g DHR and 44 liters of water with 600 g/L of arsenic to below 20 g/L using 100 g DHR.

Zhang *et al.* (2012) explored the chemical alteration of sugarcane bagasse for removing phosphate from contaminated water. Phosphorus biosorption kinetics and equilibrium between water and modified sugarcane bagasse (MSBG) were investigated. At a pH of 7, MSBG had a maximal adsorption capacity of 21.3 mg/g. The PSO was the most accurate kinetic model for describing the biosorption process. The Langmuir isotherm model provides a substantially superior fit than the Freundlich model.

Pehlivan *et al.* (2013) investigated sugarcane bagasse modified with hydrous ferric oxide (SCB-HFO) for the elimination of As(V) from water. Under ideal circumstances of pH 4, contact period 3 h, and temperature 22º C, it was discovered that SCB-HFO had an As(V) biosorption capacity of 22.1 mg/g. With 30% HCl, As(V) desorption from the biosorbent was 17%, while with 1 M NaOH solution, it was 85%. According to the results of the FTIR study, the bio-sorbent has carboxyl and hydroxyl groups that serve as exchangeable cation and complexation sites for the removal of arsenic.

The effectiveness of Zr(IV)-loaded apple peels for removing phosphate from the water was investigated by batch biosorption method. The maximum phosphate removal adsorption capacity of the adsorbent at pH 2 was obtained to be 20.35 mg/g. The Langmuir Biosorption isotherms and PSO kinetics provided the best explanation for the biosorption data (Mallampati & Valiyaveettil, 2013).

As(V) biosorption onto *M. oleifera* was examined in batch mode. The greatest adsorption capacity was 6.23 mg/g at pH 7.0. The rate-determining step was mostly surface biosorption, and the biosorption mechanism was discovered to be chemisorption. The Langmuir model showed a superior match to the data, showing that the application of arsenic monolayer coverage to rising temperatures enhanced the rate of arsenic biosorption. Arsenic biosorption on *M. oleifera* was further corroborated by equilibrium data that the Temkin equation accurately explained. The negative $\Delta G°$ values demonstrated the viability and spontaneity of As(V) biosorption onto *M. oleifera*. The endothermic character of the biosorption was shown by the positive $\Delta H°$ values. The positive $\Delta H°$ readings showed the enhanced randomness at the solid-solution interface (Sumathi & Alagumuthu, 2014).

Nguyen *et al.* (2014) studied the sequestration of phosphate from water utilizing Zr(IV) loaded okara as a biosorbent. The influence of temperature, contact duration, beginning phosphate concentration, biosorbent doses, and pH were investigated in the batch mode tests. The pH range of 2 to 6 was discovered to be the most favorable for biosorption. The assessed adsorption capacity of phosphate was 44.13 mg/g. The elimination of phosphate proceeded quickly, reaching 95% in 30 minutes.

Bahar *et al.* (2018) studied the potential of coir pith ash (CPA) for the elimination of As(V) from water. With a biosorbent dosage of 5 g/L, it was discovered that the CPA could adsorb As(V) throughout a pH range of 2 to 12. The biosorption kinetics data are most closely matched by the PSO kinetic model. The biosorption equilibrium data were extremely well represented by the Langmuir and Dubinin-Radushkevich isotherms. The highest biosorption capacity was determined via the Langmuir isotherm to be 36.5 mg/g.

Li *et al.* (2018) investigated the series of La(OH)$_3$ modified magnetic pineapple biochar for phosphate biosorption. With rise in La(OH)$_3$ concentration, the phosphate adsorption capacity rose but the magnetic property declined. Up to 101 mg/g of biosorption capacity was evaluated, which is 27 times more than pineapple biochar. The PSO kinetics model and the Langmuir model, respectively, provided superior fits for the adsorption isotherm and adsorption kinetics. In the occurrence of co-existing ions, the removal effectiveness was higher than 96.04%.

Lin *et al.* (2018) conducted a batch biosorption investigation to remove Cr(VI) from an aqueous solution using aminated rice straw grafted polyvinyl alcohol. The Freundlich isotherm and Elovich models, according to the authors, provided the strongest support for the experimental results. At a pH of 2.0, they discovered the highest biosorption up to 140.39 mg/g. In compared to the raw rice straw's highest biosorption (34.90 mg/g), the maximum biosorption was much higher. The reaction was spontaneous and endothermic.@@@

Eggshells, java plum seed, water chestnut shell, maize cob, tea waste, and pomegranate peel were some of the biosorbents tested by Shakoor *et al.* (2019) to examine how successfully they removed arsenic from water. The maximum As(III) removal efficiency was achieved by java plum seed and eggshell at pH 7, followed by

water chestnut shell (75%), maize cob (67%), tea waste (74%), and pomegranate peel (65%). The maximum As(V) elimination was observed for eggshell (71%) and java plum seed (67%), respectively, at pH 4 and 5.3. After a two-hour contact time, eggshell and Java plum seeds showed the largest As(V) and As(III) biosorption. The PSOkinetic model and the Langmuir isotherm model best fit the experimental equilibrium data for the sorption of As(III) and As(V) onto the bio-sorbents.

Noli *et al.* (2019) studied the biosorption of uranium and cadmium utilizing aloe vera wastes. To improve the raw material's ability to adsorb the tested metals, acidic and alkaline reagents were added. Several models, including Elovich and intra-particle diffusion models, PFO and PSO equations, were successfully utilized to generate the kinetics data that showed how intricate the biosorption mechanism was. Langmuir and Freundlich models were utilized to simulate the biosorption isotherms, and thermodynamic data were gathered for evaluating uptake behavior. It was discovered that the biosorbent that had been altered by the alkaline reagent had a high capacity for biosorption, with q_m values for uranium and cadmium of 370.4 and 104.2 mg/g, respectively.

Li *et al.* (2020) investigated the removal of hexavalent chromium from water using a chemically altered walnut shell. The batch biosorption technique was used to conduct the investigation. With a solution pH of 3, they obtained a maximum biosorption of 50.1 mg/g at 303 K. The PSO kinetic model and the Langmuir isotherm offered the greatest explanations for the experimental results, respectively.

Wang *et al.* (2020) used pomelo peel and $FeCl_3$ – modified pomelo peel (FPP) as biomass biosorbents to study the removal of cr(VI) from aqueous solutions. To assess the effects of pH, time, temperature, starting concentration, and biosorbent dosage on Cr(VI) removal by PP and FPP, they conducted batch biosorption studies. At a pH of 2.0 and a temperature of 40°C, the highest adsorption capacity of Cr(VI) was determined to be 21.55 mg/g for FPP and 0.57 mg/g for PP. The results demonstrated that FPP had much greater biosorption capability than PP, suggesting that FPP may be a suitable, high-efficiency biosorbent for the removal of hexavalent chromium.

Nuhoğlu *et al.* (2021) used raw and modified waste from the tea industry as the biosorbent material in their study of the Pb(II) biosorption performance from

synthetic wastewater. In the sorption kinetic experiments, the beginning pH value, particle size, initial Pb(II) concentration and dose of biosorbent, stirring speed, and temperature were all changed. In 15 minutes, biosorption achieved equilibrium. The Freundlich, Langmuir, BET, and Temkin isotherm models were employed for the adsorption process, and actual biosorption values were consistent with the Freundlich biosorption model. pH 3.5, particle size 0.125-0.25 mm, agitation speed 200 rpm, biosorbent dose 7 g/L, and 25 °C were found to be the ideal testing conditions. The maximum biosorption efficiency under these circumstances was 94.07%, and following the chemical modification process, the efficiency increased to 97.73% at 70 mg/L. Raw tea factory waste was observed to have a maximum Pb(II) adsorption capacity of 22.111 mg/g at 200 mg/L. The PSO model has been supported by biosorption kinetics.

Younes *et al.* (2021) researched the removal of Cd(II) from wastewater onto a magnetic nanocomposite made of maize cobs and nano-zero valent iron. The ideal biosorption conditions were considered after several factors, including solution pH, contact duration, biosorbent dosage, etc., were assessed. After 10.0 minutes of shaking at 25°C, a total biosorption capacity of 145 mg/g was found. The PSO kinetic Langmuir isotherm model was supported by biosorption data, which demonstrate. The biosorption process is also spontaneous, exothermic, and irreversible.

Salmana *et al.* (2021) studied the biosorption of Pb(II), Cd(II), and Cr(VI) from water under various experimental conditions, including initial heavy metals concentration (20-500 mg/L), contact time (10-120 min), pH (1-7), and biosorbent dosage (1-30 g/L). They used chemically modified Bauhinia variegata leaves. The biosorption of the selected heavy metals more effectively follows the Langmuir isotherm model. The greatest biosorption capacity of the biosorbent was 92.592 mg/g for Pb(II), 114.943 mg/g for Cd(II), and 70.921 mg/g for Cr(VI). The PSO kinetic model was more appropriate for the kinetic data. The biosorption of the selected metals was a successful, exothermic, spontaneous process, as determined by the analyzed thermodynamic characteristics.

Threepanich & Praipipat (2021) investigated the removal of lead from wastewater using iron (III) oxide-hydroxide doped with lemon peels in powdered and beaded form. Lead biosorptions were evaluated in a series of batch tests using dosage, contact

duration, pH, and initial concentration of Pb(II). We also looked at several biosorption kinetics and isotherms. All of the biosorbent materials exhibited good lead removal effectiveness, according to the results, with lemon peel with iron(III) oxide-hydroxide beads (LPFB) having the best potential. All biosorbent materials were examined using the Freundlich model, and LPFB revealed the maximum biosorption capacity of 5.67 mg/g than the various biosorbents. Every biosorbent substance adhered to PSO biosorption kinetics.

Chakraborty *et al.* (2021) used sawdust that had been formaldehyde-modified to study the biosorption of Cr(VI) ions from water. They looked at how variables like pH, contact time, biosorbent dosage, and starting metal ion concentration affected the results. The Freundlich isotherm model, according to the authors, provided the best explanation for the experimental results. At pH 2.0, a starting concentration of 10 mg/L, and an biosorbent dosage of 4 g/L, the maximum biosorption of 100% was noted. The maximal biosorption capacity was observed to be 8.84 mg/g. A PSO kinetic model best described the acquired data, and the biosorption process was discovered to be endothermic and spontaneous.

Oliveira *et al.* (2021) investigated the use of the carnauba (*Copernicia prunifera*) fruit biomass (CFB) for the elimination of Pb(II) and Cd(II) from water. The *Copernicia prunifera* fruit's exocarp was used to obtain the CFB. The CFB was cleaned with distilled water first, then dried for 48 hours at 60°C. To get particle sizes ranging from 48 mesh to 32 mesh, the material was crushed and sieved. The pH value of 5.0, 5 mg/L biosorbent doses, and 120 min of contact time were shown to have the best removal capabilities. Biosorption kinetic tests revealed that the PSO mathematical model offered a superior match to the experimental data. After 120 minutes of interaction, equilibrium was achieved. For Pb(II) and Cd(II), respectively, Temkin and Freundlich presented the greatest fits to the data. The Langmuir model determined that the q_m values for Pb(II) and Cd(II) were 26 mg/g and 58 mg/g, correspondingly.

Giri *et al.* (2022) studied the remediation of Pb(II) ions from wastewater using two biosorbents made from seeds of *Syzygiumcumini* (SB*Sc*) and *Artocarpus heterophyllus* (SB*Ah*). Pb(II) removal was 96% for SBAh and 93% for SBSc at 300 rpm when response surface approach provided optimum conditions (Pb concentration

44

2 g/mL, pH 5.8, and biosorbent dosage 60 mg). After 70 minutes, it was discovered that SB*Ah*'s biosorption capacity was 4.93 mg/g and SB*Sc*'s was 3.95 mg/g. Under ideal experimental circumstances, the inter-particle diffusion model for SB*Ah* and the Elovich model for SB*Sc* best explained the kinetics of biosorption. Additionally, both biosorbents adhered to the Temkin isotherm model.

2.2 Biosorption on raw and modified pomegranate peel

In wastewater treatment, the utilization of renewable substrates as biosorbents is receiving a lot of attention. One of these substrates is the pomegranate peel. In this section, the potential of pomegranate peel for treating wastewater is investigated through a review. The performance and sorption capacity of raw and modified pomegranate peels for metals and non-metals, dyes, and organic contaminants are assessed. However, there haven't been much research done to look into the possibilities of raw and modified pomegranate peels for wastewater treatment. Here, the most published papers on the potential of pomegranate peel as a biosorbent are reviewed.

2.2.1 Applications of pomegranate peels for removal of metallic/non-metallic pollutants

Najim & Yassin (2009) studied the usage of raw and formaldehyde-modified pomegranate peel for the elimination of Cr(VI). Raw pomegranate peel powder (MPGP) was treated with 8% formaldehyde to create the formaldehyde-modified pomegranate (FMPGP). Batch biosorption experiments were performed for Cr(VI) in the range of 10 to 40 mg/L with a contact time of 100 minutes. The pH range of the examined solutions was between 1 to 6. Batch biosorption tests were performed with a contact time of 100 minutes in a Cr(VI) concentration range of 10 to 40 mg/L. The pH range of the tested solutions was 1 to 6. Biosorption isotherm tests were conducted at various temperatures (20, 30, 40, and 50° C). The ideal circumstances were discovered to be a biosorbent dosage of 2 g/L, a pH of 2, and an equilibrium duration of 80 min. At 303 K, it was discovered that MPGP and FMPGP had maximal biosorption capacities of 26.882 mg/g and 35.336 mg/g for removing Cr(VI), respectively. The Dubinin-Radushkevich isotherm model offered the greatest match to the data on Cr(VI) biosorption onto MPGP and FMPGP, according to the findings.

The PSO kinetic models more closely matched the biosorption data than the PFOand Elovich models.

Raw pomegranate peel powder was created by Abbasi *et al.* (2009) for removing Co(II) and Ni(II) ions from wastewater. Fruit peels were taken off, thoroughly washed, and dried for three days in the sun before being dried in a 90°C oven. Pomegranate peel that had been dried out was trampled and sieved to a size of 200-400 µm. The effects of solutions with pH values between 1-6 were investigated. With an raise in biosorbent dosage from 1 to 3 g/L, the removal of Co(II) and Ni(II) metal ions rose from 38% to 78% and from 46% to 87%, respectively. The tested contact times varied from 5 to 60 minutes, and a 35-minute equilibrium time was attained. The ideal pH was determined to be pH 6 because Co(II) and Ni(II) biosorption ability of pomegranate peel improved as pH climbed. Both the Freundlich and Langmuir models well predicted the experimental findings. Maximum Langmuir biosorption capacities of 8.98 mg/g for Co(II) and 7.54 mg/g for Ni(II) were discovered. The Co(II) and Ni(II) ion biosorption processes onto raw pomegranate peel powder were shown to be endothermic and spontaneous by the thermodynamic study.

Bhatnagar & Minocha (2010) investigated the biosorption of Ni(II) onto activated pomegranate peel (PPAC). Pomegranate peels were dried overnight at 80°C after being carefully washed with double-distilled water. Peels that had been dried out were thermally activated for one hour at 600 ± 5°C in the presence of air. Before being dried overnight at 110 ± 5°C in an oven, the thermally activated dried peels were washed with distilled water to get rid of the ash content. The resulting materials were sieved with a range of 75-104 µm. We looked at the intraparticle diffusion, PFO, and PSO kinetic models. The PSO model accurately predicted the Ni(II) biosorption on PPAC. The equilibrium data were satisfactorily matched by the Langmuir model, which was shown to have a qm of 52.2 mg/g for PPAC for Ni(II) ions. Thermodynamic measurements pointed to the endothermic and spontaneous character of the biosorption.

Ay *et al.* (2012) studied the removal of Pb(II) using raw pomegranate peel. The peels were thoroughly cleaned with deionized water, then crushed to eliminate any remaining soluble components. They were then sieved to a particle size of 150 µm after being dried at 80°C for 48 hours. Investigations into isotherms, kinetics, and

thermodynamics were carried out once the biosorbent had been described. The Langmuir, Freundlich, and Dubinin-Radushkevich isotherm models were examined. The Langmuir model best matched the biosorption data. The biosorbent's maximal Langmuir biosorption capacity for lead (II) ions was found to be 166.63 mg/g at 293 K and 193.94 mg/g at 323 K and pH 5.5. The kinetic study made use of the PFO, PSO, Elovich, and intraparticle diffusion models. The PSO kinetic model has been connected to studies of Pb(II) biosorption. The findings of a thermodynamic research revealed that the process was endothermic and spontaneous.

Using pomegranate peel-activated carbon, Rouabeh & Amrani (2012) studied the biosorption of NO_3^- from an aqueous solution. After being thoroughly cleansed with distilled water, pomegranate peels were dried for two hours at 105°C before being crushed and sieved to generate particles with sizes ranging from 0.3 to 0.6 mm. Two sections of the materials were obtained; the first, designated AC, underwent an hour of carbonization at 500°C. The second part was submerged for 24 hours in a solution of 1:1 (V/V) H_3PO_4 (1M) and $ZnCl_2$, then dried and carbonized as previously stated (1M). The resulting activated carbon was then washed completely with deionized water, neutralized with a solution of 1% sodium hydroxide, and dried at 90 degrees Celsius. It was named AC1. They characterized and contrasted AC and AC1. Using AC1, biosorption tests were conducted. They looked at the impact of pH and contact duration (0-200 min) (2–11). The equilibrium duration was discovered to be 45 minutes, and maximum elimination occurred at pH 7.5–8.5. Freundlich and Langmuir are the two biosorption isotherm models that were utilized. The Langmuir model well fits the adsorption data. The maximal Langmuir adsorption capacity of AC1 for nitrate was found to be 78.125 mg/g. The biosorption kinetics data were modelled utilizing the PFO, PSO, and intraparticle diffusion models. The intraparticle diffusion model had little effect during the first phases of the biosorption process, and the PSO kinetics model provided the best fit to the biosorption kinetic data, according to the results.

Thapa and Pokhrel (2012) looked into the biosorption of As(III) onto charred pomegranate peel waste that was laden with Fe(III) (FeCPW). After being cleansed and dried in the sun for a week, the raw pomegranate peel (RPW) was processed into powder in a grain mill. Then, RPW was treated with concentrated H_2SO_4 (1:2, W/V

ratio). The mixture was steeped for 24 hours at room temperature. Before being crushed and sieved to a size of 212 μm, it was washed in distilled water until it reached neutrality, filtered, and dried at 100 °C for 6 hours. The thus obtained material was known as CPW, and it was agitated for 24 hours after being combined with 500 mL of $FeCl_3$ solution at pH 3. Once the pH of the filtrate was neutral, it was filtered, rinsed with distilled water, and dried for 24 h at 100°C. It was sieved to a 212 μm particle size. The material, named Fe-CPW, was employed to remove As(III) ions. pH 9 and 120 minutes of equilibrium time were ideal for maximum As(III) removal. At 298 K, the maximum biosorption capacity of Fe-CPW for removing As(III) ions was estimated to be 50 mg/g. Kinetic and thermodynamic studies have not been done by them.

Arbind & Vipin (2015) investigated the biosorption of Cd(II) ions onto formaldehyde-modified pomegranate peel (FMPGP). At various starting pH ranges (2–10), biosorption studies were conducted. After examining the biosorption contact duration over a range of 0-200 min, the equilibrium time was found to be approximately 120 min. From 0.5 to 3 g/L, the impact of the biosorbent dosage was investigated; 2 g/L was found to be the optimum biosorbent dose. Additionally, it was shown that raising the temperature accelerated the removal of metals, which may be connected to an endothermic biosorption process. Analysis was done on the Freundlich and Langmuir isotherm models. The Langmuir model was found to better explain biosorption data. The FMPGP was discovered to have a maximum cadmium Langmuir biosorption capacity of 18.52 mg/g at 303 K. The biosorption kinetics data were modelled using the PFO, PSO, and intraparticle diffusion models. The PSO model gave the best data fit. A thermodynamic analysis supported the endothermic and spontaneous nature of Cd(II) biosorption onto FMPGP.

The usage of activated pomegranate peel (PPAC) for removing Ni(II) ions from aquaous solution was investigated by Khawaja *et al.* (2015). The peels were washed and let 48 hours to dry in the sun. For 10 hours, the dried pomegranate peel was cooked over a medium heat. Particles of 0.6 mm in size were created from the recovered charcoal. Following that, it was immersed for 24 hours in 1:4 conc. HCl. After filtering the mixture, the leftover material was carefully washed with distilled water to get rid of any residual acid. The finished AC was dried at 110°C for two

hours. For Ni(II) concentrations in the range of 10-150 mg/L with a 60-minute contact duration, batch biosorption experiments were performed. The tested solutions have a pH range of 3-11. 2, 5, 10, and 15 g/L of absorbent dose were used. The ideal biosorption conditions were discovered to be a biosorbent dosage of 10 g/L, a pH of 7, and an equilibrium duration of 50 min. Making use of the Freundlich and Langmuir models, the biosorption isotherm was studied. Both theories suit the experimental data quite well. PPAC was observed to have a maximum Ni Langmuir biosorption capacity of 10.82 mg/g (II).

To remove Cu(II) from water, Ben-Ali *et al.* (2017) looked at the use of raw pomegranate peel. The maximum Cu (II) adsorption capacity was achieved at pH 5.8, 313 K, and 2 hours of contact time. They used the isotherm models developed by Langmuir, Freundlich, Dubinin-Radushkevich, and Temkin. The Freundlich model could not be fitted to the data. To match the experimental findings, the PSO, PFO, intraparticle diffusion, and Elovich kinetic models were applied. The model that included PSO had the best fit. A spontaneous endothermic biosorption of Cu(II) has been discovered by thermodynamic study on raw pomegranate peel. The highest Cu(II) removal capacity of raw pomegranate peel was reported to be 20.492 mg/g at 303 K and 30.12 mg/g at 313 K.

Salmani *et al.* (2017) utilized pomegranate waste treated with Fe(II) and Fe(III) ions followed by carbonization to explore the removal of Pb(II) ions from water. Wastes from pomegranates were dried at room temperature without exposure to sunlight, and the granules were then mixed separately for 12 hours with 10 mL of 0.1 M solutions of Fe(III) and Fe(II). Prior to being carbonized for three hours at 400°C without air, the impregnated granules were dried. It was rinsed 3 times with distilled water to get rid of excess ions from the changed carbons. At 105°C, the iron-modified carbons were finally heated. The ideal pH for biosorption was determined to be between 6.0 and 6.5. The results showed that a contact period of 90 min, a starting concentration of 50.0 ppm, and a biosorbent dose of 1.0 g/100 mL solution were the ideal circumstances. The maximal biosorption capacity for pomegranate peel carbons (PPC) impregnated with Fe(II) and Fe(III) under these conditions was found to be 27.5 mg/g for Fe(II) and 22.5 mg/g for Fe(III). After 30 minutes, pore diffusion becomes the rate-limiting mechanism, and the impact of the boundary layer on the

biosorption of Pb(II) by Fe(II)-PPC increases. Studies of thermodynamic parameters show that the biosorption process is advantageous and spontaneous under ideal conditions.

The biosorption of Cr(VI) onto raw pomegranate peel was examined by Giri *et al.* (2021). Through batch studies, the impact of experimental conditions on Cr(VI) sorption was assessed. Excellent removal capabilities were seen at a pH of 2, a dose of 300 mg biosorbent, and a contact duration of 30 min. The PSO model was well matched with the biosorption kinetics of Cr(VI). The Cr(VI) biosorption process was represented by the Langmuir isotherm with an biosorption capacity of 20.87 mg/g. The thermodynamic study demonstrated that the Cr(VI) ion biosorption processes onto raw pomegranate peel powder were endothermic and spontaneous.

Bellahsen *et al.* (2021) studied the biosorption of phosphate from water using iron-loaded pomegranate (IL-PP). Raw pomegranate peel was modified via saponification with NaOH and then cationization with $FeCl_3$. Thus obtained IL-PP was characterized using zeta potential measurement, SEM, and FTIR analysis. Using a 150 mg dosage of IL-PP, efficient phosphate removal up to 90% was accomplished in 60 min at pH 9 and 25^0C temperature. The findings revealed that the kinetics is best fitted to the Elovich model, which posits that the chemisorption process predominates, whereas the biosorption isotherm follows both Freundlich and Langmuir models with maximum biosorption capacity of 49.12 mg/g. The spontaneity and endothermic nature of the biosorption process were revealed by an investigation of thermodynamic parameters.

Wang *et al.* (2022) investigated the use of diethylenetriaminepentaacetic acid (DTPA) modified pomegranate peel to eliminate Cd(II) ions from aqueous solution. The mercerized pomegranate peels were prepared (MPP) by degreasing and deproteinizing. Then, MPP and DTPA were combined (1:3, w/w) in 42 mL of DMF and agitated there for 20 hours at the temperature of 75°C. Centrifugation was followed by successively washing the precipitate with DMF, In that sequence, deionized water, saturated $NaHCO_3$, 95% aqueous ethanol, deionized water, and acetone. Finally, DTPA-modified pomegranate peels (DMPP) were generated after being dried to a constant weight in an oven at 50°C. DMPP has a 46.296 mg/g maximal Cd(II) biosorption capability. After 5 minutes, the biosorption reached

equilibrium, and the Langmuir isotherm and PSO kinetic model provided good fits. Ion exchange with Na(I), complexation with oxygen-containing groups, and physical biosorption are the major biosorption processes for Cd(II).

2.2.2 Applications of pomegranate peels for removal of dyes and organic contaminants

Bhatnagar & Minocha (2009) investigated pomegranate peel that has been thermally activated as a biosorbent for removing 2,4-dichlorophenol. A starting pH between 5.5 and 6.5 and a biosorbent dosage of 10 g/L was selected. 9 hours of equilibrium time was discovered. The results demonstrated that the PFO model best matched the kinetic data. To fit the experimental data, the Langmuir isotherm model was used. The maximal Langmuir biosorption capacities of the biosorbent for 2,4-dichlorophenol were found to be 75.8 mg/g and 96.2 mg/g at 298 K and 318 K, respectively. Analysis of the thermodynamics revealed that the adsorption process was endothermic and spontaneous.

Methylene blue (MB) was investigated by Güzel *et al.* (2012) as it biosorbed onto raw pomegranate peel. It was found that the optimal pH value was 7, the equilibrium time was 150 min, and the biosorbent dose was 2 g/L. The maximal methylene blue biosorption capacity of raw pomegranate peel was found to be 36.36 mg/g at 303 K, 28.74 mg/g at 313 K, and 26.67 mg/g at 323 K. The PSO model gave the greatest match to the kinetic data, according to the isotherm and kinetic findings. Compared to the Freundlich model, the Langmuir model better fitted the equilibrium data. The biosorption process was physical, exothermic, and spontaneous, according to a thermodynamic analysis. Using several desorbing agents, desorption tests to recover the MB were done. The impacts of salt solutions on MB biosorption were investigated. The outcomes revealed that MB removal effectiveness reduced from 21.67 percent to 3.96 percent when NaCl concentration rose from 0 mol/L to 1.0 mol/L.

Mashkour (2013) used concentrated H_2SO_4 - treated pomegranate peel to study the biosorption of amaranth color from an aqueous solution. Biosorption tests were conducted in batch mode. It was investigated how the experimental variables of pH, contact time, biosorbent dose, and temperature affected the results. The optimal conditions were discovered to be a contact time of 25 minutes, a pH of 3, and an

biosorbent dose of 0.25 g/L. Both the PSO kinetic model and the Langmuir biosorption model agreed with the experimental findings. The maximal Langmuir biosorption capacity of activated pomegranate peel was observed to be 3.448 mg/g. Based on thermodynamic properties, the amaranth dye's biosorption onto the pomegranate peel looked to be an endothermic process.

Radaei *et al.* (2014) studied the elimination of Reactive Blue 19 (RB19) using phosphoric acid-activated pomegranate peel carbon. The response surface technique was used as an experimental design to evaluate the optimal biosorption parameters (beginning pH, biosorbent dose, dye concentration, and contact duration) of the biosorbent for removing RB19 dye from water. pH 11, 1.025 g/L of biosorbent, 100 mg/L of starting dye concentration, and 6.8 min of contact time were found to be the optimal values. It was shown that 98.7% of dyes could be removed on average.

Najafpoor *et al.* (2016) looked into the phenol biosorption on pomegranate peel-derived activated carbon. The impacts of contact time (0 to 210 min), pH (2 to 12), biosorbent dosage (0.1 to 0.7 g/L), and beginning phenol content (10 to 100 mg/L) were examined. The optimal biosorption requirements were a pH of 7 and 0.6 g/L of biosorbent. There was an equilibrium for 120 minutes. The experimental findings more closely match the Freundlich model. The maximum adssorption capacity of phenol for the manufactured adsorbent was determined to be 344.86 mg/g.

2.3 Research gap

A thorough review of the literature revealed that there are many types of literature on the topic of employing biosorbents to remove metallic and non-metallic contaminants from aqueous solutions. The goal of this literature review is to highlight recent research on using different biosorbents to remove contaminants from polluted aqueous systems. For all different kinds of biosorbents, efforts are increasingly focused on developing less expensive and more effective biosorbents. The use of low-cost biosorbents made from environmentally acceptable materials is not only cost-effective, but it would also replace the conventional expensive technology, which is frequently complicated, cumbersome, and time-consuming. Additionally, in the past, metallic, and non-metallic contaminants were removed using synthetic ion-exchange resins and commercial activated carbon. However, issues with their expensive price,

lack of renewability, and post-use disposal limit its widespread usage in developing nations like Nepal. As a result, a new trend has emerged to use plentiful and inexpensive biomaterials, such as agricultural byproducts, for this purpose. It would be desirable to create biosorbents that are inexpensive, widely available, highly effective, highly selective, potentially renewable, and highly adaptable to diverse working circumstances.

Many researchers have employed a range of plant-based or agricultural waste-based materials to remove contaminants. Pomegranate peels have been utilized as a biosorbent in several research for removing heavy metals, non-metals, dyes, organic compounds, and other contaminants from water. To the best of our knowledge, there hasn't been any research on a low-cost natural ion-exchanger made from locally accessible pomegranate wastes for removing arsenate, arsenite, Pb(II), Cd(II), and phosphate from contaminated water. Our research attempts to investigate the efficacy of some newly developed biosorbents (SPP@Zr, PP@TiO$_2$, and SPP) for removing the above-mentioned metallic and non-metallic pollutants from water.

CHAPTER 3

MATERIALS AND METHODS

3.1 Methodological framework

Biosorption experiments were conducted in the research laboratory of the Central Department of Chemistry, Tribhuvan University, Kathmandu, Nepal, and the Solid-state Chemistry laboratory of the Jawaharlal Nehru Centre for Advanced Scientific Research (JNCASR), Bangalore, India. The primary goal of the batch experiments was to better understand the variables that influence the biosorption process. **Figure 9** provides an illustration of the methodological framework that was applied in the current study. A thorough explanation of each procedure is followed by further discussion.
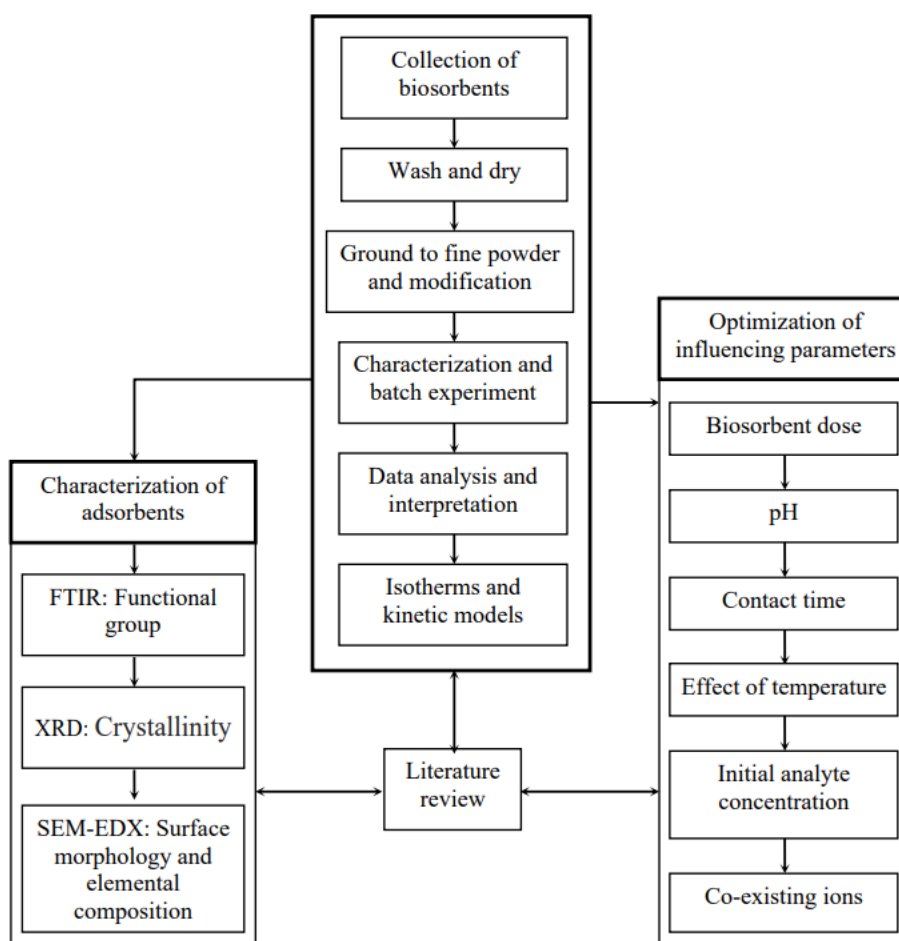
Figure 9: Methodological framework of the study

3.2 Instruments

3.2.1 X-ray diffractometer

X-ray diffraction (XRD) data for all the materials were acquired utilizing a Cu Kα (λ = 1.5406 Å) radiation on a Bruker D8 diffractometer (Bruker AXS D8 advance, Germany) and X-ray diffractometer, (Rigaku Co., Japan)

3.2.2 FTIR spectrometer

FTIR spectra of powder sample was recorded using FTIR spectrometer (IR Affinity - 1S-SHIMADZU spectrometer, Kyoto, Japan) and Bruker IFS 66v/S spectrometer, Germany. FTIR spectra were captured using the ATR (attenuated total reflection) technique with 32 scans in the spectral region of 4000-400 cm^{-1} and a resolution of 4 cm^{-1}.

3.2.3 FESEM and EDX analyzer

FESEM of the biosorbents before and after bisorption were performed using NOVA NANO SEM 600 (FEI, Germany) and JEOL, JSM-6701F (Japan) operated at 15 KV. During FESEM imaging, EDX compositional analysis was done.

3.2.4 X-ray photoelectron spectrometer (XPS)

XPS measurements have been made on Kratos Axis Ultra DLD spectrometer (Kratos Analyticals, Manchester, UK), and Nexsa XPS system (Thermo Fisher Scientific, UK).

3.2.5 Zeta potential analyzer

A zeta potential nanoparticle analyzer (HORIBA Scientific SZ-100, UK) was used to do the zeta potential measurements.

3.2.6 Inductively coupled plasma- optical emission spectrometer (ICP-OES)

Actual concentration of the arsenic, lead, cadmium, and phosphorous containing solutions (1-1000 mg/L) were analyzed by ICP-OES. Utilizing the PerkinElmer Avio 220Max (ICP-OES, Scott/crossflow) equipment, the measurements were performed. Arsenic standard (1000mg/L), Pb standard (1000 mg/L), Cd standard (1000 mg/L)

and P standard (1000 mg/L) (Sigma-Aldrich, India) were used to determine the concentration of various elements.

3.2.7 Inductively coupled plasma mass spectrometer (ICP-MS)

Element concentrations in µg/L (ppb) level (1-1000 µg/L) were analyzed utilizing ICP-MS (Agilent 7900, Santa Clara, CA, USA).

3.2.8 UV-Visible spectrophotometer

Using a UV-Vis spectrophotometer (UV-2450 Shimadzu, Japan), the concentration of arsenic and phosphate in solution were examined.

3.3 Chemical reagents

- Arsenic trioxide, As_2O_3 (AR grade, Thermo Fisher Scientific, India)
- Buffer tablets of pH 4, 7 and 9.2, (AR grade, Qualigens Fine Chemicals, India)
- Cadmium chloride, ($CdCl_2.H_2O$, (AR grade, Sigma Aldrich 99.999%, India)
- Cadmium nitrate, $Cd(NO_3)_2.4H_2O$, (AR grade, Qualigens Fine Chemicals, India)
- Calcium chloride ($CaCl_2·2H_2O$) (AR grade, Qualigens Fine Chemicals, India)
- Calcium hydroxide (AR grade, Qualigens Fine Chemicals, India)
- Ethanol (Bengal Chemicals and Pharmaceuticals, India)
- Hydrochloric acid (HCl) (AR Grade, Qualigens Fine Chemicals, India)
- Lead (II) nitrate ($Pb(NO_3)_2$, (AR grade, 99.999 %, Sigma Aldrich, India)
- Lead ICP standard solution (1000mg/L, Sigma-Aldrich, India)
- Magnesium sulphate, $MgSO_4·7H_2O$ (AR grade, Qualigens Fine Chemicals, India)
- Nitric acid (AR grade, Qualigens Fine Chemicals, India)
- Potassium Bromide, KBr (AR grade, Qualigens Fine Chemicals, India)
- potassium carbonate, K_2CO_3 (AR grade, Qualigens Fine Chemicals, India)
- Potassium dichromate, $K_2Cr_2O_7$ (AR grade, Qualigens Fine Chemicals, India
- Potassium dihydrogen phosphate, KH_2PO_4 (AR grade, Sigma Aldrich, India)
- Sodium arsenate; $Na_2HAsO_4·7H_2O$, M.W = 312.02, (purity 99-100%, fine chemical limited, Mumbai, India).
- Sodium arsenite ($NaAsO_2$) (AR grade, Sigma–Aldrich, India)
- Sodium hydroxide (NaOH) (AR grade, Qualigens Fine Chemicals, India)

- Sodium nitrate (NaNO$_3$) (AR grade, Qualigens Fine Chemicals, India)

- Sulphuric acid (H$_2$SO$_4$) (AR Grade, Qualigens Fine Chemicals, India)

- Titanium (IV) n-butoxide (AR grade, Samchun pure Chemical, Seoul, Korea)

- Zirconium oxychloride octahydrate, ZrOCl$_2$.8H$_2$O (AR grade, Sigma-Aldrich, India)

3.4 Preparation of reagents and stock solutions

Most of the chemicals were of the AR grade and were utilized without further purification. All aqueous solutions were made with deionized (DI) water. Followings chemical reagents were used in the experiments:

- **pH adjustment solution:** 0.1 N HCl and NaOH solutions were used to adjust the pH. Portable pH meter (Thermo Scientific Orion Star A221, India) was used to measure pH.

- **Preparation of 1 and 3 M sodium hydroxide (NaOH) solutions:** The solutions were made by dissolving the necessary quantity of NaOH pellets in a certain volume of DI water.

- **Preparation of 1 and 3 M Hydrochloric acid (HCl) solutions:** The solutions of required strength were prepared by appropriate dilution of concentrated hydrochloric acid.

- **Preparation of 0.1, 1 and 3 M Nitric acid (HNO$_3$) solutions:** The solutions of required strength were prepared by appropriate dilution of concentrated nitric acid.

- **Buffer solutions:** By dissolving the appropriate buffer tablets in 100 mL of DI water, buffer solutions of pH 4, 7, and 9.2 were prepared.

- The stock solution of phosphate (1000 mg/L) was made by the dissolution of calculated amount of KH$_2$PO$_4$ in 1000 mL DI water.

- The stock solution (1000 mg/L) of arsenite, As(III) was made by dissolving 1.320 g of As$_2$O$_3$ in 20 mL of 10 M NaOH solution followed by the neutralization using nitric acid and diluted to 1000 mL with DI water.

- Stock solution (1000 mg/L) of arsenate (As(V)) was prepared by dissolving 4.164 g of sodium arsenate heptahydrate (Na$_2$HAsO$_4$.7H$_2$O) in 1000 mL of DI water.

- A stock solution of Pb(II) was made by dissolving calculated amount of lead(II) nitrate salt, $(Pb(NO_3)_2$, in 1000 mL DI water.

- A stock solution of Cd(II) was prepared by dissolving cadmium chloride $(CdCl_2.H_2O)$ in DI water.

3.5 As(V) removal onto Zr(IV) modified pomegranate peels

3.5.1 Preparation of biosorbent

The pomegranate peel was purchased in Kathmandu, Nepal, from a juice vendor. It was cleansed with DI water after a couple of times with tap water. It was manually sliced into tiny chunks and dried in a 343 K oven. To create a fine powder, it was ground. The powder was passed over a copper sieve with a mesh size of 150 to sieve it. It was repetitively rinsed with DI water to remove any soluble components. The powdered wash was dried in a 343 K oven for around 24 h. It was termed "raw pomegranate peel," abbreviated as RPP hereafter, and it was utilized to make modified materials. The procedure described by Paudyal *et al.* (2013) was employed in order to prepare the Zr(IV) loaded saponified pomegranate peel. The procedure comprising the following two steps.

Step 1. Saponification: A significant amount of DI water was added along with 100g of dry RPP, 500 mL of saturated lime water, and 2-3 pellets of sodium hydroxide. The content was stirred for 24 h. The saponified product was dried at 343 K after being repeatedly rinsed with DI water the pH was neutral. This material is now known as saponified pomegranate peel (SPP).

Step 2. Loading of zirconium: 500 mL of 0.1M Zr(IV) solution and 3g of SPP were equilibrated at pH 2.2 for 24 h. It was centrifuged, cleaned with DI water many times till the pH was neutral, and then dried. The product is called Zr(IV) loaded saponified pomegranate peel that will be referred to as SPP@Zr from here on. **Figure 10** shows the mechanism exhibiting the two-step synthesis of SPP@Zr (Poudel *et. al.*, 2021).
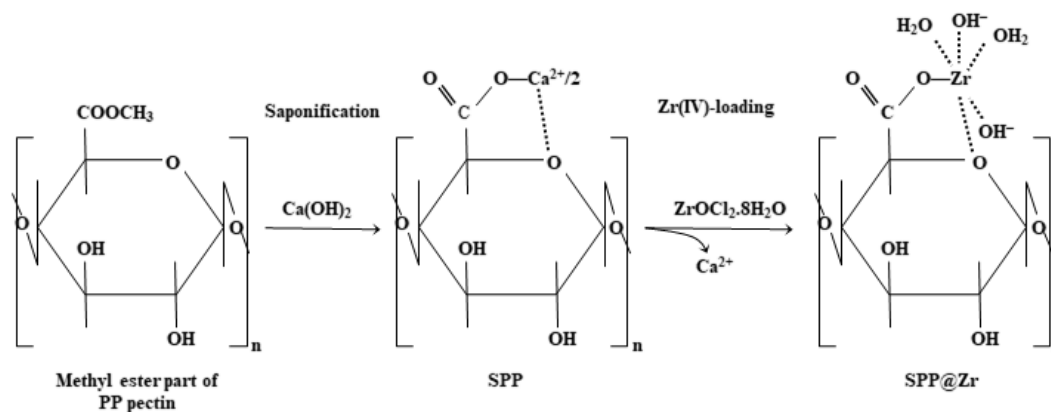
Figure 10: Reaction mechanism for the synthesis of SPP@Zr.

3.5.2 Characterization of biosorbents

Using FESEM coupled with an EDX spectrometer, the morphology and elemental composition of as synthesized biosorbent were examined. The crystallinity of the biosorbent was determined utilizing XRD patterns. Using FTIR spectroscopy, the surface functionalities of the biosorbent were examined. Using a zeta potential analyzer, pH_{pzc} of the biosorbent was determined.

3.5.3 Effect of pH

The pH studies were performed by taking 25 mL of As(V) solution with 25 mg of the SPP@Zr in conical flasks and maintaining preliminary pH values from 2.0 to 12.0, before adding the biosorbent. Each sample was shaken using a mechanical shaker at room temperature. The equilibrium pH was evaluated by utilizing a digital pH meter. The filtrate was utilized for the residual As(V) concentration. The initial pH value at which maximum biosorption occurred at equilibrium, was adjusted for further studies to ensure maximum biosorption.

3.5.4 Biosorption kinetics

With a preliminary As(V) concentration of ~20 mg/L and biosorbent dosage of 1 g/L, kinetic experiment of As(V) biosorption onto SPP@Zr was performed. The pH was held constant at 4.0 during the experiment. The sample from each flask was filtered after a certain length of time, and the As(V) concentration was analyzed. Calculations were made to determine the biosorption capacity of As(V) at a certain time (t). To further understand the biosorption mechanism, the experimental findings were fitted

to the PSO and PFO kinetic models. The Weber-Morris model and Boyd's equations were used to examine the kinetics results to clarify the diffusion mechanism and rate-determining step.

3.5.5 Biosorption isotherm studies

With a range of starting As(V) concentrations (5 to 600 mg/L), a dosage of 1 g/L and solution pH of 4.0, a biosorption isotherm experiment was conducted. At 298 K, the flasks were swirled for 12 h. Following biosorption, samples were filtered, and the equilibrium As(V) concentrations were analyzed. As(V) biosorption behavior was modeled using the Freundlich and Langmuir isotherms. In addition, the crucial aspects of the Langmuir model were examined using a dimensionless separation factor (R_L).

3.5.6 The error analyses

It is not reasonable to select the most accurate isotherm and kinetics models only based on the correlation coefficient (R^2) value. Some error analysis tools were used to determine the appropriate model based on how well it suited the experimental data. This work has employed three error analysis tools, including the chi-square (χ^2) test, root mean square error (RMSE), and average percentage error (APE), to choose the best model to represent As(V) biosorption. These error functions are computed using the following equations (Ahamad et. al., 2018).

$$\chi^2 = \sum_{i=1}^{N} \frac{(q_{exp,i} - q_{cal,i})^2}{q_{exp,i}} \qquad (3.1)$$

$$RMSE = \sqrt{\frac{\Sigma_{i=1}^{N} (q_{cal,i} - q_{exp,i})^2}{N}} \qquad (3.2)$$

$$APE\ (\%) = \frac{\Sigma_{i=1}^{N} \left| \frac{q_{exp,i} - q_{cal,i}}{q_{exp,i}} \right|}{N} \times 100 \qquad (3.3)$$

where q_{exp} and q_{cal} are the biosorption capacities (mg/g) derived from the experiment and from a theoretical calculation with the model. N is the number of experimental data. The values of χ^2, RMSE, and APE (%) will be lower if the model's projected

60

biosorption capacity closely matches the actual result, whereas they will be larger if they diverge.

3.5.7 Thermodynamic studies

Using experimental data at different temperatures and isotherm constants, the change in standard Gibbs free energy change (ΔG^0), standard enthalpy change (ΔH^0), and standard entropy change (ΔS^0) were computed. These variables are crucial for determining the nature and viability of the biosorption process.

3.5.8 Influence of competitive ions

By adding three different concentration levels of each coexisting ions into a 25 mg/L arsenate solution, it was possible to assess the effects of coexisting anions found in natural water, including chloride, sulphate, bicarbonate, and phosphate on biosorption of arsenate. A similar procedure was used to prepare a blank sample without the use of a coexisting anion. The solution's pH was maintained at 4.0. The mixture was stirred for 12 h at room temperature following the addition of the biosorbent dose of 1 g/L. A collection of the filtrates was made for As(V) analysis.

3.5.9 Regeneration and reusability of SPP@Zr

0.1 M NaOH solution (stripping solution) was mixed with 25 mg of the spent biosorbent for 12 h to liberate the arsenate ion to evaluate the regeneration of SPPP@Zr. It was filtered and dried. As(V) biosorption was again accomplished using the recovered biosorbent. To evaluate the reusability of the biosorbent, five consecutive cycles of the biosorption/regeneration process were performed. For each succeeding cycle, the % biosorption of As(V) was assessed.

3.5.10 XPS analysis

The valence states and speciation of the arsenic adsorbed on the SPP@Zr was examined using an X-ray photoelectron spectrometer.

3.6 Zirconium modified pomegranate peel for efficient removal of As(III)

3.6.1 Preparation of the SPP@Zr

The synthesis procedure of biosorbent (SPP@Zr) has been described in detail in **Section 3.5.1**.

3.6.2 Characterization

Using FESEM coupled with an EDX spectrometer, the morphology and elemental composition, and using FTIR spectroscopy, the surface functionalities of the biosorbents before and after biosorption of As(III) were examined.

3.6.3 Effect of the pH of the solutions

The pH studies were performed by taking 25 mL of As(III) solution with 25 mg of the SPP@Zr in conical flasks and maintaining preliminary pH values from 2.0 to 13.0, before adding the biosorbent. Each sample was shaken using a mechanical shaker at room temperature. The equilibrium pH was evaluated by utilizing a digital pH meter. The filtrate was utilized for the residual As(III) concentration. The initial pH value at which maximum biosorption occurred at equilibrium, was adjusted for further studies to ensure maximum biosorption.

3.6.4 Biosorption kinetics

Kinetic investigations of As(III) biosorption on PP@TiO2 were conducted until equilibrium. In each experiment, 25 mg of SPP@Zr and 25 mL of 28.32 mg/L of arsenite solution at pH 9.5 were taken in a mL conical flask and shaken vigorously at room temperature. We carried out biosorption experiments with different contact periods. Each flask's sample was filtered after a set period of time, and the equilibrium As(III) concentration was analyzed. To further understand the biosorption mechanism, the experimental findings were fitted to the PSO and PFO kinetic models.

3.6.5 Biosorption isotherms

With a range of starting As(III) concentrations (10 to 500 mg/L), a dosage of 1 g/L and solution pH of 9.5, a biosorption isotherm experiment was conducted. At 298 K, the flasks were swirled for 12 h. Following biosorption, samples were filtered, and the equilibrium As(III) concentrations were analyzed. As(III) biosorption behavior was modeled using the Freundlich and Langmuir isotherms. In addition, the crucial

aspects of the Langmuir model were examined using a dimensionless separation factor (R_L).

3.6.6 Influence of coexisting ions

By adding three different concentrations of each coexisting ions into a 25 mg/L arsenite solution, it was possible to assess the effects of competitive ions found in natural water on the biosorption of As(III). A similar procedure was used to prepare a blank sample without the use of a coexisting anion. The solution's pH was maintained at 9.5. The mixture was stirred for 12 h at room temperature after the addition of the biosorbent dose of 1 g/L. To analyze the As(III) content, the filtrate were collected.

3.6.7 Desorption and reusability of biosorbent

0.1 M NaOH solution (stripping solution) was mixed with 25 mg of the spent biosorbent for 12 h to liberate the As(III) ion to evaluate the regeneration of SPPP@Zr. It was filtered and dried. As(III) biosorption was again accomplished using the recovered biosorbent. To evaluate the reusability of the biosorbent, four consecutive cycles of the biosorption/regeneration process were conducted in equilibrium circumstances. For each succeeding cycle, the % biosorption of As(III) was assessed.

3.7 As(III) removal onto pomegranate peels impregnated with TiO_2 (PP@TiO_2)

3.7.1 Synthesis of PP@TiO_2

The local juice trader in Kathmandu, Nepal, graciously provided the pomegranate peel waste. First, distilled water was used to thoroughly wash the pomegranate peels. It was then dried for 48 h at 343 to 353 K in an oven. The dry bulk was crushed and put through a copper sieve with a mesh size of 150 microns. The biopolymer's hydroxyl groups were cross-linked by a condensation reaction by using Conc. H_2SO_4 as a dehydrating agent, preventing the adsorbent from dissolving in aqueous solutions. The cross-linked pomegranate peels were made according to Paudyal *et al.* (2017). In a round bottom flask, 15 g of raw peel powder was combined with 30 mL of Conc. H_2SO_4, which was then heated to 100°C and stirred for 24 h before cooling to room temperature. After being neutralized with sodium bicarbonate, the charred mass was once again stirred in 1 M HCl solution. It was rinsed repeatedly in distilled water until

it reached neutrality, and then it was dried at 343 K in a convection oven. The term PP refers to the powder made from pomegranate peels in this manner.

A previously reported modified sol-gel approach was used to create the PP@TiO$_2$ (Cai et. al., 2018; Zhang & Lu, 2018; Zhang at. al., 2017; Pant et. al., 2019). 15 mL of ethyl alcohol and 10 mL of titanium (IV) n-butoxide were combined. 2g of powdered PP was added to it after 30 minutes of room temperature stirring. Then, 15 mL of a 1:1:1 solution of ethyl alcohol, DI water, and ethanoic acid were dropped into the mixture from the burette while being stirred magnetically. The entire mixture was subsequently agitated for a further 4 h to produce sol. The sol was aged at 40°C for 2 h before being dried overnight at 80°C. The dry gel was then powdered and calcined for 2h at 400°C. The detailed methodology for preparating of PP@TiO$_2$ and its As(III) biosorption is schematically shown in **Figure 11**.
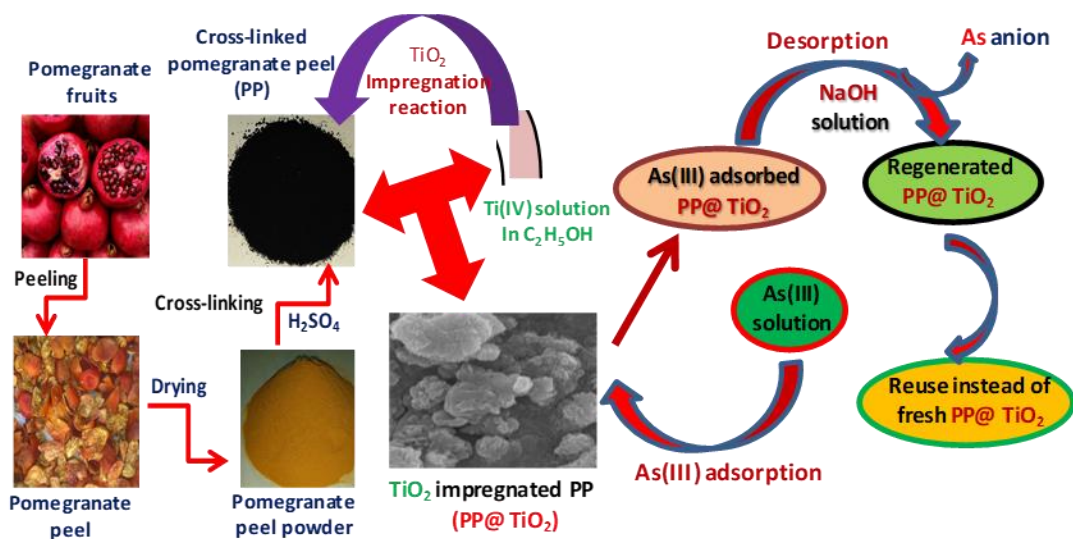
Figure 11: Flowsheet showing the details of the adsorbent synthetic route and As(III) biosorption

3.7.2 Characterizations of biosorbent

Using FESEM coupled with an EDX spectrometer, the morphology and elemental composition of as synthesized biosorbent were examined. The crystallinity of the PP@TiO$_2$ was determined using XRD patterns from an X-ray diffractometer. Using FTIR spectroscopy, the surface functionalities of the biosorbents before and after biosorption of As(III) were examined. The XPS investigations were performed by using an XPS spectrometer (Thermo Fisher Scientific, UK) to identify the elemental bonding and chemical states.

3.7.3 Batch biosorption studies

The As(III) biosorption study was performed utilizing the batch technique (V/m ~ 1000 mL/g) to investigate the biosorption behavior of the PP@TiO$_2$. To achieve equilibrium, 25 mg (dry weight) of PP@TiO$_2$ was added to several conical flasks comprising 25 mL of arsenite solution with a concentration range of 10–600 mg/L. The flasks were then stirred for 12 h at 298 K. 0.1M HCl and NaOH solutions were used to maintain the pH of the As(III) solution. Following biosorption, the PP@TiO$_2$ was filtered out of the mixture. The maximal biosorption capacity and biosorption isotherms were assessed from the equilibrium concentration.

3.7.4 Effect of pH

The pH studies were performed by taking 25 mL of As(III) solution with 25 mg of the SPP@Zr in conical flasks and maintaining preliminary pH values from 2.0 to 13.0, before adding the biosorbent. Each sample was shaken using a mechanical shaker at room temperature. The equilibrium pH was evaluated by utilizing a digital pH meter. The filtrate was utilized for the residual As(III) concentration. The initial pH value at which maximum biosorption occurred at equilibrium, was adjusted for further studies to ensure maximum biosorption.

3.7.5 Biosorption kinetics

Kinetic investigations of As(III) biosorption on PP@TiO2 were conducted until equilibrium. In each experiment, 25 mg of PP@TiO2 and 25 mL of ~30 mg/L of arsenite solution at pH 7.0 were taken in a 50 mL conical flask and shaken vigorously at room temperature. We carried out biosorption experiments with different contact periods. Each flask's sample was filtered after a set period of time, and the equilibrium As(III) concentration was analyzed. To further understand the biosorption mechanism, the experimental findings were fitted to the PSO and PFO kinetic models.

3.7.6 Effects of co-existing ions

Coexisting ions in natural water that compete with As(III) for active sorption sites may have an effect on the As(III) biosorption efficiency of PP@TiO$_2$. By introducing three different concentrations of each competitive anion into a binary mixture with a 25 mg/L solution of arsenite, it was possible to determine the impact of common

competitive ions such as chloride, sulphate and phosphate on the biosorption of As(III). The same procedure was used to prepare a blank sample without the use of a competitive ion. 0.1M HNO$_3$ and NaOH were utilized to maintain a pH of 7.0 in all the solutions. To achieve equilibrium, 1 g/L dosage of PP@TiO$_2$ was mixed, and then solutions were agitated for 24 h at 25°C. Following filtering, the final As(III) concentration was determined.

3.7.7 XPS analysis of sorption product

The elemental composition, oxidation states and speciation of the arsenic sorbed on the SPP@Zr was examined using an X-ray photoelectron spectrometer.

3.7.8 Regeneration and reusability of PP@TiO$_2$

As(III) adsorbed PP@TiO$_2$ was made by stirring 250 mg of PP@TiO2 with 250 mL of As(III) solution (25 mg/L) at pH 7.0 for 24 h at room temperature in order to conduct the regeneration study. Following filtration, ICP-MS was used to determine the residual As(III) content in the filtrate. The quantity of As(III) that had been adsorbed was calculated from the starting and residual concentration. 25 mg of dry spent PP@TiO$_2$ was stirred with 25 mL of different NaOH solution (0.01 to 0.5 M) batch-wise, like biosorption tests, to determine the optimum concentration of alkali. The suspension of each flask was filtered, and the desorbed quantity of arsenic was determined from the filtrate. Four cycles of As(III) biosorption-desorption were performed to see if PP@TiO$_2$ could be reused. After the biosorption procedure, the PP@TiO$_2$ samples were mixed with a 0.1 M NaOH solution before being filtered, washed with deionized water, and dried. To assess reusability up to four times, the regenerate PP@TiO$_2$ was again employed for biosorption tests.

3.8 As(III) removal from water using a fixed bed column packed with PP@TiO2

Fixed bed column biosorption tests were performed in a glass column with an inner diameter of 0.8 cm and a height of 20 cm, as shown in **Figure 1.5**. The biosorbent was soaked in DI water before being packed into the column. Following that, the wet adsorbent was packed into a column. The column was first filled with glass beads (5 cm), then with a layer of cotton (2 cm), and last with packed SPP@Zr that had been soaked (1.4 to 4.1 cm). To prevent the biosorbent from floating during the continuous flow, the remaining portion of the column was once more packed with a 2 cm cotton

layer followed by a 5 cm glass bead layer. Prior to sorption test, the column was conditioned by passing DI water for 5 h at the same pH as test solution. After this, As(III) solution (10 mg/L) was passed into the column at required flow rate by using (EYELA MP-1000-MP-1000-H, Tokyo Rikakikai Co. Ltd., Japan) peristaltic pump. The effluent samples for the measurement were collected at each regular interval with the help of (Advantec SF-2120, Advantec Toyo Kaish, Ltd., Japan) fraction collector. Alkali solution (0.1 M NaOH) was used to elute the loaded As(III) since they had been successfully used in earlier batch test. The Effluent samples then analyzed for measuring the final concentrations of arsenic by using ICP-MS. The column biosorption tests were performed to verify the performance of PP@ TiO_2 at different flow rates, initial As(III) concentrations, and bed height.

3.8.1 Analysis of breakthrough curve

It is crucial to study at the breakthrough curve to evaluate a column's biosorption performance. Calculating the breakthrough curve parameters can do this. The breakthrough curve illustrates the removal efficiency of As(III) in a fixed-bed column. The ratio of As(III) concentration (mg/L) from the effluent to the intake, C_e/C_i, is presented against time (h) following the commencement of the flow. The column experiments conditions are presented in **Table 4.**

3.8.2 Modeling of the breakthrough curve

The breakthrough curve must be predicted to design and optimize the column for the biosorption process. For this, several mathematical models have been proposed. Three mathematical models, the Thomas model, the Yoon-Nelson model, and the BDST model, were employed in this work to examine the dynamic biosorption efficiency of PP@ TiO_2.

3.9 Saponified pomegranate peel (SPP) for removal of Pb(II) from water

3.9.1 Preparation of biosorbent

The synthesis procedure of biosorbent (SPP) has been described in detail in **Section 3.5.1**. The reaction pathway exhibiting the preparation of SPP has been presented in **Figure 12**.

Table 4: Experimental conditions for fixed-bed column tests

Effect of flow rate	
pH	7.0
Adsorbent mass	0.86 g
Initial As(III) concentration	10.0 mg/L
Bed height	4.1 cm
Bed volume	2.06 cm^3
Variable conditions	
Flow rate	72, 150, 240 mL/h
Effect of initial As(III) concentration	
Bed height	4.1 cm
Adsorbent mass	0.86 g
Flow rate	150 mL/h
Bed volume	2.06 cm^3
pH	7.0
Variable conditions	
Initial As(III) concentration	5.0, 10.0, 15.0 mg/L
Effect of bed height	
Flow rate	60 mL/h
Initial As(III) concentration	10 mg/L
pH	7.0
Variable conditions	
Bed height	1.4, 2.6, 4.1 cm
Adsorbent mass	0.31 g for 1.4 cm, 0.55 g for 2.6 cm and 0.86 g for 4.1 cm
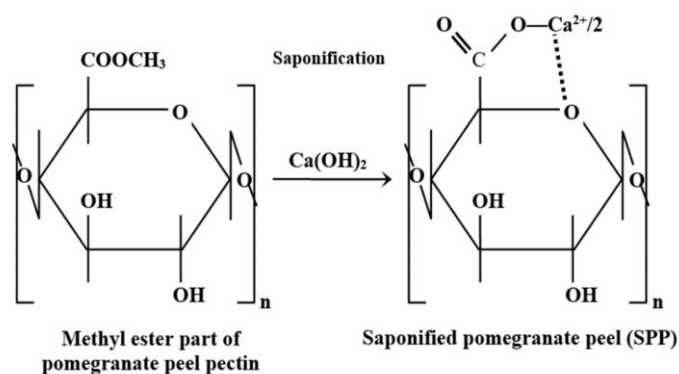
Figure 12: Reaction mechanism for the synthesis of SPP

3.9.2 Physicochemical characterization of biosorbents

Using FE-SEM coupled with an EDX spectrometer, the morphology and elemental composition of as synthesized adsorbent were evaluated. The crystallinity was determined using XRD pattern. Using FTIR spectroscopy, the surface functionalities of the biosorbent were examined. Using a zeta potential analyzer, pH_{pzc} of the biosorbent was determined.

3.9.3 Biosorption experiments

The biosorption studies of removing Pb(II) onto SPP were carried out using the batch method. In all biosorption tests, the initial and equilibrium concentrations of Pb(II) solutions (1–1000 mg/L) were measured by the ICP-OES instrument. An ICP standard lead solution (1000 mg/L, Sigma-Aldrich, India) was used to prepare the calibration solution.

3.9.4 Sequestration of Pb(II) in different pH

At pH values greater than 6.0, Pb(II) begins to precipitate out as Pb (OH)$_2$ as a result of the hydrolysis described below:

$$Pb^{2+} + OH^- \longrightarrow PbOH^+ \qquad (3.4)$$

$$PbOH^+ + OH^- \longrightarrow Pb(OH)_2 \downarrow \qquad (3.5)$$
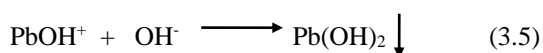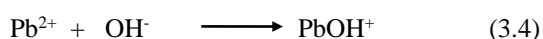
So, the impact of solution pH on Cd(II) biosorption was studied over a pH span of 2.0 to 6.0. 10 mL of P(II) with a concentration of ~30 mg L^{-1} was carried in various 15 mL centrifuging tubes, and 10 mg of SPP was added to each tube. The initial pH was respectively adjusted to 2.0, 3.0, 4.0, 5.0, and 6.0. The centrifuging tubes were shaken for 12 h with varying pH. The adsorbent was removed through centrifugation, and the initial and final amounts of Pb(II) in the supernatant were measured using ICP-OES.

3.9.5 Biosorption kinetics

Kinetic study of Pb(II) biosorption on SPP was performed till it attained equilibrium. For each experiment, 10 mg of SPP and 10 mL of a 10 mg/L Pb(II) at pH 6.0 were taken in a 15 mL centrifuging tube and well agitated at room temperature. Biosorption studies with varied contact times were conducted. The sample from each tube was immediately centrifuged or filtered after a set amount of time, and the final concentration of Pb(II) was measured. Calculations were made to determine

biosorption capacity at a certain time (t). To further understand the biosorption mechanism, the kinetic data were fitted to the PFO and PSO kinetic equations.

3.9.6 Biosorption isotherms

A biosorption isotherm investigation was performed at V/m ~1000 mL/g with solution pH 5.5 using the batch method. 10 mL of Pb(II) aqueous solution (5-450 mg/L) was taken in a 15 mL centrifuging tube. 10 mg of SPP was mixed, and the content was agitated for 12 h. Following biosorption, all the samples were filtered, and the equilibrium Pb(II) concentrations were examined. Pb(II) sorption behavior was modeled using the Freundlich and Langmuir isotherms. The essential features of the Langmuir model were also made clear using a dimensionless separation factor (R_L).

3.9.7 Effect of competitive ions

By introducing three different concentrations (25, 50, and 75 mg/L) of each competitive ions into a fixed concentration of 25 mg/L of Pb(II) solution, it was possible to assess the effects of competitive ions found in natural water, such as K^+, Ni(II), Cu(II) and Co(II) on adsorption of Pb(II). Additionally, the same procedure was used to prepare a blank sample without the use of a competitive ion. The solution's pH was maintained at 5.5. The mixture was stirred for 10 h at room temperature after the addition of the biosorbent dose of 1 g/L. To analyze the Pb(II) content, the centrifugate were collected.

3.10 Saponified pomegranate peel for removal of Cd(II) from water

3.10.1 Preparation of biosorbent

The synthesis procedure of biosorbent (SPP) has been described in detail in **Section 3.8.1**.

3.10.2 Physicochemical characterization of biosorbents

Using FE-SEM coupled with an EDX spectrometer, the morphology and elemental composition of as synthesized adsorbent were evaluated. The crystallinity was determined using XRD pattern. Using FTIR spectroscopy, the surface functionalities of the biosorbent were examined. Using a zeta potential analyzer, pH_{pzc} of the biosorbent was determined.

3.10.3 Biosorption experiments

The biosorption studies of removing Cd(II) onto SPP were carried out using the batch method. In all biosorption tests, the initial and equilibrium concentrations of Cd(II) solutions (1–1000 mg/L) were measured by the ICP-OES instrument. Cd(II) concentrations at the ppb level were analyzed using an ICP-MS instrument.

3.10.4 Effect of pH

Baseed on the pH aqueous medium, cadmium species can be found in aqueous solutions as Cd^{2+}, $Cd(OH)^+$, $Cd(OH)_2$, $Cd(OH)_3^-$, etc. (Garg *et al.*, 2008).

$$Cd^{2+} + H_2O \rightleftharpoons Cd(OH)^+ + H^+, \qquad pk_1 = 7.9 \qquad (3.6)$$

$$Cd(OH)^+ + H_2O \rightleftharpoons Cd(OH)_2 + H^+, \qquad pk_2 = 10.6 \qquad (3.7)$$

$$Cd(OH)_2 + H_2O \rightleftharpoons Cd(OH)_3^- + H^+, \qquad pk_3 = 14.3 \qquad (3.8)$$
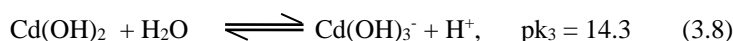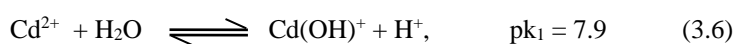
At pH values greater than 7, Cd(II) begins to precipitate out because of the hydrolysis. So, the impact of solution pH on Cd(II) biosorption was studied over a pH span of 2.0 to 7.0. 10 mL of Cd(II) with a concentration of ~30 mg L^{-1} was carried in various 15 mL centrifuging tubes, and 10 mg of SPP was added to each tube. The initial pH was respectively adjusted to 2.0, 3.0, 4.0, 5.0, 6.0, and 7.0; using 0.1M HCl and 0.1M NaOH. The centrifuging tubes were shaken for 24 h with varying pH. The adsorbent was removed through centrifugation, and the initial and final amounts of Cd(II) in the supernatant were measured using ICP-OES.

3.10.5 Biosorption kinetics

Kinetic study of Cd(II) biosorption on SPP was performed till it attained equilibrium. For each experiment, 10 mg of SPP and 10 mL of a 10 mg/L Cd(II) at pH 6.0 were taken in a 15 mL centrifuging tube and well agitated at room temperature. Biosorption studies with varied contact times were conducted. The sample from each tube was immediately centrifuged or filtered after a set amount of time, and the final concentration of Cd(II) was measured. Calculations were made to determine biosorption capacity at a certain time (t). To further understand the biosorption mechanism, the kinetic data were fitted to the PFO and PSO kinetic equations.

3.10.6 Biosorption isotherms

A biosorption isotherm investigation was performed at V/m ~1000 mL/g with solution pH 6 using the batch method. 10 mL of Cd(II) aqueous solution (5-450 mg/L) was taken in a 15 mL centrifuging tube. 10 mg of SPP was mixed, and the content was agitated for 12 h. Following biosorption, all the samples were filtered, and the equilibrium Cd(II) concentrations were examined. Cd(II) sorption behavior was modeled using the Freundlich and Langmuir isotherms. The essential features of the Langmuir model were also made clear using a dimensionless separation factor (R_L).

3.10.7 Effect of competitive ions

By introducing three different concentrations (25, 50, and 75 mg/L) of each competitive ions into a fixed concentration of 25 mg/L of Cd(II) solution, it was possible to assess the effects of competitive ions found in natural water, such as K(I), Ni(II), Cu(II) and Co(II) on adsorption of Cd(II). Additionally, the same procedure was used to prepare a blank sample without the use of a competitive ion. The solution's pH was maintained at 6.0. The mixture was stirred for 10 h at room temperature after the addition of the biosorbent dose of 1 g/L. To analyze the Cd(II) content, the filtrates were collected.

3.11   Zr(IV) modified pomegranate peel for the removal of phosphate

3.11.1 Preparation of the biosorbent

The synthesis procedure of biosorbent (SPP@Zr) has been described in detail in **Section 3.5.1**.

3.11.2 Characterization of biosorbents

Using FE-SEM coupled with an EDX spectrometer, the morphology and elemental composition of as synthesized adsorbent were evaluated. The crystallinity was determined using XRD pattern. Using FTIR spectroscopy, the surface functionalities of the biosorbent were examined.

3.11.3 Effect of pH

The pH studies were performed by taking 20 mL of PO_4^{3-} solution with 20 mg of the SPP@Zr in conical flasks and maintaining preliminary pH values from 2.0 to 11.0, before adding the biosorbent. Each sample was shaken using a mechanical shaker at room temperature. The equilibrium pH was evaluated by utilizing a digital pH meter. The filtrate was utilized for the residual PO_4^{3-} concentration. The initial pH value at which maximum biosorption occurred at equilibrium, was adjusted for further studies to ensure maximum biosorption.

3.11.4 Biosorption kinetics

With a preliminary phosphate concentration of ~25 mg/L and an adsorbent dose of 1 g/L, a kinetic experiment of PO_4^{3-} biosorption onto SPP@Zr was performed. The pH was held constant at 4.0 during the experiment. The sample from each flask was filtered after a certain length of time, and the PO_4^{3-} concentration was analyzed. Calculations were made to determine the biosorption capacity of PO_4^{3-} at a certain time (t).

3.11.5 Biosorption isotherm studies

With a range of starting PO_4^{3-} concentrations (5 to 500 mg/L) and a dose of 1 g/L, a biosorption isotherm experiment was conducted. The pH of the solution remained at 4.0 throughout the experiment. The flasks were swirled for 12 h at room temperature. Following biosorption, all the samples were filtered, and the equilibrium PO_4^{3-} concentrations were examined. Phosphate sorption behavior was modeled using the Freundlich and Langmuir isotherms.

3.11.6 Influence of competitive ions

By introducing 0.01 M of NaCl, Na_2SO_4, $NaNO_3$ and Na_2CO_3 into a 20 mg/L phosphate solution, it was possible to assess the effects of competitive ions found in natural water on the biosorption of phosphate. Additionally, the same procedure was used to prepare a blank sample without the use of a competitive ion. The solution's pH was maintained at 4.0. The mixture was stirred for 10 h at room temperature after the addition of the biosorbent dose of 1 g/L. To analyze the phosphate content, the filtrates were collected.

3.11.7 Regeneration and reusability of SPP@Zr

0.1 M NaOH solution was mixed with 25 mg of the spent biosorbent for 12 h to liberate the arsenate ion to evaluate the regeneration of SPPP@Zr. It was filtered and dried in an oven. The regenerated biosorbent was again employed for PO_4^{3-} biosorption. To evaluate the reusability of the biosorbent, five sequential cycles of the biosorption/regeneration process were performed. For each succeeding cycle, the % biosorption of PO_4^{3-} was assessed.

3.12   Application of SPP@Zr to natural groundwater

The biosorption capability of SPP@Zr was examined using groundwater tainted with arsenic to determine the viability of SPP@Zr for removing arsenic from real sample of water. For this, groundwater samples were taken in Nawalparasi West, Lumbini Province, Nepal, from an arsenic-contaminated location. The details of the sampling and analysis protocols are described as follows. Prior to sampling, the hand pumps were flushed with 30–40 L of water. Water was filled into the bottle until it was completely full, with no air bubbles present. For the determination of total arsenic and iron, samples were acidified with 2% v/v HCl. But the anion analysis samples weren't acidified. Following sampling, pH measurements were made immediately in the field. The methods prescribed in APHA-AWWA-WEF 2012, 22nd Edition were used to assess alkalinity, total dissolved solids, hardness, chlorides, phosphates, and sulfate (Baird *et al.*, 2012). Fluoride was measured using a fluoride selective electrode. By using an ICP-MS, iron and total arsenic were measured.

3.13   Statistical analyses

All investigates were accomplished in triplicate and the findings were represented as the mean ± standard deviation. Using the OriginPro 8.5 program, linear and non-linear regression analyses were carried out, and the correlation coefficient (R^2) was utilized to assess the goodness of fit to a biosorption model. All the graphs were plotted from experimental data using the OriginPro 8.5 program.

CHAPTER 4

RESULTS AND DISCUSSION

4.1 As(V) removal onto Zr(IV) modified pomegranate peels (SPP@Zr)

4.1.1 Characterizations of biosorbents

4.1.1.1 FE-SEM micrograph

In contrast to the smooth, homogenous, and non-porous morphology seen in the FE-SEM micrograph of RPP (**Figure 13(a)**), surface alteration is seen after saponification. The image of SPP (**Figure 13(b)**) shows that it has somewhat uneven, and heterogeneous surfaces. The waxy substances, such as limonene and sugar molecules, may have been bleached or removed from the surface during saponification by chemical treatment ($Ca(OH)_2$), revealing the rough surface. After the Zr(IV) loading, pores were occupied with Zr(IV) ions (**Figure 13(c)**). After As(V)biosorption, the As(V) aggregates, and forms layers on the surface, as seen in the FE-SEM image (**Figure 13(d)**).

4.1.1.2 EDX spectra with elemental colour mapping

The nature and elemental mapping of RPP, SPP, SPP@Zr and As(V) adsorbed SPP@Zr were evaluated through surface mapping with EDX analysis. The significant peaks associated with C, O, and S are seen in the EDX spectra of RPP (**Figure 13(a)**). Saponification resulted in the appearance of new peaks associated with Ca (in the EDX spectra of SPP) (**Figure 13(b)**). After zirconium impregnation (SPP@Zr), the peak associated with Ca almost vanished, and additional peaks associated with Zr were observed, indicating that the Zr(IV) ions had effectively loaded onto SPP and had replaced Ca(II) ions via a cation exchange process(**Figure 13(c)**). The EDX spectra (**Figure 13(d)**), which also showed another peak associated with arsenic, showed that the loaded Zr(IV) did not leach away following the sorption of As(V). This was further confirmed by surface color mapping, which is shown in **Figure 14(a)** and shows the elemental distribution. The EDX colour mapping investigation of the arsenic adsorbed SPP@Zr (**Figure 14(b)**) demonstrates that As(V) biosorption is uniform.
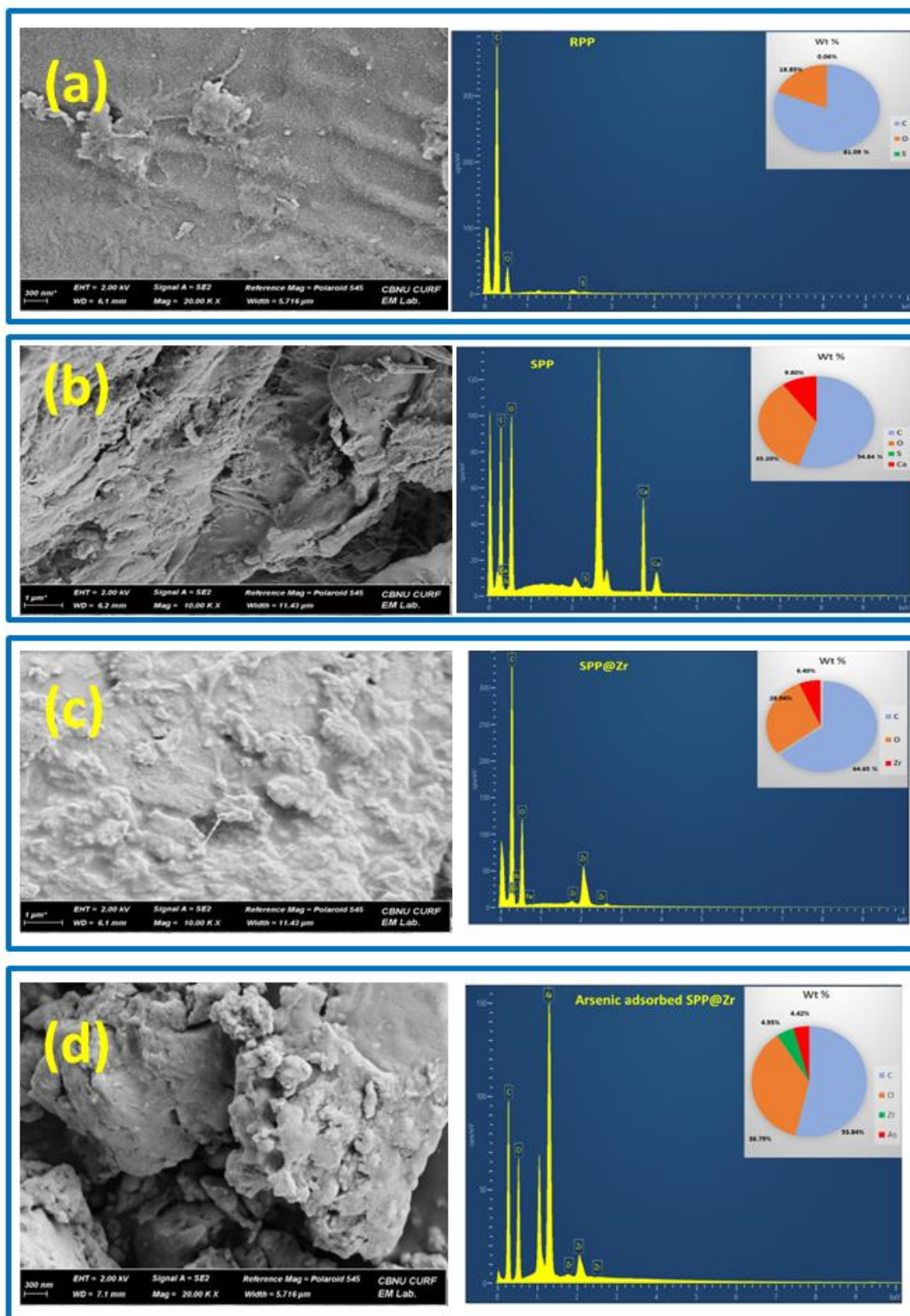
Figure 13: (a) FE-SEM micrographs and EDX spectra of (a) RPP; (b) SPP; (c) SPP@Zr, and (d) As(V) adsorbed SPP@Zr.

76
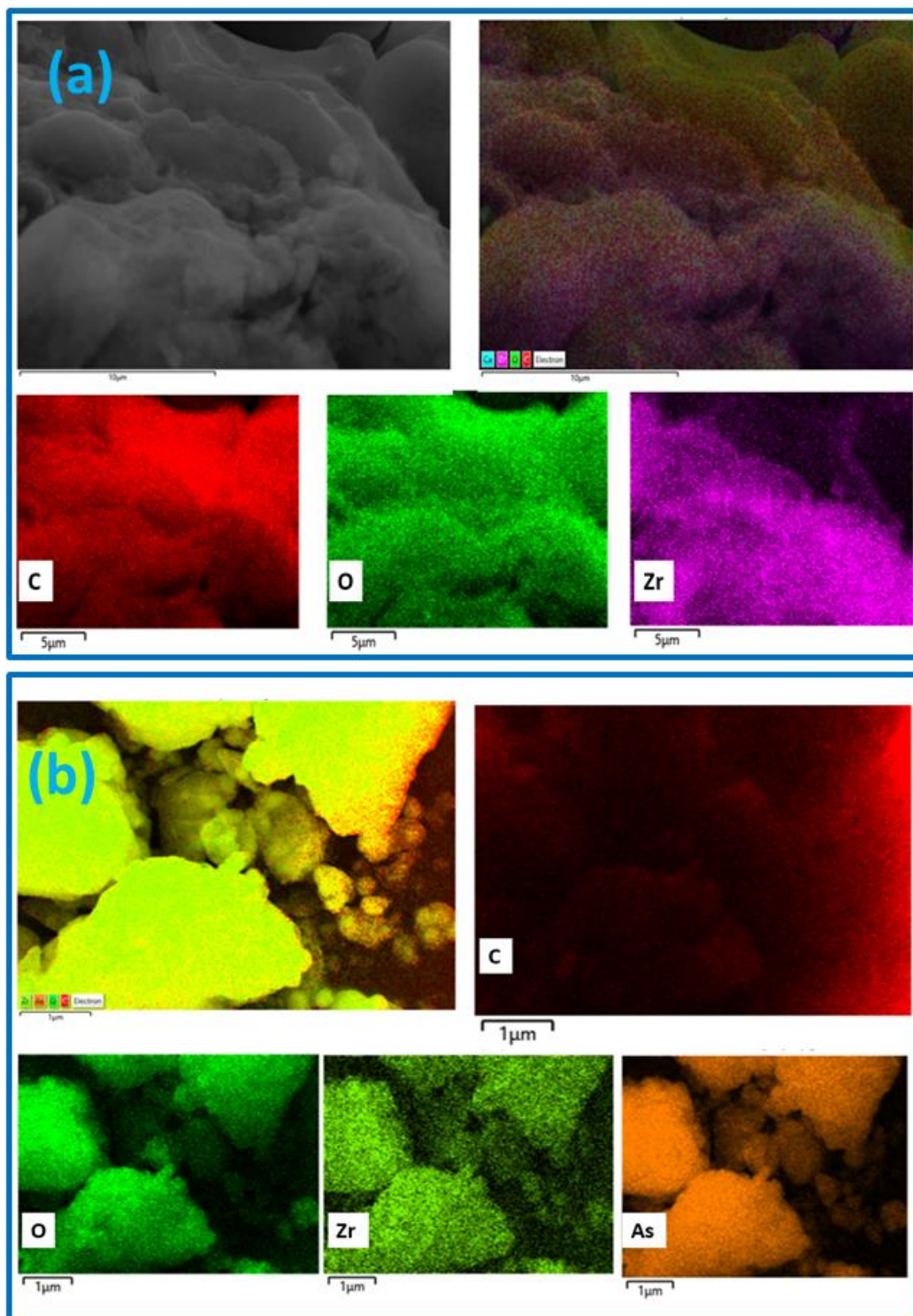
Figure 14: EDX colour mapping images of all overlapping elements of SPP@Zr (a) before and (b)after biosorption.

4.1.1.3 XRD pattern of biosorbent

The XRD pattern of raw PP and SPP@Zr is seen in **Figure 15(a)**. The XRD plot analysis of both samples revealed the absence of any observable sharp peaks that may be attributable to the crystalline structure. In the spectrum of the SPP@Zr, there were likewise no confirmed peaks associated with zirconium modification. Due to the lack of calcine used in the adsorbent's synthesis, which is a crucial step in the crystallization of zirconium hydroxide, it predominately had an amorphous form (Rahman et. al., 2021; Guo & Chen, 2004).

4.1.1.4 Functional group analysis using FTIR Spectroscopy

The FTIR spectra of RPP, SPP, SPP@Zr, and As(V) adsorbed SPP@Zr are shown in **Figure 15(b)**. The broadband at 3347.13 cm^{-1} is related with the vibration of the –OH group in the spectrum of RPP, while the narrower peak at 2920.9 cm^{-1} is related with the–CH and –CH2 units. The–COO and C=O groups, respectively, are connected to the peaks at 1731.16 and 1613.98 cm^{-1}. The C=O stretching vibration of the –COO group is accountable for the band at 1629 cm^{-1} (Poudel et. al., 2020). The –C–O– linkage found in alcoholic, phenolic, and carboxylic groups accounts for the vastly intense signal at 1018.12 cm^{-1} (Poudel et. al., 2020; Paudyal et. al., 2013). Pectic acid, an important component found in pomegranate peel, is thought to have a characteristic functional group called carboxyl that is used to prepare ion exchangers.

The band of the carboxylic group at 1731.16 cm^{-1} vanished after saponification, and two additional peaks formed at 1605.88 and 1420.79 cm^{-1} in the FTIR spectra of SPP, indicating the existence of the O-Ca linkage of calcium pectate. The peaks for SPP that were previously seen at 1605.88 and 1420.79 cm^{-1} have now moved to 1625.95 and 1410.66 cm^{-1} following Zr(IV) loading (in SPP@Zr). These band shifts indicate the formation of zirconium pectate after Zr(IV) ions are substituted for Ca(II) ions. The -Zr-OH vibration may be related to the two peaks at 1148.17 and 1076.12 cm^{-1} (Lou et. al., 2021). Like the previous peak, the strong peak at 945.13 cm^{-1} is connected to -Zr-O linkage (Rahman *et al.*, 2021). It shows that SPP@Zr contains a lot of Zr-OH groups and provides convincing proof that Zr(IV) was effectively loaded onto SPP. After As(V) biosorption, the band at 3325.97 cm^{-1} (OH stretching vibration) was observed to be weaker. It was most likely caused by the role of OH-groups in

As(V) biosorption. In the same way, the band at 1076.12 cm^{-1} (Zr-OH) was reduced, and a further band for Zr-O-As vibration was seen at around 816.23 cm^{-1}. This implies that the As(V) anion replaced the -OH group.
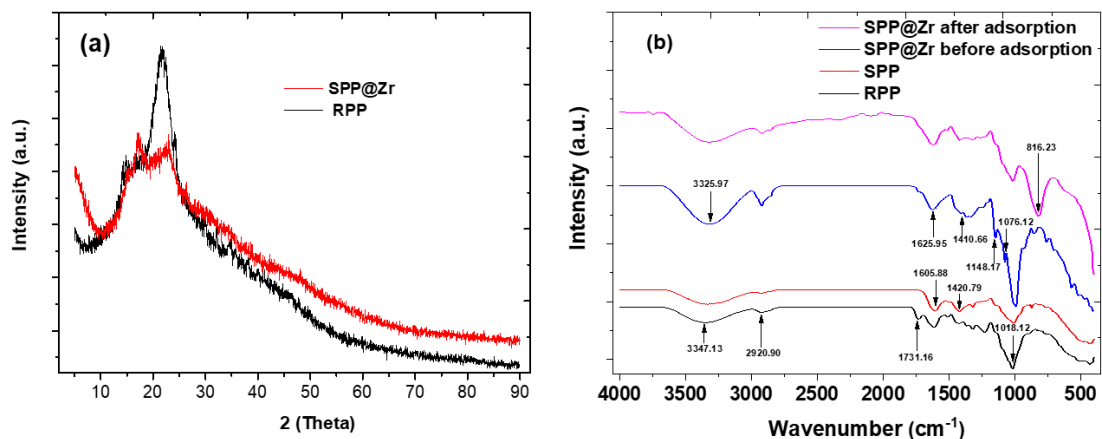
Figure 15: (a) XRD spectra of RPP and SPP@Zr; (b) FTIR spectra of RPP, SPP, SPP@Zr and As(V) adsorbed SPP@Zr

4.1.1.5 Zeta potential analysis of biosorbent

Figure 16 shows the zeta potential of SPP@Zr as determined at several pH levels. A raise in pH caused in a decline in zeta potential value.
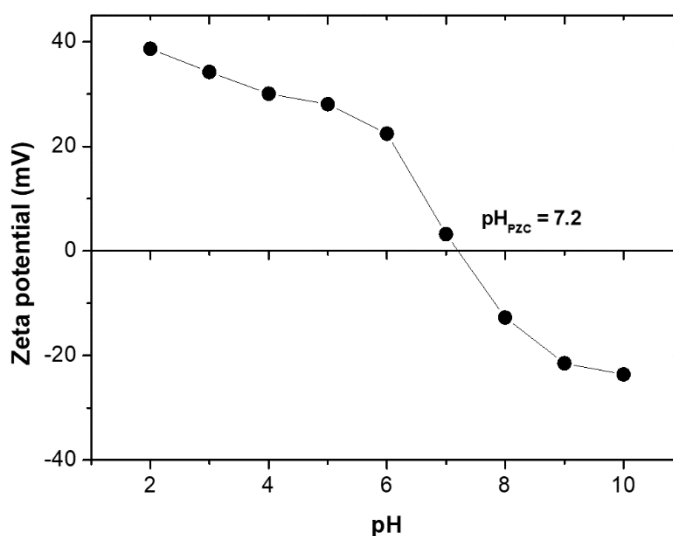
Figure 16: Zeta potential of SPP@Zr.

The calculated point of zero charges (pH$_{PZC}$) was 7.2. The SPP@Zr surface becomes positively charged when the pH of the solution falls below pH$_{PZC}$, which is

79

advantageous for the strong electrostatic attraction-based biosorption of the As(V) anion. At pH > pH$_{PZC}$, the repulsion between negatively charged SPP@Zr and negatively charged As(V) anions causes poor biosorption. As a result, at pH < 7.2, SPP@Zr may eliminate As(V) species more effectively.

4.1.2 Preliminary batch experiment

To compare the As(V) ion biosorption capacities of raw pomegranate peel (RPP) and SPP@Zr, simple batch biosorption studies were conducted. Several conical flasks were filled with starting As(V) solutions of 10, 20, 50, and 100 mg/L at pH 4.0 and biosorbent dosage of 1 g/L. Before filtering, the suspensions were stirred for 12.0 h at 298 K. The concentration of As(V) in the filtrates was determined. The findings displayed in **Table 5** demonstrated that SPP@Zr has a superior capability for adsorbing As(V) than RPP. It was found that very low As(V) could be absorbed by RPP. As a result, the sole adsorbent for the subsequent experiments was SPP@Zr.

Table 5: Comparing the biosorption capacity of PP and SPP@Zr to remove As(V).

Biosorbent	q_e (mg/g) for different initial concentrations of As(V)			
	10 mg/L	20 mg/L	50 mg/L	100 mg/L
RPP	2.15 ± 0.08	3.78 ± 1.20	6.85 ± 0.31	11.50 ± 0.50
SPP@Zr	8.8 ± 0.35	16.34 ± 0.73	38.87 ± 1.8	59.24 ± 1.30

4.1.3 Effect of solution pH

Regarding As(V) speciation and biosorbent charge, the pH of the wastewater that has to be treated is a critical control factor in the As(V) biosorption process. Various arsenate species can be provided in an aqueous medium at varying pH levels. Equations (4.1) -(4.3) demonstrated As(V) speciation with an equilibrium constant (Shabbir et. al., 2020; Awual et. al., 2008). **Figure 17** presents a curve that depicts the aqueous As(V) species at various pH levels.

$$H_3AsO_4 \rightleftharpoons H_2AsO_4^- + H^+ \qquad pK_{a1} = 2.3 \qquad (4.1)$$
$$H_2AsO_4^- \rightleftharpoons HAsO_4^{2-} + H^+ \qquad pK_{a2} = 6.8 \qquad (4.2)$$
$$HAsO_4^{2-} \rightleftharpoons AsO_4^{3-} + H^+ \qquad pK_{a3} = 11.6 \qquad (4.3)$$
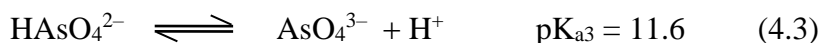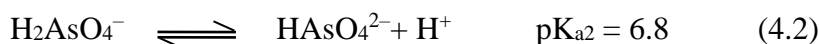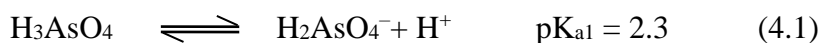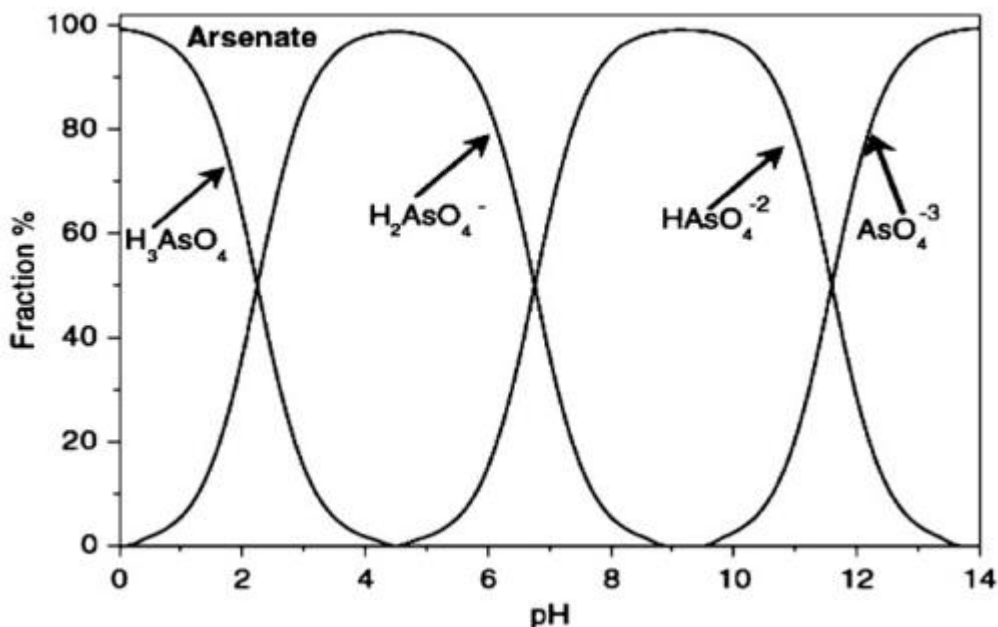
Figure 17: Curve depicting the As(V) species at various pH values (Adapted with permission from Camacho *et al.*, 2011, Copyright, Elsevier).

Figure 18(a) shows the % removal of As(V) *vs* equilibrium pH. Arsenate was removed to the greatest extent at weakly acidic and neutral conditions, as shown in the figure. At pH 3.0 to 7.0, a larger percentage of biosorption was seen, and at a pH higher than 7.2, the percentage of biosorption dramatically decreased. Due to the significant electrostatic interaction between the negatively charged arsenate ion ($H_2AsO_4^-$, $HAsO_4^{2-}$) and the substantially positive surface charge on SPP@Zr at pH $<pH_{PZC}$, the strongly positive surface charge of the biosorbent is beneficial in As(V) biosorption. Nevertheless, when pH $>pH_{PZC}$, the concentration of OH^- ions rises with pH, increasing the negative surface charge on SPP@Zr. As a result, the negative surface charge of SPP@Zr and the arsenate anions ($HAsO_4^{2-}$, AsO_4^{3-}) are repelled from each other. Biosorption of As(V) anions may be significantly reduced at high pH due to competition for biosorption sites between OH^- ions and As(V) anions (Biswas et. al., 2008b). Because As(V) occurs in an aqueous solution as neutral H_3AsO_4 at pH < 2.3 and lacks the binding force to be completely adsorbed by the adsorbent under extremely acidic conditions, sorption at pH < 2.0 is relatively low. As a result, the pH of 4.0 was determined to be optimal for removing (V) from an aqueous solution using SPP@Zr. **Figure 18(b)** shows the percent biosorption versus starting pH as well as the equilibrium pH versus starting pH. The equilibrium pH increased following the

81

sorption, suggesting that a ligand exchange mechanism was used throughout the process to release the hydroxide ions into the solution.
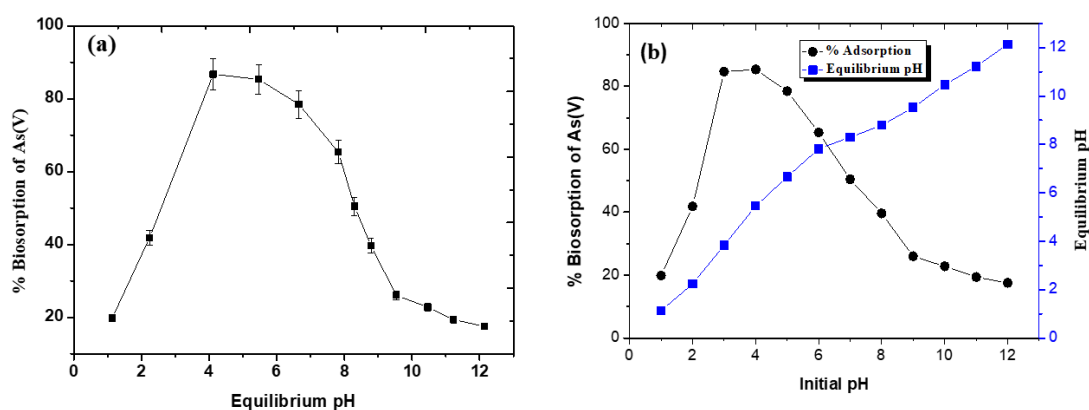
Figure 18: The influence of pH on the biosorption of As(V). (a) % biosorption of As(V) *vs* Equilibrium pH; (b) Equilibrium pH and % biosorption of As(V) vs initial pH.

4.1.4 Biosorption kinetics

The kinetics of As(V) biosorption on SPP@Zr have been investigated. **Figure 19(a)** depicts the equilibrium concentration and percent biosorption of arsenate vs. contact time. The biosorption efficiency improved dramatically over time. At first, the biosorption rate was high; after that, it dropped, and after 5 h, equilibrium was reached. Since the equilibrium is established in less than 5 h, the contact period was set at 12 h in the tests that followed to ensure that As(V) completely adsorbs to SPP@Zr. To further understand the kinetic process, the PFO and PSO models were suited to the kinetic data.
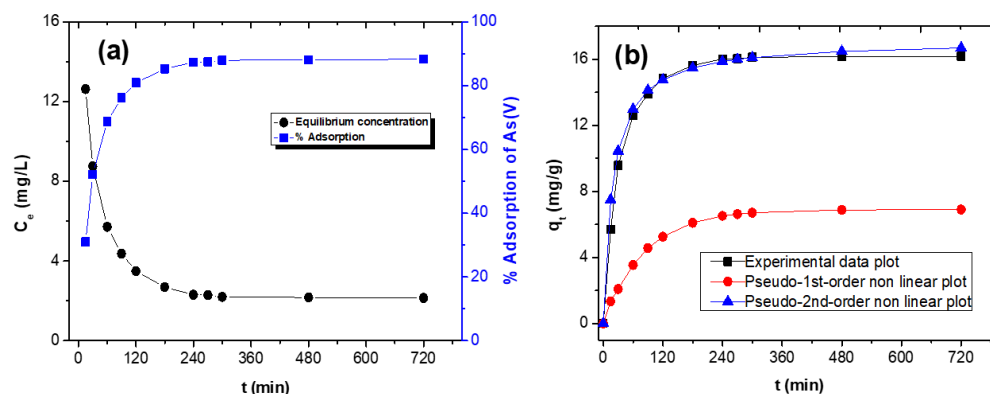
Figure 19: Biosorption kinetics study of As(V): (a) equilibrium concentration and % biosorption *vs* t; (b) kinetic data and non-linear kinetics modeling with the PFO and PSO kinetics.

82

To calculate k_1 and k_2, q_e, and R^2, two independent graphs of log(q_e–q_t) against t (**Figure 20**) and t/q_t against t (**Figure 21**) were drawn. **Table 6** lists the estimated values for the kinetic parameters. Compared to the PFO model, R^2 of the PSO model (0.999) was nearer to unity. Additionally, the theoretical equilibrium biosorption capacity of SPP@Zr in the PSO kinetic (q_e(cal)) = 16.95 mg/g is near the actual result (q_e(exp)) = 16.20 mg/g. Due to the better fitting with PSO kinetics, biosorption of arsenate may be led by chemisorption. The best match of the kinetic data to the PSO kinetics is also shown by the non-linear kinetic plot (**Figure 19(b)**) of q_t *vs* t.
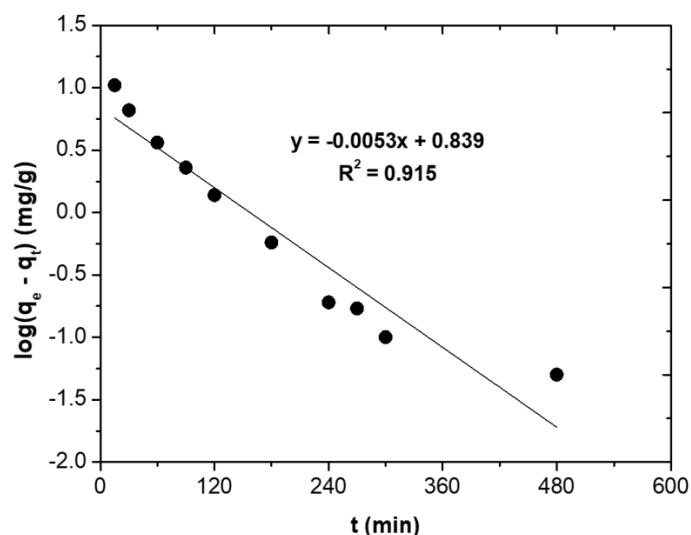
Figure 20: PFO kinetics plot of SPP@Zr with As(V) system.
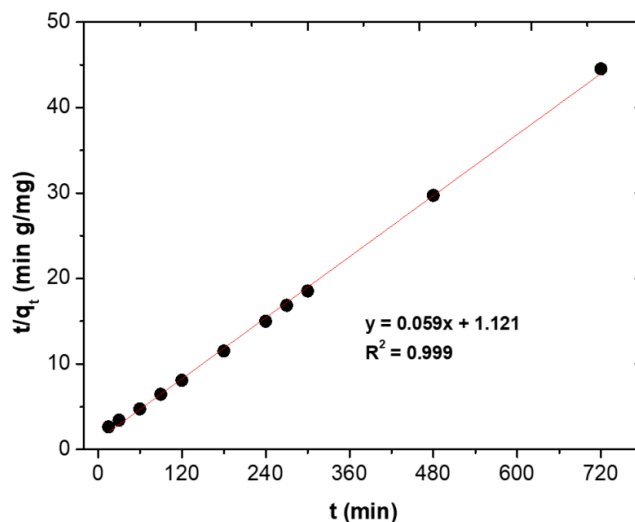
Figure 21: PSO kinetics plot of SPP@Zr with As(V) system.

Table 6: Kinetic parameters for As(V) biosorption on SPP@Zr.

Model	R^2	q_e (exp) (mg/g)	q_e (cal) (mg/g)	k_1 (min^{-1})	k_2 (g /mg.min)
PSO	0.999	16.20 ± 0.73	16.95 ± 0.33	-	3.10×10^{-3}
PFO	0.910	16.20 ± 0.73	6.90 ± 0.21	12.20×10^{-3}	-

The kinetic models described above do not forestall the diffusion mechanism and the rate-controlling stage in the biosorption. Hence, the Weber-Morris and Boyd models are used to assess the kinetic data. The fitted Weber-Morris model (**Figure 22**) has three linear portions, signifying the three stages in biosorption. Each of these 3 parts represents the film diffusion, intraparticle diffusion, and time to equilibrium (Lebron et. al., 2021). However, the measured c values did not equal zero, it is plausible to infer that there were other rate-controlling steps in the sorption process in addition to intraparticle diffusion. Furthermore, the Weber-Morris model's lower R^2 values than those for the PSO model lend credence to the claim that intra-particle diffusion is not likely to be the solely rate-controlling stage. **Table 7** lists the estimated Web-Morris parameter values.
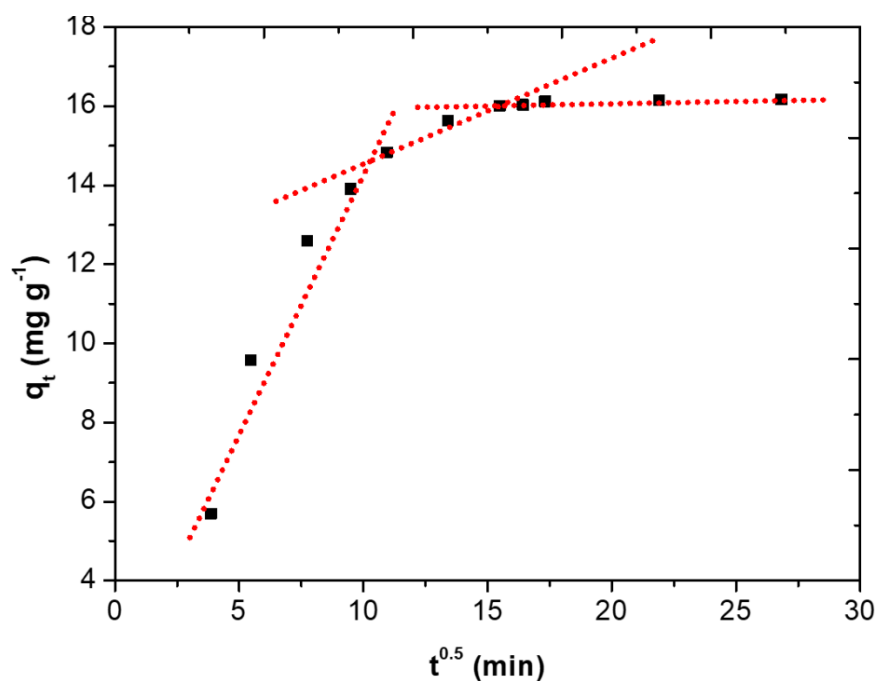
Figure 22: Rate limiting step evaluation for As(V) biosorption onto SPP@Zr by Weber and Morris model.

Table 7: Diffusion parameters of As(V) biosorption onto SPP@Zr.

Model	Parameters	Value
Weber & Morris		
	$k_{2,0\ W\&B}$ (mg g^{-1} min$^{-0.5}$)	0.383 ± 0.004
	c_0 (mg g^{-1})	8.703 ± 0.32
	R^2	0.575
Weber & Morris- Boundary layer diffusion		
	$k_{2,1\ W\&B}$ (mg g^{-1} min$^{-0.5}$)	1.4 ± 0.02
	c_1 (mg g^{-1})	0.865 ± 0.07
	R^2	0.927
Weber & Morris- Intraparticle diffusion		
	$k_{2,2\ W\&B}$ (mg g^{-1} min$^{-0.5}$)	0.341 ± 0.005
	c_2 (mg g^{-1})	10.88 ± 0.41
	R^2	0.916
Weber & Morris- Equilibrium		
	$k_{2,3\ W\&B}$ (mg g^{-1} min$^{-0.5}$)	0.012 ± 0.002
	c_3 (mg g^{-1})	15.89 ± 0.37
	R^2	0.721

It is discovered that Weber-Morris $k_{2,i\ W\&B}$ values are in the order $k_{2,1\ W\&M} > k_{2,2\ W\&M} > k_{2,3\ W\&M}$. Once the surface sites have been completely occupied by arsenate ions, the biosorbent is exhausted, and the rate-limiting phase is the transition from the outside to the interior adsorbent sites (Moreira *et al.*, 2019). The equilibrium period for the biosorption of arsenate was approximately 240 minutes ($t^{0.5} = 15.5$ min).

The findings of the Weber-Morris model were further corroborated by Boyd's model, which exhibited that the plot (**Figure 23**) did not overlap the origin despite a linear relationship between B_t and t ($R^2 = 0.911$).
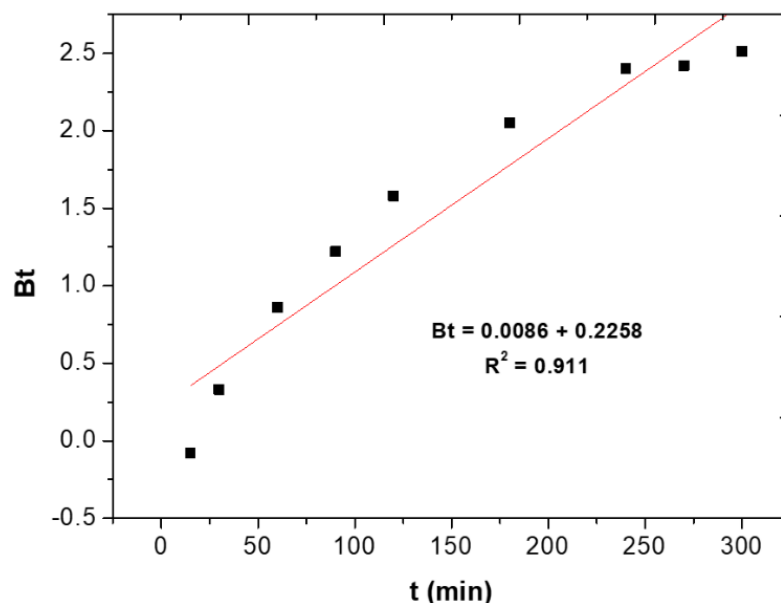
Figure 23: Boyd plots for arsenate biosorption onto SPP@Zr.

4.1.5 Biosorption isotherm

The fluctuation of the initial As(V) concentration was used to designate the biosorption isotherm. **Figure 24(a)** displays the arsenate biosorption isotherms at different temperatures. The results exhibit that when the As(V) ion concentration increased, the biosorption capacity increased quickly, then gradually until it reached saturation (plateau) at high concentrations. The initial high biosorption rate might be due to the increasing amount of accessible sorption sites for the biosorbent. Since the biosorption capacity has peaked at a high concentration area, no more sites are available for further biosorption.

The experimental data were examined utilizing the Langmuir and Freundlich isotherm models to elucidate the As(V) biosorption performance. **Figure 25** depicts the plot of C_e/q_e vs C_e utilizing the Langmuir model. **Figure 26** depicts the graph of the Freundlich model's linear relationship between $\log q_e$ and $\log C_e$. The assessed values for the isotherm parameters are listed in **Table 8**. The results showed that the equilibrium data depicted by the Langmuir model had a superior R^2 than the Freundlich model. Therefore, the Langmuir model would be a better fit to explain how As(V)adsorbs onto SPP@Zr. It showed that the biosorption processes, which were thought to be monolayer homogenous biosorption processes, occurred on the

86

biosorbent surface. The non-linear fitting of experimental data with modeling findings from both models at 298 K was compared with the experimental data to further confirm the superior fit to the Langmuir model. The non-linear isotherm plot between C_e and q_e (**Figure 24(b)**) illustrates this.
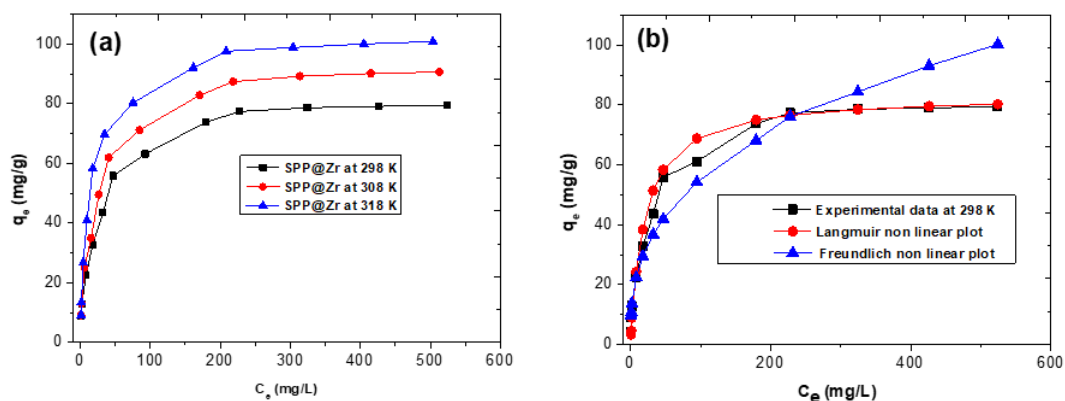
Figure 24: (a) Temperature-dependent biosorption isotherm for As(V) onto SPP@Zr; (b) Non-linear plot of equilibrium data and modeling results by the Langmuir and Freundlich isotherms at 298 K.
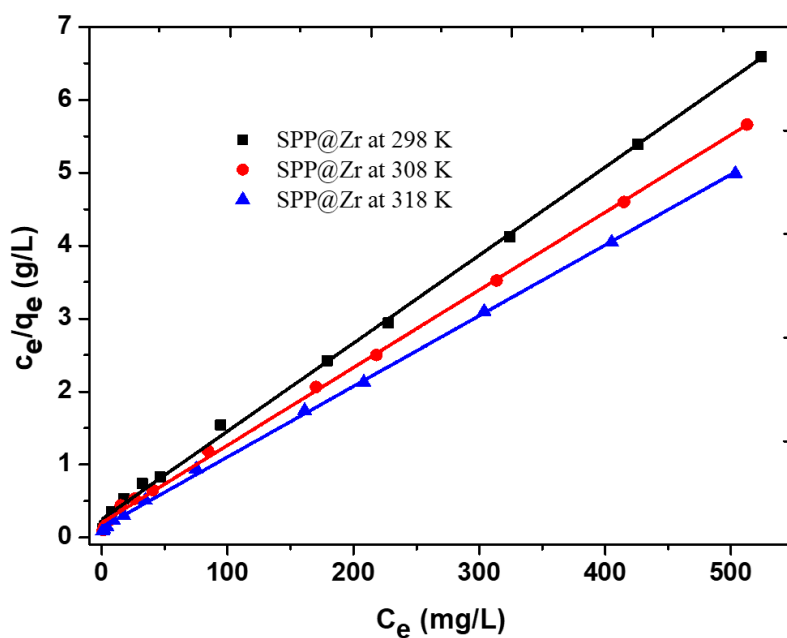
Figure 25: Linearized Langmuir plot of SPP@Zr with As(V) at various temperatures.
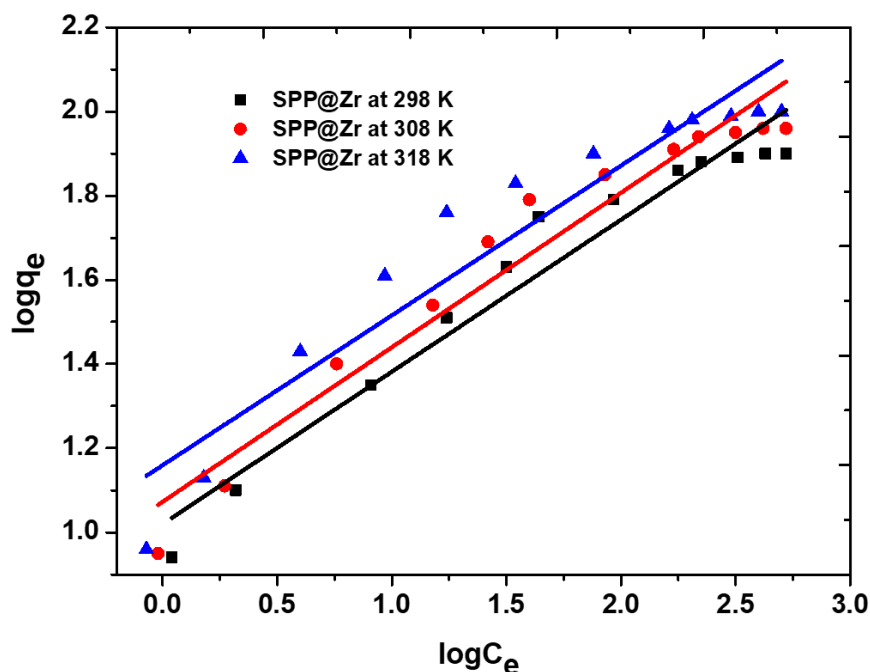
Figure 26:   Linearized Freundlich plot of SPP@Zr with As(V) at various temperatures.

At room temperature (298 K), the q_m of SPP@Zr for As(V) estimated applying the Langmuir model was 83.33 mg/g. This value is greater than several other materials mentioned in earlier research, as shown in **Table 9**. It implies that SPP@Zr might be an effective anion exchanger for removing As(V) from contaminated water.

Table 8: Isotherm parameters for As(V) biosorption onto SPP@Zr.

Isotherm model	Parameter	298 K	308 K	318 K
Langmuir isotherm	q_m(mg/mg)	83.33 ± 2.37	93.89 ± 2.53	103.30 ± 3.37
	b (L/mg)	0.048 ± 0.002	0.053 ± 0.004	0.071 ± 0.003
	R^2	0.999	0.999	0.999
Freundlich isotherm	K_F (mg/g) (L/mg)$^{1/n}$	10.47 ± 0.23	11.82 ± 0.37	14.52 ± 0.87
	n	2.77 ± 0.04	2.72 ± 0.04	2.80 ± 0.04
	R^2	0.949	0.942	0.940

Table 9: Comparison of q_m of SPP@Zr for As(V) with other biosorbents.

Adsorbent	Optimum pH	q_m (mg/g)	Reference
Iron loaded *Aegle marmelous* leaves	3.0	69.65	(Sahu *et al.*, 2019)
Iron impregnated *Citrus limetta* fruit waste	3.0	2.0	(Verma *et al.*, 2019)
Fe(III) treated sawdust of spruce	6.0	9.86	(Urik *et al.*, 2009)
Fe_2O_3 treated Sugarcane bagasse	4.0	22.1	(Pehlivan *et al.*, 2013)
Zr(IV) loaded orange waste	3.0	88.0	(Biswas *et al.*, 2008a)
Iron-grafted luffa fiber	7.0	2.55*	(Nguyen *et al.*, 2020b)
Zirconium-grafted luffa fiber	7.0	2.89*	(Nguyen *et al.*, 2020b)
Jute fiber and Fe_2O_3 nanocomposite	3.0	48.06	(Sahu *et al.*, 2017)
Iron modified orange peel	6.0	81.3	(Meng *et al.*, 2017)
Iron-Zirconium binary oxide	7.0	46.1	(Ren *et al.*, 2011)
Fe(III) treated *Staphylococcus xylosus*	3.0	61.34	(Aryal *et al.*, 2010)
Zirconium modified biochar	6.0	33.1	(Rahman *et al.*, 2021)
Zirconium-iron modified biochar	6.0	62.5	(Rahman *et al.*, 2021)
Zr-chitosan modified sodium alginate composite	2.0-3.0	76.78	(Lou *et al.*, 2021)
CuO impregnated biochar	4.0	12.47	(Imran *et al.*, 2021)
Zirconium-based magnetic sorbent	2.6-3.3	45.6	(Zheng *et al.*, 2009)
Zirconium modified pomegranate peel (SPP@Zr)	4.0	83.33	This work

*Initial concentration of As(V) solution = 0.5 mg L^{-1}
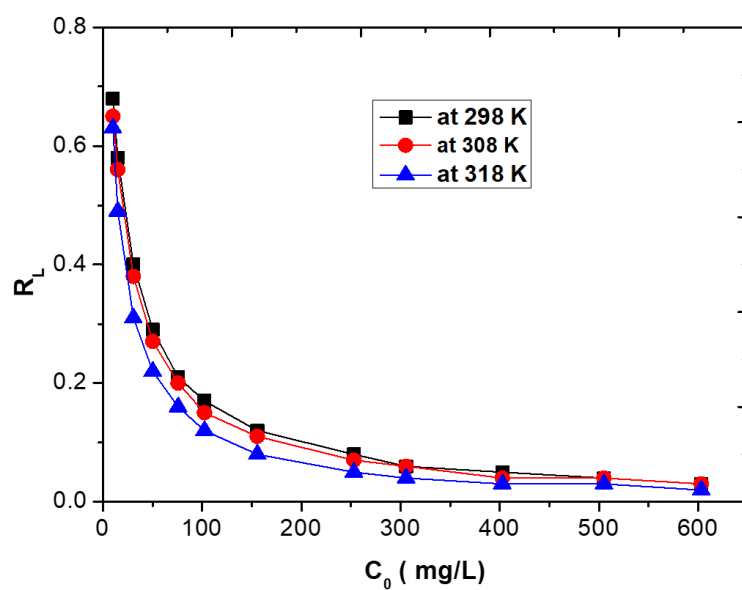
Figure 27: Value of R_L at various temperatures.

Figure 27 displays the estimated values of R_L based on the experimental data. In this investigation, $0 < R_L > 1$ was observed, suggesting that As(V) adsorption onto SPP@Zr is favorable and that there is a strong bond between As(V) anions and the surface of SPP@Zr.

4.1.6 The error analysis

For two isotherms and two kinetics models, the error values of the As(V) biosorption capacity of SPP@Zr were determined and are shown in **Table 10**. According to the table, As(V) biosorption onto SPP@Zr demonstrated a superior match to the PSO kinetics and Langmuir isotherm models with smaller computed error values. The As(V) biosorption onto SPP@Zr was consistent between the error values and R^2 values, according to the results of the error analysis.

Table 10: Error analysis for isotherm and kinetics models.

Error function	Isotherm model		Kinetics model	
	Langmuir	Freundlich	PSO	PFO
χ^2	0.24 ± 0.04	3.37 ± 0.41	0.62 ± 0.032	47.9 ± 2.15
RMSE	0.57 ± 0.03	6.31 ± 0.33	0.53 ± 0.028	8.76 ± 0.35
APE (%)	4.89 ± 0.05	10.38 ± 0.34	3.41 ± 0.14	62.73 ± 1.8

4.1.7 Thermodynamic studies

The ΔH^0 and ΔS^0 were obtained from the van't Hoff plot of $\ln K_C$ *vs* $1/T$ as revealed in **Figure 28**. A straight line with an R^2 of 0.999 results from the plot. The estimated thermodynamic parameter values are displayed in **Table 11**. All temperatures under study had negative $\Delta G°$ values, suggesting that this biosorption process is feasible, thermodynamically favorable, and spontaneous (Chiban *et al.*, 2016). The positive value of $\Delta H°$ suggested an endothermic sorption process. The fact that the q_m increased as the temperature increased supports this conclusion as well.

Table 11: Thermodynamic parameters.

T (K)	K_C	ΔG^0 (kJ/mol)	ΔH^0 (kJ/mol)	ΔS^0 (J /mol. K)
298	19.96×10^4	-30.23 ± 1.35		
308	22.04×10^4	-31.50 ± 1.72	15.82 ± 1.32	154.47 ± 4.32
318	29.52×10^4	-33.31 ± 1.47		
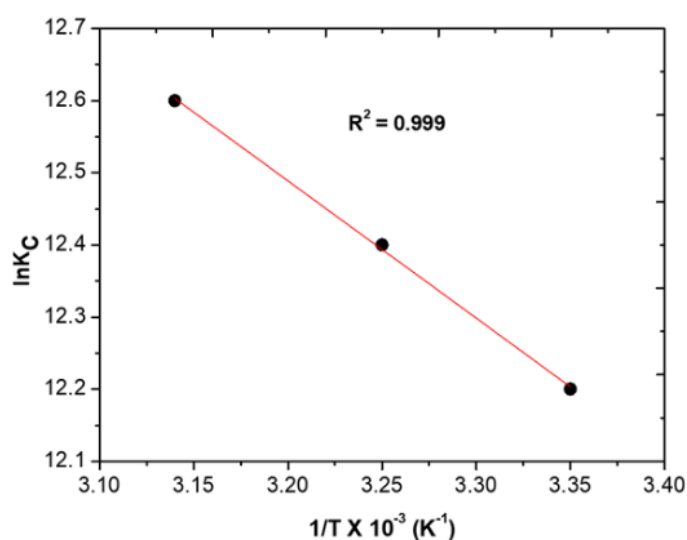
Figure 28: Van't Hoff plot of lnK_C *vs* of $1/T$

4.1.8 Influence of competitive ions

It was investigated how different competing ions affected the removal of arsenate ions, and the findings are shown in **Figure 29**.
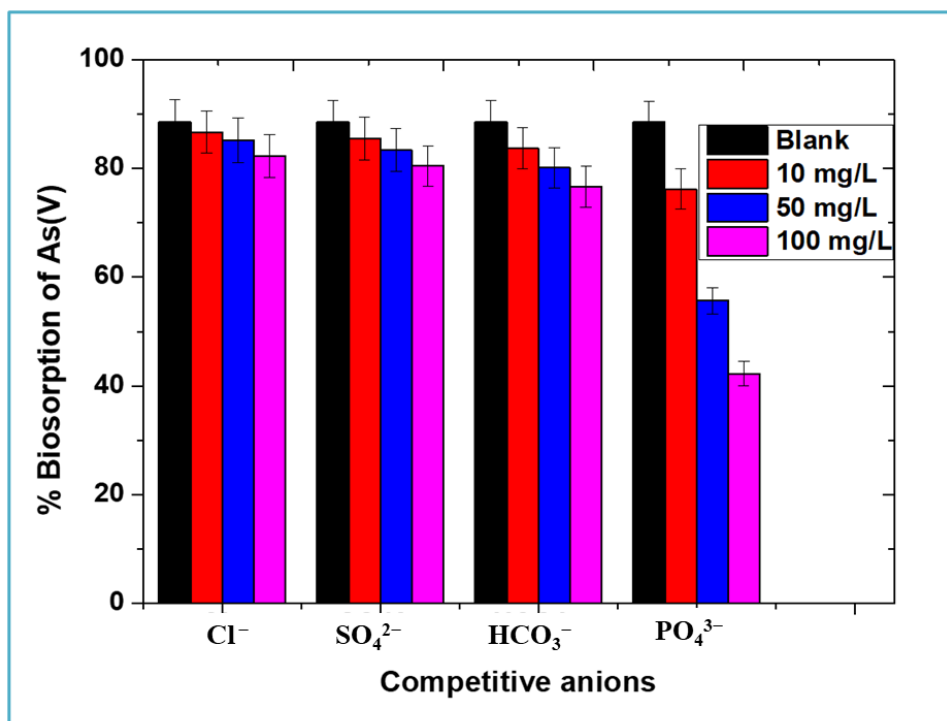
Figure 29: Effect of competitive anions for the removal of As(V) on SPP@Zr.

As seen in the figure, relative to the blank, the presence of Cl^-, SO_4^{2-}, and HCO_3^- at any concentration level very slightly reduces the percentage of As(V) that is adsorbed.

This could be since these ions are less capable of binding than arsenate ions (Verma *et al.*, 2019; Sawood & Gupta, 2020). However, because phosphate and arsenate ions compete for binding sites on the adsorbent, the addition of PO_4^{3-} significantly reduced As(V) biosorption. Arsenate and phosphate have chemical and structural similarities in an aqueous solution, which contributes to the dramatic drop in arsenate biosorption in its presence (Sahu *et al.*, 2019; Sahu *et al.*, 2017).

4.1.9 Regeneration and reusability of SPP@Zr

A good biosorbent has a superior biosorption capacity while simultaneously being easily regenerable or desorbable and maintaining a high capacity for biosorption after recycling to save operational expenses. Even though As(V) is weakly adsorbed on SPP@Zr at pH greater than 10, using an alkali solution makes it simple to desorb As(V) from the exhausted adsorbent. Therefore, the used SPP@Zr can be revived for recycling using a 0.1 M NaOH solution.
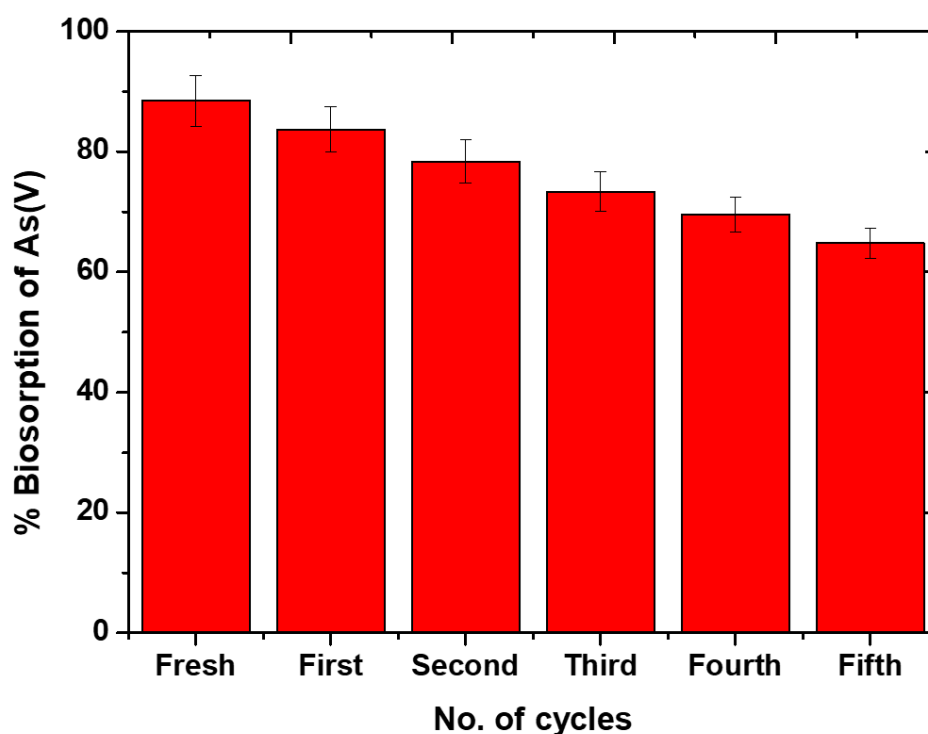
Figure 30:   Variation of the % biosorption of As(V) in 5 cycles' biosorption-desorption process.

The sorbed arsenate ion may have been replaced *via* a ligand exchange mechanism due to the high concentration of OH^- in the alkaline medium. The SPP@Zr desorbed by NaOH was isolated and neutralized for reuse by rinsing with DI water. After

desorption, up to five series of biosorption/desorption were used to investigate the reusability of the adsorbent. The As(V) biosorption capacity declined from 88.6% to 64.9% after five consecutive cycles, as illustrated in **Figure 30.**

4.1.10 XPS analysis

The chemical structure and oxidation state of sorbed arsenic were determined using XPS analysis of the sorption product. The XPS survey scan of it is displayed in **Figure 31(a)**. Similar to EDX analysis, C, O, As, and Zr were the main elements found, with peaks of As 3d, Zr 3d, C 1s, and O 1s found at 44.65, 181.7, 284.22, and 531.85 eV, respectively. The identification of distinguishing Zr peaks confirmed the effective loading of Zr(IV) on the biomass. Like this, distinguishing peaks of arsenic (As 3d) verified the successful biosorption of As(V) on the SPP@Zr. **Figure 31(b)** shows two peaks in the Zr 3d high-resolution XPS spectrum, which are the Zr $3d^{5/2}$ and Zr $3d^{3/2}$ (Rahman *et al.*, 2021).
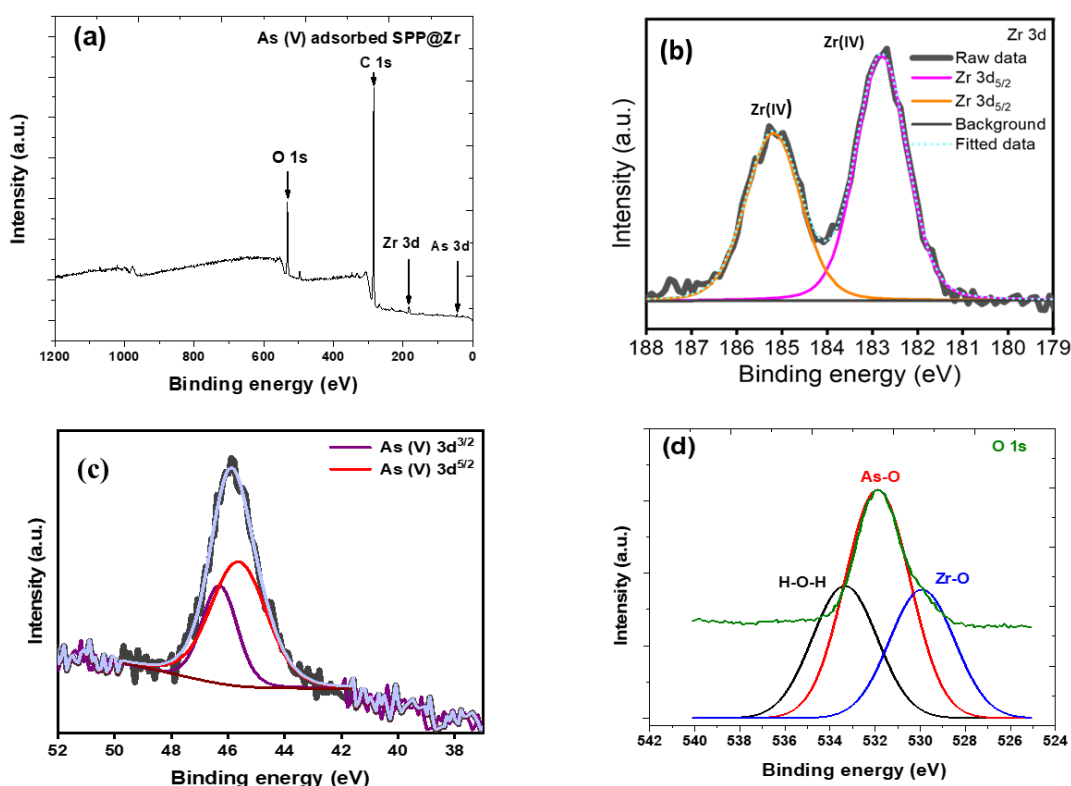
Figure 31: XPS spectra of As(V) sorbed SPP@Zr: (a) Wide scan; (b) Zr 3d; (c) As 3d; (d) O 1s.

Figure 31(c) shows two peaks corresponding to As(V) $3d^{5/2}$ at 44.65 eV and As(V) $3d^{3/2}$ at 46.18 eV, demonstrating that only As(V) exists and that As(V) has not been

reduced to As(III) throughout the biosorption process (Rahman *et al.*, 2021; Pintor *et al.*, 2018). The Zr-O, As-O, and sorbed H_2O molecules may all be ascribed to three bands in the O 1s spectra that are respectively centered at 529.88, 531.9, and 533.37 eV (**Figure 31(d)**).

4.1.11 As(V) biosorption/desorption mechanism

The PSO model well matches the kinetic data for As(V) biosorption on SPP@Zr, indicating that chemisorption may be the driving force behind As(V) biosorption. The thermodynamic analysis revealed that increasing the temperature improved As(V) biosorption, implying surface complexation. The % biosorption of As(V) was substantially greater at pH < pH_{PZC} than at pH > pH_{PZC}, per the pH study. By electrostatic attraction between oxyanion of As(V) and the positively charged biosorbent surface, which results in outer-sphere complexation, certain oxyanions of As(V) were able to nonspecifically bind to the surface of the SPP@Zr when the pH was less than 7.2. However, oxyanions of As(V) ($H_2AsO_4^-$; $HAsO_4^{2-}$) and surface hydroxyl groups of the SPP@Zr were substituted by the most common ligand exchange mechanisms that resulted in inner-sphere complexation (Mohan & Pittman, 2007; Nguyen *et al.*, 2020a). After biosorption, the peak at 1076.12 cm^{-1} (Zr-OH) decreased, and a new peak for Zr-O-As vibration was seen at around 816.23 cm^{-1}, demonstrating that the -OH groups were exchanged by oxyanions of As(V) (Sahu *et al.*, 2019). After biosorption, the solution's pH increased (**Figure 18(b)**), showing that OH$^-$ ions were released into the solution *via* a ligand exchange reaction during the biosorption process.

When zirconium is loaded onto SPP, pectic acid and Zr(IV) form stable chelates (Biswas *et al.*, 2008a). Through a ligand exchange process, the OH$^-$ ions present in the coordination sphere of Zr(IV) were anticipated to be swapped As(V) anions. Additionally, since laden Zr(IV) ions have a propensity to hydrolyze in water., the coordination sphere of hydrated zirconium has enough hydroxide ions and H_2O molecules to give ample biosorption sites for As(V) species (Ghimire *et al.*, 2003; Paudyal *et al.*, 2013). Similarly, in the regeneration of the used biosorbent, the adsorbed As(V) ions may be readily desorbed with an alkali solution. This process includes the ligand exchange mechanism between the sorbed oxyanions of arsenic and

OH⁻ ions in the alkali solution. The ligand exchange mechanism for the biosorption and desorption of As(V) is displayed in **Figure 31**.
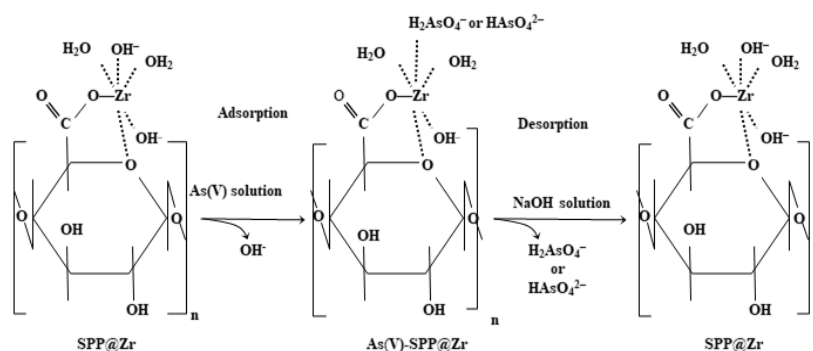
Figure 32: Biosorption-desorption mechanism of arsenate on SPP@Zr (Ghimire *et al.*, 2008).

4.2 As(III) removal onto Zr(IV) modified pomegranate peels

4.2.1 Characterization of the adsorbents

SEM pictures and EDX spectra of SPP, SPP@Zr, and As(III) adsorbed SPP@Zr are shown in **Figure 33**. The image of SPP (**Figure 33(a)**) shows that it has somewhat uneven, heterogeneous, and rough surfaces. The waxy substances, such as limonene and sugar molecules, may have been bleached or removed from the surface during saponification by lime water treatment, revealing the uneven and porous surface. Following the Zr(IV) loading, the pores were occupied with Zr(IV) ions (**Figure 33(b)**). After As(III) biosorption, the As(III) aggregates, and forms layers on the surface, as seen in the FE-SEM image (**Figure 33(c)**).

The strong Ca peak in the EDX spectra of SPP (**Figure 33(d)**) shows that Ca is the main components of the saponification product. After zirconium impregnation (SPP@Zr), the peak associated with Ca almost vanished, and additional peaks associated with Zr were observed, indicating that the Zr(IV) ions had effectively loaded onto SPP and had replaced Ca(II) ions via a cation exchange process (**Figure 33(e)**). The EDX spectra (**Figure 33(f)**), which also showed another peak associated with arsenic, showed that the impregnated Zr(IV) did not leach away following the sorption of As(V). **Table 12** displays the elemental composition of the materials.
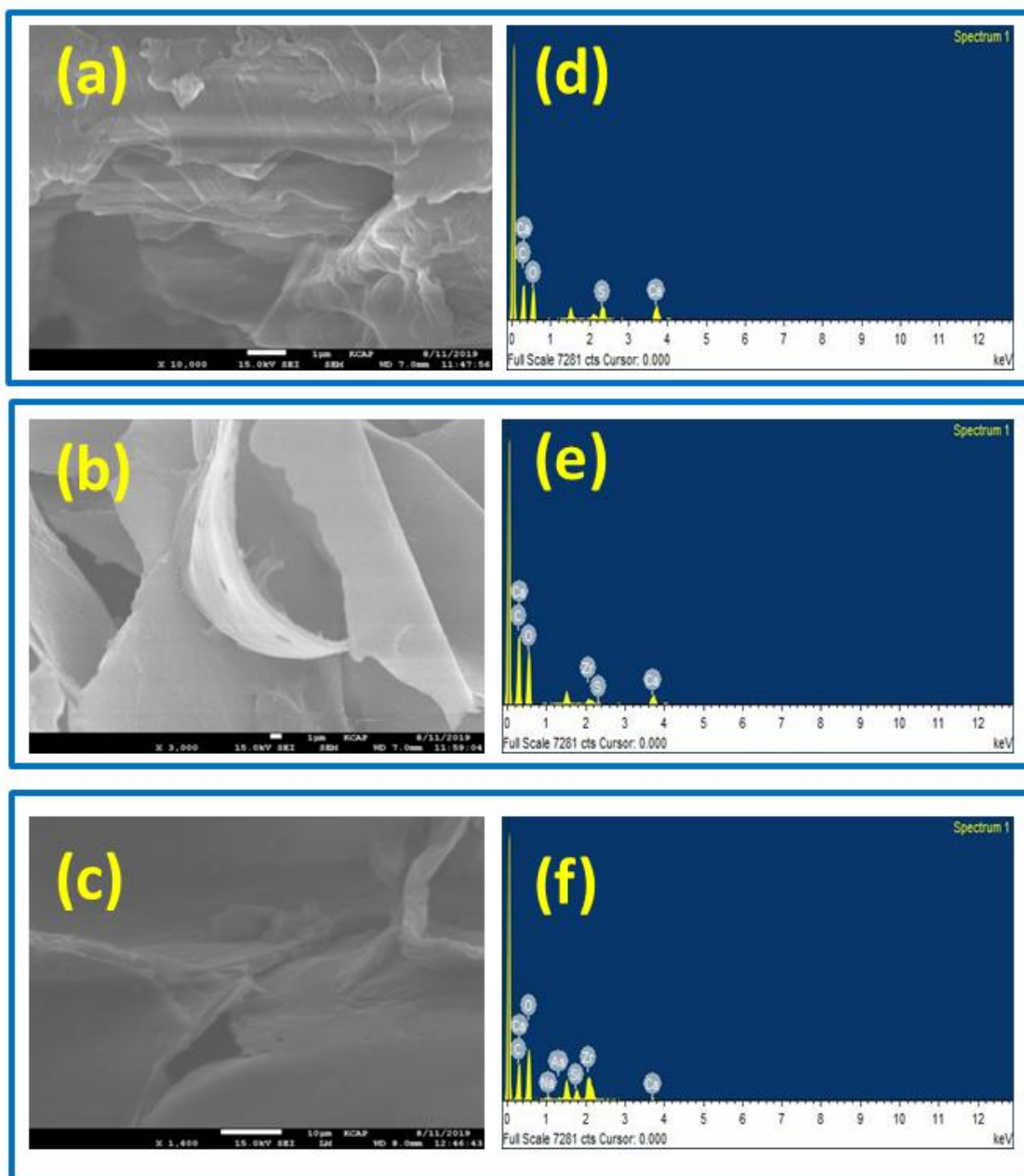
Figure 33: FE-SEM micrographs and EDX spectra of (a), (d) SPP; (b), (e) SPP@Zr; and (c), (f) As(III) adsorbed SPP@Zr.

The FTIR spectra of RPP, SPP, SPP@Zr and As(III) adsorbed SPP@Zr are shown in **Figure 34**. The broadband at 3345 cm^{-1} is related with the –OH bond in the spectrum of RPP, while the narrower peak at 2923 cm^{-1} is related with the –CH and –CH$_2$ groups (Poudel *et al.*, 2021). The –COO and C=O groups, respectively, are connected to the peaks in 1729 and 1613 cm^{-1}. The C=O stretching vibration of the –COO group is accountable for the band at 1629 cm^{-1} (Poudel et. al., 2020). The –C–O– linkage

96

accounts for the vastly intense signal at 1015 cm^{-1} (Poudel et. al., 2020; Paudyal et. al., 2013). The band of the –COOH group at 1729 cm^{-1} vanished after saponification, and an additional peak formed at 1607 cm^{-1} in the FTIR spectra of SPP, indicating the existence of the O-Ca linkage of calcium pectate. This peak has now shifted to 1626 cm^{-1} following Zr(IV) loading (in SPP@Zr). This indicates the formation of zirconium pectate after heavier Zr(IV) ions are substituted for lighter Ca(II) ions. The -Zr-OH vibration may be related to the peak at 1076 cm^{-1} (Lou et. al., 2021; Rahman *et al.*, 2021). It provides convincing proof that Zr(IV) was effectively loaded onto SPP. After As(III) biosorption, the band at 1076 cm^{-1} (Zr-OH) was declined, and a further band for Zr-O-As vibration was seen at around 815 cm^{-1}. This implies that the As(V) anion replaced the -OH group.
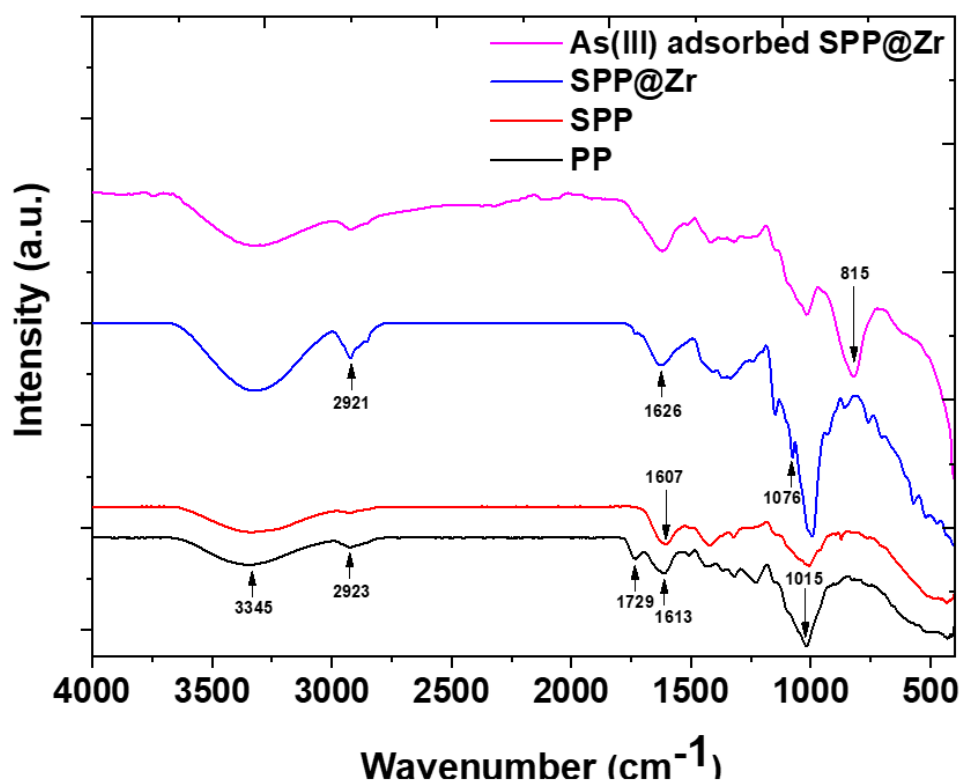
Figure 34: FTIR spectra of RPP, SPP, SPP@Zr, and As(III) adsorbed SPP@Zr

Table 12: Elemental composition of SPP, SPP@Zr, and As(III) adsorbed SPP@Zr

Elements	SPP (Wt %)	SPP@Zr (Wt%)	As-SPP@Zr (Wt%)
C K	41.29	44.72	38.62
O K	43.82	40.36	41.01
Na K	ND	ND	0.42
Si K	ND	ND	2.12
Ca K	13.89	0.56	0.46
As L	ND	ND	3.87
Zr L	ND	14.35	13.49
Total	100.00	100.00	100.00

4.2.2 Effect of the pH of the solutions

Figure 35(a) shows the % biosorption of As(III) *vs* equilibrium pH. The pH range between 9.0 and 10.0 was favorable for As(III) biosorption. At pH 9 to 10, the % biosorption of As(III) was maximum. Therefore, pH 9.5 was chosen as the ideal pH for the additional biosorption experiment. As(III) occurs largely as a neutral species (H_3AsO_3) up to pH 8.0, oxyanion species ($H_2AsO_3^-$ and $HAsO_3^{2-}$) at pH 8.0–12.0, and as an AsO_3^{3-} species at pH > 12.0, depending on the chemistry of the aqueous solution (Hao *et al.*, 2018). **Figure 35(b)** presents a curve that depicts the aqueous As(III) species at various pH levels.

Low pH inhibits the ligand exchange reaction between neutral As(III) species, such as H_3AsO_3, and the OH^- ions of SPP@Zr, leading to limited biosorption. At a pH of around 9-10, the anionic As(III) species predominate, creating the substitution of OH^- by the oxyanion more advantageous and leading to an increase in As(III) absorption. As(III) biosorption may be hindered by competition between the oxyanions of As(III) and OH^- ions. Even at the ideal pH, it was found that As(III)biosorption performance of RPP was noticeably inferior to that of SPP@Zr. Therefore, only SPP@Zr was chosen as the biosorbent for the subsequent studies.
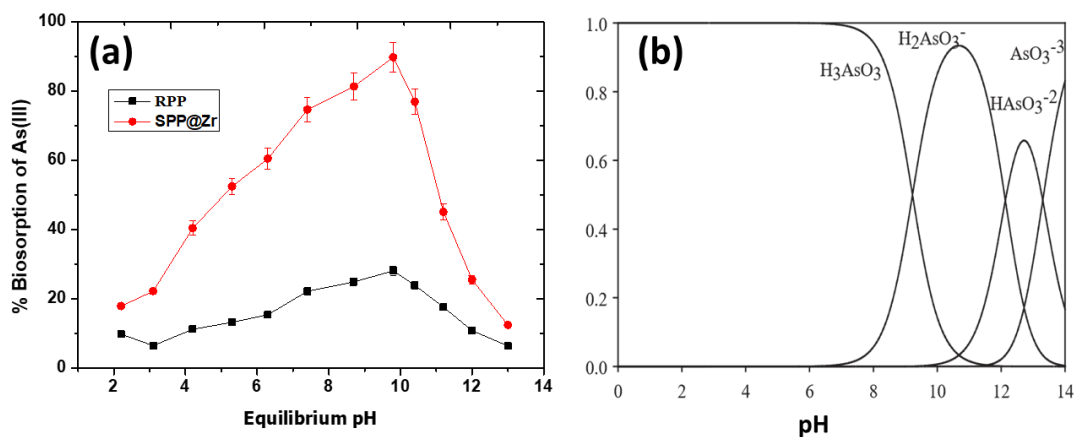
Figure 35: (a) Effect of pH in the biosorption of As(III) onto SPP and SPP@Zr; and (b) curve depicting the As(III) species at various pH values (Ghimire *et al.*, 2003).

4.2.3 Biosorption kinetics

The kinetics of As(III)biosorption on SPP@Zr have been investigated. **Figure 36(a)** depicts the As(III)biosorption capacity (q_t) vs contact times (t). The biosorption efficiency improved dramatically over time. At first, the biosorption rate was high; after that, it dropped, and after 3 h, equilibrium was reached. Since the equilibrium is established in less than 3 h, the contact period was set at 12 h in the tests that followed to ensure that As(III) completely adsorbs to SPP@Zr.To further understand the kinetic process, the PFO and PSO models were suited to the kinetic data. To calculate k_1 and k_2, q_e, and R^2, two independent graphs of log (q_e–q_t) against t (**Figure 36(b)**) and t/$q_t$against t (**Figure 36(c)**) were drawn. **Table 13** lists the assessed quantities for the kinetic parameters. Compared to PFO model, R^2 of the PSO model (0.999) was nearer to unity. Additionally, the theoretical equilibrium biosorption capacity of SPP@Zr in the PSO kinetic (q_e(cal)) = 25.25 mg/g is close to experimental value (q_e(exp)) = 24.98 mg/g. Due to the PSO kinetics of the As(III) biosorption processes on SPP@Zr, biosorption of As(III) may be driven by chemisorption.

Table 13: Kinetics parameters for As(III) biosorption onto SPP@Zr.

Order	R^2	q_e (exp) (mg/g)	q_e (cal) (mg/g)	k_1 (min^{-1})	k_2 (g /mg. min)
PSO	0.999	24.98 ± 1.10	25.25 ± 1.30	-	8.30×10^{-3}
PFO	0.887	24.98 ± 1.10	7.96 ± 0.34	22.3×10^{-3}	-
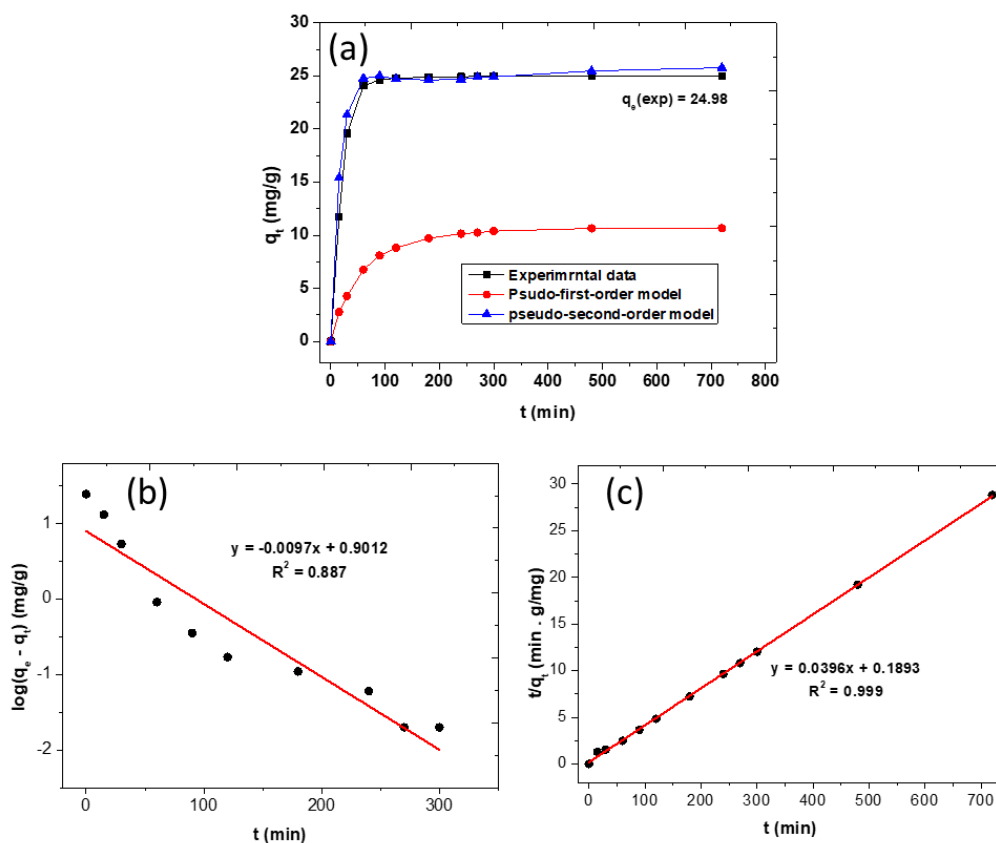
Figure 36: Biosorption kinetics study of As(III): (a) Kinetic data and non-linear kinetics modeling with PFO and PSO models; (b) PFO kinetics plot; (c) PSO kinetics plot.

4.2.4 Biosorption isotherms

Figure 37(a) displays the As(III) biosorption isotherms at pH 9.5 and 298 K. The findings exhibit that as the As(III) ion concentration increased, the biosorption capacity increased quickly, then gradually until it reached saturation (plateau) at high concentrations. The initial high biosorption rate might be due to the increasing number of accessible sorption sites for the adsorbent. The experimental data were examined utilizing the Langmuir and Freundlich isotherm models to elucidate the As(III) biosorption performance. **Figure 37(b)** depicts the plot of C_e/q_e *vs* C_e utilizing the Langmuir model. **Figure 37(c)** depicts the graph of the Freundlich model's linear relationship between $\log q_e$ and $\log C_e$. The assessed values for the isotherm parameters are listed in **Table 14**. The results showed that the data described by the Langmuir model had a superior R^2 (> 0.99) than the Freundlich model (> 0.94). Therefore, the Langmuir model would be a better fit to explain how As(III) adsorbs

onto SPP@Zr. The non-linear fitting of experimental data with modeling findings from both models was compared with the results to further verify the superior fitting of the equilibrium data to the Langmuir model. The non-linear isotherm plot between C_e and q_e (**Figure 37(a)**) illustrates this. It showed that the biosorption processes, which were thought to be monolayer homogenous biosorption processes.
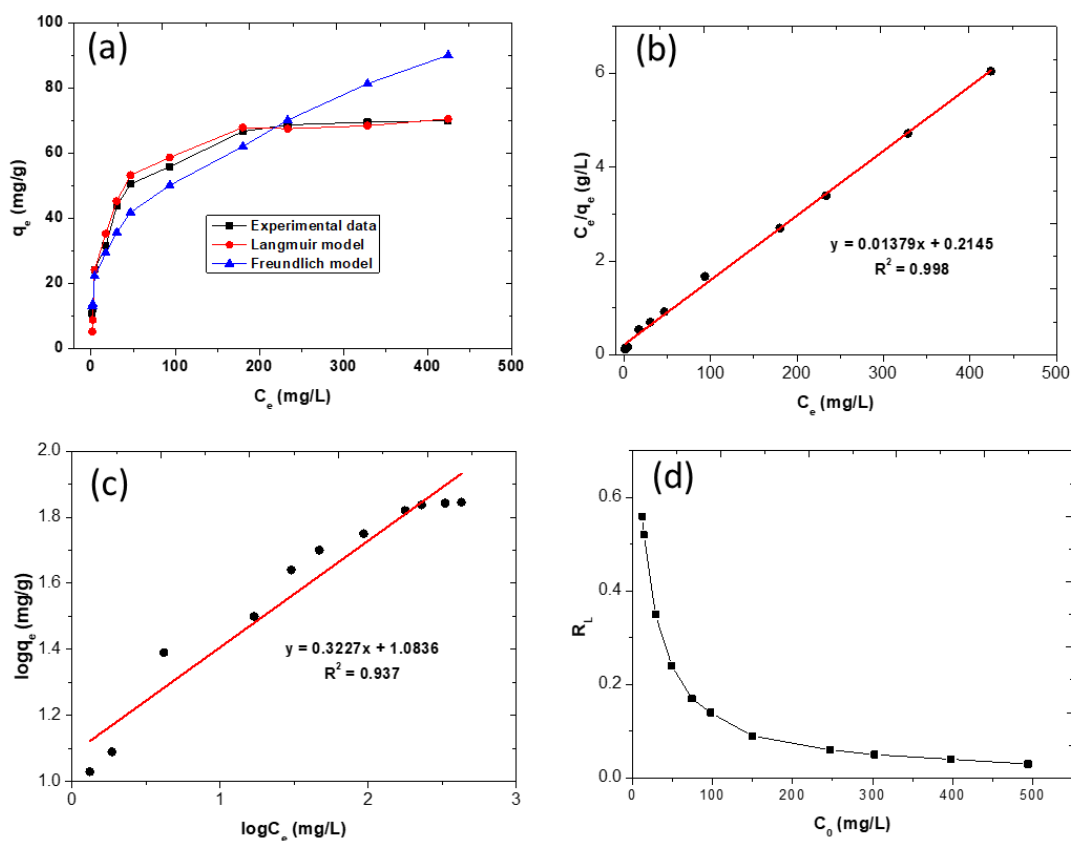
Figure 37: (a) Experimental data and non-linear modeling data by Langmuir and Freundlich isotherm; (b) Linearized Langmuir isotherm plot of SPP@Zr with As(III) system; (c) Linearized Freundlich isotherm plot of SPP@Zr with As(III) system; (d) Value of R_L as a function of initial concentration of As(III).

Table 14: Isotherms parameters for As(III) biosorption onto SPP@Zr.

Model	Parameter	Value
Langmuir isotherm	q_m(mg/g)	72.52 ± 2.40
	b (L/mg)	0.064 ± 0.002
	R^2	0.998
Freundlich isotherm	K_F (mg/g) (L/mg)$^{1/n}$	12.12 ± 0.83
	n	3.10 ± 0.14
	R^2	0.937

101

At room temperature, the q_m of the biosorbent for As(III) determined applying the Langmuir model was 72.52 mg/g. This value is greater than several other materials mentioned in earlier research, as shown in **Table 15**. It implies that SPP@Zr might be an effective biosorbent for removing As(III) from contaminated water.

Figure 37(d) displays the estimated values of R_L based on the experimental data. In this investigation, $0 < R_L > 1$ was observed, implying that As(III) adsorption onto SPP@Zr is favorable and that there is a strong bond between As(III) anions and the surface of SPP@Zr.

Table 15: Comparison of As(III) biosorption capacities of various biosorbents with SPP@Zr.

Adsorbent	Optimal pH	q_m(mg/g)	Reference
Zr(IV)-loaded apple peels	9.0	15.68	(Mallampati & Valiyaveettil, 2013)
La(III)-loaded saponified watermelon rind	12.08	37.73	(Aryal *et al.*, 2022b)
Zr-chitosan modified sodium alginate composite	-	43.19	(Lou *et al.*, 2021)
Powdered almond shell	7.2	4.6	(Ali *et al.*, 2020)
Modified hazelnut shell	9.0	11.84	(Sert *et al.*, 2017)
Iron-coated seaweeds	7.0	4.2	(Vieira *et al.*, 2017)
ZrO$_2$-coated sawdust	7.0	29.0	(Setyono & Valiyaveettil, 2014)
La$_2$O$_3$-coated sawdust	7.0	22.0	(Setyono & Valiyaveettil, 2014)
Iron dopped amino-functionalized sawdust	7.0	10.1	(Hao *et al.*, 2016)
SPP@Zr	8.0	72.52	This study

4.2.5 Influence of coexisting ions

It was investigated how different competing ions affected the biosorption of As(III), and the results are revealed in **Figure 38**. As seen in the figure, relative to the blank, the existence of Cl^-, and SO_4^{2-} at any concentration level very slightly reduces the percentage of As(III) that is adsorbed. This could be since these ions are less capable of binding than As(III) ions. However, because phosphate and arsenite ions compete

for binding sites on the adsorbent, the addition of PO_4^{3-} significantly reduced As(III) biosorption. Arsenite and phosphate have chemical and structural similarities in an aqueous solution, which contributes to the dramatic drop in arsenate biosorption in its presence (Poudel *et al.*, 2022).
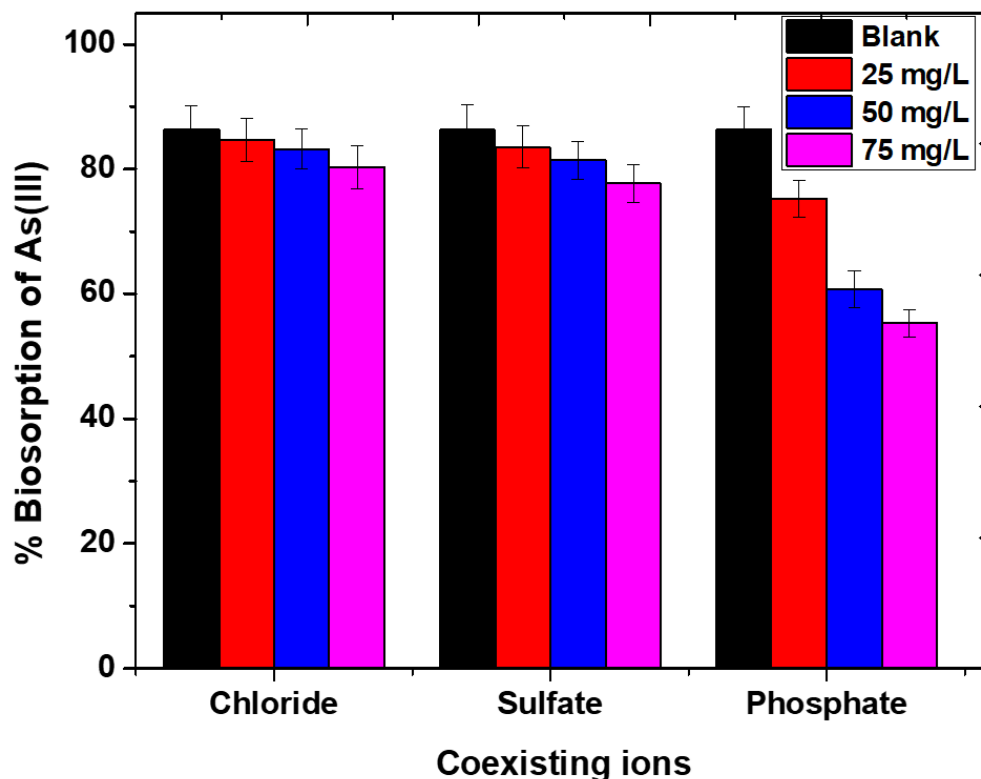
Figure 38: Influence of competitive ions for the biosorption of As(III) ions onto SPP@Zr.

4.2.6 Desorption and reusability of adsorbent

Even though As(III) ion is weakly adsorbed on SPP@Zr at pH greater than 11, using an alkali solution makes it simple to desorb As(III) from the exhausted adsorbent. Therefore, the used SPP@Zr can be rejuvenated for reutilizing applying a 0.1 M NaOH solution. The adsorbed As(III) anion may have been swapped through a ligand exchange process due to the high concentration of OH^- in the alkaline medium. The SPP@Zr desorbed by NaOH was isolated and neutralized for reuse by rinsing with DI water. After desorption, up to four series of biosorption/desorption were used to investigate the reusability of the adsorbent. The As(III) biosorption capacity declined from 86.4% to 61.2% after four consecutive cycles, as illustrated in **Figure 39**. It was discovered that few attractive sites cannot be fully reversed through the desorption

process. Even though its biosorption capacity decreased with repeated recycling, the SPP@Zr was a greatly ecological and favorable biosorbent for removing As(III) from aqueous solution.
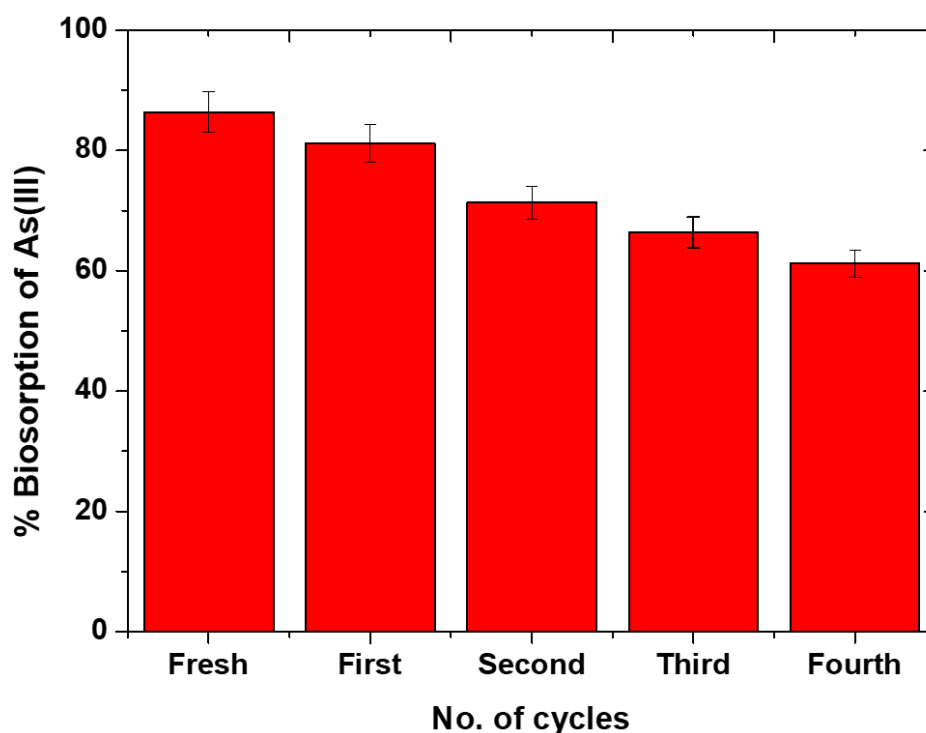
Figure 39: Variation of the % biosorption of As(III) in 4 cycles' biosorption-desorption process.

4.2.7 As(III) biosorption/desorption mechanism

The PSO model well matches the kinetic data for As(III) biosorption on SPP@Zr, indicating that chemisorption may be the driving force behind As(III) biosorption. The oxyanions of As(III) ($H_2AsO_3^-$; $HAsO_3^{2-}$) and surface hydroxyl groups of the SPP@Zr were substituted by the most common ligand exchange mechanisms that resulted in inner-sphere complexation (Mohan & Pittman, 2007). The biosorption of As(III) depends significantly on the impregnated Zr(IV) metal ion. When zirconium is loaded onto SPP, pectic acid and Zr(IV) form stable chelates (Biswas *et al.*, 2008a). Through a ligand exchange process, the OH^- ions present in the coordination sphere of Zr(IV) were anticipated to be swapped As(III) anions. The coordination sphere of hydrated zirconium has enough hydroxide ions and H_2O molecules to give ample biosorption sites for As(III) species (Ghimire *et al.*, 2003; Paudyal *et al.*, 2013). Similarly, in the regeneration of the used biosorbent, the adsorbed As(III) ions may be

readily desorbed with an alkali solution. This process includes the ligand exchange interaction between the sorbed As(III) anions and the OH$^-$ ions provided by the eluant solution. The ligand substitution mechanism for the biosorption and desorption of As(III) is displayed in **Figure 40**.
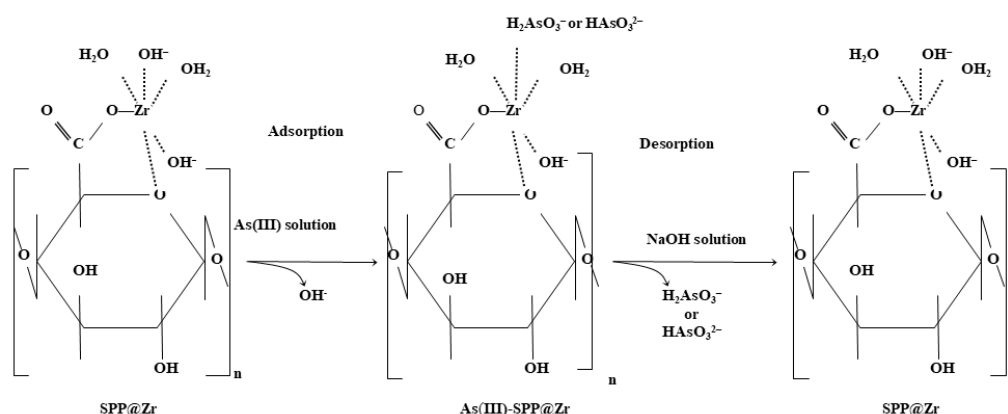
Figure 40: Biosorption-desorption mechanism of As(III) onto SPP@Zr.

4.3 As(III) removal onto PP@TiO$_2$

4.3.1 Adsorbent characterization

4.3.1.1 SEM images of biosorbent

The surface morphology of biosorbent was investigated using SEM measurements. **Figure 41(a)** and **Figure 41(b)**, taken from SEM micrographs, shows porous nature and irregular morphology of PP and PP@TiO$_2$. The occlusion of pores by TiO$_2$ particles is likely the cause of the reduction in porosity in PP@TiO$_2$ (**Figure 41(b)**) as compared to PP (Figure 4.29(a)). As shown, several TiO$_2$ particles are affixed to the surface of the PP. It follows that the successful impregnation of PP with TiO$_2$ is justifiable. The SEM picture of As(III) sorbed PP@TiO$_2$ (**Figure 41(c)**) indicates that arsenic has formed a layer on the adsorbent surfaces, completely covering them.

4.3.1.2 EDX spectra biosorbent before and after As(III) biosorption

The EDX spectra of PP, PP@TiO$_2$, and As(III) adsorbed PP@TiO$_2$ are revealed in **Figure 41(d)**, **Figure 41(e)**, and **Figure 41(f)**, correspondingly. The major peaks for C, O, and Si were found in PP, as shown in **Figure 41(d)**. New peaks associated with Ti were seen after TiO$_2$ impregnation (PP@TiO$_2$), indicating that the biomass had been effectively impregnated with TiO$_2$ (**Figure 41(e)**). As a result of arsenic

biosorption, the EDX spectra of As(III) adsorbed PP@TiO₂ showed an additional peak associated with arsenic (**Figure 41(f)**). This demonstrated that arsenic had been effectively adsorbable from an aqueous solution by PP@TiO₂.
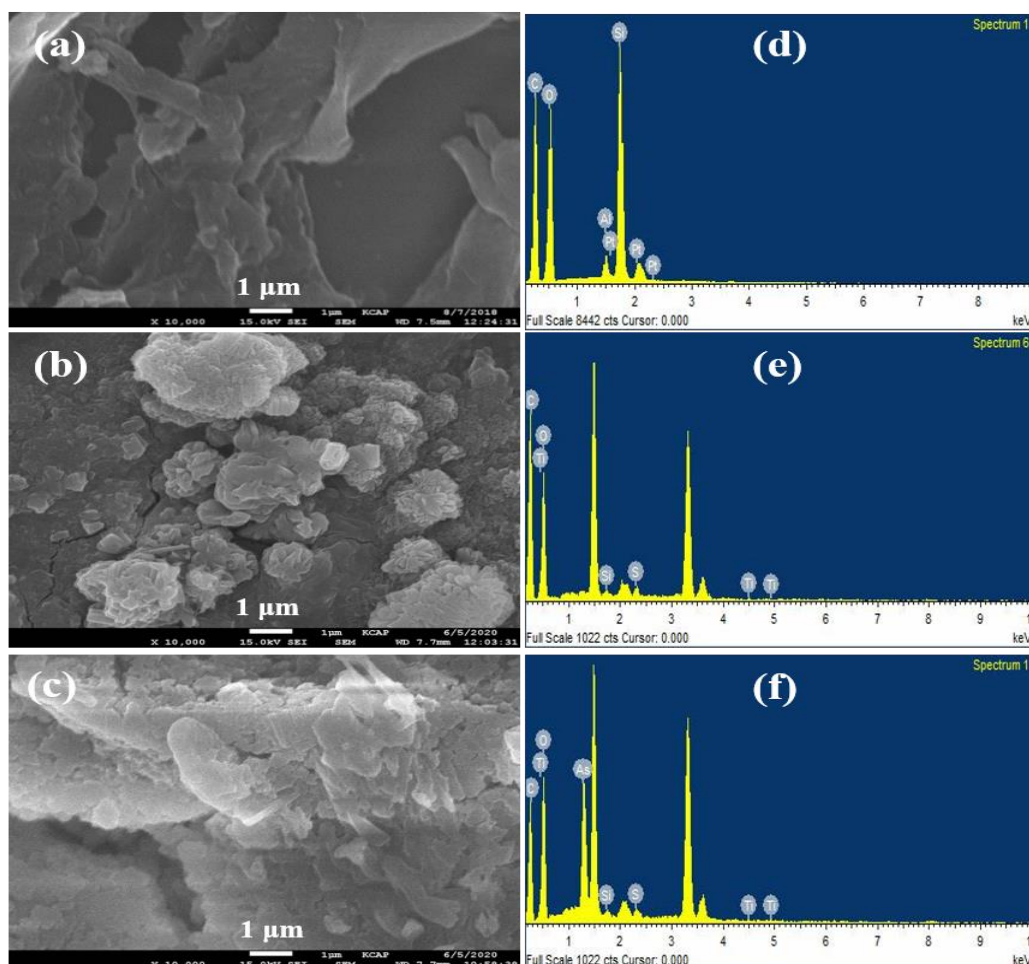
Figure 41: FE-SEM micrographs and EDX spectra of (a), (d) PP; (b), (e) PP@TiO₂; and (c), (f) As(III) adsorbed PP@TiO₂.

4.3.1.3 XRD pattern of biosorbent

Figure 42(a) displays the PXRD pattern of PP and PP@TiO₂. The absence of sharp peaks in the PP signaled its amorphous nature. The diffraction peaks associated with crystalline TiO₂ in the case of PP@TiO₂ emerge at $2\theta = 25.2°$, $38.1°$, $48°$, $55°$, $63°$, $70°$, and $75°$. The (1 0 1), (0 0 4), (2 0 0), (1 0 5), (2 0 4), (2 2 0), and (2 1 5) planes, respectively, are represented by these peaks. This demonstrates that TiO₂ was successfully imbedded in biomass in the form of crystalline anatase. These peaks demonstrate excellent agreement with JCPDS card No. 00-021-1272 of the TiO₂ anatase phase (Pant *et al.*, 2020; Choi *et al.*, 2016).

4.3.1.4 Functional group analysis

FTIR spectra were used to confirm the functional groups on the biosorbents, as given in **Figure 42(b)**. In PP, the stretching vibrations of –OH, –CH$_2$, –COO, and C=O are responsible for the absorption bands seen at 3346, 2915, 1735, and 1621 cm^{-1}, correspondingly. The band with the greatest intensity, found at 1023 cm^{-1}, is caused by the C–O stretching. In PP@TiO$_2$, the Ti-O vibration, which represents the interaction of TiO$_2$ with PP, is attributed to absorption peaks between 420 and 700 cm^{-1} (Fausey *et al.*, 2019; Pant *et al.*, 2020). This offers convincing proof of TiO$_2$ impregnation and the creation of the Ti-O-C bond. The intensities of bands belonging to the oxygen-containing functional groups in PP@TiO$_2$ were substantially lower than in PP, proving that PP had been loaded with TiO$_2$. In the FTIR spectra of As(III) adsorbed PP@TiO$_2$, a extra peak related to As-O vibrations was discovered at 825 cm^{-1} following arsenic biosorption. This supports the biosorption of As(III) onto PP@TiO$_2$.
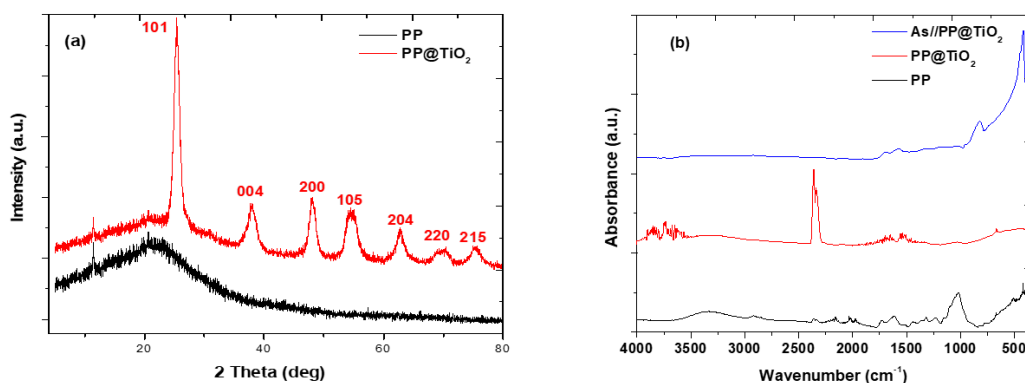
Figure 42: (a) PXRD spectra of PP and PP@TiO$_2$; (b) FTIR of PP, PP@TiO$_2$, and As(III) adsorbed PP@TiO$_2$.

4.3.2 Effect of pH

An essential factor that regulates biosorption at the solution-adsorbent interface is the pH of the solution. As a result, while maintaining other variables constant, the effects of equilibrium solution pH on As(III) biosorption by PP@TiO$_2$ was examined at various pH values varying from 2 to 12. The outcomes are presented in **Figure 43**. The pH range between 7.0 and 10.0 was favorable for As(III) biosorption. At pH 7.0, a maximum biosorption capacity of As(III) of 81.4% was seen. Therefore, pH 7.0 was

selected as the ideal pH for the additional biosorption experiment. As(III) only occurs as neutral H_3AsO_3 species at lower pH levels, and the surfaces of PP@TiO$_2$ are protonated. As a result, As(III) does not bind well to positively charged adsorbent (Biswas *et al.*, 2008a). Lower As(III)biosorption has been observed at pH values greater than 10, where the major As(III) species $H_2AsO_3^-$, $HAsO_3^{2-}$ and AsO_3^{3-} are repulsed by the negatively charged biosorent's surface (Ghimire et. al., 2002). Electrostatic repulsion and anionic arsenic species' competition with the hydroxyl ions for biosorption sites are both responsible for the decline in As(III) biosorption. This is consistent with the finding made about the As(III) removal from water utilizing an iron oxide/nano-porous carbon magnetic composite (Joshi et. al., 2019).
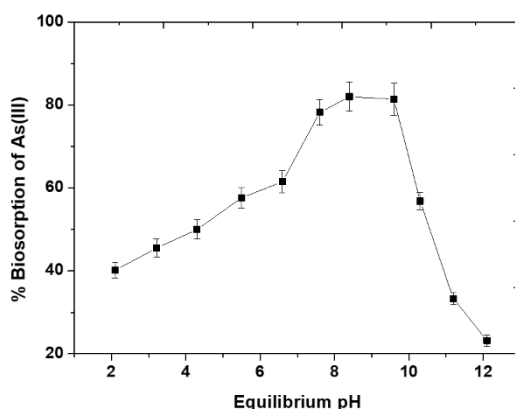
Figure 43: Influence of solution pH in the biosorption of As(III) onto PP@TiO$_2$

4.3.3 Biosorption kinetics

The impact of contact time on As(III) biosorption on PP@TiO$_2$ is illustrated in **Figure 44(a)**. The figure reveals that biosorption goes on increasing with time and the equilibrium is reached almost within 5 h. The kinetic data were simulated by PFO and PSO kinetic equations. The correlation coefficient value of PSO kinetic was higher and closure to unity than that of the PFO kinetic rate equation. Thus the biosorption was found to be controlled by PSO kinetics. The subsequent kinetic parameters are presented in **Table 16**. The PSO model is appropriate for As(III) biosorption, suggesting that the biosorption is chemisorption.
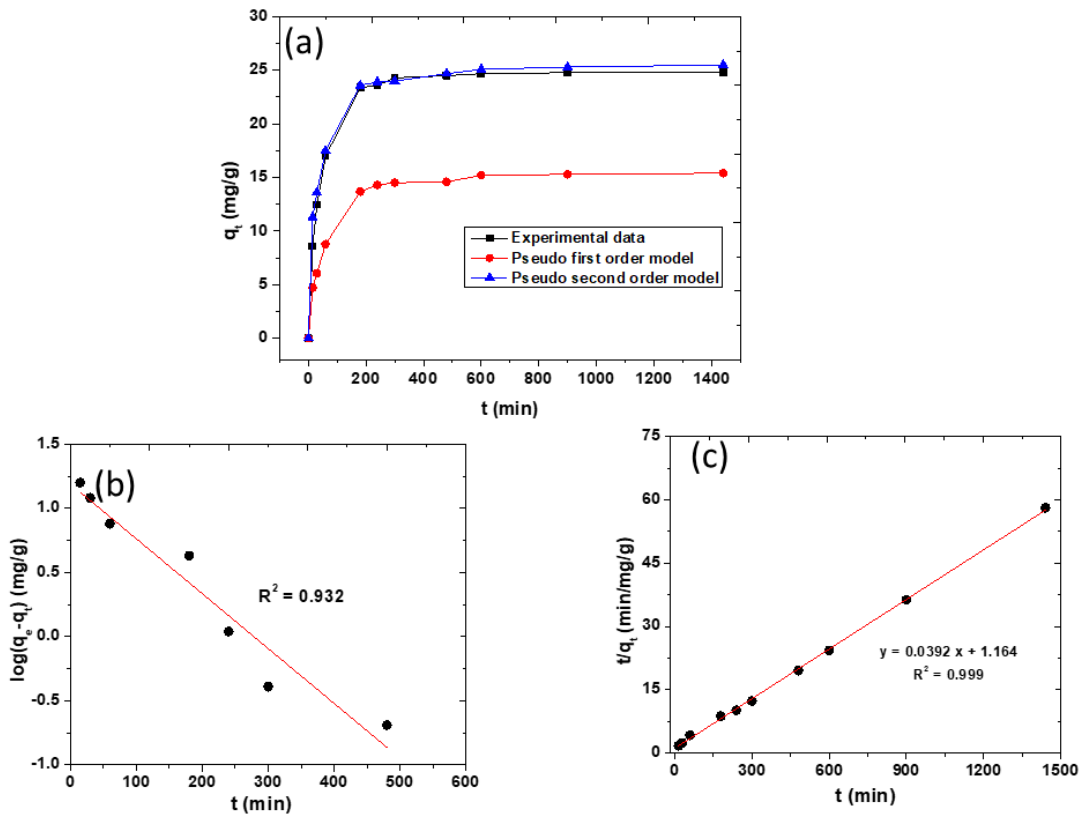
Figure 44: Biosorption kinetics study of As(III): (a) kinetic data and non-linear kinetics modeling with the PFO and PSO kinetics; (b) PFO kinetics plot of PP@TiO$_2$ with As(III) system; (c) PSO kinetics plot of PP@TiO$_2$ with As(III) system

Table 16: Kinetic parameters for the biosorption of As(III) onto PP@TiO$_2$

Order	R^2	q_e (exp) (mg/g)	q_e (cal) (mg/g)	k_1 (min^{-1})	k_2 (mg/g/min)
PSO	0.999	24.7 ± 1.2	25.51 ± 1.3	–	1.32×10^{-3}
PFO	0.932	24.7 ± 1.2	15.45 ± 0.84	9.85×10^{-3}	–

4.3.4 Biosorption isotherm

Figure 45(a) shows the relationship between the As(III) concentration in the solution at equilibrium (C_e) and equilibrium biosorption capacity (q_e) of PP@TiO$_2$ for As(III). Using the Langmuir and Freundlich binding models, the equilibrium data were fitted. From the slope and intercept of the Langmuir plot of C_e against C_e/q_e shown in **Figure 45(b)**, qm (mg/g), and b (L/mg), were calculated. The slope (1/n) and intercept (log K_F) of the Freundlich isotherm plot of log C_e against logq_e shown in **Figure 45(c)** were used to determine the two constants K_F and n. **Table 17** contains

the assessed values for the isotherm parameters of the two models. The conclusion that the PP@TiO$_2$ is an appropriate adsorbent for the biosorption of As(III) from water is clear from the results.

Table 17: Langmuir and Freundlich isotherm parameters for the biosorption of As(III) onto PP@TiO$_2$.

Langmuir model			Freundlich model		
q$_m$ (mg/g)	b (L/mg)	R^2	K$_F$ (mg/g)(L/mg)$^{1/n}$	n	R^2
76.92 ± 2.33	0.03 ± 0.15	0.999	8.72 ± 0.42	2.72 ± 0.41	0.954
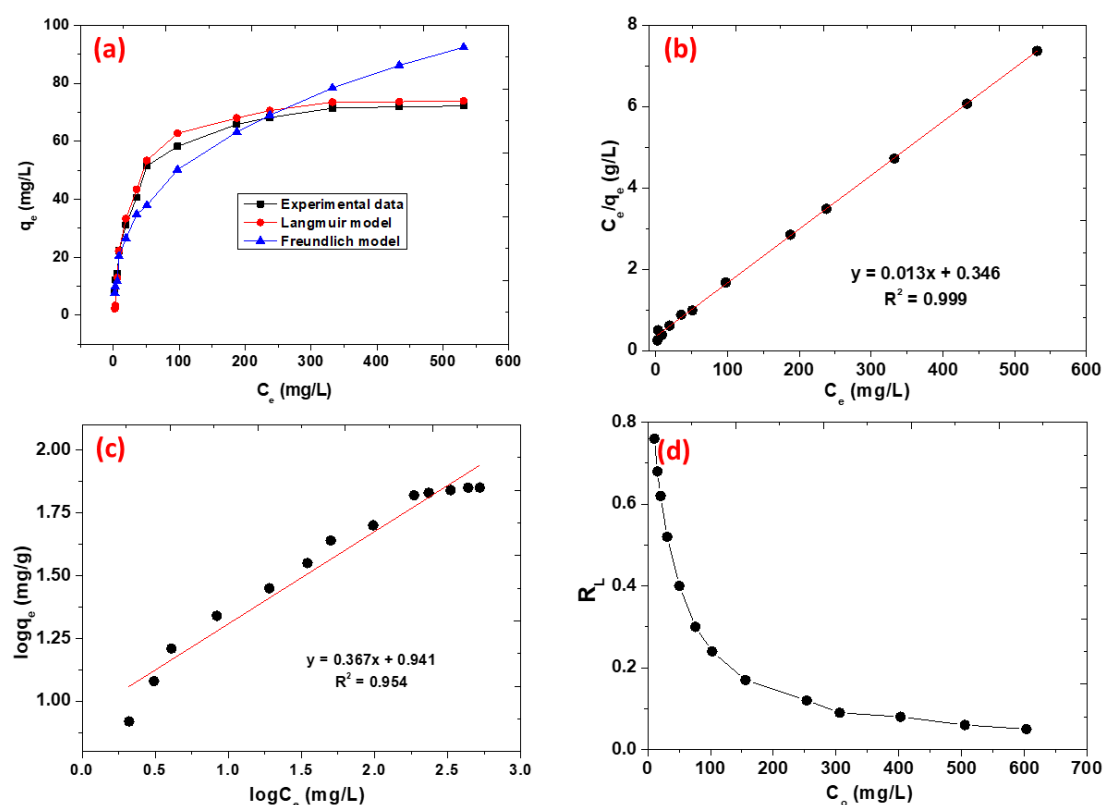
Figure 45: As(III) biosorption isotherm utilizing PP@TiO$_2$ from water: (a) Non-linear plot of equilibrium data and modeling results by Langmuir and Freundlich isotherm; (b) The modeling of experimental data using the Langmuir isotherm; (c) The modeling of experimental data using Freundlich isotherm; (d) Variation of R$_L$ with starting As(III) concentration.

The Freundlich constant (n) varied from 1 to 10 for excellent adsorbent (*i.e.*, 1/n < 1). **Table 17** clearly shows that the value of "n" was determined to be 2.72, demonstrating a robust interaction between the adsorbent and the adsorbate. This demonstrates that the outcome of the Freundlich isotherm cannot be ignored. Thus,

the experimental equilibrium results match well with both the Freundlich and Langmuir isotherms. Both Chandra *et al.* (2010) and Shehzad *et al.* (2019) stated a analogous finding for the biosorption of As(III) on ZrO_2 nanosheets and magnetite-reduced graphene oxide, respectively. The maximum As(III) biosorption capacity that was measured, q_m, was 76.92 mg/g. The previously reported materials are given in Table 18 for comparison. This comparison shows that PP@TiO_2 has a greater biosorption capacity than previously researched adsorbents. As a result, the produced PP@TiO_2 could be a viable material for As(III) removal from water.

The examination of the dimensionless separation factor, R_L, further supported the Langmuir isotherm characteristic. The assessed R_L values ranged from 0.06 to 0.76 based on the experimental results for all concentrations examined (see **Figure 45(d)**). These all fall between 0 and 1 ($0 < R_L < 1$), indicating more benevolent As(III) biosorption onto PP@TiO_2.

Table 18: Comparison of q_m of several adsorbents for As(III).

Adsorbent	Optimum pH	q_m (mg/g)	Reference
Orange juice residue	10.0	68.16	(Ghimire *et al.*, 2002)
Watermelon rind	8.2	3.40	(Shakoor *et al.*, 2018)
Thiol functionalized sugarcane bagasse	7	28.57	(Gupta *et al.*, 2015)
Granular titanium dioxide	7	32.4	(Bang *et al.*, 2005)
Fe_3O_4 nanoparticles	7	46.06	(Feng *et al.*, 2012)
Iron–modified activated carbon	7.6–8.0	38.8	(Chen *et al.*, 2007)
Amorphous iron hydroxide	6–8	28.0	(Lenoble *et al.*, 2002)
Fe_3O_4/sugarcane bagasse activated carbon composite	8	6.69	(Joshi *et al.*, 2019)
ZrO_2 nanosheets	6	74.9	(Shehzad *et al.*, 2019)
Iron modified bamboo charcoal	4–5	7.23	(Liu *et al.*, 2012)
Fe(III) loaded pomegranate waste	9	50.0	(Thapa & Pokhrel, 2012)
Al-based MOF graphene–oxide nanocomposite	6.1	65.0	(Chowdhury *et al.*, 2018)
ZrO_2–sawdust	7	29.0	(Setyono & Valiyaveettil, 2014)
Copper–impregnated coconut husk carbon	6.5	20.35	(Manju *et al.*, 1998)
TiO_2 impregnated pomegranate peels (PP@TiO_2)	7	76.92	This study

4.3.5 As(III) biosorption mechanism onto PP@TiO$_2$

The external surface of PP@TiO$_2$ develops more biosorption sites after being impregnated with TiO$_2$. It is implied that steric hindrance makes it challenging to neutralize all four of the positive charges on the tetravalent Ti during impregnation by the functional groups (–OH, –COOH) found in biomass. Therefore, a carboxyl group in PP neutralizes with one or two positive charges of tetravalent Ti, while the leftover charges are counteracted by hydroxyl ions and water molecules. In an aqueous, hydrated titanium oxide, Polymer≡ Ti(OH)$_n$(H$_2$O)$_{6-n}$, is produced (**Equation 4.4**). As(III) occurs as the anionic species H$_2$AsO$_3^-$ and HAsO$_3^{2-}$ as well as neutral H$_3$AsO$_3$ molecule at pH 6 to 9, which is close to neutral and mildly alkaline (Biswas *et al.*, 2008a). The replacement of hydroxyl anions or neutral H$_2$O molecules may be seen as a ligand exchange process for the biosorption of As(III) on PP@TiO$_2$. Thus, the adsorption of oxyanion and neutral As(III) (**Equation 4.5** and **4.6**) may be caused *via* the following process.

$$\text{Polymer} \equiv \text{TiO}_2 + (6-n)\,\text{H}_2\text{O} + n\text{H}^+ \longrightarrow \text{Polymer} \equiv \text{Ti(OH)}_n(\text{H}_2\text{O})_{6-n} \tag{4.4}$$

$$\text{Polymer} \equiv \text{Ti(OH)}_n(\text{H}_2\text{O})_{6-n} + \text{H}_2\text{AsO}_3^- \longrightarrow \text{Polymer} \equiv \text{Ti(OH)}_{n-1}(\text{H}_2\text{AsO}_3)(\text{H}_2\text{O})_{6-n} + \text{OH}^- \tag{4.5}$$

$$\text{Polymer} \equiv \text{Ti(OH)}_n(\text{H}_2\text{O})_{6-n} + \text{H}_3\text{AsO}_3 \longrightarrow \text{Polymer} \equiv \text{Ti(OH)}_n(\text{H}_3\text{AsO}_3)(\text{H}_2\text{O})_{5-n} + \text{H}_2\text{O} \tag{4.6}$$
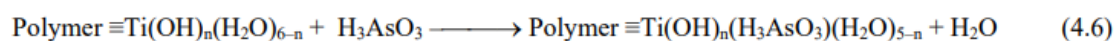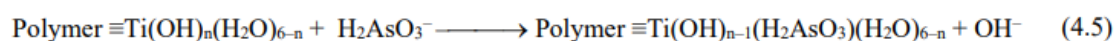
Additionally, in batch tests conducted in room temperature conditions, 10% or so of As(III) is likely converted into less poisonous and easier to adsorb As(V) by the straightforward contact with TiO$_2$ on biosorbent surface (Bang et. al., 2005). According to **Equation 4.7**, oxyanion of As(V), H$_2$AsO$_4^-$, could be adsorbed.

$$\text{Polymer} \equiv \text{Ti(OH)}_n(\text{H}_2\text{O})_{6-n} + \text{H}_2\text{AsO}_4^- \longrightarrow \text{Polymer} \equiv \text{Ti(OH)}_{n-1}(\text{H}_2\text{AsO}_4)(\text{H}_2\text{O})_{6-n} + \text{OH}^- \tag{4.7}$$
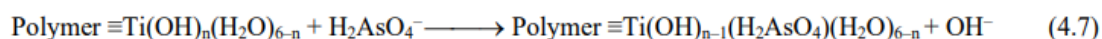
4.3.6 XPS analysis

Following As(III) biosorption studies, the elemental composition, and oxidation states of element were investigated further using XPS. The significant peaks from Ti, O, C, and As were found in the As(III) adsorbed PP@TiO$_2$, according to the wide scan spectrum (**Figure 46(a)**). The peaks at 458.5 and 464.2 eV, which correspond to the Ti 2p$^{3/2}$ and Ti 2p$^{1/2}$ peaks of Ti^{4+}, were seen in the high-resolution XPS scan of Ti 2p

(**Figure 46(b)**) (Pant *et al.*, 2014). The Ti2p$^{3/2}$ peak of Ti^{3+} is responsible for an additional peak at roughly 458.58 eV (Cai *et al.*, 2018). This showed that Ti^{4+} was partially reduced to Ti^{3+} while As(III) was oxidized. Two peaks for the As(III) and As(V) oxidation states, respectively, at 44.4 and 45.85 eV, were present in the As 3d high-resolution XPS scan (**Figure 46(c)** (Tamayo *et al.*, 2019). The high resolution As 3d XPS spectra showed that some As(III) oxidized to As(V) at the surface of PP@TiO$_2$.The Ti-O, O-As, and O-H bonds, correspondingly, are associated with the three peaks at 529.8, 531.5, and 532.3 eV in the high-resolution XPS scan of O 1s (**Figure 46(d)**).

According to XPS measurements, As(III) is therefore adsorbed onto PP@TiO$_2$ and partly oxidized to As(V). (Tamayo *et al.*, 2019) observed a similar pattern of action for the removal of As(III) from water using CaTiO$_3$ nanoparticles. The presence of surface hydroxyl groups and physio-sorbed oxygen probably caused this oxidation. All of the findings showed that PP@TiO$_2$ may concurrently oxidize some As(III) to As(V) on biosorbent surface while also remediating As(III) from water. (Bang et. al., 2005) reported that in batch experiments conducted in a room environment, 10% of As(III) is oxidized to As(V) due to direct contact with TiO$_2$, which is less poisonous and easier to absorb.

When exposed to UV light, 3.0 g/L TiO$_2$/ACF in the presence of 0.80 mg/L As(III) may totally oxidize to As(V) in 30 minutes, according to Yao *et al.* (Yao *et al.*, 2010). They noticed that the oxidation of As(III) was greatly reduced by the occurrence of silicate and phosphate ions. TiO$_2$ completely oxidized As(III) to As(V) in the presence of oxygen and UV radiation, according to previous research (Bissen *et al.*, 2001; Ferguson *et al.*, 2005). As more n-TiO$_2$ is loaded into the composite biomaterial/TiO$_2$, it becomes more capable of adsorbing As(III) and photo-oxidizing it (Pincus *et al.*, 2018). More research is needed, however, to investigate the detailed As(III) oxidation features of PP@TiO$_2$.
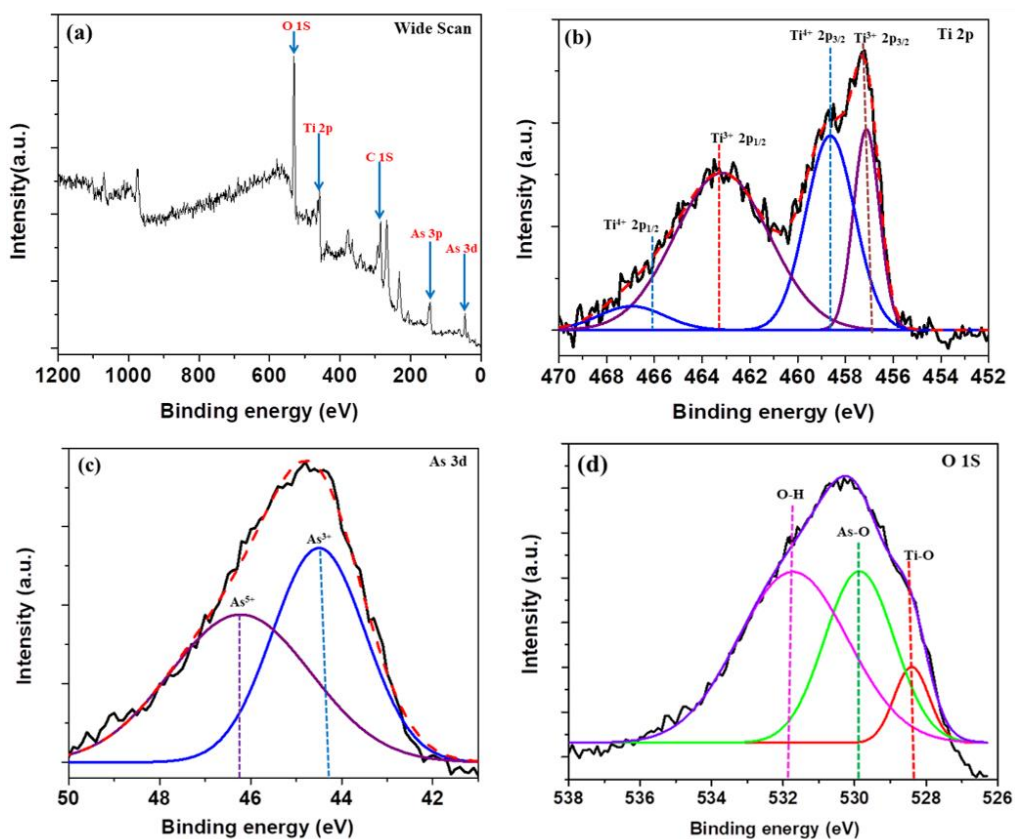
Figure 46: XPS spectra of As(III) adsorbed PP@TiO$_2$: (a) Survey scan; (b) Ti 2p; (c) As 3d; (d) O 1s.

4.3.7 Effect of common co-existing anions

Different concentrations of Cl$^-$, SO$_4^{2-}$, and PO$_4^{3-}$ were used to investigate their influence on As(III) biosorption. **Figure 47** shows that for all of the tested ions, increasing the concentration of coexisting ions reduces the effectiveness of As(III) biosorption compared to the blank. In the presence of Cl$^-$, there was only a small amount of interference, but PO$_4^{3-}$, which has a greater concentration than As(III) and may cause a biosorption loss of up to 27.9% at its greatest concentration (100 mg/L), caused a larger interference. Phosphate competes fiercely with arsenic ions for adsorption sites on PP@TiO$_2$. This is explained by the fact that the oxyanion structures of phosphate and arsenic ions are identical (Su et. al., 2017).
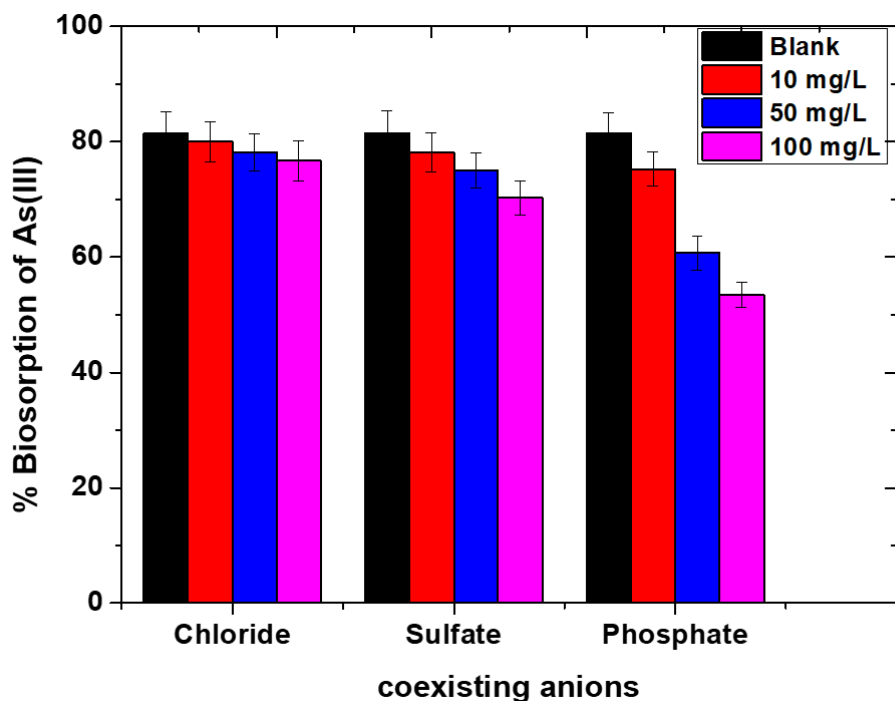
Figure 47: Influence of competitive ions for the biosorption of As(III) ions onto PP@TiO$_2$.

4.3.8 Desorption study and reusability of PP@TIO$_2$

Following the biosorption procedures, batch desorption experiments were conducted utilizing the As(III)-loaded adsorbent. As(III) is readily adsorbed on PP@TiO$_2$ at pH ranges between 6 and 9, it is ineffectively adsorbed at higher pH levels (>9). This suggests that the desorption of adsorbed As(III) may be accomplished with ease by using alkali solution. As a result, the desorption test was conducted using various NaOH concentrations ranging from 0.01 to 0.5 M, as shown in **Figure 48(a)**. **Equation 4.8** was used to compute the As(III) % desorption (% D) as shown below (Paudyal *et al.*, 2020).

$$\% \ D = \frac{D_{amount}}{A_{amount}} \ x \ 100 \tag{4.8}$$

where A$_{amount}$ and D$_{amount}$ are the amounts (mg/g) of As(III) ions adsorbed and desorbed, correspondingly. By raising the concentration of NaOH from 0.01 to 0.1 M, the desorption of arsenic rises from 29.1% to 97.8% and then stays constant when the concentration is raised further. Therefore, it was discovered that a 0.1 M NaOH solution was an effective eluting agent for regeneration of the used adsorbent. The adsorbed arsenic anions on the PP@TiO$_2$ surface were replaced by hydroxyl ions

115

liberated from the NaOH solution. As seen below, it is thought that the ligand substitution process contributes to desorption by replacing adsorbed arsenic species with OH$^-$ ions provided by eluent solution (**Equation 4.9**).

$$\text{Polymer} \equiv \text{Ti(OH)}_{n-1}\,(\text{H}_2\text{AsO}_3)(\text{H}_2\text{O})_{6-n} + \text{OH}^- \longrightarrow \text{Polymer} \equiv \text{Ti(OH)}_n\,(\text{H}_2\text{O})_{6-n} + \text{H}_2\text{AsO}_3^- \qquad (4.9)$$

The PP@TiO$_2$ was put through four sets of biosorption/desorption cycles to gauge its reusability. **Figure 48(b)** reveals that the biosorption capacity of As(III) was reduced by 14.5% following fourth cycles. While maintaining the adsorbent's chemical stability, As(III) anions are replaced by OH$^-$ present in an alkaline solution and leave the sorption sites before the next cycle of biosorption. Since both the adsorbent and the arsenic were effectively recycled and regenerated, the high desorption efficiency of arsenic from the PP@TiO$_2$ provided low-cost removal technology.
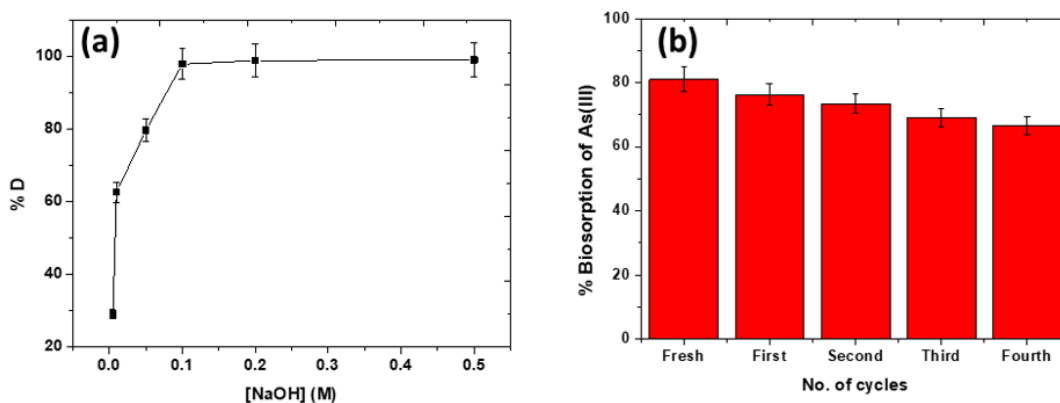
Figure 48: (a) Desorption of arsenic from arsenic loaded PP@TiO$_2$; (b) Variation of the % biosorption of As(III) in 4 cycles' biosorption-desorption process

4.4 As(III) removal from water using a fixed bed column packed with PP@TiO2

4.4.1 Effect of the flow rate

The impact of the flow rate of the inflowing solution on the As(III) biosorption by PP@ TiO$_2$ was investigated at different flow rates (72, 150 and 240 mL/h) and a fixed bed height (4.1 cm), and preliminary As(III) concentration (10.0 mg/L). The breakthrough data presented in **Figure 49(a)**, indicates that a lesser treated bed volume happened at a greater flow rate. The treated bed volumes were determined to be 297.1, 327.7, and 349.5 at flow rates of 72, 150, and 240 mL/h, respectively. A greater volume of solution passed across the bed at a greater flow rate. Consequently,

more As(III) ions became in contact with the adsorbent sites, making them get saturated more rapidly.
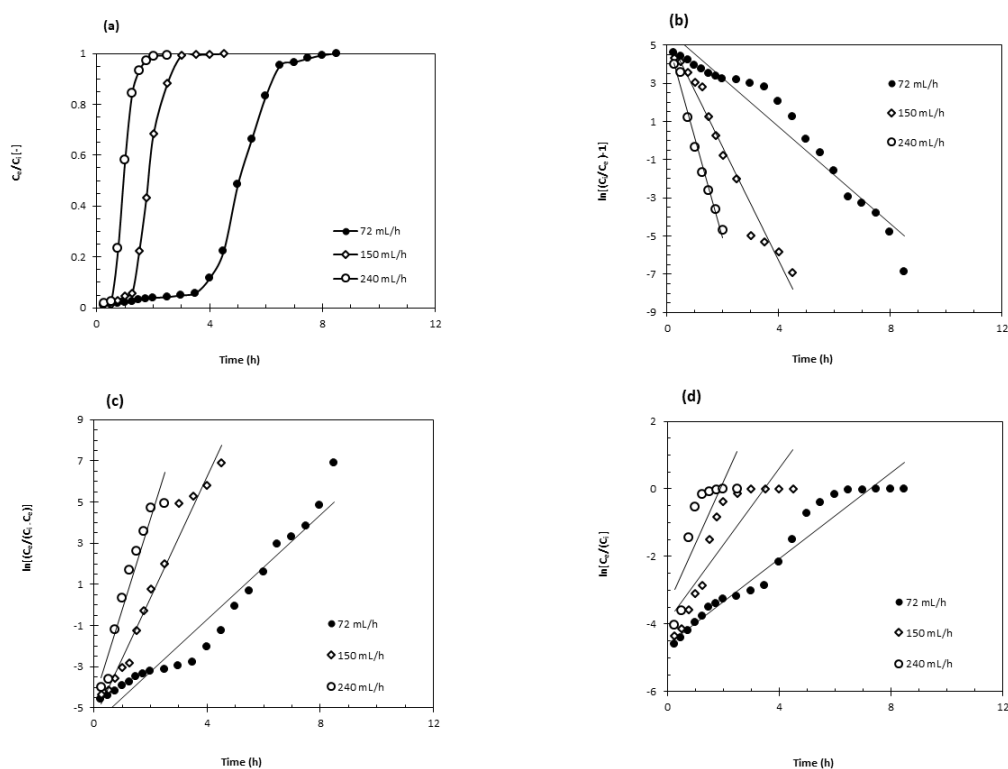
Figure 49: Biosorption of As(III) onto PP@TiO$_2$ in fixed bed system at different flow rates (a) breakthrough profile, and modeling using (b) Thomas, (c) Yoon Nelson, and (d) Adams-Bohrats models.

Likewise, a higher biosorption capacity was achieved at a gentler flow rate. It was probably because the longer contact duration between the As(III) ions and the adsorbent surface. The longer contact time led to more efficient sorption As(III) onto PP@ TiO$_2$, and thus a higher biosorption capacity was attained. Similar results have also been reported by Paudyal *et al.* (2013).

4.4.2 Effect of initial As(III) concentration

The breakthrough curves at varying initial As(III) concentrations for a flow rate of 150 mL/h and bed height of 4.1 cm are shown in **Figure 50**. The treated bed volumes were 436.9, 327.7, and 145.63 for initial As(III) concentrations of 5.0, 10.0, and 15.0 mg/L, respectively. The figure clearly shows that with increasing initial As(III) concentration, the biosorption approached saturation more quickly and the breakthrough time was decreased. A similar trend was reported by Paudyal *et al.* (2013).

117
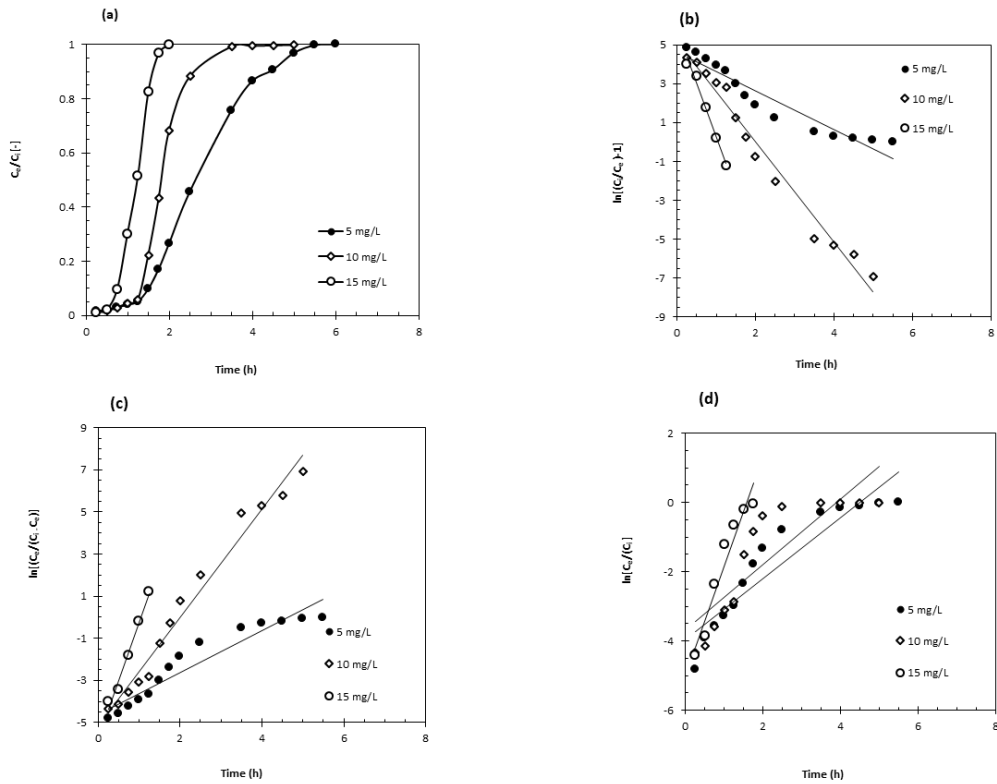
Figure 50: Biosorption of As(III) onto PP@TiO$_2$ in fixed bed system at different concentrations (a) breakthrough profile, and modeling using (b) Thomas, (c) Yoon Nelson, and (d) Adams-Bohrats models.

The biosorption capacity of PP@TiO$_2$ for As(III) also increased (2.31 to 3.14 mg/g) with increasing initial As(III) concentration, which can be probably since higher concentration offers more driving force for the transfer process to overwhelm the mass transfer barrier in the packed bed.

4.4.3 Effect of bed height

Figure 51(a) depicted the impact of bed height on the breakthrough curves about As(III) biosorption onto the PP@TiO$_2$. The treated bed volumes of As(III) solution increased from 515.5 to 625.0, and 687.8 with an increasing bed height of 1.4, 2.6, and 4.1 cm, respectively, which may relate to a extended contact duration. The evaluated As(III) removal capacity of PP@TiO$_2$ for the bed height of 4.1, 2.6, and 1.4 cm are presented in **Table 19**. The result recommended that increasing the bed height led to an increase in the As(III) biosorption capacity of PP@TiO$_2$. This can be probably to the higher biosorption sites at higher bed heights (Jain *et al.*, 2013).

118
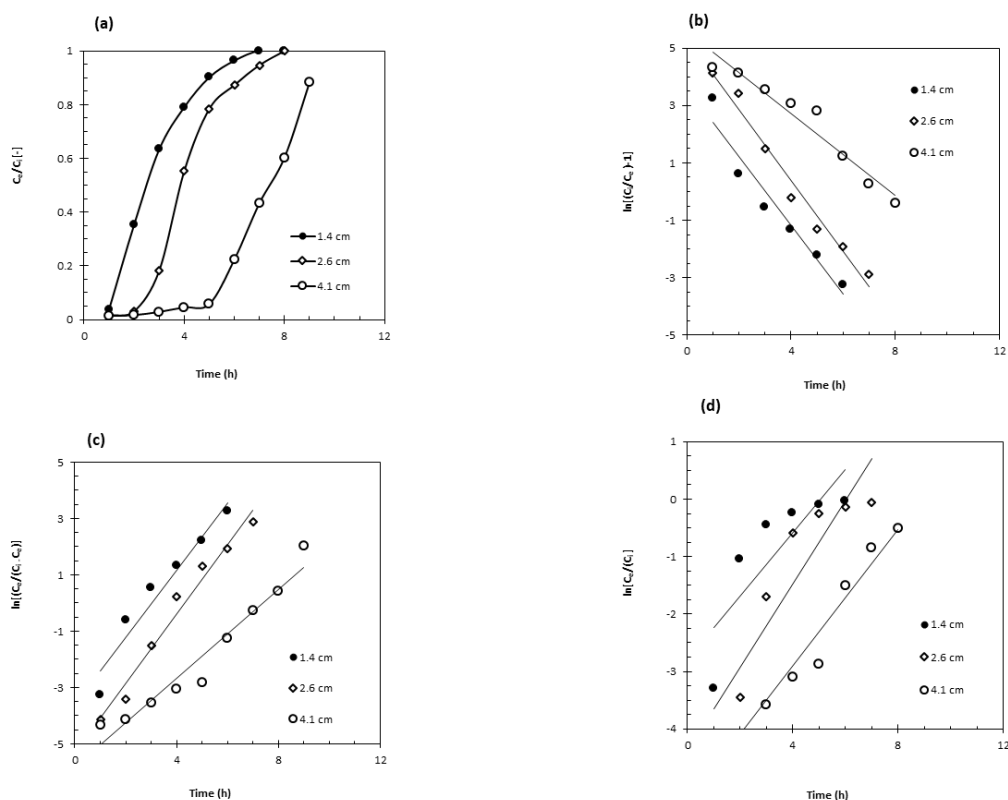
Figure 51: Biosorption of As(III) onto PP@TiO$_2$ in fixed bed system at different bed height (a) breakthrough profile, and modeling using (b) Thomas, (c) Yoon Nelson, and (d) Adams-Bohrats models.

4.4.4 Modeling of the breakthrough curve

This study explores the dynamic biosorption behaviour of PP@TiO$_2$ using the Thomas, Yoon-Nelson, and Adams-Bohart models. **Table 19** shows the results for Thomas, Yoon-Nelson, and Adams-Bohart models.

The entire breakthrough curve may be analyzed using the Thomas model. This model presupposes that mass transfer at the interface limits biosorption and that the data follows second-order kinetics and Langmuir isotherms. The dynamic biosorption capacity rose from 3.81 to 2.86 mg/g as the flow rate increased from 72 to 240 mL/h, whereas the Thomas rate constant increased from 0.127 to 0.521 L/mg.h. In a packed bed system, homogeneous contact decreases due to channeling, which causes q$_0$ to decline at greater flow rates. The Thomas rate constant increased from 0.1992 to 0.2567 L/mg.h and the biosorption capacity increased from 2.31 to 3.13 mg/g as the initial As(III) concentration rose from 5.0 to 15.0 mg/L. The higher concentration gradient and greater driving force can be attributed to a better biosorption capacity at

119

the higher initial As(III) concentration (Paudyal *et al.*, 2013). The Thomas rate constant increased from 0.139 to 0.095 L/mg.h with the increase in bed depth from 1.4 to 4.1 cm, and the biosorption capacity increased from 11.59 to 14.59 mg/g.

Table 19: Thomas, Yoon-Nelson, Adams-Bohart models parameters for the biosorption of As(III) in the fixed bed column of PP@TiO$_2$.

Experimental parameters				Thomas parameters			Yoon Nelson parameters			Adams-Bohart parameters		
F (mL/h)	Ci (mg/L)	Z (cm)	q_{exp} (mg/g)	q_0 (mg/g)	k_{Th} (L/mg h)	R^2	Ţ (h)	K_{YN} (1/h)	R^2	N_0 (mg/L)	K_{AB} (L/mg h)	R^2
72	10	4.1	4.06	3.81	0.1271	0.94	4.54	1.271	0.94	2532	0.063	0.95
150	10	4.1	3.57	3.28	0.2961	0.97	1.87	2.961	0.97	2529	0.112	0.78
240	10	4.1	3.07	2.86	0.5216	0.98	1.04	4.439	0.93	2195	0.1815	0.68
150	5	4.1	2.31	4.04262	0.1992	0.94	4.63	0.996	0.91	1.63	0.1758	0.85
150	10	4.1	2.79	3.49109	0.2567	0.97	2.00	2.567	0.97	2.83	0.0946	0.74
150	15	4.1	3.13	2.74202	0.3648	0.98	1.04	5.472	0.98	7.91	0.0422	0.95
60	10	1.4	10.58	11.59	0.139	0.94	3.01	1.194	0.94	10798	0.0725	0.69
60	10	2.6	12.40	11.76	0.101	0.97	4.31	1.231	0.97	6924	0.0552	0.86
60	10	4.1	13.58	14.59	0.095	0.95	6.76	0.047	0.94	6780	0.0549	0.96

About the Yoon-Nelson model, it was discovered that, with an increase in flow rate from 72 to 240 mL/h, k_{YN} rose from 1.271 to 2.961 h^{-1} and τ reduced from 4.54 to 1.04 h, respectively. The k_{YN} values fall from 1.194 to 0.047 h^{-1} when the bed height rises from 1.4 to 4.1 cm, while τ increases from 89.3 to 165.1 h. An increase in the k_{YN} values from 0.996 to 5.472 h^{-1} and a drop in τ from 4.63 to 1.04 h was brought on by a change in the initial As(III) concentration from 5 to 15 mg/L. Sharma & Singh (2013) attributed these findings to the column saturating more quickly at greater flow rates and initial As(III) concentrations.

The Adams-Bohart model, which is used to evaluate the initial part of the breakthrough curve ($C_t/C_0 = 0$ to 0.5), assumes that equilibrium is not instantaneous. When the initial As(III) concentration was increased from 5 to 10 mg/L, the kinetic constant k_{AB} reduced from 0.175 to 0.042 L/mg.h, but it rose when the flow rate was increased from 72 to 240 mL/h from 0.063 to 0.181 L/mg.h. Additionally, a rise in bed height from 1.4 to 4.1 cm caused the k_{AB} to fall from 0.0725 to 0.0552 L/mg.h.

With an increase in flow rate from 72 to 240 mL/h, the capacity of the adsorbent (N_0) decreased from 2532 to 2195 mg/L, respectively. When the initial As(III) concentration was increased from 5 to 15 mg/L, N_0 values increased from 1.63 to 7.91 mg/L, respectively. According to the analysis of correlation coefficients, the Thomas model provided a better description of the As(III) biosorption process than the Yoon-Nelson and Adams-Bohart models.

4.5 Saponified pomegranate peel (SPP) for removal of Pb(II) from water

4.5.1 Zeta potential analysis of SPP

Figure 52 shows the zeta potential of SPP as determined at several pH levels. An increase in pH resulted in a decrease in zeta potential value. The calculated point of zero charges (pH_{PZC}) was 4.6. The SPP surface becomes negatively charged when the pH of the solution is higher than pH_{PZC}, which is advantageous for the strong electrostatic attraction-based biosorption of the Pb(II)/ Cd(II)cation. At pH levels lower than pH_{PZC}, the repulsion between positively charged SPP and positively charged Pb(II) ions cause poor biosorption. As a result, at pH > 4.6, SPP may eliminate Pb(II)ions more effectively.
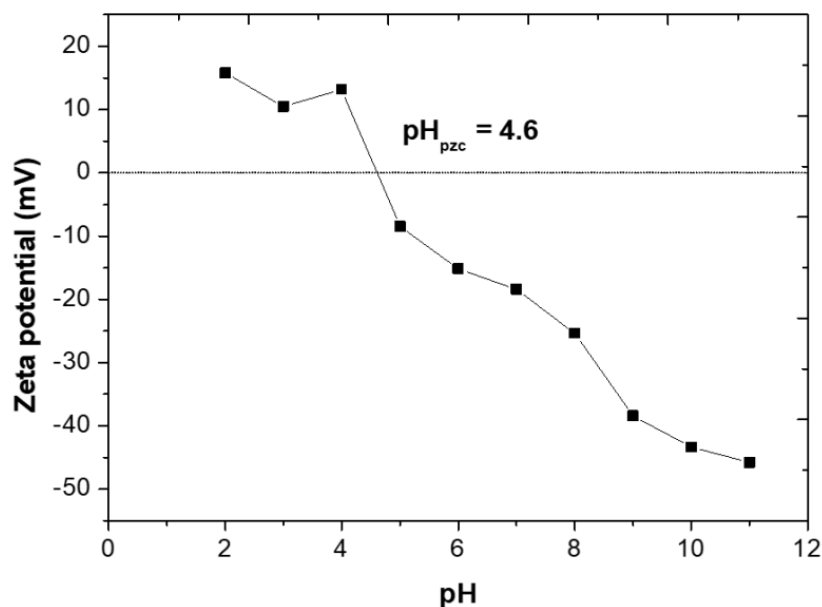
Figure 52: Zeta potential of SPP.

4.5.2 Effect of pH

Figure 53 displays the plot of Pb(II)biosorption % onto RPP and SPP (dosage 1.0 g/L) with the equilibrium pH of the solution (C_o = 25 mg/L). The solution pH has a significant influence on the degree of ionization of the adsorbate during reactions; the solubility of the metallic ions; and the kind of charge on the surface of the biosorbent (Bhat *et al.*, 2015). The pH_{pzc} of the SPP biosorbent was 4.6, indicating that biosorption of Pb(II) at pH <4.6 is unfavorable for SPP because Pb(II) ions must compete with H^+ ions on the positively charged surface of the adsorbents. Instead, Pb(II) should be adsorbed at pH > pH_{pzc} when the surface of the biosorbents turns negative. The outcomes of the experiments support this assertion. The amount of Pb(II)biosorption on SPP was minimal at pH 2 to 3, while increased from pH 4 to 6. At pH 5 to 6, nearly 95% biosorption was accomplished using a 25 mg/L Pb(II) solution and a 1.0 g/L dosage of biosorbent. Because the point of zero charges of SPP was lower than the biosorption pH, electrostatic attractions may have played a role in the biosorption process between the negatively charged biosorbent surface and cationic Pb(II) species.
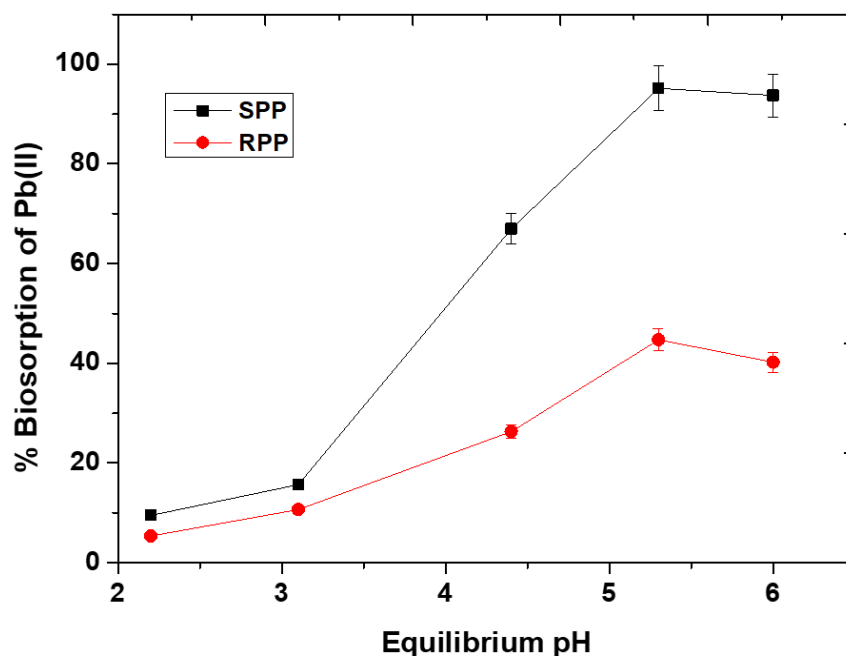
Figure 53: Influence of solution pH for the biosorption of Pb(II) using RPP and SPP.

The natural pH of Pb(II) solutions ranged from 5 to 6. Thus, the natural pH of Pb(II) solution was used for all subsquent experiments. Even at the ideal pH, it was found that Pb(II) biosorption performance of RPP was noticeably inferior to that of SPP. Therefore, only SPP was chosen as the adsorbent for the subsequent testing.

4.5.3 Biosorption kinetics

The kinetics of Pb(II) biosorption on SPP against reaction time at preliminary concentration 41.27 mg/L, pH 5.4, and bisorbent dose 1.0 g/L have been investigated. **Figure 54(a)** depicts the equilibrium concentration and % biosorption of Pb(II) *vs* reaction time. **Figure 54(b)** depicts the Pb(II)biosorption capacity (q_t) over a range of reaction times. The biosorption efficiency improved dramatically over time. At first, the biosorption rate was high; after that, it dropped, and after 60 minutes, equilibrium was reached. To further understand the kinetic process, the PFO and PSO models were suited to the kinetic data.
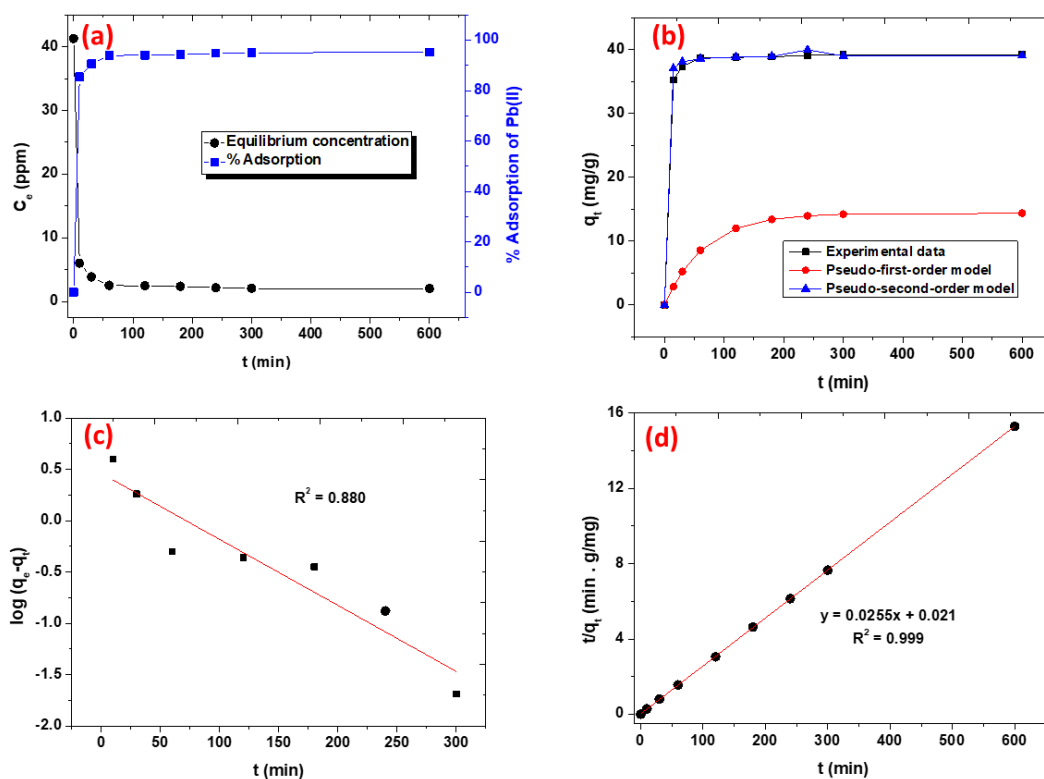
Figure 54: Biosorption kinetics study of Pb(II): (a) equilibrium concentration and % biosorption versus contact time; (b) kinetic data and non-linear kinetics modeling with the PFO and PSO kinetics; (c) PFO kinetics plot of SPP with Pb(II) system; (d) PSO kinetics plot of SPP with Pb(II) system.

To calculate k_1 and k_2, q_e, and R^2, two independent graphs of $\log(q_e-q_t)$ against t (**Figure 54(c)**) and t/q_t against t (**Figure 54(d)**) were drawn. **Table 20** lists the estimated values for the kinetic parameters. Compared to the PFO model, R^2 of the PSO model (0.999) was nearer to unity. Additionally, the theoretical equilibrium adsorption capacity of SPP in the PSO kinetic (q_e(cal)) = 39.21 mg/g is near the actual result (q_e (exp)) = 39.24mg/g. Due to the PSO kinetics of the arsenate adsorption processes on SPP, this process may be driven by chemisorption. Other studies on the biosorption of divalent metal ions on heterogeneous adsorbents demonstrated that the biosorption kinetics were often governed by a PSO model (Jha *et al.*, 2008; Reddad *et al.*, 2002).

Table 20: Kinetic parameters for Pb(II) biosorption onto SPP.

Order	R^2	q_e (exp) (mg/g)	q_e (cal) (mg/g)	k_1 (min^{-1})	k_2 (g /mg. min)
PSO	0.999	39.24 ± 1.73	39.21 ± 1.51	-	3.10×10^{-2}
PFO	0.880	39.24 ± 1.73	4.37 ± 0.24	1.47×10^{-2}	-

4.5.4 Bisorption isotherms

Figure 55(a) shows the relationship between the Cd(II) concentration in the solution at equilibrium (C_e) and equilibrium biosorption capacity (q_e) of SPP for Pb(II). The results show that when the Pb(II) concentration increased, the biosorption capacity increased quickly, then gradually until it reached saturation (plateau) at high concentrations. The initial high biosorption rate might be due to the increasing amount of accessible sorption sites for the biosorbent. Since the biosorption capacity has peaked at a high concentration area, no more sites are available for further biosorption. The experimental data were analyzed utilizing the Langmuir and Freundlich isotherm models to elucidate the Pb(II) biosorption performance.

Figure 55(b) depicts the plot of C_e/q_e vs C_e utilizing the Langmuir model. **Figure 55(c)** depicts the graph of the Freundlich model's linear relationship between $\log q_e$ and $\log C_e$. The assessed values for the Langmuir and Freundlich parameters, as well as the corresponding R^2 value, are listed in **Table 21**. The results showed that the Langmuir model would be a better fit to explain how Pb(II) adsorbs onto SPP. It showed that the biosorption processes, which were thought to be monolayer

homogenous biosorption processes, occurred on the biosorbent surface. The non-linear isotherm plot between C_e and q_e (**Figure 55(a)**) illustrates the superior fit of the equilibrium data to the Langmuir model. Accordingly, R_L values ranged from 0 to 1, which is consistent with the favorable biosorption (**Figure 55(d)**).
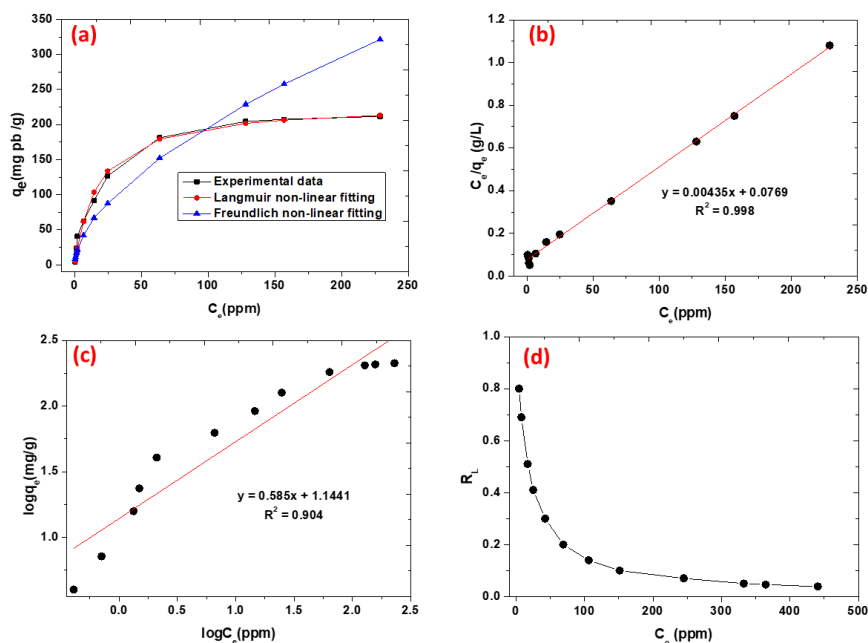
Figure 55: Biosorption isotherm for Pb(II) onto SPP from water: (a) non-linear plot of equilibrium data and modeling results of Pb(II) biosorption by the Langmuir and Freundlich isotherms; (b) Linearized Langmuir isotherm plot of SPP with Pb(II) system; (c) Linearized Freundlich isotherm plot of SPP@Zr with Pb(II) system; (d) Value of R_L as a function of initial concentration of Pb(II).

Similar outcomes for the Pb(II) biosorption from water by activated carbon (AC) generated from coconut shell and magnetic acid-treated AC nanocomposite treated were reported (Jafari Kang *et al.*, 2016; Sharaf & Sharaf, 2016). The q_m of SPP for Pb(II) estimated utilizing Langmuir model was 229.88 mg/g.

Table 21: Isotherms parameters for Pb(II) biosorption onto SPP

Model	Parameter	Value
Langmuir isotherm	q_m(mg/g)	229.88 ± 2.3
	b (L/mg)	0.056 ± 0.002
	R^2	0.998
Freundlich isotherm	K_F (mg /g) (L/mg)$^{1/n}$	13.93 ± 0.51
	1/n	1.70 ± 0.06
	R^2	0.904

4.5.5 FE-SEM images and EDX spectra of SPP and Pb(II) adsorbed SPP

The SEM image of SPP (**Figure 56(a)**) shows that it has somewhat uneven, heterogeneous, and porous surfaces. The waxy substances, such as limonene and sugar molecules, may have been bleached or removed from the surface during saponification, revealing the rough and porous surface. After the Pb(II), the pores were occupied and the Pb(II) aggregated and formed layers on the surface (**Figure 56(b)**).

The elemental mapping of SPP before and after biosorption was assessed by EDX analysis. The significant peaks associated with C, O, and Ca are seen in the EDX spectra of SPP (**Figure 56(c)**). After Pb(II)biosorption, the peak associated with Ca almost vanished, and additional peaks associated with Pb(II) were observed, indicating that the Pb(II) ions had effectively adsorbed onto SPP and had replaced Ca(II) ions via a cation exchange process (**Figure 56(d)**).
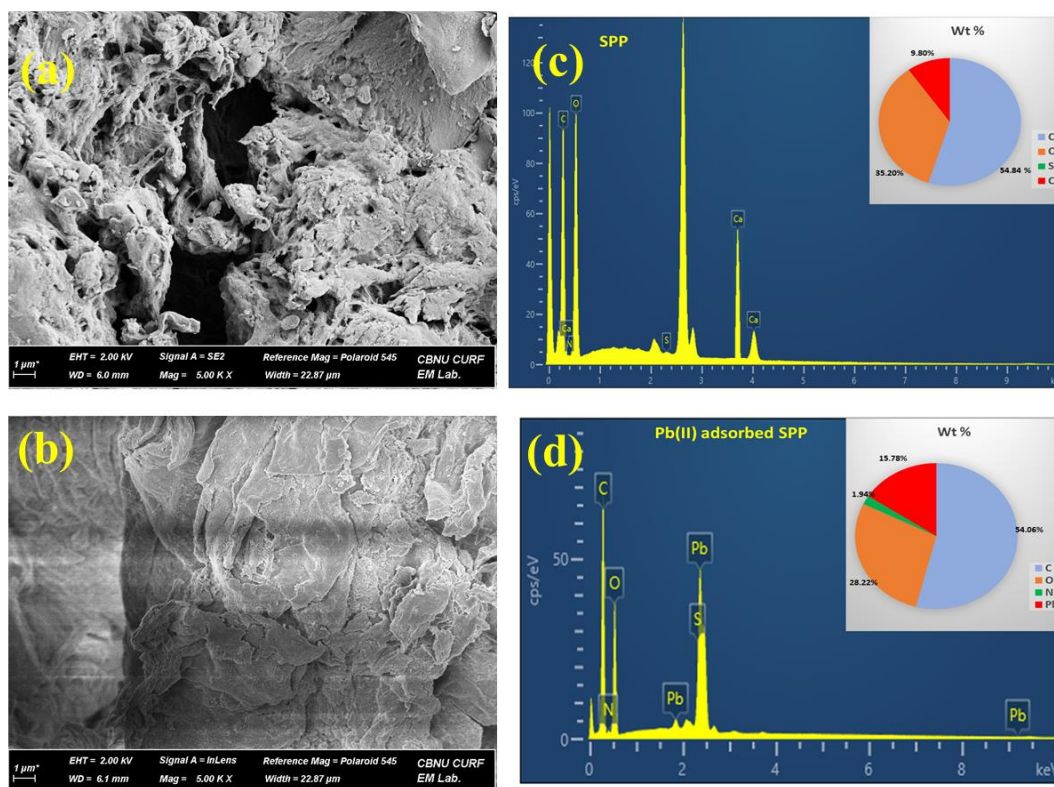
Figure 56:   (a) FE-SEM micrographs of SPP; (b) FE-SEM micrograph of Pb(II) adsorbed SPP; (c) EDX spectra of SPP; and (d) EDX spectra of Pb(II) adsorbed SPP.

4.5.6 FTIR spectra of SPP and Pb(II) adsorbed SPP

The FTIR spectra of RPP, SPP, Pb(II) adsorbed SPP are shown in **Figure 57**. The broadband at 3347.13 cm^{-1} is related with the –OH group in the spectrum of RPP, while the narrower peak at 2920.9 cm^{-1} is related with the–CH and –CH$_2$ groups. The –COO and C=O groups, respectively, are connected to the peaks at 1731.16 and 1613.98 cm^{-1}. The C=O stretching vibration of the –COO group is accountable for the band at 1629 cm^{-1} (Poudel et. al., 2020). The –C–O– linkage found in alcoholic, phenolic, and carboxylic groups accounts for the vastly intense signal at 1018.12 cm^{-1} (Poudel et. al., 2020; Paudyal et. al., 2013). The band of the carboxylic group at 1731.16 cm^{-1} vanished after saponification, and two additional peaks formed at 1605.88 and 1420.79 cm^{-1}in the FTIR spectra of SPP, indicating the existence of the O-Ca linkage of calcium pectate. The peaks for SPP that were previously seen at 1606.08 and 1421.39 cm^{-1} have now moved to 1574.27 and 1298.55 cm^{-1} following Pb(II) biosorption (in Pb(II) adsorbed SPP). These band shifts indicate the formation of lead pectate after Pb(II) ions are substituted for Ca (II) ions.
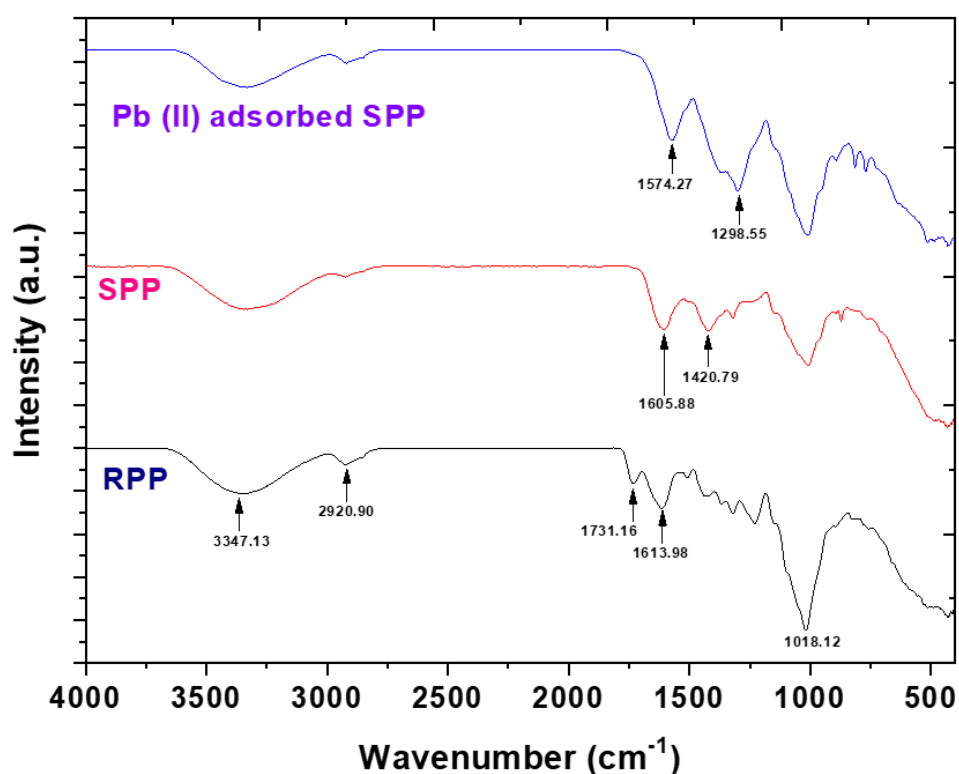
Figure 57: FTIR spectra of RPP, SPP, and Pb(II) adsorbed SPP.

4.5.7 Mechanism of Pb(II) biosorption

As was previously noted, SPP is rich in calcium salt of pectic acid, where the O-atom in the pyranose ring of pectic acid and carboxyl group play a crucial role in forming stable chelate with Ca(II) ions as shown in **Figure 58**. It is assumed that the lead ions can easily replace these Ca(II) ions of the SPP through a cation exchange mechanism, which was further supported the previously mentioned EDX spectra of SPP before and after Pb(II) biosorption.
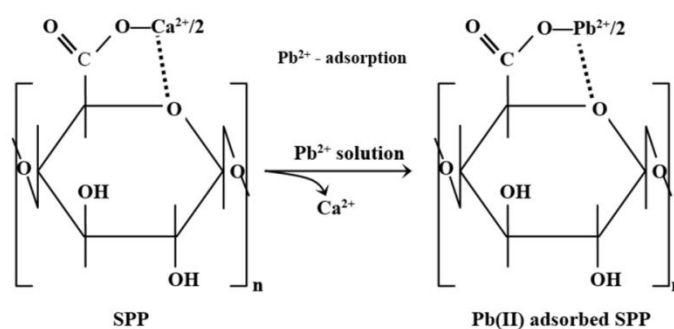
Figure 58: Mechanism of Pb(II) biosorption onto SPP

4.5.8 Effect of competitive ions

Pb(II) had a fixed starting concentration of 25 mg/L while the initial concentrations of competitive ion solutions (K(I), Ni(II), Cu(II), and Co(II)) varied (25, 50, and 75 mg/L). SPP biosorbent dosage was set at 1 g/L.
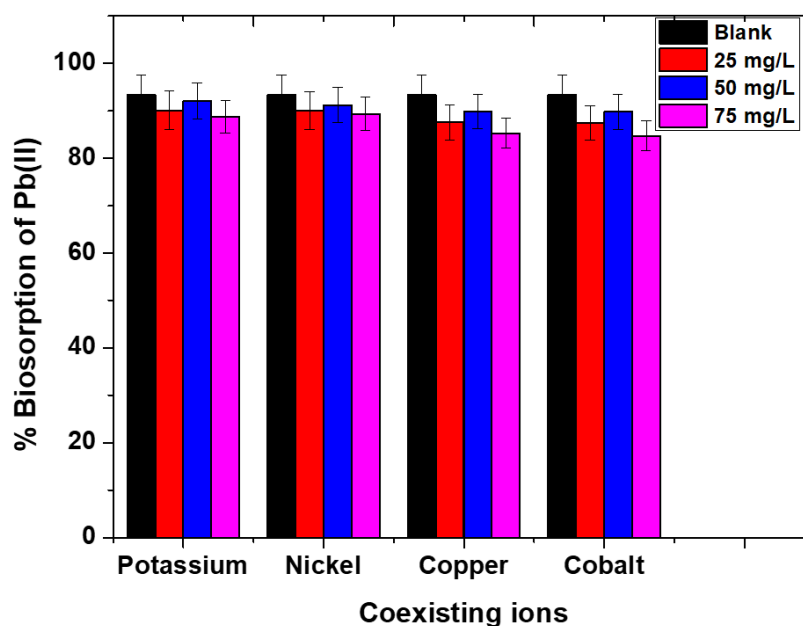
Figure 59:   Effect of competitive ions for the biosorption of Pb(II) ions onto SPP.

The experiment's findings are displayed in **Figure 59**. The results make it abundantly evident that the removal of Pb(II)from water using SPP was mostly unaffected by the occurrence of K(I), Ni(II), Cu(II), and Co(II) ions in an aqueous solution.

4.5.9 Desorption and regeneration study

Since Pb(II) biosorption at pH 2 to 4 is minimal, it should be desorbed with lower pH. To desorb Pb(II) from Pb(II) adsorbed SPP, 0.1 M HNO_3 was utilized. A 40 mg/L Pb(II) solution was mixed with 0.5 g of SPP and agitated for an hour. It was revealed that 94.7% of Pb(II) was removed from the solution. After that, the Pb(II) adsorbed SPP was dried at 70°C and then given an hour of vigorous shaking in a 0.1 M HNO_3 solution to regenerate it. After regeneration, Pb(II) concentration in the filtrate was analyzed. There was 86.4% desorption of Pb(II). These findings have shown that employing 01 M HNO_3, 86.4% Pb(II) could be recovered from the spent biosorbent.

4.6 SPP for removal of Cd(II) from water

4.6.1 Effect of pH

Figure 60 displays the plot of Cd(II)biosorption capacities onto SPP (dosage 1.0 g/L) with the equilibrium pH of Cd(II) aqueous solution (C_o =20.57 mg/L).
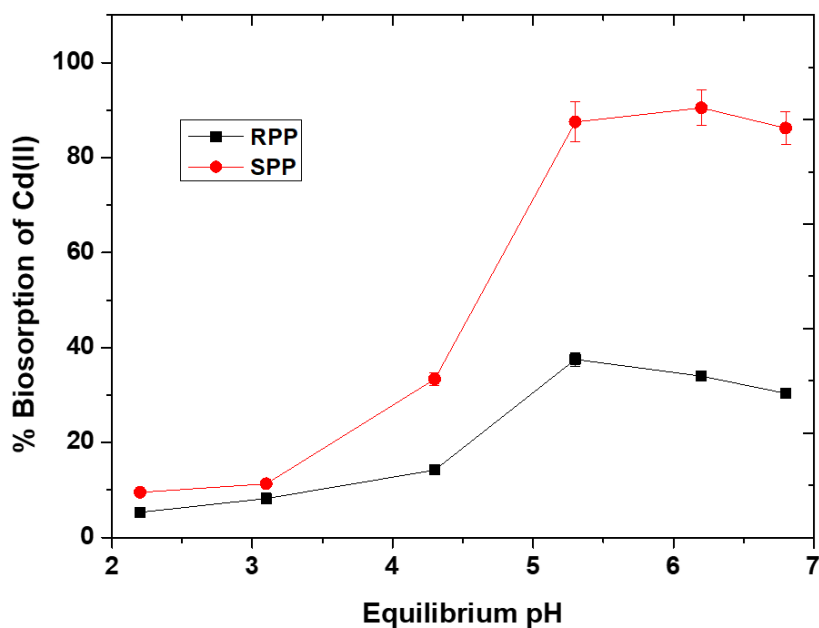
Figure 60: Effect of pH for the biosorption of Cd(II).

The pH_{pzc} of the SPP biosorbent was 4.6, indicating that biosorption of Cd(II) at pH < 4.6 is unfavorable for SPP because Cd(II) ions must compete with H^+ ions on the positively charged surface of the adsorbents. Instead, Cd(II) should be adsorbed at pH > pH_{pzc} when the surface of the biosorbents turns negative. The outcomes of the experiments support this assertion. The amount of Pb(II)biosorption on SPP was minimal at pH 2 and 3, while increased from pH 4 to 6. Similar outcomes for the biosorption of Cd(II) in agricultural waste biomass have been reported (Garg *et al.*, 2008). In a Cd(II) solution, maintaining the pH at 7 without precipitation proved particularly challenging. Thus, pH 6 was used for all further experiments. Since the pH_{PZC} value of SPP is 4.6, the unfavorable biosorption of Cd(II) at pH 3 and 4 is obvious. Even at the ideal pH, it was found that Cd(II)biosorption performance of RPP was noticeably inferior to that of SPP. Therefore, only SPP was chosen as the adsorbent for the subsequent testing.

4.6.2 Biosorption kinetics

The kinetics of Cd(II) biosorption on SPP as a function of reaction time at an preliminary concentration of 38.72 mg/L, pH 6.0, and biosorbent dosage 1.0 g/L have been investigated. **Figure 61(a)** depicts the equilibrium concentration and % biosorption of Cd(II) vs. reaction time. **Figure 61(b)**depicts the Cd(II) biosorption capacity (q_t) over a range of reaction times. The biosorption efficiency improved dramatically over time. At first, the biosorption rate was high; after that, it dropped, and after 120 minutes, equilibrium was reached. To further understand the kinetic process, the PFO and PSO models were suited to the kinetic data.

To calculate k_1 and k_2, q_e, and R^2, two independent graphs of $\log(q_e-q_t)$ against t (**Figure 61(c)**) and t/q_t against t (**Figure 61(d)**) were drawn. **Table 22** lists the estimated values for the kinetic parameters. Compared to the PFO model, R^2 of the PSO model (0.999) was nearer to unity. Additionally, the theoretical equilibrium biosorption capacity of SPP in the PSO kinetic (q_e(cal)) = 35.08 mg/g is near the actual result (q_e(exp)) = 34.77 mg/g. Due to the PSO kinetics of the arsenate biosorption processes on SPP, the biosorption of Cd(II) may be driven by chemisorption.
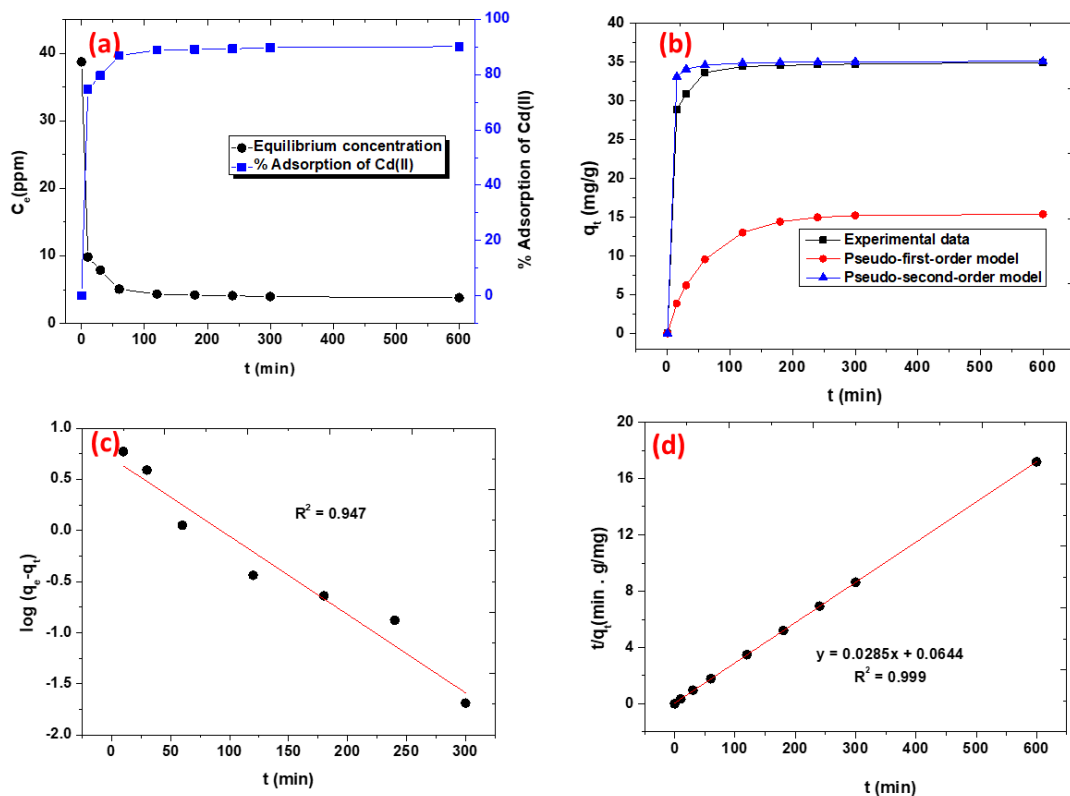
Figure 61: Biosorption kinetics study of Cd(II): (a) equilibrium concentration and % biosorption versus contact time; (b) kinetic data and non-linear kinetics modeling with the PFO and PSO kinetics; (c) PFO kinetics plot of SPP with Cd(II) system; (d) PSO kinetics plot of SPP with Cd(II) system.

Table 22: Kinetics parameters for Cd(II) biosorption onto SPP.

Order	R^2	q_e (exp) (mg/g)	q_e (cal) (mg/g)	k_1 (min^{-1})	k_2 (g /mg. min)
PSO	0.999	34.77 ± 1.33	35.08 ± 1.4	-	1.26×10^{-2}
PFO	0.947	34.77 ± 1.33	5.10 ± 0.23	1.75×10^{-2}	-

4.6.3 Biosorption isotherms

Figure 62(a) shows the relationship between the Cd(II) concentration in the solution at equilibrium (C_e) and equilibrium biosorption capacity (q_e) of SPP for Cd(II). The results show that when the Cd(II) concentration increased, the biosorption capacity increased quickly, then gradually until it reached saturation (plateau) at high concentrations. The initial high biosorption rate might be due to the increasing amount of accessible sorption sites for the biosorbent. Since the biosorption capacity has peaked at a high concentration area, no more sites are available for further

biosorption. The experimental data were analyzed utilizing the Langmuir and Freundlich isotherm models to elucidate the Cd(II) biosorption performance.

Figure 62(b) depicts the plot of C_e/q_e *vs* C_e utilizing the Langmuir model. **Figure 62(c)** depicts the graph of the Freundlich model's linear relationship between $logq_e$ and $logC_e$. The assessed values for the isotherm parameters are listed in **Table 23**. The results showed that the Langmuir model would be a better fit to explain how Cd(II) adsorbs onto SPP. It showed that the biosorption processes, which were thought to be monolayer homogenous biosorption processes, occurred on the biosorbent surface.
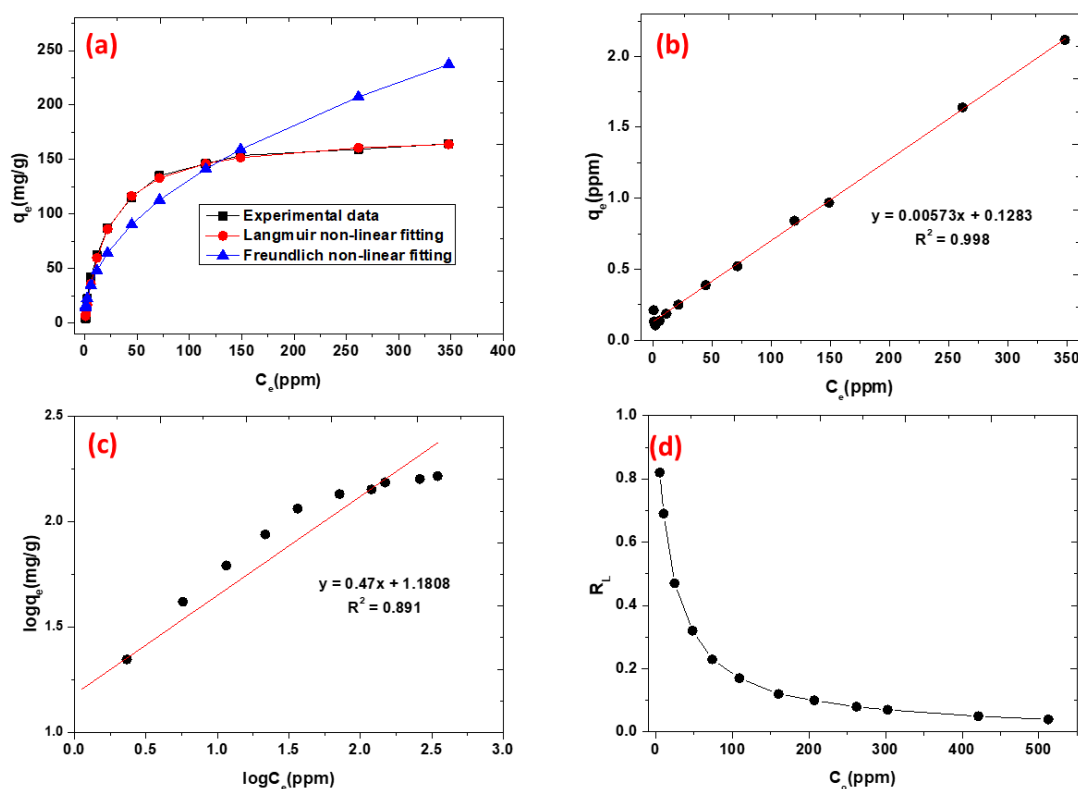
Figure 62: Biosorption isotherm for Cd(II) onto SPP from water: (a) Non-linear plot of equilibrium data and modeling results of Cd(II) biosorption by the Langmuir and Freundlich isotherms (b) Linearized Langmuir isotherm plot of SPP with Cd(II) system; (c) Linearized Freundlich isotherm plot of SPP with Cd(II) system; (d) Value of R_L as a function of initial concentration of Cd(II).

The non-linear isotherm plot between C_e and q_e (**Figure 62(a)**) further confirm the superior fit of the equilibrium data to the Langmuir model. The q_m of SPP for Cd(II) estimated utilizing Langmuir model was 174.52 mg/g. Accordingly, R_L values ranged from 0 to 1, which is consistent with the favorable biosorption (**Figure 62(d)**).

Table 23: Isotherms parameters for Cd(II) biosorption onto SPP

	Parameter	Value
Langmuir isotherm	q_m(mg g^{-1})	174.52 ± 2.0
	b (L mg^{-1})	0.045 ± 0.003
	R^2	0.998
Freundlich isotherm	K_F (mg g^{-1}) (L mg^{-1})$^{1/n}$	15.16 ± 0.53
	n	2.12 ± 0.82
	R^2	0.891

4.6.4 FE-SEM images and EDX spectra of SPP and Cd(II) adsorbed SPP

The SEM image of SPP (**Figure 63(a)**) shows that it has somewhat uneven, heterogeneous, and porous surfaces. The waxy substances, such as limonene and sugar molecules, may have been bleached or removed from the surface during saponification, revealing the rough and porous surface.
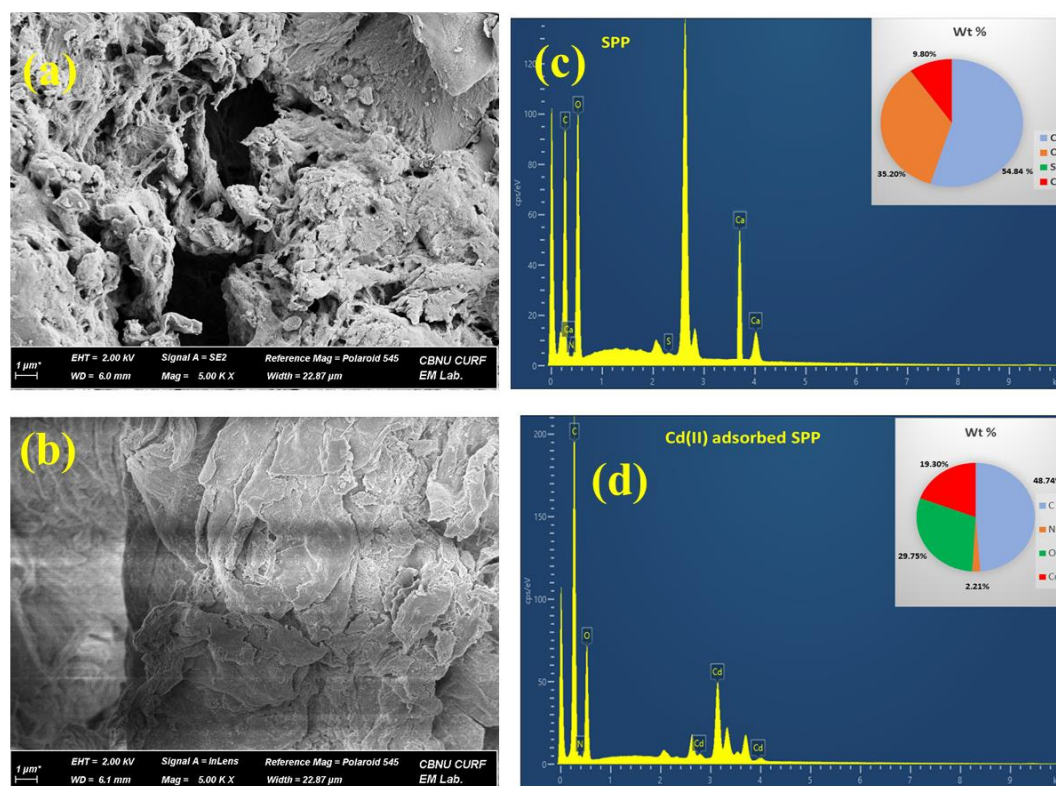
Figure 63:   (a) FE-SEM micrographs of SPP; (b) FE-SEM micrograph of Cd(II) adsorbed SPP; (c) EDX spectra of SPP; and (d) EDX spectra of Cd(II) adsorbed SPP.

After the Cd(II), the pores were occupied and the Cd(II) aggregated and formed layers on the surface (**Figure 63(b)**). The elemental mapping of SPP before and after

133

biosorption was assessed by EDX analysis. The significant peaks associated with C, O, and Ca are seen in the EDX spectra of SPP (**Figure 63(c)**). After Cd(II) biosorption, the peak associated with Ca almost vanished, and additional peaks associated with Cd(II) were observed, indicating that the Cd(II) ions had effectively adsorbed onto SPP and had replaced Ca(II) ions via a cation exchange process (**Figure 63(d)**).

4.6.5 FTIR spectra of SPP and Cd(II) adsorbed SPP

The FTIR spectra of RPP, SPP, Cd(II) adsorbed SPP are shown in **Figure 64**. The broadband at 3347.13 cm^{-1} is related with the –OH group in the spectrum of RPP, while the narrower peak at 2920.9 cm^{-1} is related with the–CH and –CH$_2$ groups. The –COO and C=O groups, respectively, are connected to the peaks at 1731.16 and 1613.98 cm^{-1}. The C=O stretching vibration of the –COO group is accountable for the band at 1629 cm^{-1} (Poudel et. al., 2020). The –C–O– linkage found in alcoholic, phenolic, and carboxylic groups accounts for the vastly intense signal at 1018.12 cm^{-1} (Poudel et. al., 2020; Paudyal et. al., 2013).

Figure 64: FTIR spectra of RPP, SPP, and Cd(II) adsorbed SPP.

The band of the carboxylic group at 1731.16 cm^{-1} vanished after saponification, and two additional peaks formed at 1605.88 and 1420.79 cm^{-1}, indicating the existence of the O-Ca linkage of calcium pectate. The peaks for SPP that were previously seen at 1606.08 and 1421.39 cm^{-1} have now moved to 1415.32 and 1320.11 cm^{-1} following Cd(II) biosorption (in Cd(II) adsorbed SPP). These band shifts indicate the formation of cadmium pectate after Cd(II) ions are substituted for Ca (II) ions.

4.6.6 Mechanism of Cd(II) biosorption

As was previously noted, SPP is rich in calcium salt of pectic acid, where the O-atom in the pyranose ring of pectic acid and carboxyl group play a crucial role in forming stable chelate with Ca(II) ions as illustrated in **Figure 65**. It is assumed that the Cd(II) ions can easily replace these Ca(II) ions of the SPP through a cation exchange mechanism.
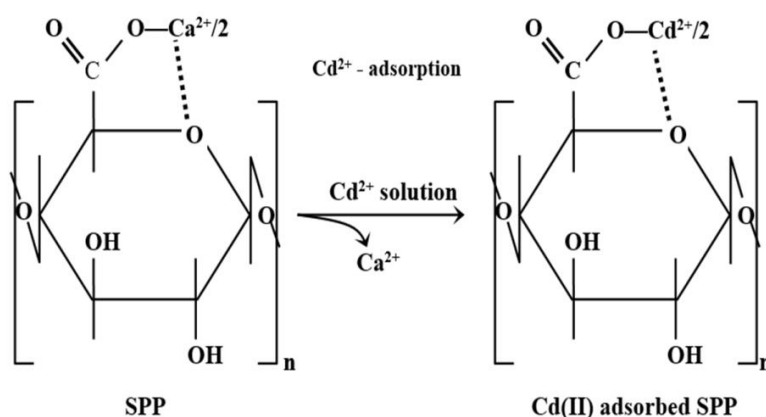
Figure 65: Mechanism of Cd(II) biosorption onto SPP.

4.7 SPP@Zr for the removal of phosphate from water

4.7.1 Preliminary batch experiment

To compare the phosphate biosorption capacities of RPP and SPP@Zr, simple batch biosorption studies were conducted. Several conical flasks were filled with starting phosphate solutions of 9.87, 18.27, 48.12, and 103.10 mg/L at pH 4.0 and biosorbent dose of 1 g/L. Before filtering, the suspensions were stirred for 12.0 h at 298 K. The concentration of phosphate in the filtrates was determined. The collected findings are displayed in **Table 24**. The findings demonstrated that SPP@Zr has a superior capability for adsorbing phosphate than RPP. It was found that very low phosphate

could be absorbed by RPP. As a result, the sole adsorbent for the subsequent phosphate removal experiments was SPP@Zr.

Table 24: Comparision of the phosphate biosorption capacity of RPP and SPP@Zr

Adsorbent	q_e (mg/g) for different initial concentrations of Phosphate			
	9.87 mg/L	18.27 mg/L	48.12 mg/L	103.10 mg/L
RPP	2.15± 0.09	3.78± 0.13	6.85± 0.33	11.50± 0.43
SPP@Zr	8.85± 0.43	16.90± 0.82	43.34± 1.9	90.64± 3.2

4.7.2 Effect of pH

When the pH is below 2.15, phosphate species occur in solutions predominately as H_3PO_4. When the pH is between 2.12 and 7.20, the main form of phosphate is $H_2PO_4^-$, and when it is between 7.20 and 12.36, the major form is HPO_4^{2-} (Yang *et al.*, 2018a). **Figure 66** presents a curve that depicts the aqueous phosphate species at various pH levels.

Figure 67(a) reveals the % removal of phosphate *vs* equilibrium pH. Phosphate was removed to the greatest extent at weakly acidic and neutral conditions (at pH 3.0 to 7.0), as shown in the figure. At a pH higher than 7.0, % biosorption dramatically decreased. The value of pH_{pzc} of biosorbent was observed to be 7.2. Because of the significant coulombic attraction between the negatively charged phosphate ($H_2PO_4^-$) and the substantially positive surface charge on SPP@Zr at pH <pH_{PZC}, the strongly positive surface charge of the biosorbent is beneficial in phosphate biosorption. Nevertheless, when pH > pH_{PZC}, deprotonation of the surface charge took place, creating a strong electrostatic repulsion between the negative surface of the biosorbent and the phosphate species. At higher pH conditions, the increased OH^- concentration increases competition for biosorption sites between OH^-ions and phosphate anions (Jung *et al.*, 2017). The highest % biosorption (88.46%) was observed at pH 4.0 compared to that at pH 3.0 (84.33%) and 5.0 (80.37%).
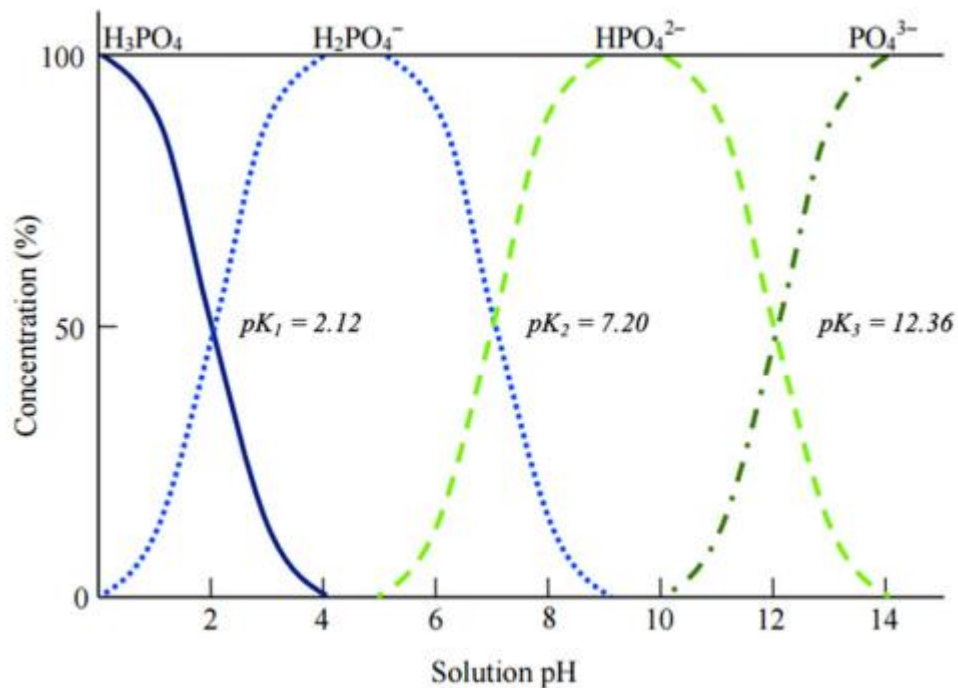
Figure 66: Curve depicting the phosphate species at various pH values (Suzaimi *et al.*, 2020).
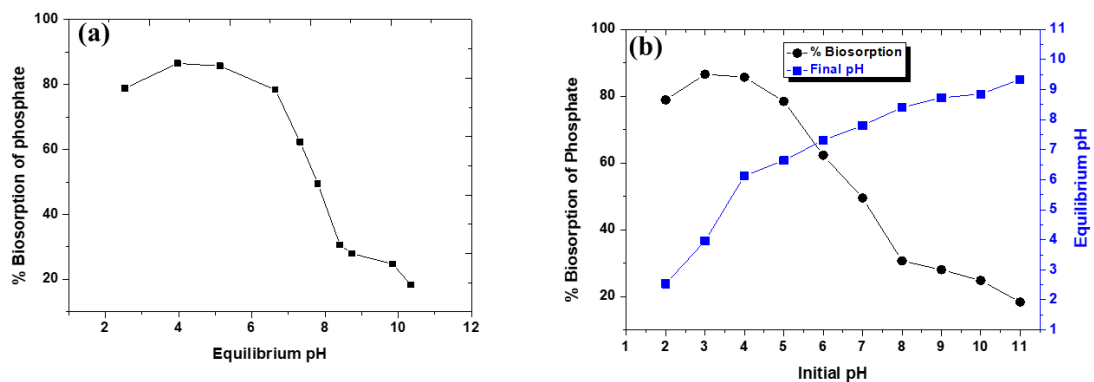
Figure 67: The Effect of solution pH on phosphate biosorption: (a) % biosorption of phosphate *vs* equilibrium pH; (b) Equilibrium pH and % biosorption of phosphate vs initial pH.

Figure 67(b) shows the % of phosphate biosorption versus starting pH as well as the equilibrium pH versus starting pH. The equilibrium pH increased following the biosorption, suggesting that a ligand exchange mechanism was used throughout the process to release the OH⁻ ions into the solution. The further release of OH⁻ ions from the biosorbent would be inhibited by the increasing concentration of OH⁻ in the solution, resulting in a reduction in % biosorption at higher pH.

4.7.3 Biosorption kinetics

Biosorption kinetics is typically used to evaluate the rate of biosorption, which is a crucial factor in determining how well an adsorbent performs. **Figure 68(a)** depicts the equilibrium concentration, % biosorption, and biosorption capacity (q_t) of phosphate onto SPP@Zr *vs* contact time at an preliminary phosphate concentration of 38.37 mg/L. The biosorption efficiency improved dramatically over time. Because of the abundance of newly available adsorption sites, the rate of phosphate adsorption increased significantly during the first 60 minutes of contact time, when approximately 87.5% of the maximum phosphate biosorption was achieved. Thereafter, the rate of phosphate biosorption gradually increased concerning contact time until reaching an equilibrium stage within 3 h of contact time. This tendency is explained by two factors: i) the steady reduction in the concentration gradient between the bulk solution and the adsorbent; and (ii) the progressive saturation of the accessible binding sites, which may cause repulsive forces between the adsorbed phosphate on the surface (Jung *et al.*, 2017). Since the equilibrium is established in less than 3 h, the agitation duration was set at 12 h in the tests that followed to make sure that phosphate completely adsorbs to SPP@Zr. **Figure 68(b)** represents a non-linear kinetic plot between q_t *vs* t.

To further understand the kinetic process, the PFO and PSO models were suited to the kinetic data. To calculate k_1 and k_2, q_e, and R^2, two independent graphs of $\log(q_e–q_t)$ against t (**Figure 69(a)**) and t/q_t against t (**Figure 69(b)**) were drawn. **Table 25** lists the estimated values for the kinetic parameters. Compared to the PFO model, R^2 of the PSO model (0.999) was nearer to unity. Additionally, the theoretical equilibrium biosorption capacity of SPP@Zr in the PSO kinetic (q_e(cal)) = 34.55 mg/g is near the actual result (q_e (exp)) = 34.39 mg/g. Due to the PSO kinetics of the phosphate biosorption processes on SPP@Zr, the biosorption of phosphate may be driven by chemisorption.
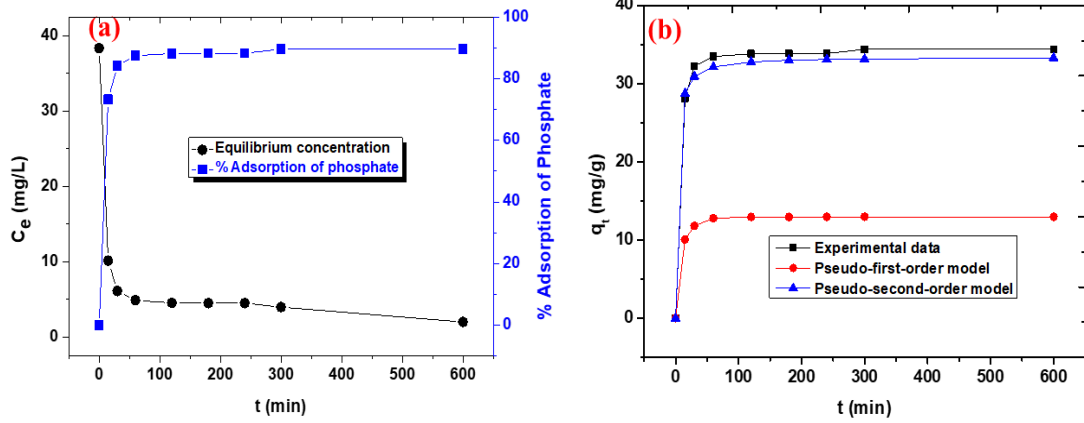
Figure 68: Biosorption kinetics study of phosphate: (a) equilibrium concentration and % biosorption vs contact time; (b) kinetic data and non-linear kinetics modeling with the PFO and PSO kinetics.
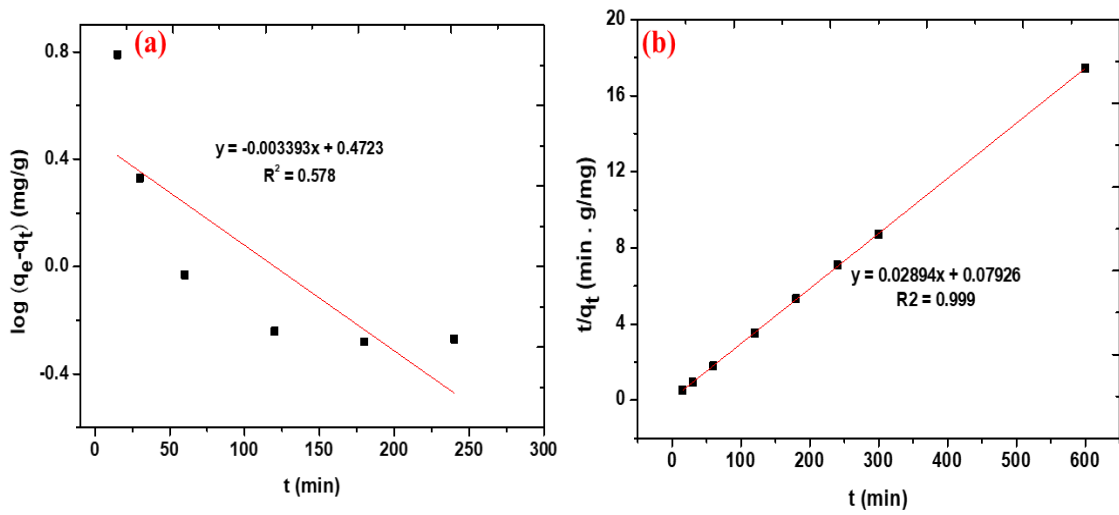
Figure 69: (a) PFO kinetics plot of SPP@Zr with phosphate system; (d) PSO kinetics plot of SPP@Zr with phosphate system.

Table 25: Kinetic parameters for the biosorption of phosphate onto SPP@Zr with two different models

Order	R^2	q_e (exp) (mg/g)	q_e (cal) (mg/g)	k_1 (min^{-1})	k_2 (mg/g/min)
PSO	0.999	34.39 ± 1.4	34.55 ± 1.3	-	1.16×10^{-2}
PFO	0.578	34.39 ± 1.4	12.97 ± 0.53	9.09×10^{-3}	-

139

4.7.4 Biosorption isotherm studies

The fluctuation of the initial phosphate concentration was used to designate the biosorption isotherm. **Figure 70** displays the phosphate biosorption isotherms at 298 K. The findings exhibit that when the phosphate concentration increased, the biosorption capacity increased quickly, then gradually until it reached saturation (plateau) at high concentrations. The initial high biosorption rate might be due to the increasing amount of accessible sorption sites for the biosorbent. Since the biosorption capacity has peaked at a high concentration area, no more sites are available for further biosorption.
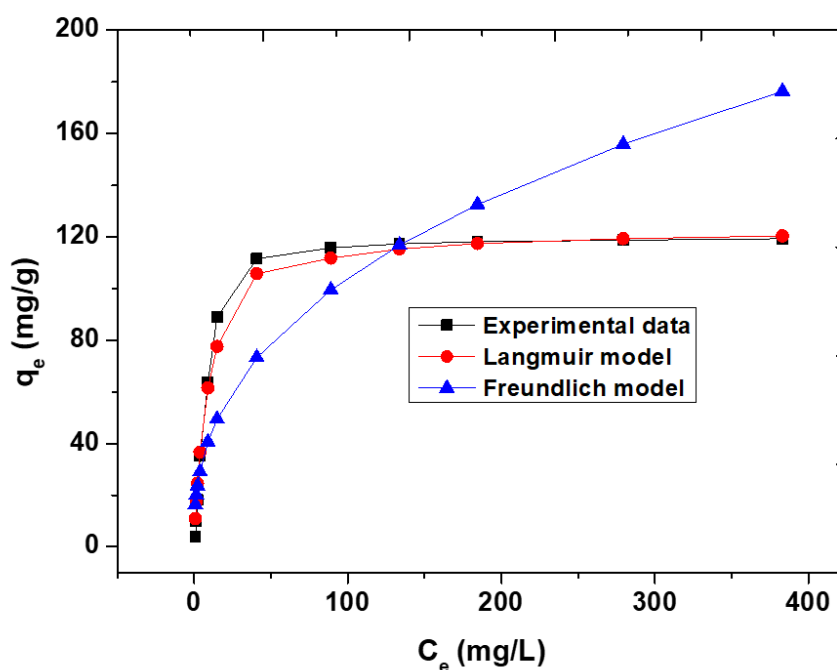
Figure 70: Biosorption isotherm for phosphate onto SPP@Zr from water.

The experimental data were examined utilizing the Langmuir and Freundlich isotherm models to elucidate the phosphate biosorption performance. **Figure 71(a)** depicts the plot of C_e/q_e *vs* C_e utilizing the Langmuir model. **Figure 71(b)** depicts the graph of the Freundlich model's linear relationship between $\log q_e$ and $\log C_e$. The assessed values for the isotherm parameters are listed in **Table 26**. The Langmuir model would be a better fit to explain how phosphate adsorbs onto SPP@Zr. It showed that the biosorption processes, which were thought to be monolayer homogenous biosorption processes, occurred on the biosorbent surface.

140
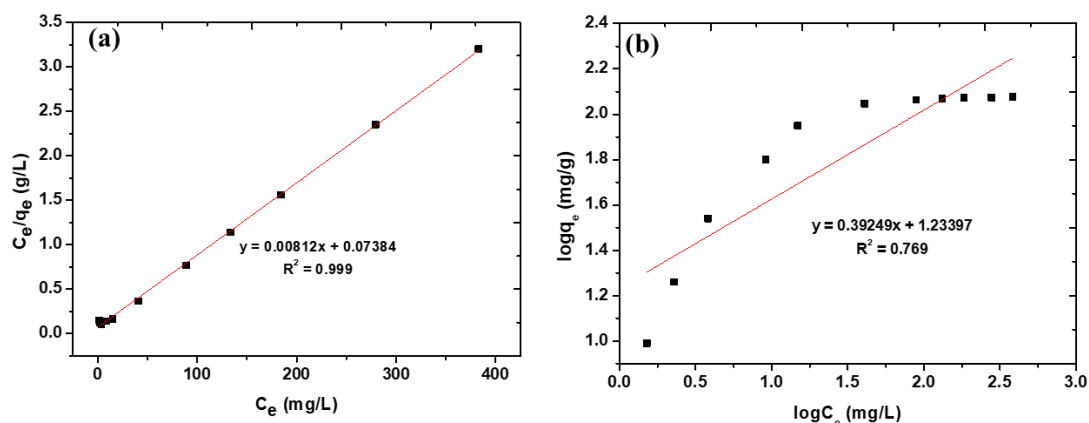
Figure 71: Linearized (a) Langmuir; and (b) Freundlich plot of phosphate biosorption onto SPP@Zr.

Table 26: Isotherms parameters for phosphate biosorption onto SPP@Zr

	Parameter	Value
	q_m (mg/g)	123.15 ± 3.5
Langmuir isotherm	b (L/mg)	0.109 ± 0.005
	R^2	0.999
	K_F (mg/g) (L/mg)$^{1/n}$	17.14 ± 0.83
Freundlich isotherm	1/n	0.392 ± 0.01
	R^2	0.769

Table 27: Comparison of phosphate biosorption capacities of different adsorbents

Adsorbent	q_m (mg/g)	Reference
Zr(III)-loaded okara	44.13	(Nguyen *et al.*, 2014)
Zr(IV)-loaded saponified watermelon rind	27.63	(Aryal *et al.*, 2022a)
$Zncl_2$-activated coir-pith carbon	5.10	(Namasivayam & Sangeetha, 2004)
Zr(IV) modified corn bracts	17.80	(Jiang *et al.*, 2019)
Zr(IV)-loaded apple Peels	20.35	(Mallampati & Valiyaveettil, 2013)
Iron-impregnated waste-activated sludge biochar	111.0	(Yang *et al.*, 2018a)
MgO-impregnated magnetic biochar	121.25	(Li *et al.*, 2016)
Fe(III)-loaded litchi seed	96.5	(Shrestha *et al.*, 2018)
SPP@Zr	123.15	This study

The q_m of SPP@Zr for phosphate estimated applying the Langmuir model was 123.15 mg/g. This value is greater than several other materials mentioned in earlier research, as shown in **Table 27**.

4.7.5 FE-SEM and EDX spectra of SPP@Zr before and after phosphate biosorption

It is found that the SPP@Zr surface structure is uniform, smooth, and has fewer pores and voids (**Figure 72(a)**). In the FE-SEM image (**Figure 72(b)**), the phosphate ions aggregate and form layers on the surface.
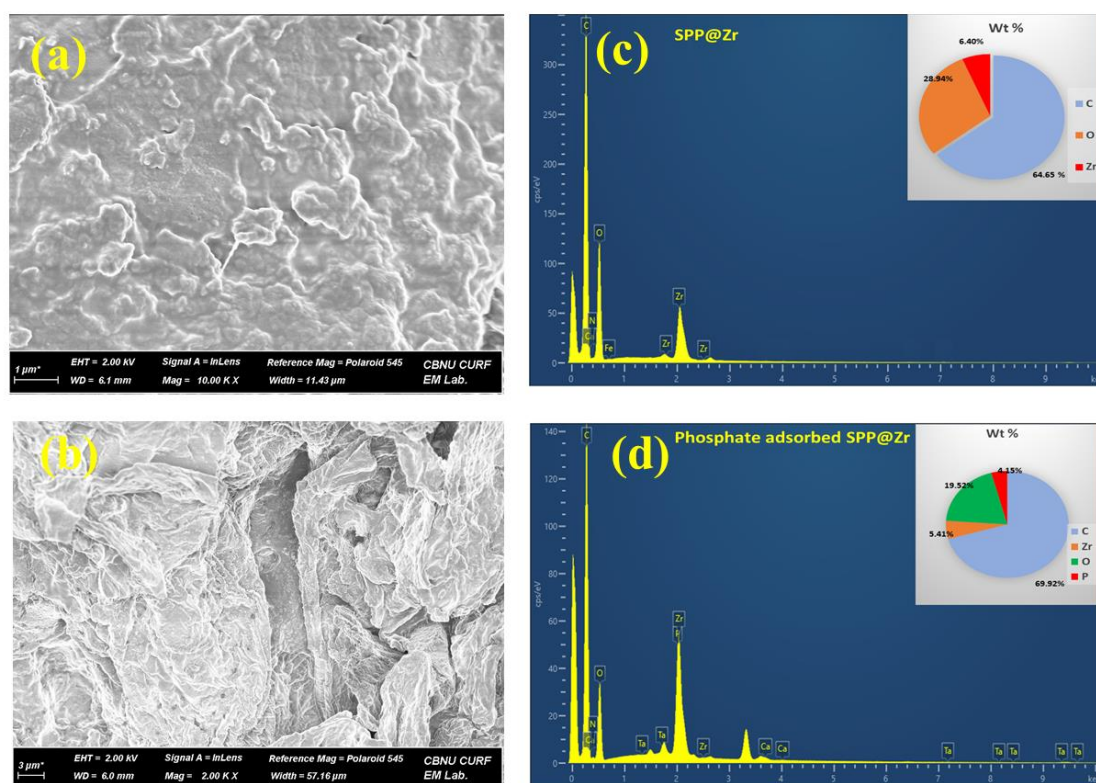
Figure 72: (a) FE-SEM micrographs of SPP@Zr; (b) FE-SEM micrograph of phosphate adsorbed SPP@Zr; (c) EDX spectra of SPP@Zr; and (d) EDX spectra of phosphate adsorbed SPP@Zr.

The significant peaks associated with C, O, and Zr are seen in the EDX spectra of SPP@Zr (**Figure 72(c)**). After phosphate biosorption, the additional peak associated with P was observed, indicating that the phosphate ions had effectively adsorbed onto SPP@Zr (**Figure 72(d)**). The persistence of the peak associated with Zr showed that the impregnated Zr(IV) did not leach away following the biosorption of phosphate.

142

This was further confirmed by EDX colour mapping images of all overlapping elements of SPP@Zr before phosphate biosorption (**Figure 73**), and after phosphate biosorption (**Figure 74**). The colour mapping investigation of the biosorption product demonstrates that phosphate biosorption is uniform.
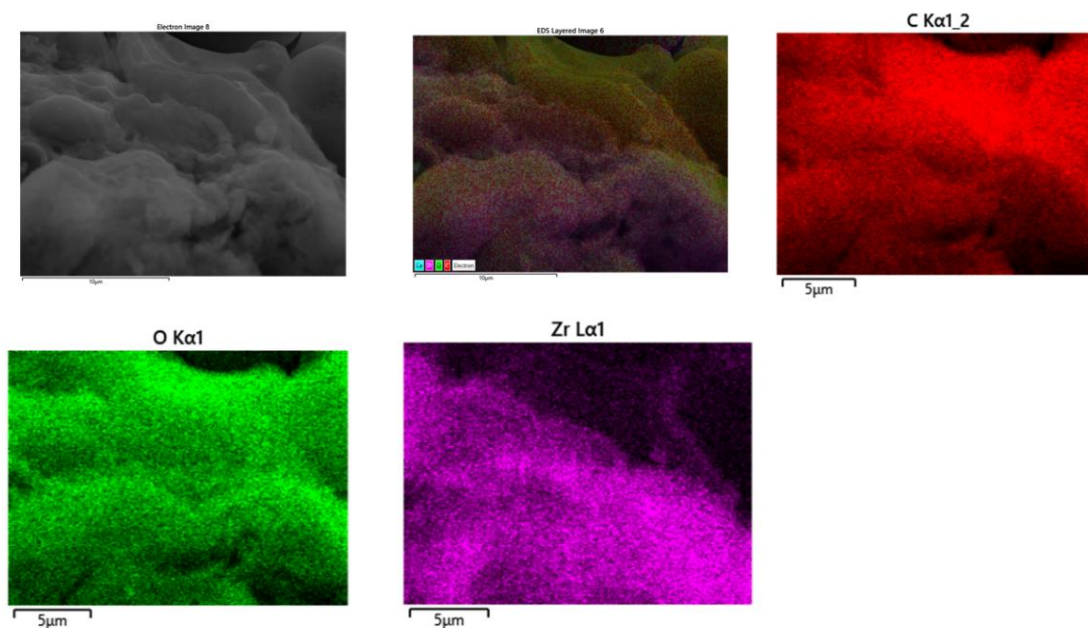
Figure 73: EDX electron image, layered image, and EDX colour mapping images of all overlapping elements of SPP@Zr before phosphate biosorption.
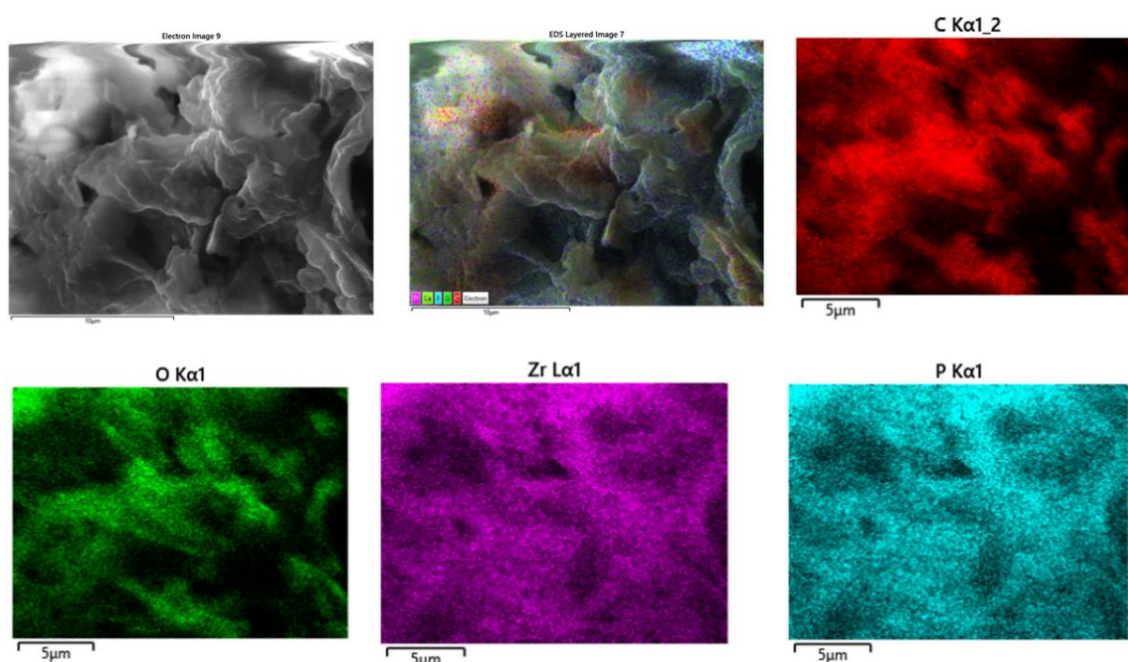
Figure 74: EDX electron image, layered image, and EDX colour mapping images of all overlapping elements of SPP@Zr after phosphate biosorption.

4.7.6 FTIR spectra of SPP@Zr and phosphate adsorbed SPP@Zr

The FTIR spectra are shown in **Figure 75**. In SPP@Zr, the broadband at 3326.67 cm^{-1} is related with the –OH bond, while the narrower peak at 2920.19 cm^{-1} is related with the –CH and –CH$_2$ groups. The -Zr-OH vibration may be related to the two peaks at 1148.17 and 1075.92 cm^{-1} (Lou et. al., 2021). Like the previous peak, the strong peak at 932.74 cm^{-1} is connected to -Zr-O linkage (Rahman *et al.*, 2021). It shows that SPP@Zr contains a lot of Zr-OH groups and provides convincing proof that Zr(IV) was effectively loaded onto SPP. After phosphate biosorption, the band at 3326.67 cm^{-1} was observed to be weaker and shifted to 3333.84 cm^{-1}. It was most likely caused by the role of -OH groups in phosphate biosorption. In the same way, the band at 1075.92 cm^{-1} (Zr-OH) was weakened, indicating that the -OH group was exchanged by phosphate. This outcome was consistent with that of phosphate absorption on Zr(IV) modified corn bracts (Jiang *et al.*, 2019) and Zr(IV) loaded cross-linked chitosan particles (Liu *et al.*, 2016).
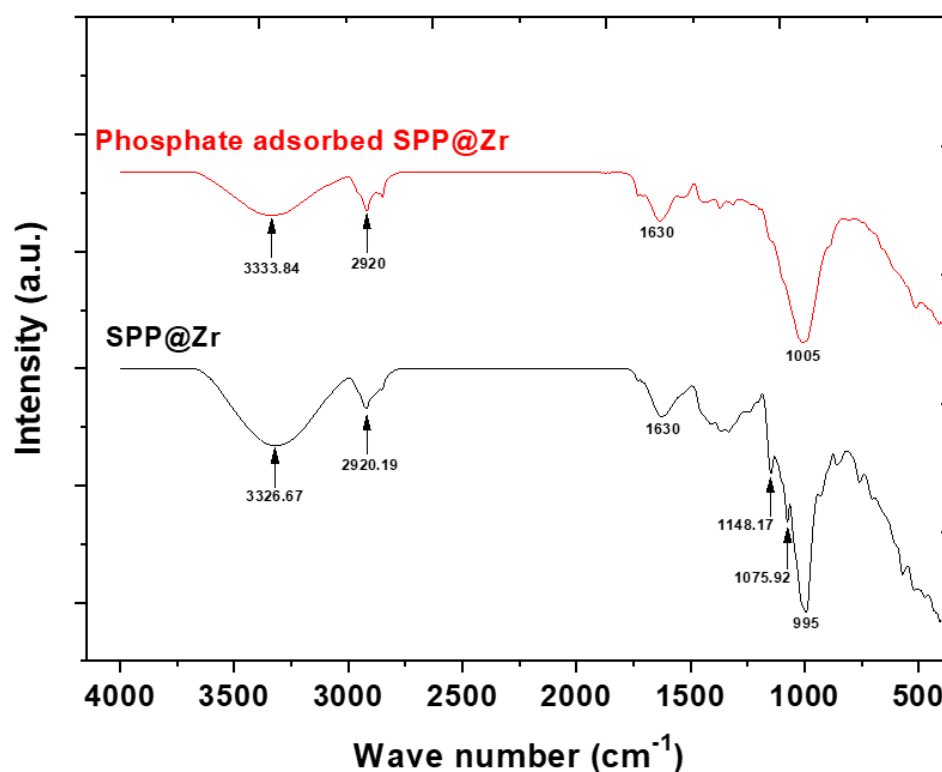
Figure 75: FTIR of SPP@Zr and phosphate adsorbed SPP@Zr.

144

4.7.7 Influence of competitive ions

In real wastewater, ions like Cl^-, SO_4^{2-}, NO_3^-, and CO_3^{2-} frequently coexist, which might interfere with the biosorption of phosphate. Consequently, the competitive ion biosorption experiment was carried out, and the outcomes are shown in **Figure 76**. Despite the coexisting ion concentration (0.01M) being higher than that of phosphate, the three ions, i.e., chloride, sulfate, and nitrate, had no discernible impact on the biosorption of phosphate relative to the blank solution. This shows that there was little competition between these three ions and phosphate ions for the binding site on SPP@Zr. The removal efficiency of phosphate, however, was only 44.37% in the presence of carbonate. The phenomenon demonstrated that phosphate and carbonate might engage in intense competition for the same biosorption sites on SPP@Zr.
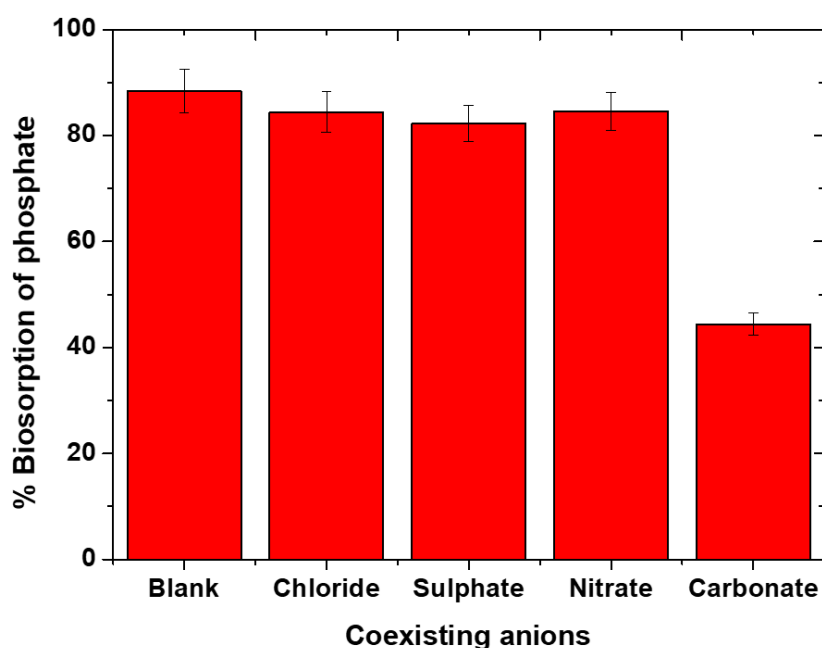
Figure 76: Effect of coexisting anions on phosphate biosorption onto SPP@Zr.

4.7.8 Desorption and reusability of SPP@Zr

For the biosorption process to become more cost-effective, a biosorbent with repeated biosorption-desorption cycles must be stable and recyclable. It was observed that the phosphate is only slightly adsorbed on SPP@Zr at an alkaline condition (pH > pHpzc). This suggests that the phosphate in the exhausted SPP@Zr can be desorbed by an alkaline solution. In this light, the phosphate adsorbed SPP@Zr can be

renewed for recycling utilizing a 0.1 M NaOH solution. The SPP@Zr desorbed by NaOH was isolated and neutralized for reuse by rinsing with DI water. After desorption, up to five series of biosorption/desorption were used to investigate the reusability of the adsorbent. The phosphate biosorption capacity declined from 87.9% to 62.7% after five consecutive cycles, as illustrated in **Figure 77**. There is the potential for a small amount of loaded Zr(IV) to leak during continuing biosorption, elution, and re-biosorption cycles, which would reduce the number of accessible active biosorption sites. Even though its biosorption capacity decreased with repeated recycling, the SPP@Zr was a highly ecological and promising biosorbent for removing phosphate from water. Even after the fifth cycle, the phosphate removal efficiency was still better than 62%.
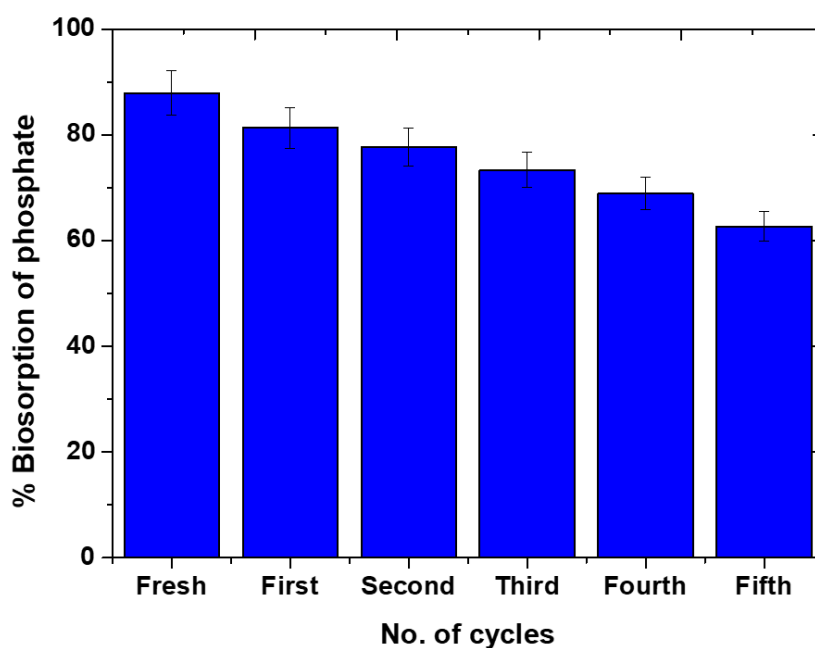
Figure 77: Variation of the % biosorption of Phosphate in 5 cycles' biosorption-desorption process.

4.7.9 Phosphate biosorption and desorption mechanism

The PSO model well matches the kinetic data for phosphate biosorption on SPP@Zr, indicating that chemisorption may be the driving force behind phosphate biosorption. By using the pH_{pzc} value and an FTIR analysis, the mechanism of phosphate biosorption on the SPP@Zr might be explained. The % adsorption of phosphate was substantially greater at $pH < pH_{PZC}$ than at $pH > pH_{PZC}$, per the pH study.

However, phosphate ions ($H_2PO_4^-$; HPO_4^{2-}) and surface hydroxyl groups of the SPP@Zr were substituted by the most common ligand exchange mechanisms that resulted in inner-sphere complexation. The FTIR spectra of SPP@Zr and phosphate adsorbed SPP@Zr endorsed this. After phosphate biosorption, the band at 1075.92 cm^{-1} (Zr-OH) was weakened, indicating that -OH group was exchanged by phosphate. After biosorption, the solution's pH increased, showing that OH^- ions were released into the solution via a ligand exchange reaction during the biosorption process. When zirconium is loaded onto SPP, pectic acid and Zr(IV) form stable chelates (Biswas *et al.*, 2008b). Utilizing a ligand exchange process, the OH^-ions present in the coordination sphere of Zr(IV) were anticipated to be swapped phosphate. The coordination sphere of hydrated zirconium has enough hydroxide ions and H_2O molecules to give ample biosorption sites for P species. Similarly, in the regeneration of used biosorbent, the adsorbed phosphate may be readily desorbed with NaOH solution. This process includes the ligand exchange mechanism between the adsorbed phosphate anions and the high concentration of OH^- ions present in the asolution. The ligand substitution mechanism for the biosorption and desorption of phosphate onto SPP@Zr is displayed in **Figure 78**.
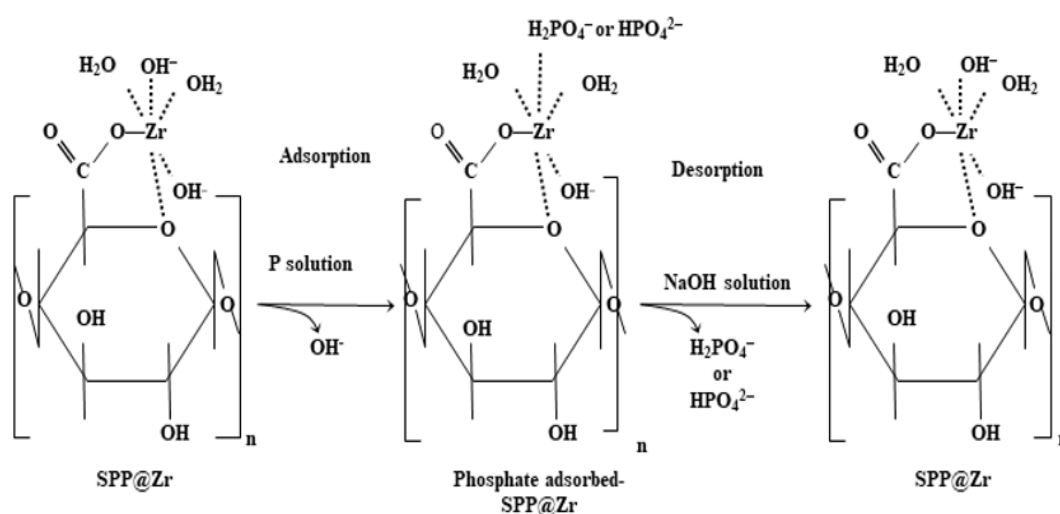
Figure 78: Biosorption-desorption mechanism of phosphate onto SPP@Zr.

4.8 Application of SPP@Zr to natural water

The results of the analysis of the different parameters of water samples gathered from arsenic-polluted location of Nawalparasi West, Nepal, are shown in **Table 28**.

Table 28: Water quality parameters of arsenic-contaminated groundwater.

Parameters	G1	G2	G3
pH	7.16 ± 0.3	7.21 ± 0.3	7.37 ± 0.3
Total hardness (mg/L)	387 ± 6.5	321 ± 5.7	353 ± 5.1
Total dissolved solids (mg/L)	457 ± 5.3	513 ± 5.4	492 ± 4.8
Chloride (mg/L)	224 ± 2.9	233 ± 2.7	227 ± 3.1
Fluoride (mg/L)	0.32 ± 0.02	0.28 ± 0.02	0.39 ± 0.03
Sulphate (mg/L)	14.7 ± 0.72	18.5 ± 0.65	20.1 ± 0.63
Phosphate (mg/L)	1.3 ± 0.03	1.2 ± 0.02	1.5 ± 0.04
Iron (mg/L)	0.57 ± 0.04	0.62 ± 0.05	0.46 ± 0.04
Total arsenic (µg/L)	87.2 ± 2.0	98.0 ± 2.7	67.3 ± 1.8

Three groundwater samples were collected, and batch biosorption tests using two different biosorbent doses (2.0 and 4.0 g/L) were performed on them at their native pH. The residual total arsenic concentrations were examined, and the findings are shown in **Table 29**. It displays that arsenic uptake increased as the adsorbent dosage was increased. At a dosage of 2.0 g/L, arsenic content was found to be much lower than the mark of drinking water tolerance threshold established by WHO and USEPA (10 µg/L), while arsenic removal effectiveness was determined to be greater than 99% at a dose of 4.0 g/L. These results support the idea that SPP@Zr offers a possible method for removing arsenic from polluted water.

Table 29: Application of SPP@Zr to real groundwater samples.

Parameters	Total Arsenic (µg/L) before biosorption	Residual total arsenic (µg/L) after biosorption	
		Dose 2.0 g/L	Dose 4.0 g/L
G1	87.2 ± 2.0	6.1 ± 0.3	ND
G2	98.0 ± 2.7	7.6 ± 0.3	ND
G3	67.3 ± 1.8	5.3 ± 0.2	ND

CHAPTER 5

CONCLUSIONS AND RECOMMENDATION

5.1 Conclusions

The major objectives of this study were preparation and characterization of low-cost ion-exchange type adsorbents from readily obtainable agricultural waste (pomegranate peel) as alternative materials to replace non-degradable synthetic ion-exchangers and to explore their viability for the efficient removal of some hazardous metallic ions (As, Pb, and Cd) and non-metallic ions (phosphate ions) from water. The findings of my investigations led to the following conclusions:

- Pomegranate peel waste was used to prepare biosorbents SPP, SPP@Zr, and SPP@TiO$_2$ as natural ion exchangers.

- The Zr, Ti, and Ca peaks, respectively, appeared in the EDX spectra of the SPP@Zr, SPP@TiO$_2$, and SPP, indicating that the pomegranate peel biomass had successfully been modified to become ion-exchangers. Like this, the EDX spectra of the biosorbents after the biosorption of hazardous ions clearly showed peaks of the corresponding hazardous ions, confirming the biosorption of the adsorbate on the adsorbents.

- Using FTIR spectra, the surface functionalities of the biosorbents were examined. There is a shifting of the absorption bands of the FTIR spectra of biosorbent towards higher or lower wavenumber sides with a change in intensity of the peaks due to the biosorption of hazardous ions. It shows the hazardous ions interact with surface functional groups of biosorbents, confirming the biosorption of the ions onto biosorbents. Specifically, in the FTIR spectra of SPP@Zr after arsenic and phosphate biosorption, the bands corresponding to OH- groups are prominently decreased, indicating that the OH group was exchanged by oxyanions of arsenic and phosphorous by a ligand exchange mechanism.

- The pHpzc of SPP@Zr and SPP were determined to be 7.2 and 4.6 respectively.

- SPP@Zr showed high biosorption capabilities for As(V), As(III) and phosphate ions from an aqueous solution when compared to other biosorbents mentioned in the literature. For As(V), As(III), and phosphate the q$_m$ of SPP@Zr were evaluated to be 83.33 mg/g, 72.52 mg/g and 123.15 mg/g, respectively. The

Langmuir isotherm model and the PSO kinetic model provided the best fits for all three biosorption processes.

- The biosorption processes of AS(V) onto SPP@Zr were found to be thermodynamically feasible, spontaneous, and endothermic.

- Biosorption of arsenic and phosphate were not impacted by the addition of other co-existing anions like Cl^-, SO_4^{2-}, NO_3^-, and CO_3^{2-}. However, the presence of phosphate ions intensely slows down the biosorption of arsenic and the presence of carbonate ions dramatically slow the biosorption of phosphate onto SPP@Zr.

- Using 0.1 M NaOH solution, As(V), As(III) and phosphate were eluted without any leakage of the loaded zirconium. Up to five biosorption-desorption cycles, the SPP@Zr demonstrated exceptional reusability and stability.

- The XPS analysis of the As(V) adsorbed SPP@Zr confirmed that only As(V) existed and that As(V) had not been reduced to As(III) during the biosorption process.

- According to the biosorption mechanism investigation, ligand exchange is essential for the biosorption of arsenic anions and phosphate ions onto SPP@Zr surfaces. Oxyanions of arsenic and phosphorous substituted the surface hydroxyl groups of the SPP@Zr by the most common ligand exchange mechanisms that resulted in inner-sphere complexation.

- The As(III) maximal biosorption capacity of PP@TiO$_2$ was 76.92 mg/g. The Langmuir isotherm model and the PSO kinetic model provided the best fits for the biosorption process. The coexisting ions such as chloride, and sulphate have an insignificant effect on removing As(III) by SPP@TiO$_2$, but the presence of phosphate ions significantly inhibits the biosorption of As(III) anion. Arsenic was successfully desorbed from the sorption product by using a 0.1 M NaOH solution for its safe disposal, and the biosorbent can be reused.

- The XPS analysis of As(III) adsorbed PP@TiO$_2$ showed that arsenic was present as As(III) and partly oxidized to As(V) in the As(III) adsorbed PP@TiO$_2$, demonstrating TiO$_2$ functions as both an adsorbent and a photocatalyst.

- Studies on fixed bed columns utilizing PP@TiO$_2$ showed that bed height, flow rate, and starting As(III) concentration had a substantial impact on column

performance. Column packing with SPP@Zr was found to be capable of completely removing As(III).

- For Pb(II) and Cd(II), the q_m of the SPP was assessed to be 229.88 mg/g and 174.52 mg/g, respectively. Both biosorption processes were discovered to be governed by a PSO kinetic model, with the Langmuir isotherm model providing the greatest match.

- The co-existing cations such as K^+, Ni^{2+}, Cu^{2+}, and Co^{2+} showed negligible effects on Pb(II) and Cd(II) removal by SPP.

- 0.1 M HNO_3 can be used for the effective desorption of Pb(II) and Cd(II) ions from exhausted SPP for safe disposal.

- Pb(II) and Cd(II) ions can be adsorbed onto SPP by replacing the Ca^{2+} ions of the SPP through a cation exchange mechanism.

- The SPP@Zr was used to remove total inorganic arsenic from naturally occurring groundwater samples obtained from an area in Nawalparasi West, Lumbini Province, that was arsenic-contaminated, and it was found to be extremely effective at removing arsenic much lower than the mark of the drinking water tolerance threshold established by the WHO and USEPA (10 μg/L).

- According to the deduction made above, the tested biosorbents (SPP@Zr, PP@TiO₂, and SPP) may be regarded as effective, economical, eco-friendly, and reusable ion-exchanger for removing hazardous cationic and anionic contaminants from aqueous solutions.

5.2 Recommendation

Pomegranate peel waste is successfully used to prepare natural ion-exchanger alternatives to the highly expensive synthetic ion-exchange resins and activated carbon for contaminants' removal from an aqueous environment. Among the developed biosorbents, SPP@Zr acts as an anion exchanger for the effective uptake of hazardous oxyanions (arsenate, arsenate, and phosphate); PP@TiO₂ acts as an anion exchanger as well as a photocatalyst, and SPP acts as a cation exchanger for efficient and rapid sequestration of metallic ions like Pb(II), and Cd(II). The demand for and usage of biomass-based adsorbents is anticipated to increase soon because of their simplicity of accessibility, affordability, and environmental friendliness. The

following is a list of some recommendations from this study for application and future prospective:

- Future research should examine extremely efficient, economical, and environmentally favorable biosorbents that are simple to regenerate from several operating cycles without noticeably losing their biosorption performance.

- The further modification technique of the surface functional groups of biomasses may prove to be a promising field of research in future courses of study.

- It is possible to study the micro-mechanics of the biosorption of different hazardous ions on biosorbents.

- To improve the widespread use of biosorbents, future research should focus on real contaminated water and industrial effluents employing the continuous column approach.

- A cost-benefit analysis on the usage of SPP@Zr as biosorbents for the removal and recovery of pollutants should be investigated.

CHAPTER 6

SUMMARY

The rapid urbanization expansion and sophisticated lifestyle of people in this 21st century are causing two important issues related to our fragile environment, which are the generation of solid waste and the poisoning of our water resources by pollutants. The global community is very concerned about water pollution, but poor nations like Nepal are particularly affected. The surface water and groundwater of Nepal are polluted by both metallic and non-metallic pollutants.

There are six chapters in this thesis. The following lists the important points of each chapter.

Chapter 1 describes the context of this study and provides a detailed research background for this study. The impacts of hazardous heavy metals and non-metals as well as water treatment techniques have been discussed. The applicability of biosorbents for toxic metallic and non-metallic ion removal is discussed. This chapter also describes the several theories that are used to interpret the outcomes of our experiments. The research objectives and rationale of the study are highlighted.

Chapter 2 presents a summary of the literature review on biosorption. A literature review concerning raw and chemically modified pomegranate peel and other various agro-wastes as biosorbents for removing hazardous metallic and non-metallic ions revealed that the pectin-rich pomegranate peel waste can be a cost-effective precursor for the preparation of an ion-exchanger to remove hazardous ions from aqueous solutions by the biosorption process.

Chapter 3 covers the materials and methods which describe the experimental procedure for preparing biosorbents, their physicochemical characterization, and the biosorption of As(V), As(III), Pb(II), Cd(II), and phosphate ions onto as-prepared biosorbents in an aqueous medium.

Chapter 4 refers the results and discussion containing the physicochemical characterization of biosorbents and the biosorption of aforementioned ions on prepared biosorbents in an aquatic environment, the reasoning behind the biosorption behavior, and analysis of the experimental result.

Chapter 5 alludes to overall conclusions drawn from the findings of this research work and finishes with recommendations for upcoming research.

Chapter 6 presents the summary of this thesis and ends with the references cited.

Based on the results and discussions, the studied biosorbents (SPP@Zr, PP@TiO$_2$, and SPP) may be regarded as effective, economical, eco-friendly, and recyclable ion-exchangers for removing hazardous cationic and anionic pollutants from aqueous solutions.

REFERENCES

Abbas, A., Al-Amer, A. M., Laoui, T., Al-Marri, M. J., Nasser, M. S., Khraisheh, M., & Atieh, M. A. (2016). Heavy metal removal from aqueous solution by advanced carbon nanotubes: critical review of adsorption applications. *Separation and Purification Technology*, **157**: 141-161.

Abbasi, Z., Alikarami, M., & Homafar, A. (2009). Adsorption study on pomegranate peel: removal of Ni^{2+} from aqueous solution and Co^{2+}. *Inorganic Chemistry*, **3**: 3-6.

Abdul, K. S. M., Jayasinghe, S. S., Chandana, E. P., Jayasumana, C., & De Silva, P. M. C. (2015). Arsenic and human health effects: A review. *Environmental Toxicology and Pharmacology*, **40**(3): 828-846.

Abdullah, N., Othman, F., Yusof, N., Matsuura, T., Lau, W., Jaafar, J., Ismail, A., Salleh, W., & Aziz, F. (2020). Preparation of nanocomposite activated carbon nanofiber/manganese oxide and its adsorptive performance toward lead (II) from aqueous solution. *Journal of Water Process Engineering*, **37**: 101430.

Ahamad, K. U., Singh, R., Baruah, I., Choudhury, H., & Sharma, M. R. (2018). Equilibrium and kinetics modeling of fluoride adsorption onto activated alumina, alum and brick powder. *Groundwater for Sustainable Development*, **7**: 452-458.

Ahluwalia, S. S., & Goyal, D. (2007). Microbial and plant derived biomass for removal of heavy metals from wastewater. *Bioresource Technology*, **98**(12): 2243-2257.

Ajith, N., Bhattacharyya, K., Ipte, P. R., Satpati, A. K., Tripathi, A. K., Verma, R., & Swain, K. K. (2019). Interaction of arsenic (III) and arsenic (V) on manganese dioxide: XPS and electrochemical investigations. *Journal of Environmental Science and Health, Part A*, **54**(4): 277-285.

Ajmal, M., Adeel, S., Azeem, M., Zuber, M., Akhtar, N., & Iqbal, N. (2014). Modulation of pomegranate peel colourant characteristics for textile dyeing using high energy radiations. *Industrial Crops and Products*, **58**: 188-193.

Akpor, O., & Muchie, M. (2010). Remediation of heavy metals in drinking water and wastewater treatment systems: processes and applications. *International Journal of Physical Sciences*, **5**(12): 1807-1817.

Aksu, Z., & İşoğlu, İ. A. (2005). Removal of copper (II) ions from aqueous solution by biosorption onto agricultural waste sugar beet pulp. *Process Biochemistry*, **40**(9): 3031-3044.

Alengebawy, A., Abdelkhalek, S. T., Qureshi, S. R., & Wang, M.-Q. (2021). Heavy metals and pesticides toxicity in agricultural soil and plants: Ecological risks and human health implications. *Toxics*, **9**(3): 42.

Al-Ghouti, M. A., & Da'ana, D. A. (2020). Guidelines for the use and interpretation of adsorption isotherm models: A review. *Journal of Hazardous Materials*, **393**: 122383.

Ali, I., Asim, M., & Khan, T. A. (2012). Low cost adsorbents for the removal of organic pollutants from wastewater. *Journal of Environmental Management*, **113**: 170-183.

Ali, S., Rizwan, M., Shakoor, M. B., Jilani, A., & Anjum, R. (2020). High sorption efficiency for As(III) and As(V) from aqueous solutions using novel almond shell biochar. *Chemosphere*, **243**: 125330.

Alqadami, A. A., Naushad, M., ALOthman, Z. A., Alsuhybani, M., & Algamdi, M. (2020). Excellent adsorptive performance of a new nanocomposite for removal of toxic Pb (II) from aqueous environment: adsorption mechanism and modeling analysis. *Journal of Hazardous Materials*, **389**: 121896.

Anantha, R. K., & Kota, S. (2016). Removal of lead by adsorption with the renewable biopolymer composite of feather (Dromaius novaehollandiae) and chitosan (Agaricus bisporus). *Environmental Technology & Innovation*, **6**: 11-26.

Arbind, K., & Vipin, K. (2015). Kinetic, equilibrium isotherm and thermodynamic study for removal of cadmium from wastewater by using modified pomegranate peel. *Journal of Chemical and Pharmaceutical Research*, **7**(1): 685-697.

Arslanoğlu, E., Eren, M. Ş., Arslanoğlu, H., & Çiftçi, H. (2021). Modification of grape pulp with citric acid for the production of natural ion exchanger resin and removal of Pb(II) and Cd(II) from aqueous solutions: kinetic, thermodynamics, and mechanism. *Biomass Conversion and Biorefinery*, 1-14.

Aryal, M., Ziagova, M., & Liakopoulou-Kyriakides, M. (2010). Study on arsenic biosorption using Fe(III)-treated biomass of *Staphylococcus xylosus*. *Chemical Engineering Journal*, **162**(1): 178-185.

Aryal, M., Ziagova, M., & Liakopoulou-Kyriakides, M. (2011). Comparison of Cr (VI) and As (V) removal in single and binary mixtures with Fe(III)-treated *Staphylococcus xylosus* biomass: thermodynamic studies. *Chemical Engineering Journal*, **169**(1-3): 100-106.

Aryal, R. L., Bhurtel, K. P., Poudel, B. R., Pokhrel, M. R., Paudyal, H., & Ghimire, K. N. (2022a). Sequestration of phosphate from water onto modified watermelon waste loaded with Zr (IV). *Separation Science and Technology*, **57**(1): 70-82.

Aryal, R. L., Thapa, A., Poudel, B. R., Pokhrel, M. R., Dahal, B., Paudyal, H., & Ghimire, K. N. (2022b). Effective biosorption of arsenic from water using La(III) loaded carboxyl functionalized watermelon rind. *Arabian Journal of Chemistry,* **15**(3):103674.

Awual, M. R., & Jyo, A. (2011). Assessing of phosphorus removal by polymeric anion exchangers. *Desalination*, **281**: 111-117.

Awual, M. R., Urata, S., Jyo, A., Tamada, M., & Katakai, A. (2008). Arsenate removal from water by a weak-base anion exchange fibrous adsorbent. *Water Research*, **42**(3): 689-696.

Ay, Ç. Ö., Özcan, A. S., Erdoğan, Y., & Özcan, A. (2012). Characterization of Punica granatum L. peels and quantitatively determination of its biosorption behavior towards lead (II) ions and Acid Blue 40. *Colloids and Surfaces B: Biointerfaces*, **100**: 197-204.

Ayele, A., Haile, S., Alemu, D., & Kamaraj, M. (2021). Comparative utilization of dead and live fungal biomass for the removal of heavy metal: a concise review. *The Scientific World Journal*, **2021**: 558811.

Azizullah, A., Khattak, M. N. K., Richter, P., & Häder, D.-P. (2011). Water pollution in Pakistan and its impact on public health-a review. *Environment International*, **37**(2): 479-497.

Babalola, B. M. (2018). *Investigating adsorption characteristics of Delonix regia for heavy metals removal in wastewater and its potential for remediating contaminated soils* (doctoral dissertation). Lancaster University (United Kingdom).

Bahar, M. M., Mahbub, K. R., Naidu, R., & Megharaj, M. (2018). As (V) removal from aqueous solution using a low-cost adsorbent coir pith ash: Equilibrium and kinetic study. *Environmental Technology & Innovation*, **9**: 198-209.

Baird, R. B., Eaton, A. D., & Clesceri, L. S. (2012). *Standard methods for the examination of water and wastewater* (Vol. 10). E. W. Rice (Ed.). Washington, DC: American public health association.

Bang, S., Patel, M., Lippincott, L., & Meng, X. (2005). Removal of arsenic from groundwater by granular titanium dioxide adsorbent. *Chemosphere*, **60**(3): 389-397.

Barakat, M., & Kumar, R. (2014). CHAPTER 10: Modified and new adsorbents for removal of heavy metals from wastewater. In *Heavy Metals In Water: Presence, Removal and Safety* (pp. 193-212). The Royal Society of Chemistry.

Bashar, R., Gungor, K., Karthikeyan, K., & Barak, P. (2018). Cost effectiveness of phosphorus removal processes in municipal wastewater treatment. *Chemosphere*, **197**: 280-290.

Bellahsen, N., Kakuk, B., Beszédes, S., Bagi, Z., Halyag, N., Gyulavári, T., Kertész, S., Amarti, A. E., Tombácz, E., & Hodúr, C. (2021). Iron-loaded pomegranate peel as a bio-adsorbent for phosphate removal. *Water*, **13**(19): 2709.

Ben-Ali, S. (2021). Application of raw and modified pomegranate peel for wastewater treatment: a literature overview and analysis. *International Journal of Chemical Engineering*, **2021**: 8840907

Ben-Ali, S., Jaouali, I., Souissi-Najar, S., & Ouederni, A. (2017). Characterization and adsorption capacity of raw pomegranate peel biosorbent for copper removal. *Journal of Cleaner Production*, **142**: 3809-3821.

Benyoucef, S., & Amrani, M. (2011). Removal of phosphorus from aqueous solutions using chemically modified sawdust of Aleppo pine (Pinus halepensis Miller): kinetics and isotherm studies. *The Environmentalist*, **31**(3): 200-207.

Bhardwaj, S., Soni, R., Gupta, S. K., & Shukla, D. P. (2020). Mercury, arsenic, lead and cadmium in waters of the Singrauli coal mining and power plants industrial zone, Central East India. *Environmental Monitoring and Assessment*, **192**(4): 1-20.

Bhat, A., Megeri, G. B., Thomas, C., Bhargava, H., Jeevitha, C., Chandrashekar, S., & Madhu, G. (2015). Adsorption and optimization studies of lead from aqueous solution using γ-Alumina. *Journal of Environmental Chemical Engineering*, **3**(1): 30-39.

Bhatnagar, A., & Minocha, A. (2009). Adsorptive removal of 2, 4-dichlorophenol from water utilizing Punica granatum peel waste and stabilization with cement. *Journal of Hazardous Materials*, **168**(2-3): 1111-1117.

Bhatnagar, A., & Minocha, A. K. (2010). Biosorption optimization of nickel removal from water using Punica granatum peel waste. *Colloids and Surfaces B: Biointerfaces*, **76**(2): 544-548.

Bissen, M., Vieillard-Baron, M. M., Schindelin, A. J., & Frimmel, F. H. (2001). TiO2-catalyzed photooxidation of arsenite to arsenate in aqueous samples. *Chemosphere*, **44**(4): 751-757.

Biswas, B. K., Inoue, J.-i., Inoue, K., Ghimire, K. N., Harada, H., Ohto, K., & Kawakita, H. (2008a). Adsorptive removal of As (V) and As (III) from water

by a Zr (IV)-loaded orange waste gel. *Journal of Hazardous Materials*, **154**(1-3): 1066-1074.

Biswas, B. K., Inoue, K., Ghimire, K. N., Harada, H., Ohto, K., & Kawakita, H. (2008b). Removal and recovery of phosphorus from water by means of adsorption onto orange waste gel loaded with zirconium. *Bioresource Technology*, **99**(18): 8685-8690.

Bodalo, A., Gomez, J.-L., Gomez, E., Leon, G., & Tejera, M. (2005). Ammonium removal from aqueous solutions by reverse osmosis using cellulose acetate membranes. *Desalination*, **184**(1-3): 149-155.

Boer, M. A. d., Wolzak, L., & Slootweg, J. C. (2019). Phosphorus: reserves, production, and applications. In *Phosphorus Recovery and Recycling* (pp. 75-100). Springer, Singapore.

Boyd, G. E., Adamson, A. W., & Myers Jr, L. S. (1947). The exchange adsorption of ions from aqueous solutions by organic zeolites. II. Kinetics[1]. *Journal of the American Chemical Society*, **69**(11): 2836-2848.

Bulgariu, D., & Bulgariu, L. (2013). Sorption of Pb (II) onto a mixture of algae waste biomass and anion exchanger resin in a packed-bed column. *Bioresource Technology*, **129**: 374-380.

Cai, X., Li, J., Liu, Y., Yan, Z., Tan, X., Liu, S., ... & Jiang, L. (2018). Titanium dioxide-coated biochar composites as adsorptive and photocatalytic degradation materials for the removal of aqueous organic pollutants. *Journal of Chemical Technology & Biotechnology*, **93**(3): 783-791.

Camacho, L. M., Parra, R. R., & Deng, S. (2011). Arsenic removal from groundwater by MnO2-modified natural clinoptilolite zeolite: Effects of pH and initial feed concentration. *Journal of Hazardous Materials*, **189**(1-2): 286-293.

Cao, S., Duan, X., Zhao, X., Wang, B., Ma, J., Fan, D., Sun, C., He, B., Wei, F., & Jiang, G. (2015). Health risk assessment of various metal (loid) s via multiple exposure pathways on children living near a typical lead-acid battery plant, China. *Environmental Pollution*, **200**: 16-23.

Carolin, C. F., Kumar, P. S., Saravanan, A., Joshiba, G. J., & Naushad, M. (2017). Efficient techniques for the removal of toxic heavy metals from aquatic environment: A review. *Journal of Environmental Chemical Engineering*, **5**(3): 2782-2799.

Chakraborty, R., Verma, R., Asthana, A., Vidya, S. S., & Singh, A. K. (2021). Adsorption of hazardous chromium (VI) ions from aqueous solutions using modified sawdust: kinetics, isotherm and thermodynamic modelling. *International Journal of Environmental Analytical Chemistry*, **101**(7): 911-928.

Chandra, V., Park, J., Chun, Y., Lee, J. W., Hwang, I. C., & Kim, K. S. (2010). Water-dispersible magnetite-reduced graphene oxide composites for arsenic removal. *ACS nano*, **4**(7): 3979-3986.

Chen, W., Parette, R., Zou, J., Cannon, F. S., & Dempsey, B. A. (2007). Arsenic removal by iron-modified activated carbon. *Water Research*, **41**(9): 1851-1858.

Chen, Y., Shen, Z., & Li, X. (2004). The use of vetiver grass (Vetiveria zizanioides) in the phytoremediation of soils contaminated with heavy metals. *Applied Geochemistry*, **19**(10): 1553-1565.

Chiban, M., Carja, G., Lehutu, G., & Sinan, F. (2016). Equilibrium and thermodynamic studies for the removal of As(V) ions from aqueous solution using dried plants as adsorbents. *Arabian Journal of Chemistry*, **9**: S988-S999.

Choi, C., Hwang, K. J., Kim, Y. J., Kim, G., Park, J. Y., & Jin, S. (2016). Rice-straw-derived hybrid TiO_2–SiO_2 structures with enhanced photocatalytic properties for removal of hazardous dye in aqueous solutions. *Nano Energy*, **20**: 76-83.

Chowdhury, T., Zhang, L., Zhang, J., & Aggarwal, S. (2018). Removal of arsenic (III) from aqueous solution using metal organic framework-graphene oxide nanocomposite. *Nanomaterials*, **8**(12): 1062.

Chuang, C. L., Fan, M., Xu, M., Brown, R. C., Sung, S., Saha, B., & Huang, C. P. (2005). Adsorption of arsenic (V) by activated carbon prepared from oat hulls. *Chemosphere*, **61**(4): 478-483.

Danh, L. T., Truong, P., Mammucari, R., Tran, T., & Foster, N. (2009). Vetiver grass, Vetiveria zizanioides: a choice plant for phytoremediation of heavy metals and organic wastes. *International Journal of Phytoremediation*, **11**(8): 664-691.

Davydiuk, T., Chen, X., Huang, L., Shuai, Q., & Le, X. C. (2020). Removal of inorganic arsenic from water using metal organic frameworks. *Journal of Environmental Sciences (China)*, **97**: 162-168.

De Gisi, S., Lofrano, G., Grassi, M., & Notarnicola, M. (2016). Characteristics and adsorption capacities of low-cost sorbents for wastewater treatment: a review. *Sustainable Materials and Technologies*, **9**: 10-40.

Demirbas, A. (2008). Heavy metal adsorption onto agro-based waste materials: a review. *Journal of Hazardous Materials*, **157**(2-3): 220-229.

Dhoble, R. M., Lunge, S., Bhole, A. G., & Rayalu, S. (2011). Magnetic binary oxide particles (MBOP): a promising adsorbent for removal of As(III) in water. *Water Research*, **45**(16): 4769-4781.

Ding, Y., Jing, D., Gong, H., Zhou, L., & Yang, X. (2012). Biosorption of aquatic cadmium (II) by unmodified rice straw. *Bioresource Technology*, **114**: 20-25.

Dursun, A. Y. (2006). A comparative study on determination of the equilibrium, kinetic and thermodynamic parameters of biosorption of copper (II) and lead (II) ions onto pretreated Aspergillus niger. *Biochemical Engineering Journal*, **28**(2): 187-195.

Ekka, B., Rout, L., Kumar, M. K. S. A., Patel, R. K., & Dash, P. (2015). Removal efficiency of Pb (II) from aqueous solution by 1-alkyl-3-methylimidazolium bromide ionic liquid mediated mesoporous silica. *Journal of Environmental Chemical Engineering*, **3**(2): 1356-1364.

Ekrayem, N. A., Alhwaige, A. A., Elhrari, W., & Amer, M. (2021). Removal of lead (II) ions from water using chitosan/polyester crosslinked spheres derived from chitosan and glycerol-based polyester. *Journal of Environmental Chemical Engineering*, **9**(6): 106628.

Elwakeel, K. Z., Elgarahy, A. M., Khan, Z. A., Almughamisi, M. S., & Al-Bogami, A. S. (2020). Perspectives regarding metal/mineral-incorporating materials for water purification: with special focus on Cr (VI) removal. *Materials Advances*, **1**(6): 1546-1574.

Eris, S., & Azizian, S. (2017). Analysis of adsorption kinetics at solid/solution interface using a hyperbolic tangent model. *Journal of Molecular Liquids*, **231**: 523-527.

Fausey, C. L., Zucker, I., Shaulsky, E., Zimmerman, J. B., & Elimelech, M. (2019). Removal of arsenic with reduced graphene oxide-TiO_2-enabled nanofibrous mats. *Chemical Engineering Journal*, **375**: 122040.

Feng, L., Cao, M., Ma, X., Zhu, Y., & Hu, C. (2012). Superparamagnetic high-surface-area Fe_3O_4 nanoparticles as adsorbents for arsenic removal. *Journal of hazardous Materials*, **217**: 439-446.

Ferguson, M. A., Hoffmann, M. R., & Hering, J. G. (2005). TiO_2-photocatalyzed As(III) oxidation in aqueous suspensions: reaction kinetics and effects of adsorption. *Environmental Science & Technology*, **39**(6): 1880-1886.

Foo, K. Y., & Hameed, B. H. (2010). Insights into the modeling of adsorption isotherm systems. *Chemical Engineering Journal*, **156**(1): 2-10.

Foo, K., Lee, L., & Hameed, B. (2013). Preparation of tamarind fruit seed activated carbon by microwave heating for the adsorptive treatment of landfill leachate: a laboratory column evaluation. *Bioresource Technology*, **133**: 599-605.

Freundlich, H. (1907). Über die adsorption in lösungen. *Zeitschrift für physikalische Chemie*, **57**(1): 385-470.

Garg, U., Kaur, M., Jawa, G., Sud, D., & Garg, V. (2008). Removal of cadmium (II) from aqueous solutions by adsorption on agricultural waste biomass. *Journal of Hazardous Materials*, **154**(1-3): 1149-1157.

Gavlighi, H. A., Tabarsa, M., You, S., Surayot, U., & Ghaderi-Ghahfarokhi, M. (2018). Extraction, characterization and immunomodulatory property of pectic polysaccharide from pomegranate peels: Enzymatic vs conventional approach. *International Journal of Biological Macromolecules*, **116**: 698-706.

Ghimire, K. N., Inoue, K., Makino, K., & Miyajima, T. (2002). Adsorptive removal of arsenic using orange juice residue. *Separation Science and Technology*, **37**(12): 2785-2799.

Ghimire, K. N., Inoue, K., Ohto, K., & Hayashida, T. (2007). Adsorptive separation of metallic pollutants onto waste seaweeds, *Porphyra yezoensis* and *Ulva japonica*. *Separation Science and Technology*, **42**(9): 2003-2018.

Ghimire, K. N., Inoue, K., Ohto, K., & Hayashida, T. (2008). Adsorption study of metal ions onto crosslinked seaweed *Laminaria japonica*. *Bioresource Technology*, **99**(1): 32-37.

Ghimire, K. N., Inoue, K., Yamaguchi, H., Makino, K., & Miyajima, T. (2003). Adsorptive separation of arsenate and arsenite anions from aqueous medium by using orange waste. *Water Research*, **37**(20): 4945–4953.

Ghimire, S., Pokhrel, N., Pant, S., Gyawali, T., Koirala, A., Mainali, B., Angove, M. J., & Paudel, S. R. (2022). Assessment of technologies for water quality control of the Bagmati River in Kathmandu valley, Nepal. *Groundwater for Sustainable Development*, **18**: 100770.

Ghodbane, I., & Hamdaoui, O. (2008). Removal of mercury (II) from aqueous media using eucalyptus bark: kinetic and equilibrium studies. *Journal of Hazardous Materials*, **160**(2-3): 301-309.

Ghosh, M., & Singh, S. (2005). A review on phytoremediation of heavy metals and utilization of it's by products. *Asian Journal of Energy and Environment*, **6**(4): 18.

Gibbons, M. K. (2010). *The use of water treatment residual solids for arsenate and phosphate adsorption*. Library and Archives Canada=Bibliothèque et Archives Canada, Ottawa.

Giri, D. D., Alhazmi, A., Mohammad, A., Haque, S., Srivastava, N., Thakur, V. K., Gupta, V. K., & Pal, D. B. (2022). Lead removal from synthetic wastewater by biosorbents prepared from seeds of Artocarpus Heterophyllus and Syzygium Cumini. *Chemosphere*, **287**: 132016.

Giri, R., Kumari, N., Behera, M., Sharma, A., Kumar, S., Kumar, N., & Singh, R. (2021). Adsorption of hexavalent chromium from aqueous solution using pomegranate peel as low-cost biosorbent. *Environmental Sustainability*, **4**(2): 401-417.

Govindaswamy, S., Schupp, D. A., & Rock, S. A. (2011). Batch and continuous removal of arsenic using hyacinth roots. *International Journal of Phytoremediation*, **13**(6): 513-527.

Grassi, M., Kaykioglu, G., Belgiorno, V., & Lofrano, G. (2012). Removal of emerging contaminants from water and wastewater by adsorption process. In *Emerging compounds removal from wastewater* (pp. 15-37). Springer, Dordrecht.

Guo, G. Y., & Chen, Y. L. (2004). New zirconium hydroxide. *Journal of Materials Science*, **39**(12): 4039-4043.

Gupta, A., Vidyarthi, S. R., & Sankararamakrishnan, N. (2015). Concurrent removal of As(III) and As(V) using green low cost functionalized biosorbent–Saccharum officinarum bagasse. *Journal of Environmental Chemical Engineering*, **3**(1): 113-121.

Güzel, F., Aksoy, Ö., & Akkaya, G. (2012). Application of pomegranate (Punica granatum) pulp as a new biosorbent for the removal of a model basic dye (methylene blue). *World Appllied Sciences Journal*, **20**(7): 965-975.

Hall, K. R., Eagleton, L. C., Acrivos, A., & Vermeulen, T. (1966). Pore-and solid-diffusion kinetics in fixed-bed adsorption under constant-pattern conditions. *Industrial & Engineering Chemistry Fundamentals*, **5**(2): 212-223.

Hanief, A., & Laursen, A. E. (2019). Meeting updated phosphorus reduction goals by applying best management practices in the Grand River watershed, southern Ontario. *Ecological Engineering*, **130**: 169-175.

Hao, L., Liu, M., Wang, N., & Li, G. (2018). A critical review on arsenic removal from water using iron-based adsorbents. *RSC Advances*, **8**(69): 39545-39560.

Hao, L., Zheng, T., Jiang, J., Zhang, G., & Wang, P. (2016). Removal of As (III) and As (V) from water using iron doped amino functionalized sawdust: characterization, adsorptive performance and UF membrane separation. *Chemical Engineering Journal*, **292**: 163-173.

Hasnaoui, N., Wathelet, B., & Jiménez-Araujo, A. (2014). Valorization of pomegranate peel from 12 cultivars: Dietary fibre composition, antioxidant capacity and functional properties. *Food Chemistry*, **160**: 196-203.

Hernández, F., Legua, P., Melgarejo-Sánchez, P., & Martinez Font, R. (2012). The pomegranate tree in the world: Its problems and uses. In *Options Méditerranéennes. Séries A: Mediterranean Seminars*, CIHEAM-IAMZ, Zaragoza, Spain; Universidad Miguel Hernández,, Elche, Spain.

Hinrichsen, D., & Tacio, H. (2002). The coming freshwater crisis is already here. *The linkages between population and water. Washington, DC: Woodrow Wilson International Center for Scholars*, 1-26.

Ho, Y.-S., & McKay, G. (1999). Pseudo-second order model for sorption processes. *Process Biochemistry*, **34**(5): 451-465.

Homagai, P. L., Ghimire, K. N., & Inoue, K. (2010). Adsorption behavior of heavy metals onto chemically modified sugarcane bagasse. *Bioresource Technology*, **101**(6): 2067-2069.

Huang, X., Liao, X., & Shi, B. (2009). Adsorption removal of phosphate in industrial wastewater by using metal-loaded skin split waste. *Journal of Hazardous Materials*, **166**(2-3): 1261-1265.

Hubicki, Z., & Kołodyńska, D. (2012). Selective removal of heavy metal ions from waters and waste waters using ion exchange methods. *Ion Exchange Technologies*, **7**: 193-240.

Imran, M., Iqbal, M. M., Iqbal, J., Shah, N. S., Khan, Z. U. H., Murtaza, B., ... & Rizwan, M. (2021). Synthesis, characterization and application of novel MnO and CuO impregnated biochar composites to sequester arsenic (As) from water: modeling, thermodynamics and reusability. *Journal of Hazardous Materials*, **401**: 123338.

Iqbal, M., Saeed, A., & Zafar, S. I. (2009). FTIR spectrophotometry, kinetics and adsorption isotherms modeling, ion exchange, and EDX analysis for understanding the mechanism of Cd^{2+} and Pb^{2+} removal by mango peel waste. *Journal of Hazardous Materials*, **164**(1): 161-171.

Jafari Kang, A., Baghdadi, M., & Pardakhti, A. (2016). Removal of cadmium and lead from aqueous solutions by magnetic acid-treated activated carbon nanocomposite. *Desalination and Water Treatment*, **57**(40): 18782-18798.

Jain, M., Garg, V., & Kadirvelu, K. (2013). Cadmium (II) sorption and desorption in a fixed bed column using sunflower waste carbon calcium–alginate beads. *Bioresource Technology*, **129**: 242-248.

Jaishankar, M., Tseten, T., Anbalagan, N., Mathew, B. B., & Beeregowda, K. N. (2014). Toxicity, mechanism and health effects of some heavy metals. *Interdisciplinary Toxicology*, **7**(2): 60.

Jha, V. K., Matsuda, M., & Miyake, M. (2008). Sorption properties of the activated carbon-zeolite composite prepared from coal fly ash for Ni^{2+}, Cu^{2+}, Cd^{2+} and Pb^{2+}. *Journal of Hazardous Materials*, **160**(1): 148-153.

Jiang, Y., Chen, Y., Du, Q., & Shi, J. (2019). Adsorption of different forms of phosphorus on modified corn bracts. *Water Environment Research*, **91**(8): 748-755.

Joshi, S., Sharma, M., Kumari, A., Shrestha, S., & Shrestha, B. (2019). Arsenic removal from water by adsorption onto iron oxide/nano-porous carbon magnetic composite. *Applied Sciences*, **9**(18): 3732.

Jung, K.-W., Lee, S., & Lee, Y. J. (2017). Synthesis of novel magnesium ferrite (MgFe2O4)/biochar magnetic composites and its adsorption behavior for phosphate in aqueous solutions. *Bioresource Technology*, **245**: 751-759.

Jyothi, M. D., Kiran, K. R., & Ravindhranath, K. (2012). Phosphate pollution control in waste waters using new biosorbents. *International Journal of Water Resources and Environmental Engineering*, **4**(4): 73-85.

Kalmykova, Y., & Fedje, K. K. (2013). Phosphorus recovery from municipal solid waste incineration fly ash. *Waste Management*, **33**(6): 1403-1410.

Kanamarlapudi, S., Chintalpudi, V. K., & Muddada, S. (2018). Application of biosorption for removal of heavy metals from wastewater. *Biosorption*, **18**(69): 70-116.

Karabegovic, L., Uldal, M., Werker, A., & Morgan-Sagastume, F. (2013). Phosphorus recovery potential from a waste stream with high organic and nutrient contents via struvite precipitation. *Environmental Technology*, **34**(7): 871-883.

Karachalios, A. (2013). *Nutrient removal from water by various quaternized wood agricultural residues using a choline based ionic liquid analogue* (Doctoral thesis). Stevens Institute of Technology, New Jersey, United States.

Karmacharya, M. S., Gupta, V. K., Tyagi, I., Agarwal, S., & Jha, V. K. (2016). Removal of As(III) and As(V) using rubber tire derived activated carbon modified with alumina composite. *Journal of Molecular Liquids*, **216**: 836-844.

Kartel, M. T., Kupchik, L. A., & Veisov, B. K. (1999). Evaluation of pectin binding of heavy metal ions in aqueous solutions. *Chemosphere*, **38**(11): 2591-2596.

Kayastha, S. P. (2015). Heavy metals Fractionation in Bagmati River Sediments, Nepal. *Journal of Hydrology and Meteorology*, **9**(1): 119-128.

Khambhaty, Y., Mody, K., Basha, S., & Jha, B. (2009). Kinetics, equilibrium and thermodynamic studies on biosorption of hexavalent chromium by dead fungal biomass of marine Aspergillus niger. *Chemical Engineering Journal*, **145**(3): 489-495.

Khawaja, M., Mubarak, S., Zia-Ur-Rehman, M., Kazi, A. A., & Hamid, A. (2015). Adsorption studies of pomegranate peel activated charcoal for nickel (II) ion. *Journal of the Chilean Chemical Society*, **60**(4): 2642-2645.

Khuzestani, R. B., & Souri, B. (2013). Evaluation of heavy metal contamination hazards in nuisance dust particles, in Kurdistan Province, Western Iran. *Journal of Environmental Sciences*, **25**(7): 1346-1354.

Kong, S., Lu, B., Ji, Y., Zhao, X., Chen, L., Li, Z., Han, B., & Bai, Z. (2011). Levels, risk assessment and sources of PM10 fraction heavy metals in four types dust from a coal-based city. *Microchemical Journal*, **98**(2): 280-290.

Krishnan, K. A., & Haridas, A. (2008). Removal of phosphate from aqueous solutions and sewage using natural and surface modified coir pith. *Journal of Hazardous Materials*, **152**(2): 527-535.

Kumar, R., & Pal, P. (2015). Assessing the feasibility of N and P recovery by struvite precipitation from nutrient-rich wastewater: a review. *Environmental Science and Pollution Research*, **22**(22): 17453-17464.

Lagergren, S. (1898). Zur theorie der sogenannten adsorption geloster stoffe. *Kungliga svenska vetenskapsakademiens. Handlingar*, **24**: 1-39.

Lambert, J., Rakib, M., Durand, G., & Avila-Rodríguez, M. (2006). Treatment of solutions containing trivalent chromium by electrodialysis. *Desalination*, **191**(1-3): 100-110.

Langmuir, I. (1916). The Constitution and fundamental properties of solids and liquids. *Journal of the American Chemical Society,* **38**(11): 2221-2295.

Lansky, E. P., & Newman, R. A. (2007). Punica granatum (pomegranate) and its potential for prevention and treatment of inflammation and cancer. *Journal of Ethnopharmacology*, **109**(2): 177-206.

Lebron, Y. A. R., Moreira, V. R., & de Souza Santos, L. V. (2021). Biosorption of methylene blue and eriochrome black T onto the brown macroalgae Fucus vesiculosus: equilibrium, kinetics, thermodynamics and optimization. *Environmental Technology*, **42**(2): 279-297.

Lenoble, V., Bouras, O., Deluchat, V., Serpaud, B., & Bollinger, J. C. (2002). Arsenic adsorption onto pillared clays and iron oxides. *Journal of Colloid and Interface Science*, **255**(1): 52-58.

Li, J., Ma, J., Guo, Q., Zhang, S., Han, H., Zhang, S., & Han, R. (2020). Adsorption of hexavalent chromium using modified walnut shell from solution. *Water Science and Technology*, **81**(4): 824-833.

Li, R., Wang, J. J., Zhou, B., Awasthi, M. K., Ali, A., Zhang, Z., Lahori, A. H., & Mahar, A. (2016). Recovery of phosphate from aqueous solution by magnesium oxide decorated magnetic biochar and its potential as phosphate-based fertilizer substitute. *Bioresource Technology*, **215**: 209-214.

Li, T., Su, X., Yu, X., Song, H., Zhu, Y., & Zhang, Y. (2018). La (OH) 3-modified magnetic pineapple biochar as novel adsorbents for efficient phosphate removal. *Bioresource Technology*, **263**: 207-213.

Li, X., Guo, J., Dong, R., Ahring, B. K., & Zhang, W. (2016). Properties of plant nutrient: comparison of two nutrient recovery techniques using liquid fraction of digestate from anaerobic digester treating pig manure. *Science of the Total Environment*, **544**: 774-781.

Li, Y., Yu, H., Liu, L., & Yu, H. (2021). Application of co-pyrolysis biochar for the adsorption and immobilization of heavy metals in contaminated environmental substrates. *Journal of Hazardous Materials*, **420**: 126655.

Li, Y., Zhao, R., Chao, S., Sun, B., Wang, C., & Li, X. (2018). Polydopamine coating assisted synthesis of MnO_2 loaded inorganic/organic composite electrospun fiber adsorbent for efficient removal of Pb^{2+} from water. *Chemical Engineering Journal*, **344**: 277-289.

Lin, C., Luo, W., Luo, T., Zhou, Q., Li, H., & Jing, L. (2018). A study on adsorption of Cr (VI) by modified rice straw: Characteristics, performances and mechanism. *Journal of Cleaner Production*, **196**: 626-634.

Lin, S.-H., & Juang, R.-S. (2002). Removal of free and chelated Cu (II) ions from water by a nondispersive solvent extraction process. *Water Research*, **36**(14): 3611-3619.

Lin, S.-H., Kao, H.-C., Su, H.-N., & Juang, R.-S. (2005). Effect of formaldehyde on Cu (II) removal from synthetic complexed solutions by solvent extraction. *Journal of Hazardous Materials*, **120**(1-3): 1-7.

Liu, Q., Hu, P., Wang, J., Zhang, L., & Huang, R. (2016). Phosphate adsorption from aqueous solutions by zirconium (IV) loaded cross-linked chitosan particles. *Journal of the Taiwan Institute of Chemical Engineers*, **59**: 311-319.

Liu, X., Ao, H., Xiong, X., Xiao, J., & Liu, J. (2012). Arsenic removal from water by iron-modified bamboo charcoal. *Water, Air, & Soil Pollution*, **223**(3): 1033-1044.

Liu, X., Ma, R., Wang, X., Ma, Y., Yang, Y., Zhuang, L., Zhang, S., Jehan, R., Chen, J., & Wang, X. (2019). Graphene oxide-based materials for efficient removal of heavy metal ions from aqueous solution: A review. *Environmental Pollution*, **252**: 62-73.

Lou, S., Liu, B., Qin, Y., Zeng, Y., Zhang, W., & Zhang, L. (2021). Enhanced removal of As (III) and As (V) from water by a novel zirconium-chitosan modified spherical sodium alginate composite. *International Journal of Biological Macromolecules*, **176**: 304-314.

Maji, S. K., Pal, A., Pal, T., & Adak, A. (2007). Modeling and fixed bed column adsorption of As (III) on laterite soil. *Separation and Purification Technology*, **56**(3): 284-290.

Mallampati, R., & Valiyaveettil, S. (2013). Apple Peels - A Versatile Biomass for Water Purification? *ACS Applied Materials & Interfaces*, **5**(10): 4443-4449.

Manju, G. N., Raji, C., & Anirudhan, T. S. (1998). Evaluation of coconut husk carbon for the removal of arsenic from water. *Water Research*, **32**(10): 3062-3070.

Martin, B., Parsons, S., & Jefferson, B. (2009). Removal and recovery of phosphate from municipal wastewaters using a polymeric anion exchanger bound with hydrated ferric oxide nanoparticles. *Water Science and Technology*, **60**(10): 2637-2645.

Martínez-Miranda, V., García-Sánchez, J., & Solache-Ríos, M. (2011). Fluoride ions behavior in the presence of corrosion products of iron: effects of other anions. *Separation Science and Technology*, **46**(9): 1443-1449.

Mashkour, S. (2013). Removal of amaranth dye from aqueous solution using pomegranate peel. *International Journal of Basic & Appllied Sciences*, **13**(4): 57-64.

Melgarejo, P., Núñez-Gómez, D., Legua, P., Martínez-Nicolás, J. J., & Almansa, M. S. (2020). Pomegranate (*Punica granatum L.*) a dry pericarp fruit with fleshy seeds. *Trends in Food Science & Technology*, **102**: 232-236.

Meng, F., Yang, B., Wang, B., Duan, S., Chen, Z., & Ma, W. (2017). Novel dendrimerlike magnetic biosorbent based on modified orange peel waste: Adsorption–reduction behavior of arsenic. *ACS Sustainable Chemistry & Engineering*, **5**(11): 9692-9700.

Michalak, I., Chojnacka, K., & Witek-Krowiak, A. (2013). State of the art for the biosorption process-a review. *Applied Biochemistry and Biotechnology*, **170**(6): 1389-1416.

Mohammadi, T., Moheb, A., Sadrzadeh, M., & Razmi, A. (2005). Modeling of metal ion removal from wastewater by electrodialysis. *Separation and Purification Technology*, **41**(1): 73-82.

Mohan, D., & Pittman Jr, C. U. (2007). Arsenic removal from water/wastewater using adsorbents - A critical review. *Journal of Hazardous Materials*, **142**(1-2): 1-53.

Mor, S., Chhoden, K., & Ravindra, K. (2016). Application of agro-waste rice husk ash for the removal of phosphate from the wastewater. *Journal of Cleaner Production*, **129**: 673-680.

Moreira, V. R., Lebron, Y. A. R., Lange, L. C., & Santos, L. V. S. (2019). Simultaneous biosorption of Cd (II), Ni (II) and Pb (II) onto a brown macroalgae Fucus vesiculosus: Mono-and multi-component isotherms, kinetics and thermodynamics. *Journal of Environmental Management*, **251**: 109587.

Mthombeni, N. H., Mbakop, S., Ochieng, A., & Onyango, M. S. (2018). Adsorptive removal of V (V) ions using clinoptilolite modified with polypyrrole and iron oxide nanoparticles in column studies. *MRS Advances*, **3**(36): 2119-2127.

Mueller, B., & Hug, S. J. (2018). Climatic variations and de-coupling between arsenic and iron in arsenic contaminated ground water in the lowlands of Nepal. *Chemosphere*, **210**: 347-358.

Najafpoor, A. A., Dousti, S., Joneidi Jafari, A., & Hosseinzadeh, A. (2016). Efficiency in phenol removal from aqueous solutions of pomegranate peel ash as a natural adsorbent. *Environmental Health Engineering and Management Journal*, **3**(1): 41-46.

Najim, T. S., & Yassin, S. A. (2009). Removal of Cr (VI) from aqueous solution using modified pomegranate peel: equilibrium and kinetic studies. *E-Journal of Chemistry*, **6**(S1): S129-S142.

Namasivayam, C., & Sangeetha, D. (2004). Equilibrium and kinetic studies of adsorption of phosphate onto $ZnCl_2$ activated coir pith carbon. *Journal of Colloid and Interface Science*, **280**(2): 359-365.

Naujokas, M. F., Anderson, B., Ahsan, H., Aposhian, H. V., Graziano, J. H., Thompson, C., & Suk, W. A. (2013). The broad scope of health effects from chronic arsenic exposure: update on a worldwide public health problem. *Environmental Health Perspectives*, **121**(3): 295-302.

Netzer, A., & Hughes, D. (1984). Adsorption of copper, lead and cobalt by activated carbon. *Water Research*, **18**(8): 927-933.

Nguyen, T. T. Q., Loganathan, P., Nguyen, T. V., & Vigneswaran, S. (2020a). Removing arsenate from water using modified manganese oxide ore: column adsorption and waste management. *Journal of Environmental Chemical Engineering*, **8**(6): 104491.

Nguyen, T. T. Q., Loganathan, P., Nguyen, T. V., Vigneswaran, S., & Ngo, H. H. (2020b). Iron and zirconium modified luffa fibre as an effective bioadsorbent to remove arsenic from drinking water. *Chemosphere*, **258**: 127370.

Nguyen, T., Ngo, H., Guo, W., Zhou, J., Wang, J., Liang, H., & Li, G. (2014). Phosphorus elimination from aqueous solution using 'zirconium loaded okara'as a biosorbent. *Bioresource Technology*, **170**: 30-37.

Nhiem, D. N., Duc, D. H., Lim, D. T., Bac, N. Q., Chuc, P. N., Dung, D. T., ... & Khieu, D. Q. (2021). Strong adsorption of arsenite and phosphate from aqueous solution using La_2O_3–CeO_2 composite. *Journal of Polymers and the Environment*, **29**(4): 1310-1323.

Nieminen, J. (2010). Phosphorus recovery and recycling from municipal wastewater sludge. *Vesitalous*, **3**: 15-17.

Nies, D. H. (1999). Microbial heavy-metal resistance. *Applied Microbiology and Biotechnology*, **51**(6): 730-750.

Noli, F., Kapashi, E., & Kapnisti, M. (2019). Biosorption of uranium and cadmium using sorbents based on Aloe vera wastes. *Journal of Environmental Chemical Engineering*, **7**(2): 102985.

Nuhoğlu, Y., Ekmekyapar Kul, Z., Kul, S., Nuhoğlu, Ç., & Ekmekyapar Torun, F. (2021). Pb (II) biosorption from the aqueous solutions by raw and modified tea factory waste (TFW). *International Journal of Environmental Science and Technology*, **18**(10): 2975-2986.

Ohtake, H., & Tsuneda, S. (Eds.). (2019). *Phosphorus recovery and recycling*. Singapore: Springer Singapore.

Okada, K., Jha, V., Kameshima, Y., Nakajima, A., & MacKenzie, K. (2004). Sorption properties of activated carbon derived from used paper and of amorphous 2CaO. Al_2O_3. $2SiO_2$ from paper sludge ash. *WIT Transactions on Ecology and the Environment*, **79**: 1-10

Oliveira, M. R. F., do Vale Abreu, K., Romão, A. L. E., Davi, D. M. B., de Carvalho Magalhães, C. E., Carrilho, E. N. V. M., & Alves, C. R. (2021). Carnauba (Copernicia prunifera) palm tree biomass as adsorbent for Pb (II) and Cd (II) from water medium. *Environmental Science and Pollution Research*, **28**(15): 18941-18952.

Ortega, A., Oliva, I., Contreras, K. E., González, I., Cruz-Díaz, M. R., & Rivero, E. P. (2017). Arsenic removal from water by hybrid electro-regenerated anion exchange resin/electrodialysis process. *Separation and Purification Technology*, **184**: 319–326.

Padmavathy, V. (2008). Biosorption of nickel (II) ions by baker's yeast: Kinetic, thermodynamic and desorption studies. *Bioresource Technology*, **99**(8): 3100-3109.

Pandey, G., & Madhuri, S. (2014). Heavy metals causing toxicity in animals and fishes. *Research Journal of Animal, Veterinary and Fishery Sciences*, **2**(2): 17-23.

Pangeni, B., Paudyal, H., Inoue, K., Kawakita, H., Ohto, K., Gurung, M., & Alam, S. (2014). Development of low cost adsorbents from agricultural waste biomass for the removal of Sr (II) and Cs (I) from water. *Waste and Biomass Valorization*, **5**(6): 1019-1028.

Pant, B., Pant, H. R., & Park, M. (2020). Fe1−xS modified TiO$_2$ NPs embedded carbon nanofiber composite via electrospinning: A potential electrode material for supercapacitors. *Molecules*, **25**(5): 1075.

Pant, B., Pant, H. R., Park, M., Liu, Y., Choi, J. W., Barakat, N. A., & Kim, H. Y. (2014). Electrospun CdS–TiO$_2$ doped carbon nanofibers for visible-light-induced photocatalytic hydrolysis of ammonia borane. *Catalysis Communications*, **50**: 63-68.

Pant, B., Park, M., & Park, S. J. (2019). Recent advances in TiO$_2$ films prepared by sol-gel methods for photocatalytic degradation of organic pollutants and antibacterial activities. *Coatings*, **9**(10): 613.

Patel, H. (2019). Fixed-bed column adsorption study: a comprehensive review. *Applied Water Science*, **9**(3): 1-17.

Pathak, P. D., Mandavgane, S. A., & Kulkarni, B. D. (2016). Characterizing fruit and vegetable peels as bioadsorbents. *Current Science*, 2114-2123.

Paudyal, H., Ohto, K., Kawakita, H., & Inoue, K. (2020). Recovery of fluoride from water through adsorption using orange-waste gel, followed by desorption using saturated lime water. *Journal of Material Cycles and Waste Management*, **22**(5): 1484-1491.

Paudyal, H., Pangeni, B., Inoue, K., Harada, H., Kawakita, H., Ohto, K., & Alam, S. (2017). Adsorptive removal of trace concentration of fluoride using orange waste treated using concentrated sulfuric acid. *IJMSA*, **6**: 212.

Paudyal, H., Pangeni, B., Inoue, K., Kawakita, H., Ohto, K., & Alam, S. (2013). Adsorptive removal of fluoride from aqueous medium using a fixed bed column packed with Zr (IV) loaded dried orange juice residue. *Bioresource Technology*, **146**: 713-720.

Paudyal, H., Pangeni, B., Inoue, K., Kawakita, H., Ohto, K., Ghimire, K. N., Harada, H., & Alam, S. (2013). Adsorptive removal of trace concentration of fluoride ion from water by using dried orange juice residue. *Chemical Engineering Journal*, **223**: 844–853.

Pehlivan, E., Tran, H. T., Ouédraogo, W. K. I., Schmidt, C., Zachmann, D., & Bahadir, M. (2013). Sugarcane bagasse treated with hydrous ferric oxide as a potential adsorbent for the removal of As(V) from aqueous solutions. *Food Chemistry*, **138**(1): 133-138.

Peng, W., Li, H., Liu, Y., & Song, S. (2017). A review on heavy metal ions adsorption from water by graphene oxide and its composites. *Journal of Molecular Liquids*, **230**: 496-504.

Pincus, L. N., Melnikov, F., Yamani, J. S., & Zimmerman, J. B. (2018). Multifunctional photoactive and selective adsorbent for arsenite and arsenate: Evaluation of nano titanium dioxide-enabled chitosan cross-linked with copper. *Journal of Hazardous Materials*, **358**: 145-154.

Pintor, A. M., Vieira, B. R., Santos, S. C., Boaventura, R. A., & Botelho, C. M. (2018). Arsenate and arsenite adsorption onto iron-coated cork granulates. *Science of the Total Environment*, **642**: 1075-1089.

Pirilä, M., Martikainen, M., Ainassaari, K., Kuokkanen, T., & Keiski, R. L. (2011). Removal of aqueous As (III) and As (V) by hydrous titanium dioxide. *Journal of Colloid and Interface Science*, **353**(1): 257-262.

Podgorski, J., & Berg, M. (2020). Global threat of arsenic in groundwater. *Science*, **368**(6493): 845–850.

Pokhrel, M. R., Poudel, B. R., Aryal, R. L., Paudyal, H., & Ghimire, K. N. (2019). Removal and recovery of phosphate from water and wastewater using metal-loaded agricultural waste-based adsorbents: a review. *Journal of Institute of Science and Technology*, **24**(1): 77-89.

Poudel, B. R., Ale, D. S., Aryal, R. L., Ghimire, K. N., Gautam, S. K., Paudyal, H., & Pokhrel, M. R. (2022). Zirconium modified pomegranate peel for efficient removal of arsenite from water. *BIBECHANA*, **19**(1-2): 1-13.

Poudel, B. R., Aryal, R. L., Bhattarai, S., Koirala, A. R., Gautam, S. K., Ghimire, K. N., Pant, B., Park, M., Paudyal, H., & Pokhrel, M. R. (2020). Agro-waste derived biomass impregnated with TiO_2 as a potential adsorbent for removal of as (III) from water. *Catalysts*, **10**(10): 1125.

Poudel, B. R., Aryal, R. L., Gautam, S. K., Ghimire, K. N., Paudyal, H., & Pokhrel, M. R. (2021). Effective remediation of arsenate from contaminated water by zirconium modified pomegranate peel as an anion exchanger. *Journal of Environmental Chemical Engineering*, **9**(6): 106552.

Qi, F., Lamb, D., Naidu, R., Bolan, N. S., Yan, Y., Ok, Y. S., Rahman, M. M., & Choppala, G. (2018). Cadmium solubility and bioavailability in soils amended with acidic and neutral biochar. *Science of the Total Environment*, **610**: 1457-1466.

Quintelas, C., Pereira, R., Kaplan, E., & Tavares, T. (2013). Removal of Ni (II) from aqueous solutions by an Arthrobacter viscosus biofilm supported on zeolite: from laboratory to pilot scale. *Bioresource Technology*, **142**: 368-374.

Radaei, E., Alavi Moghaddam, M. R., & Arami, M. (2014). Removal of reactive blue 19 from aqueous solution by pomegranate residual-based activated carbon: optimization by response surface methodology. *Journal of Environmental Health Science and Engineering*, **12**(1): 1-8.

Rahman, M. A., Lamb, D., Rahman, M. M., Bahar, M. M., Sanderson, P., Abbasi, S., Bari, A. F., & Naidu, R. (2021). Removal of arsenate from contaminated waters by novel zirconium and zirconium-iron modified biochar. *Journal of Hazardous Materials*, **409**: 124488.

Rahman, M. A., Lamb, D., Rahman, M. M., Bahar, M. M., Sanderson, P., Abbasi, S., Bari, A. S. M. F., & Naidu, R. (2021). Removal of arsenate from contaminated

waters by novel zirconium and zirconium-iron modified biochar. *Journal of Hazardous Materials*, **409**: 124488

Rajendran, M., &Thangavelu, D. (2021). Removal of As (V) from water using galvanically coupled sacrificial metals. *Journal of Hazardous Materials*, **409**: 124564.

Ranjan, D., Talat, M., & Hasan, S. (2009). Rice polish: an alternative to conventional adsorbents for treating arsenic bearing water by up-flow column method. *Industrial & Engineering Chemistry Research*, **48**(23): 10180-10185.

Rathore, E., Maji, K., & Biswas, K. (2021). Nature-inspired coral-like layered $[Co_{0.79} Al_{0.21}(OH)_2 (CO_3)_{0.11}]\cdot mH_2O$ for fast selective ppb level capture of Cr (VI) from contaminated water. *Inorganic Chemistry*, **60**(13): 10056-10063.

Rathore, E., Pal, P., & Biswas, K. (2017). Layered metal chalcophosphate (K-MPS-1) for efficient, selective, and ppb level sequestration of Pb from water. *The Journal of Physical Chemistry C*, **121**(14): 7959-7966.

Reddad, Z., Gerente, C., Andres, Y., & Le Cloirec, P. (2002). Adsorption of several metal ions onto a low-cost biosorbent: kinetic and equilibrium studies. *Environmental Science & Technology*, **36**(9): 2067-2073.

Ren, Z., Zhang, & G., Chen, J. P. (2011). Adsorptive removal of arsenic from water by an Iron–zirconium binary oxide adsorbent. *Journal of Colloid and Interface Science*, **358**(1): 230–237.

Rouabeh, I., & Amrani, M. (2012). Equilibrium modeling for adsorption of NO3 from aqueous solution on activated carbon produced from pomegranate peel. *Advances in Environmental Research*, **1**(2): 143-151.

Roy, P., Mondal, N. K., Bhattacharya, S., Das, B., & Das, K. (2013). Removal of arsenic (III) and arsenic (V) on chemically modified low-cost adsorbent: batch and column operations. *Applied Water Science*, **3**(1): 293-309.

Saad, H., Charrier-El Bouhtoury, F., Pizzi, A., Rode, K., Charrier, B., & Ayed, N. (2012). Characterization of pomegranate peels tannin extractives. *Industrial Crops and Products*, **40**: 239-246.

Saad, H., Pizzi, A., Charrier, B., Ayed, N., Rode, K., & Charrier, F. (2015). Valorization of Tunisian pomegranate peel tannins in green adhesives formulation. *Journal of Renewable Materials*, **3**(1): 34-43.

Sahu, U. K., Mahapatra, S. S., & Patel, R. K. (2017). Synthesis and characterization of an eco-friendly composite of jute fiber and Fe_2O_3 nanoparticles and its application as an adsorbent for removal of As (V) from water. *Journal of Molecular Liquids*, **237**: 313-321.

Sahu, U. K., Sahu, S., Mahapatra, S. S., & Patel, R. K. (2019). Synthesis and characterization of magnetic bio-adsorbent developed from Aegle marmelos leaves for removal of As (V) from aqueous solutions. *Environmental Science and Pollution Research*, **26**(1): 946-958.

Saifuddin M, N., & Kumaran, P. (2005). Removal of heavy metal from industrial wastewater using chitosan coated oil palm shell charcoal. *Electronic Journal of Biotechnology*, **8**(1): 43-53.

Salmana, S. M., Zahoorb, M., Majeeda, A., Wahaba, M., e Shahwarc, D., Shahd, S. N., & Khane, E. (2021). Effective removal of Cd (II), Pb (II) and Cr (VI) from aqueous solution using Bauhinia variegata leaves after chemical modifications. *Desalination and Water Treatment*, **220**: 182-191.

Salmani, M. H., Abedi, M., Mozaffari, S. A., & Sadeghian, H. A. (2017). Modification of pomegranate waste with iron ions a green composite for removal of Pb from aqueous solution: equilibrium, thermodynamic and kinetic studies. *AMB Express*, **7**(1): 1-8.

Sarma, P., Kumar, R., & Pakshirajan, K. (2015). Batch and Continuous Removal of Copper and Lead from Aqueous Solution using Cheaply Available Agricultural Waste Materials. *International Journal of Environmental Research*, **9**(2): 1-13.

Sasidharan, A. P., Meera, V., & Raphael, V. P. (2022). Nanochitosan impregnated polyurethane foam in the removal of phosphate and coliforms from greywater. *Nanotechnology for Environmental Engineering*, **2022**: 1-12.

Sasidharan, A., Meera, V., & Raphael, V. (2021). Novel polyurethane foams loaded with nanoparticles-synthesis, characterisation, and evaluation of phosphate removal efficacies. *International Journal of Environmental Science and Technology*, **2021**: 1-20.

Sawood, G. M., & Gupta, S. K. (2020). Arsenate adsorption from aqueous solution using iron-loaded Azadirachta indica roots: batch and fixed-bed column study. *Desalination & Water Treatment*, **203**: 292-308.

Schaum, C. (2018). *Phosphorus: Polluter and Resource of the Future: Motivations, Technologies and Assessment of the Elimination and Recovery of Phosphorus from Wastewater*. IWA Publishing, London UK.

Schweitzer, L., & Noblet, J. (2018). Water contamination and pollution. In *Green Chemistry* (pp. 261-290). Elsevier.

Sehn, P. (2008). Fluoride removal with extra low energy reverse osmosis membranes: three years of large scale field experience in Finland. *Desalination*, **223**(1-3): 73-84.

Sengupta, S., & Pandit, A. (2011). Selective removal of phosphorus from wastewater combined with its recovery as a solid-phase fertilizer. *Water Research*, **45**(11): 3318-3330.

Sert, S., Celik, A., & Tirtom, V. N. (2017). Removal of arsenic (III) ions from aqueous solutions by modified hazelnut shell, *Desalination & Water Treatment,* **75**: 115-123.

Setyono, D., & Valiyaveettil, S. (2014). Chemically modified sawdust as renewable adsorbent for arsenic removal from water. *ACS Sustainable Chemistry and Engineering*, **2**(12): 2722–2729.

Shabbir, Z., Shahid, M., Khalid, S., Khalid, S., Imran, M., Qureshi, M. I., & Niazi, N. K. (2020). Use of agricultural bio-wastes to remove arsenic from contaminated water. *Environmental Geochemistry and Health*, **2020**: 1-10.

Shakoor, M. B., Niazi, N. K., Bibi, I., Shahid, M., Saqib, Z. A., Nawaz, M. F., Shaheen, S. M., Wang, H., Tsang, D. C., & Bundschuh, J. (2019). Exploring the arsenic removal potential of various biosorbents from water. *Environment International*, **123**: 567-579.

Shakoor, M. B., Niazi, N. K., Bibi, I., Shahid, M., Sharif, F., Bashir, S., ... & Rinklebe, J. (2018). Arsenic removal by natural and chemically modified watermelon rind in aqueous solutions and groundwater. *Science of the Total Environment*, **645**: 1444-1455.

Sharaf El-Deen, G., & Sharaf El-Deen, S. (2016). Kinetic and isotherm studies for adsorption of Pb (II) from aqueous solution onto coconut shell activated carbon. *Desalination and Water Treatment*, **57**(59): 28910-28931.

Sharma, R., & Singh, B. (2013). Removal of Ni (II) ions from aqueous solutions using modified rice straw in a fixed bed column. *Bioresource Technology*, **146**: 519-524.

Sharma, V. K., & Sohn, M. (2009). Aquatic arsenic: toxicity, speciation, transformations, and remediation. *Environment International*, **35**(4): 743-759.

Shehzad, K., Ahmad, M., He, J., Liu, T., Xu, W., & Liu, J. (2019). Synthesis of ultra-large ZrO_2 nanosheets as novel adsorbents for fast and efficient removal of As(III) from aqueous solutions. *Journal of Colloid and Interface Science*, **533**: 588–597.

Sherchand, O., Mehta, K., Poudel, P., Deo, B., & Baral, N. (2014). Blood Lead Levels of Primary School Children in Kathmandu Municipality, Nepal. *Journal of Institute of Medicine*, **36**(3) 1-8.

Sherlala, A., Raman, A., Bello, M., & Asghar, A. (2018). A review of the applications of organo-functionalized magnetic graphene oxide nanocomposites for heavy metal adsorption. *Chemosphere*, **193**: 1004-1017.

Shrestha, A., Poudel, B. R., Silwal, M., & Pokhrel, M. R. (2018). Adsorptive removal of phosphate onto iron loaded litchi chinensis seed waste. *Journal of Institute of Science and Technology*, **23**(1): 81-87.

Shrestha, R. K., Regmi, D., & Kafle, B. P. (2014). Seasonal variation of arsenic concentration in ground water of Nawalparasi district of Nepal. *International Journal of Applied Sciences and Biotechnology*, **2**(1): 59-63.

Sial, R., Chaudhary, M., Abbas, S., Latif, M., & Khan, A. (2006). Quality of effluents from Hattar industrial estate. *Journal of Zhejiang University SCIENCE B*, **7**(12): 974-980.

Silva Simplicio, W. (2020). *Phosphorus recovery through adsorption using iron modified cellulose* (Doctoral dissertation). NUI Galway.

Singh, T. S., & Pant, K. (2006). Experimental and modelling studies on fixed bed adsorption of As (III) ions from aqueous solution. *Separation and Purification Technology*, **48**(3): 288-296.

Srivastava, S., & Goyal, P. (2010). *Novel biomaterials: decontamination of toxic metals from wastewater*. Springer Science & Business Media.

Su, H., Lv, X., Zhang, Z., Yu, J., & Wang, T. (2017). Arsenic removal from water by photocatalytic functional Fe_2O_3–TiO_2 porous ceramic. *Journal of Porous Materials*, **24**(5): 1227-1235.

Sumathi, T., & Alagumuthu, G. (2014). Adsorption studies for arsenic removal using activated Moringa oleifera. *International Journal of Chemical Engineering*, **2014**: 430417.

Suzaimi, N. D., Goh, P. S., Malek, N. A. N. N., Lim, J. W., & Ismail, A. F. (2020). Enhancing the performance of porous rice husk silica through branched polyethyleneimine grafting for phosphate adsorption. *Arabian Journal of Chemistry*, **13**(8): 6682-6695.

Tamayo, R., Espinoza-González, R., Gracia, F., Rodrigues-Filho, U. P., Flores, M., & Sacari, E. (2019). As (III) removal from aqueous solution by calcium titanate nanoparticles prepared by the sol gel method. *Nanomaterials*, **9**(5): 733.

Tangaromsuk, J., Pokethitiyook, P., Kruatrachue, M., & Upatham, E. (2002). Cadmium biosorption by Sphingomonas paucimobilis biomass. *Bioresource Technology*, **85**(1): 103-105.

Thapa, S., & Pokhrel, M. R. (2012). Removal of As(III) from aqueous solution using Fe (III) loaded pomegranate waste. *Journal of Nepal Chemical Society*, **30**: 29-36.

Threepanich, A., & Praipipat, P. (2021). Powdered and beaded lemon peels-doped iron (III) oxide-hydroxide materials for lead removal applications: Synthesis, characterizations, and lead adsorption studies. *Journal of Environmental Chemical Engineering*, **9**(5): 106007.

Tran, H. N., You, S. J., Hosseini-Bandegharaei, A., & Chao, H. P. (2017). Mistakes and inconsistencies regarding adsorption of contaminants from aqueous solutions: a critical review. *Water Research*, **120**: 88-116.

Uddin, M. M., Zakeel, M. C. M., Zavahir, J. S., Marikar, F. M., & Jahan, I. (2021). Heavy metal accumulation in rice and aquatic plants used as human food: A general review. *Toxics*, **9**(12): 360.

Ullah, R., Malik, R. N., & Qadir, A. (2009). Assessment of groundwater contamination in an industrial city, Sialkot, Pakistan. *African Journal of Environmental Science and Technology*, **3**(12): 429-446.

UNEP. "Lead Exposure and Human Health." UNEP- United Nations Environment Programme. 2013. http://www.chem.unep.ch/pops/pdf/lead/leadexp.pdf (accessed 07/07/2022).

United States Environmental Protection Agency (USEPA). 2017. Drinking Water Requirements for States and Public Water System. https://www.epa.gov/dwreginfo/chemical--contaminant--rules (accessed 12/07/2022).

Uppal, J. S., Zheng, Q., & Le, X. C. (2019). Arsenic in drinking water—recent examples and updates from Southeast Asia. *Current Opinion in Environmental Science & Health*, **7**: 126-135.

Urik, M., Littera, P., & Sevc, J. (2009). Removal of arsenic(V) from aqueous solutions using chemically modified sawdust of spruce (*Picea abies*): Kinetics and isotherm studies. *International Journal of Environmental Science & Technology*, **6**(3): 451-456.

Uysal, M., & Ar, I. (2007). Removal of Cr(VI) from industrial wastewaters by adsorption: Part I: Determination of optimum conditions. *Journal of Hazardous Materials*, **149**(2): 482-491.

Verma, L., Siddique, M. A., Singh, J., & Bharagava, R. N. (2019). As(III) and As(V) removal by using iron impregnated biosorbents derived from waste biomass of Citrus limmeta (peel and pulp) from the aqueous solution and ground water. *Journal of Environmental Management*, **250**: 109452.

Vieira, B. R., Pintor, A. M., Boaventura, R. A., Botelho, C. M., & Santos, S. C. (2017). Arsenic removal from water using iron-coated seaweeds. *Journal of Environmental Management*, **192**: 224-233.

Vijayaraghavan, K., & Yun, Y.-S. (2008). Bacterial biosorbents and biosorption. *Biotechnology Advances*, **26**(3): 266-291.

Wang, F., Wu, P., Shu, L., Guo, Q., Huang, D., & Liu, H. (2022). Isotherm, kinetics, and adsorption mechanism studies of diethylenetriaminepentaacetic acid-modified banana/pomegranate peels as efficient adsorbents for removing Cd(II) and Ni(II) from aqueous solution. *Environmental Science and Pollution Research*, **29**(2): 3051-3061.

Wang, J., & Chen, C. (2009). Biosorbents for heavy metals removal and their future. *Biotechnology Advances*, **27**(2): 195-226.

Wang, J., & Guo, X. (2020). Adsorption isotherm models: Classification, physical meaning, application and solving method. *Chemosphere*, **258**: 127279.

Wang, P., Zhang, Q., Li, Y., Matsiko, J., Zhang, Y., & Jiang, G. (2017). Airborne persistent toxic substances (PTSs) in China: occurrence and its implication associated with air pollution. *Environmental Science: Processes & Impacts*, **19**(8): 983-999.

Wang, Q., Zhou, C., Kuang, Y.-j., Jiang, Z.-h., & Yang, M. (2020). Removal of hexavalent chromium in aquatic solutions by pomelo peel. *Water Science and Engineering*, **13**(1): 65-73.

Weber Jr, W. J., & Morris, J. C. (1963). Kinetics of adsorption on carbon from solution. *Journal of the Sanitary Engineering Division*, **89**(2): 31-59.

Won, S. W., Kotte, P., Wei, W., Lim, A., & Yun, Y.-S. (2014). Biosorbents for recovery of precious metals. *Bioresource Technology*, **160**: 203-212.

World Health Organization, WHO. (2017). Guidelines for drinking-water quality: first addendum to the fourth edition.

Xi, J., He, L., & Yan, L.-g. (2017). Continuous extraction of phenolic compounds from pomegranate peel using high voltage electrical discharge. *Food Chemistry*, **230**: 354-361.

Xu, L., Liu, Y., Wang, J., Tang, Y., & Zhang, Z. (2021). Selective adsorption of Pb^{2+} and Cu^{2+} on amino-modified attapulgite: Kinetic, thermal dynamic and DFT studies. *Journal of Hazardous Materials*, **404**: 124140.

Xu, X., Gao, B., Yue, Q., & Zhong, Q. (2011). Sorption of phosphate onto giant reed based adsorbent: FTIR, Raman spectrum analysis and dynamic sorption/desorption properties in filter bed. *Bioresource Technology*, **102**(9): 5278-5282.

Xu, X., Gao, B.-Y., Yue, Q.-Y., & Zhong, Q. (2010). Preparation of agricultural by-product based anion exchanger and its utilization for nitrate and phosphate removal. *Bioresource Technology*, **101**(22): 8558-8564.

Yadav, D., Kumar, P., Kapur, M., & Mondal, M. K. (2019). Phosphate removal from aqueous solutions by nano-alumina for the effective remediation of

eutrophication. *Environmental Progress & Sustainable Energy*, **38**(S1): S77-S85.

Yadav, P., Farnood, R., & Kumar, V. (2021). HMO-incorporated electrospun nanofiber recyclable membranes: Characterization and adsorptive performance for Pb (II) and As (V). *Journal of Environmental Chemical Engineering*, **9**(6): 106507.

Yang, Q., Wang, X., Luo, W., Sun, J., Xu, Q., Chen, F., Zhao, J., Wang, S., Yao, F., & Wang, D. (2018a). Effectiveness and mechanisms of phosphate adsorption on iron-modified biochars derived from waste activated sludge. *Bioresource Technology*, **247**: 537-544.

Yang, X., Nisar, T., Hou, Y., Gou, X., Sun, L., & Guo, Y. (2018b). Pomegranate peel pectin can be used as an effective emulsifier. *Food Hydrocolloids*, **85**: 30-38.

Yao, S., Jia, Y., Shi, Z., & Zhao, S. (2010). Photocatalytic oxidation of arsenite by a composite of titanium dioxide and activated carbon fiber. *Photochemistry and Photobiology*, **86**(6): 1215-1221.

Younes, A. A., Abdulhady, Y. A., Shahat, N. S., & El-Din El-Dars, F. M. (2021). Removal of cadmium ions from wastewaters using corn cobs supporting nano-zero valent iron. *Separation Science and Technology*, **56**(1): 1-13.

Zhang, H., Wang, Z., Li, R., Guo, J., Li, Y., Zhu, J., & Xie, X. (2017). TiO_2 supported on reed straw biochar as an adsorptive and photocatalytic composite for the efficient degradation of sulfamethoxazole in aqueous matrices. *Chemosphere*, **185**: 351-360.

Zhang, J., Shan, W., Ge, J., Shen, Z., Lei, Y., & Wang, W. (2012). Kinetic and equilibrium studies of liquid-phase adsorption of phosphate on modified sugarcane bagasse. *Journal of Environmental Engineering*, **138**(3): 252-258.

Zhang, Q. L., Lin, Y. C., Chen, X., & Gao, N. Y. (2007). A method for preparing ferric activated carbon composites adsorbents to remove arsenic from drinking water. *Journal of Hazardous Materials*, **148**(3): 671-678.

Zhang, S., & Lu, X. (2018). Treatment of wastewater containing Reactive Brilliant Blue KN-R using TiO$_2$/BC composite as heterogeneous photocatalyst and adsorbent. *Chemosphere*, **206**: 777-783.

Zhang, Z., Wang, T., Zhang, H., Liu, Y., & Xing, B. (2021). Adsorption of Pb (II) and Cd (II) by magnetic activated carbon and its mechanism. *Science of the Total Environment*, **757**: 143910.

Zheng, Y. M., Lim, S. F., & Chen, J. P. (2009). Preparation and characterization of zirconium-based magnetic sorbent for arsenate removal. *Journal of Colloid and Interface Science*, **338**(1): 22-29.

Zubair, A., Bhatti, H. N., Hanif, M. A., & Shafqat, F. (2008). Kinetic and equilibrium modeling for Cr (III) and Cr (VI) removal from aqueous solutions by Citrus reticulata waste biomass. *Water, Air, and Soil pollution*, **191**(1): 305-318.

APPENDIX

Scientific Publications

1. **Poudel, B. R.**, Aryal, R. L., Gautam, S. K., Ghimire, K. N., Paudyal, H., & Pokhrel, M. R. (2021). Effective remediation of arsenate from contaminated water by zirconium modified pomegranate peel as an anion exchanger. *Journal of Environmental Chemical Engineering*, **9**(6): 106552. https://doi.org/10.1016/j.jece.2021.106552

2. **Poudel, B.R.**, Aryal, R.L., Bhattrai, S., Koirala, A.R., Gautam, S.K., Ghimire, K.N., Pant, B., Park, M., Paudyal, H., & Pokhrel, M.R. (2020). Agro-waste Derived Biomass Impregnated with TiO_2 as a Potential Adsorbent for Removal of As (III) from Water, *catalysts,* **10**: 1125. https://doi.org/10.3390/catal10101125

3. **Poudel, B. R.**, Ale D. S., Aryal, R. L., Ghimire, K. N., Gautam, S. K., Paudyal, H., & Pokhrel, M. R. (2021). Zirconium modified pomegranate peel for efficient removal of arsenite from water, *BIBECHANA,* **19**(1-2): 1-13. https://doi.org/10.3126/bibechana.v19i1-2.45943

4. **Poudel, B.R.**, Aryal, R.L., Ghimire, K.N., Paudyal, H., & Pokhrel, M.R. (2020). Development of Biomass-Based Anion Exchanger for the Removal of Trace Concentration of Phosphate from Water, *Journal of Nepal Chemical Society*, **41**: 56-63. https://doi.org/10.3126/jncs.v41i1.30488

Participation in International conferences

1. **International Soft Matter Summer School: Soft Matter and Topology** held on July 2-6, 2018, Korea Institute for Advanced Study (KIAS), Seoul, Korea. (Poster presentation).

2. **International Winter School 2018 on Frontiers in Materials Science** held on December 3-7, 2018, Jawaharlal Nehru Centre for Advanced Scientific Research (JNCASR), Bengaluru, India. (Poster presentation).

3. **POLY-CHAR 2019, Polymers for Sustainable Global Development** held on May 19-23, 2019, Kathmandu, Nepal. (Oral presentation).

4. **The 8th Asian Conference on Colloid & Interface Science (ACCCIS 2019),** organized by the Asian Society for Colloid & Interface Science (ASCAIS) held on September 24-27, 2019, Kathmandu, Nepal. (Poster presentation).

5. **International Winter School 2021 on Frontiers in Materials Science** held on December 6-10, 2021, Jawaharlal Nehru Centre for Advanced Scientific Research (JNCASR), Bengaluru, India. (Poster presentation)
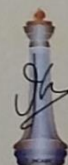
School of Advanced Materials (SAMat)
International Centre for Materials Science
and the Sheikh Saqr Laboratory
Jawaharlal Nehru Centre for Advanced Scientific Research

This is to certify that

Bhoj Raj Poudel

Tribhuvan University, NEPAL

has participated in the

International Winter School 2018
on
Frontiers in Materials Science

Directors
Prof. C.N.R. Rao & Prof. A. K. Cheetham

Prof. S. M. Shivaprasad
Convener

Prof. Umesh V. Waghmare
Convener

POLY-CHAR 2019

Certificate of Participation

This is to certify that

Prof. / Dr. / Mr. / Ms. **Bhoj Raj Poudel**

has participated as an **oral** presenter on

Adsorptive Removal of Phosphate from Aqueous Solution on Modified Arundo Donax Stem as Natural Functional Polymers in the

POLY-CHAR 2019

(Polymers for Sustainable Global Development)

May 19-23, 2019 in Kathmandu, Nepal.
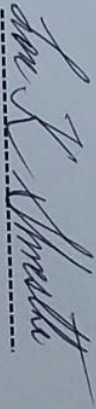
Jean M. Saiter
POLY-CHAR President

Rameshwar Adhikari
POLY-CHAR 2019 Chair

The 8th Asian Conference on Colloid & Interface Science (ACCIS 2019)

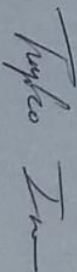Sept. 24-27, Kathmandu, Nepal

Certificate of Participation

This is to certify that

Bhoj Raj Poudel

has participated and contributed Poster Presentation in

The 8th Asian Conference on Colloid & Interface Science (ACCIS 2019) organized by the **Asian Society for Colloid and Surface Science (ASCASS)** held in Pulchowk Campus, Institute of Engineering, Tribhuvan University, Lalitpur, Kathmandu, Nepal.
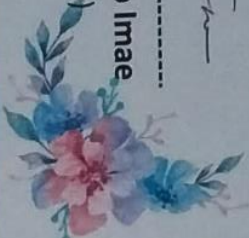
Dr. Lok Kumar Shrestha
Chairperson (ACCIS 2019)

September 27, 2019

Prof. Dr. Toyoko Imae
President (ASCASS)

ASCASS

KIΛS

KOREA INSTITUTE FOR ADVANCED STUDY
85 Hoegiro, Dongdaemun-gu,
Seoul 130-722, Korea
www.kias.re.kr

Letter of Confirmation

DATE : 2018-07-06

Name Bhojraj Poudel

Affiliation Tribhuvan University, Nepal

Email bhojrajpoudel@yahoo.com

Poster Presentation Title Removal of Chromium (VI) From Aqueous Solution using Chemically-Modified Vetiver (Vetiveria zizanioides) Root Powder as Adsorbent

This is to certify that Bhojraj Poudel of Tribhuvan University, Nepal has participated in the KIAS School, Soft Matter Summer School, which was held at Rm. 1503, KIAS, Seoul during 2018-07-02 ~ 2018-07-06.

Sincerely,

Changbong Hyeon

Professor of KIAS

Tribhuvan University
Institute of Science and Technology
Dean's Office

SEMESTER EXAMINATION 2075

Name of Student: Bhoj Raj Poudel

Level: Ph.D.

Department: Central Dept. of Chemistry

Exam Roll No.: 100003

Ph.D. Enrolment No.: 62/074

T.U. Regd. No.: 22655-93

Semester: I

Grade Sheet

Code No.	Course Title	Cr. Hrs.	Grade Point	Grade
PHS 911	Philosophy of Science	3	3.7	A-
RM 912	Research Methodology	3	3.7	A-
Sem 913	Seminar	3	4	A

SGPA: 3.8

Verified By: ~~Sndy~~

Date: oct. 9, 2018

Asst. Dean

Tribhuvan University
Institute of Science and Technology
Dean's Office

SEMESTER EXAMINATION-2075

Name of Student: Bhoj Raj Poudel   **Exam Roll No.:** 200003

Level: Ph.D.   **Ph.D. Enrolment No.:** 62/075
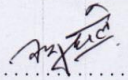
Department: Central Dept. of Chemistry   **T.U. Regd. No.:** 22655-93
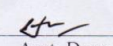
Semester: 2

Grade Sheet

Code No.	Course Title	Cr. Hrs.	Grade Point	Grade
CHE 951	Advanced Research Methodology	3	4	A
CHE 954	Separation Science and Environmental Chemistry	3	4	A
CHE 952	Seminar	3	4	A

SGPA: 4.00

Verified By: ....

Date:- Sept. 16. 2019

Asst. Dean